Sonochemically-generated Stimuli-responsive Polymeric Microspheres for Controlled Release

Cradduck, Emily

Award date:
2018

Awarding institution:
University of Bath

Sonochemically-generated Stimuli-responsive Polymeric Microspheres for Controlled Release

Emily Georgina Cradduck

A Thesis submitted for the degree of Doctor of Philosophy

Department of Chemistry

University of Bath

September 2017

Abstract

Ultrasonic irradiation at the interface between a protein solution and a gas or non-aqueous liquid facilitates the formation of protein-shelled microspheres by a phenomenon of simultaneous emulsification and encapsulation. Sonochemically-generated hollow proteinaceous microspheres have been widely reported in the literature, with a range of current and potential applications including ultrasound contrast agents, drug delivery vehicles and nutrient carriers in the food processing industry. This project builds upon preliminary investigations conducted in the field into the use of synthetic polymers as alternative shell species by developing sonochemically-generated microspheres, employing synthesised polymeric and novel stimuli-responsive block copolymeric shell species that are capable of releasing their payload in response to changes in the external environment.

Biocompatible poly(methacrylic acid) (PMAA) and PMAA-based di- and triblock copolymers, containing thermoresponsive poly(N-isopropylacrylamide) ($PNIPAA_M$), were synthesised by reversible addition-fragmentation (RAFT) polymerisation with a measured lower critical solution temperature (LCST) of 31 °C. LCST-modified polymers and block copolymers were also successfully synthesised by copolymerisation of the $PNIPAA_M$ block with hydrophobic methyl methacrylate (MMA), with an LCST of 28 °C. Functionalisation via a carbodiimide crosslinking mechanism yielded thiol-functionalised polymers, capable of undergoing radically-initiated crosslinking to form disulphide-stabilised microsphere shells.

Both thiolated and non-thiolated polymers were successfully employed in the synthesis of sonochemically-generated polymeric microspheres with comparable morphologies, supporting recent literature describing the synthesis of proteinaceous and polymeric microspheres in the absence of thiol-functionalities. Hydrophobic species, including tetradecane and naturally-occurring oils, and aqueous sodium chloride ($NaCl_{(aq)}$) within water-in-oil emulsions were successfully encapsulated. Optical microscopy was employed to measure the size and stability of the microspheres with time, whilst the encapsulation efficiency of Sudan III-labelled tetradecane-filled microspheres was characterised by Ultraviolet-Visible (UV/Vis) spectroscopy. Laser scanning confocal microscopy (LSCM) was also employed to observe the successful encapsulation of non-aqueous Nile Red-

labelled tetradecane and aqueous 5,6-carboxyfluorescein-labelled 1M NaCl aq-in-oil emulsions within the polymeric microspheres.

The release behaviour of fluorescently-labelled tetradecane from polymeric microspheres was monitored by optical microscopy, LSCM and UV/Vis spectroscopy. A range of release mechanisms were utilised, including sonochemical disruption, extreme pH and the specific release from thermoresponsive polymeric microspheres in response to an increase in temperature beyond the elevated LCST of 36-38 °C and 32-33 °C for LCST-modified microspheres. In addition to optical and confocal microscopy, the thermally-induced release of NaCl, quantified by a change in sample conductivity, was also investigated.

The work conducted during the course of this project forms the foundation for further investigation into the optimisation of thermoresponsive and stimuli-responsive microspheres, with an aim to tailor the release mechanisms of encapsulants for use as smart delivery vehicles with potential applications in the field of therapeutics, food processing, and agrochemicals.

Acknowledgements

I would first like to thank the University of Bath for funding this PhD project and for the incredible opportunities and experiences available to me both during my postgraduate and undergraduate studies. I would also like to acknowledge and thank the following people for their help and support over the last four years:

Prof. Gareth Price, thank you for making this PhD possible, enabling me to continue the research that I enjoyed so much during my Masters' project, and for your encouragement and support during these four years. Thank you for taking me out of my comfort zone by introducing me to Malaysia and for being an amazing tour guide around the sights of Kuala Lumpur, not to mention allowing me to expand my Hard Rock Café pin badge collection and experience changeable weather unlike anything I have ever witnessed.

A huge thank you to John Lowe and Catherine Lyall for your support and patience with me during my perseverance with DOSY NMR. Anne Gessell, thank you for enabling me to conclude my thesis with illuminating confocal microscopy. Cecilia, my dear, thank you for always been the crazy one in our friendship, for making rainy days in the lab a little brighter with your sunny personality, and for only teaching me the important Italian words.

Clayton, thank you for your love and patience and for being my rock during the ups and downs of research. Thank you for the wonderful experiences we have shared and for the adventures to come.

Most importantly, thank you to my amazing parents. Thank you for believing in me, for your never-ending love and support in everything I do, and for helping me make my house a home. Thank you for inspiring me, grounding me, and for being the best role models over the past 27 years.

Abbreviations and Acronyms

A/W	Air-in-water emulsion
AAc	Acrylic Acid
AAm	Acrylamide
ACP	4,4’-Azobis(4-cyanovaleric acid)
aq	Aqueous
ATRP	Atom Transfer Radical Polymerisation
CEHDA	Coaxial Electrohydrodynamic Atomisation
CMDB	S-Thiobenzoyl(thioglycolic acid)
CPADB	4-cyanopentanoic acid dithiobenzoate
CRP	Controlled Radical Polymerisation
DEAEMA	(Diethylamino)-ethyl methacrylate
DLS	Dynamic Light Scattering
DMSO	Dimethyl Sulphoxide
DOSY	Diffusion-Ordered NMR Spectroscopy
DP	Degree of Polymerisation
DTT	1,4-Dithiothreitol
EDAC	N-(3-dimethylaminopropyl)-N’-ethylcarbodiimide
FA	Folic Acid
FITC	Fluorescein Isothiocyanate
G/O/W	Gas-in-oil-in-water (Double Emulsion)
GPC	Gel Permeation Chromatography
IR	Infra-red Spectroscopy
LAMs	Less Active Monomers
LCST	Lower Critical Solution Temperature
MAA	Methacrylic Acid

MAMs	More Active Monomers
MALDI-MS	Matrix-Assisted Laser Desorption/Ionisation Mass Spectroscopy
MeI	Methyl Iodide
MeOH	Methanol
MMA	Methyl Methacrylate
M_n	Number-average Molecular Weight
MRI	Magnetic Resonance Imaging
NaCl	Sodium Chloride
NHS	N-hydroxysuccinimide
$NIPAA_M$	N-isopropylacrylamide
NMP	Nitroxide-Mediated Polymerisation
NMR	Nuclear Magnetic Resonance Spectroscopy
PFC	Perfluorocarbon
PMAA	Poly(methacrylic acid)
$PNIPAA_M$	Poly(N-isopropylacrylamide)
PVA	Poly(vinyl alcohol)
PVPON	Poly(vinyl caprolactone)
RAFT	Reversible Addition-Fragmentation Chain Transfer polymerisation
RITC	Rhodamine B Isothiocyanate
r.u.s	Repeat Units
SEC	Size Exclusion Chromatography
TMG	1,1,3,3-Tetramethylguanidine
US	Ultrasound
UV/Vis	Ultraviolet-Visible Spectroscopy
W/O	Water-in-oil (Emulsion)
W/O/W	Water-in-oil-in-water (Double Emulsion)

Oral and Poster Presentations

M4 Colloids -Cardiff, UK	2014	Poster presentation detailing initial investigations into the RAFT polymerisation of stimuli-responsive block copolymers and the use of thiolated polymers as microsphere shell material. Encapsulation of hydrophobic species and W/O emulsions within $PMAA_{SH}$-based microspheres.
European Sonochemical Society -Avignon, France	2015	Contribution of data to a poster and oral presentation by Prof. Gareth Price detailing RAFT polymerisation of stimuli-responsive block copolymers and the use of thiolated polymers as microsphere shell material.

Conferences Attended

M4 Colloids -Cardiff, UK	2014
European Sonochemical Society -Avignon, France	2015
McBain Awards Day – SCI -London, UK	2015
M4 Colloids -Bath, UK – Conference Organiser	2016

Research Collaborations

University of Nottingham -Semenyih, Malaysia	2016	Conducting research under the supervision of Prof. Sivakumar Manickam – Dept. of Chemical Engineering into the potential scale-up of microsphere synthesis by hydrodynamic cavitation.

Contents

1 Introduction

Ultrasound provides a valuable tool for the initiation and enhancement of chemical reactions via novel and interesting reaction pathways. The exploitation of ultrasound and its chemical consequences as a means to synthesise stable air-filled proteinaceous bovine serum albumin (BSA) microspheres was first discovered by Suslisk *et al*. in 1990[1]. Since then, the encapsulation of hydrophobic species[2] and the use of shell material alternatives such as lysozyme[3], DNA[4], chitosan[5] and synthetic biocompatible polymers[6], amongst other advances, have been detailed in the literature. More recently, the successful encapsulation of aqueous species has been reported[7], further broadening the scope of potential encapsulants. Advances are being made with regards to the targeting and labelling of microspheres[8,9] for particular *in vivo* applications, and early investigations into the incorporation of stimuli-responsive shell material for triggered release, initiated by physiochemical changes in the environment, have also been conducted[6].

The focus of this project is to design and tailor stimuli-responsive biopolymers, appropriate for use as microsphere shells, with an aim to create thermoresponsive microspheres capable of releasing their contents in response to temperature changes in the surrounding environment. When designing a microsphere system, factors such as the shell material, the encapsulant species, the synthetic protocol for polymer and microsphere synthesis and the stability of the microspheres must all be considered. In addition, desirable features such as release mechanism and surface functionalisation or labelling can also be included in the scope of the design.

Firstly, the shell material was considered. Microsphere systems employing proteins and naturally-occurring polymers as shell material have been extensively researched and characterised[2,5,10]. However, the extent with which a natural material can be tailored to meet the requirements of a particular application is somewhat limited. Initial investigations into the use of alternative synthetic shell species[10] have extended to scope by demonstrating the potential to design microsphere systems incorporating functional and responsive components, capable of targeting and environmentally-triggered release behaviour. This project continues to build upon the initial investigations conducted by Skinner[6] into the incorporation of stimuli-responsive components within microsphere shells. Chapter 3

reports the synthesis and characterisation of biocompatible polymeric and thermoresponsive block copolymeric shell materials by RAFT polymerisation.

It was initially proposed by Suslick and Grinstaff[2] that free thiol groups within the shell material were required to form stable microspheres by sonochemical techniques, due to the oxidation of cysteine residues during sonication and subsequent formation of stable intermolecular stable disulphide crosslinks. This theory has since been contradicted by both Gedanken[5,11] and Suslick[12], who have proposed alternative methods of stabilisation, including hydrophobic interactions, hydrogen bonding and van der Waals. The sonochemical synthesis and stability of microspheres, employing thiol-functionalised polymeric shells and non-thiolated polymeric shells stabilised by alternative covalent and non-covalent interactions, is reported in Chapter 4.

The next component to consider, of equal importance to the choice of shell material, is the encapsulant. The nature of common microsphere systems dictates that a hydrophobic or gas core is required as, during sonochemical synthesis, the oil phase is dispersed throughout the aqueous media in a simultaneous emulsification and encapsulation process. The oil layer is first deposited onto the aqueous phase containing the solubilised protein or polymer, the ultrasound horn tip is then placed at the oil:water interface, or air:water interface in microbubble systems, and the sample is sonicated. The protein or polymer then arranges itself around the dispersed oil droplet or air bubble, forming a stable dispersion[1,2,10,13]. Encapsulation of hydrophilic species has been reported, either by the partial solubilisation of a water soluble drug within the oil core upon sonication[13] or, more recently, the novel encapsulation of an aqueous phase within a preformed water-in-oil (W/O) emulsion, creating stable water-in-oil-in-water (W/O/W) dispersions[7]. The successful incorporation of an aqueous phase demonstrates the potential of microsphere systems to deliver water-soluble drugs, flavourings, and agrochemicals; a significant leap forward in the field. Chapter 4 reports successful microsphere synthesis and the use of various encapsulants including natural oils and W/O emulsions.

A mechanism for encapsulant release must also be addressed when designing polymers as delivery vehicles. The release can either occur by simple microsphere degradation, mechanical or chemical release, or stimuli-responsive release in response to a change in the external environment. Proteinaceous microspheres, stabilised by disulphide cross-linking, are known to be stable for months when stored at or below room temperature[1,14] and have

successfully exhibited release behaviour in response to mechanical release mechanisms via ultrasonic disruption[6] or the use of a disulphide cleaving agent such as dithiothreitol (DTT)[7,15]. There are no reports as yet in the literature of a sonochemically-produced thermoresponsive synthetic polymeric microsphere system successfully releasing an encapsulant in response to a change in temperature, aside from initial experimentation conducted by Skinner[6].

In an ideal stimuli-responsive microsphere system, drug-loaded microspheres with timely controlled release profiles, capable of releasing their payload in response to an external stimulus such as extreme pH, a reductive environment or a change in temperature, would enable the delivery of a specific dose to a target location over a desired duration of time. The development of tailored and targeted drug delivery vehicles has the potential to quash the use of less efficient systemic therapeutics, which offer no targeting capabilities and often harm healthy cells in the process. Although controlled delivery of this caliber is some way off, sonochemically-generated proteinaceous drug delivery vehicles have successfully enhanced drug administration to a target location *in vivo*[9]. The encapsulation efficiency and release behaviour of thiolated and non-thiolated polymeric and stimuli-responsive block copolymeric microspheres in response to various release mechanisms is discussed further in Chapter 5.

As previously mentioned, the research conducted and reported upon in this thesis builds on initial investigations performed by Skinner and Price at the University of Bath. Skinner[6] reported the functionalisation of commercially available poly(methacrylic acid) sodium salt and the one-pot sonochemical synthesis of $PMAA_{SH}$ microspheres as an alternative to proteinaceous shell species, originally demonstrated by Cavalieri *et al.*[10]. In addition to the encapsulation of hydrophobic tetradecane, Skinner and Price[7] have successfully generated novel water-in-oil emulsion-filled $PMAA_{SH}$ microspheres, first optimising the emulsion properties to generate stable nanoemulsions, followed by encapsulation within $PMAA_{SH}$ microspheres employing the same simple sonochemical protocol. Finally, Skinner[6] began investigations into the incorporation of a stimuli-responsive component within microsphere shells, reporting the novel synthesis of diblock $PMAA_{SH}$-$PNIPAA_{M}$ microspheres by RAFT polymerisation and hydrolysis of poly(tert-butyl methacrylate) (PtBMA) followed by block copolymerisation with $NIPAA_{M}$. In addition to encapsulant release from all microsphere systems instigated by non-specific release mechanisms, including sonochemical disruption

and extreme pH, Skinner reported preliminary observations of thermoresponsive microsphere breakdown and release of fluorescently-labelled tetradecane by laser scanning confocal microscopy at 40 ºC.

This chapter will provide an introduction to ultrasound, sonochemistry and the sonochemical synthesis and applications of microspheres, as well as a brief review of RAFT polymerisation and its suitability as a technique to synthesise well-defined polymers for use as microsphere shell material.

1.1 Ultrasound and Sonochemistry

The term "sonochemistry" refers to reaction initiation and enhancement induced by irradiation of a system with sound of frequencies within the ultrasonic range[16,17]. The chemical effects of ultrasound waves propagating through a liquid were first reported by Richards and Loomis in 1927[18] and since this time, ultrasound has been employed for a range of chemical, therapeutic and industrial applications. Ultrasound can be defined as the region of the sonic spectrum with frequencies that lie beyond 20 kHz, or the limit of human hearing. The range can then be subdivided further into three regions, low frequency power ultrasound, high frequency power ultrasound, and diagnostic ultrasound. Low frequency, high power ultrasound occurs within the range of 20-100 kHz, and it is here that the majority of sonochemistry occurs. It is termed conventional power ultrasound and is utilised for chemical applications due to the conditions created by acoustic energy passing through a liquid medium[19]. High frequency, low power ultrasound (1-10 MHz) is employed for diagnostic applications as it does not induce the same chemical effects as conventional power ultrasound[20].

All ultrasonic systems require a transducer to convert electrical energy into ultrasound, vibrating at a desired frequency to generate and propagate the sound wave. The most commonly employed electroacoustic transducers are piezoelectric and magnetostrictive transducers[21]. Magnetostrictive transducers, traditionally used to generate high powered ultrasound on an industrial scale, exploit the reduction in size of ferromagnetic materials in an applied magnetic field. Rapid pulsation of the applied field at a desired frequency facilitates vibration of the metal, and the oscillations generate acoustic waves[19].

In piezoelectric transducers, a pressure is applied across a surface of piezoelectric crystals along a crystallographic axis, and each perpendicular face adopts opposing charges of equal size, termed the "direct effect". The inverse is also possible, whereby an applied electric charge induces deformation and creates a mechanical stress, termed the "inverse effect". Each side then expands or contracts, depending on the charge applied, and by rapidly reversing the charges applied to each face, it is possible to generate oscillations at a desired frequency. It is this conversion of electrical energy into mechanical oscillations that generates acoustic waves[19].

To propagate the ultrasonic oscillations generated by the piezoelectric transducer through a liquid medium, an emitting surface is required. Common emitters found in the laboratory are usually in the form of a horn immersed into the liquid with longitudinal oscillation, or a bath where the oscillations propagate from the base of the bath into the liquid contained within[19]. The intensity of the ultrasound propagating from the emitter is dependent on the surface area of the emitter and measured in W cm^{-2}, therefore a 3 mm diameter horn tip will provide a higher amplitude than an ultrasonic bath of the same frequency with the same arbitrary power output setting. This is evident in the gradual destruction of 20 kHz horn tips via erosion during sonication, compared with the use of 20 kHz baths as ultrasonic cleaners of laboratory equipment, dental implements and jewellery.

Throughout this project, an ultrasound horn setup was used to propagate high intensity ultrasound through small volumes of liquid. A 3 mm titanium horn tip emitter was connected to a piezoelectric transducer converting supplied electrical energy into ultrasonic waves with a frequency of 23 kHz, within the range of conventional power ultrasound.

1.1.1 Cavitation, Sonochemistry and Sonoluminescence

A sound wave is a longitudinal pressure wave, transmitted by inducing compression and rarefaction within the medium through which the wave is travelling[19]. In a liquid, molecules of the medium oscillate parallel to the direction of the propagating wave, leading to alternate compression and rarefaction[20]. If the negative pressure during rarefaction overcomes the cohesive strength of intermolecular interactions within the fluid, small air cavities, known as cavitation bubbles, are generated. The point at which these voids are

formed is defined as the cavitation threshold. For cavitation to occur in pure water in the absence of inhomogeneities, extremely high pressures in excess of 1000 atm are required in order for voids to form. In practice, however, microscopic particulate matter and inhomogeneities within the medium provide a source of nucleation from which cavitation bubbles can grow[19].

Acoustic energy is a mechanical energy and not absorbed by molecules[20]. The applied frequencies are several orders of magnitude too low to excite vibrational or rotational motion, therefore the chemical effects of ultrasound in a liquid cannot be attributed to a direct interaction between the acoustic waves and matter within the medium at a molecular or atomic level[19]. Instead, it is the formation, growth and collapse of these generated cavitation bubbles that underlies the fundamental mechanism behind sonochemistry[22]. Once generated, the bubbles undergo compression and rarefaction in the applied field, growing with each cycle in a process called rectified diffusion, as dissolved gases and vapourised solvent diffuse into the bubble (Figure 1.1). With each cycle, stability decreases until the bubble violently collapses.

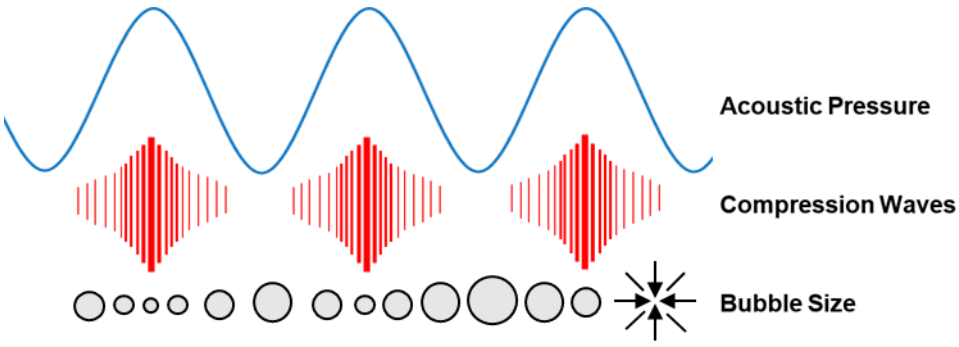

Figure 1.1 – Rarefaction and compression of a cavitation bubble in an applied acoustic field[17]. Image redrawn from reference model.

The Sonochemical Hot Spot

The collapse of cavitation bubbles generates extreme conditions of localised heat and high pressure over a very short lifetime. Temperatures within the collapsing bubble can reach 5000 K with heating and cooling rates of approximately 10^9 K/s, and localised pressure reaching 2000 atm[23], providing a unique mechanism to facilitate high energy chemistry in

liquids. It is widely accepted in the literature that the chemical effects of ultrasound stem from these localised hot spots generated during cavitation, and this process is defined as the "Hot Spot Theory"[24,18,25].

There are two types of cavitation, stable and transient[20]. During stable cavitation, bubbles oscillate over many acoustic cycles before they become unstable and violently implode, whereas in transient cavitation, bubbles only undergo one or two cycles of oscillation before implosion. Leighton[26] clarified the terminology of stable and transient cavitation by drawing attention away from the idea of temporal differentiation when considering the two modes of cavitation. Instead, he described stable cavitation as a "repetitive transient cavitation", capable of undergoing continuous oscillations of high energy collapse, until reaching a "threshold acoustic pressure" beyond which the bubble undergoes transient collapse, fragmentation, and generation of a new site for bubble nucleation[27]. Leighton[26] predicted that the nature of cavitation was therefore dependent on bubble size, whereby smaller bubbles with a higher resonant frequency are able to undergo rapid growth during rarefaction, becoming highly energetic before a compression phase during which they undergo violent transient collapse. Larger bubbles with a much lower resonant frequency, however, exhibit a slower response time and experience less growth with each rarefaction phase, therefore it can take many acoustic cycles of stable cavitation for the bubble to reach a maximum threshold size and undergo transient collapse, if at all.

A significant result of the extreme conditions created by cavitating bubbles in a liquid is the thermal dissociation of solvent molecules. In aqueous solutions the dissociation of water leads to the production of hydrogen radicals (H•), hydroxyl radicals (•OH), and protonated superoxide radicals (HO_2•)[28]. Cravotto and Cintas postulated that reactions induced by cavitation are largely determined by radical lifetimes relative to the lifetimes of collapsing bubbles[29]. At high frequencies in the diagnostic range, compression and rarefaction cycles are so rapid that the negative pressures required during rarefaction to overcome intermolecular interactions between solvent molecules, i.e. the cavitation threshold, is not reached. Cavitation is therefore very difficult to achieve at these frequencies, making it suitable for diagnostic purposes without damaging tissue. At a low frequency of 20 kHz, within the range of conventional power ultrasound, Cravotto and Cintas reported that bubble collapse occurs over 10^{-5} s. This allows time for the primary radicals produced to undergo subsequent recombination reactions to yield hydrogen peroxide, protonated

superoxide radicals and excited water molecules (Scheme 1.1). These then go on to react further in sonochemically-initiated chemical reactions within the medium. In comparison, at 500 kHz bubble collapse occurs over 4 x 10^{-7} s[29], the hot spot is too transient for the primary radicals to undergo subsequent reactions, and they transfer into the bulk phase to interact with other species.

$$H_2O \rightarrow H\bullet + \bullet OH$$
$$H\bullet + H\bullet \rightarrow H_2$$
$$\bullet OH + \bullet OH \rightarrow H_2O_2$$
$$\bullet OH + \bullet OH \rightarrow H_2O + O$$
$$\bullet OH + \bullet OH \rightarrow H_2 + O_2$$
$$H_2O + OH \rightarrow H_2O_2 + H$$
$$H\bullet + O_2 \rightarrow \bullet HO_2$$
$$\bullet HO_2 + H\bullet \rightarrow H_2O_2$$
$$\bullet HO_2 + \bullet HO_2 \rightarrow H_2O_2 + O_2$$
$$\bullet OH + H_2O \rightarrow H_2O_2 + H\bullet$$
$$\bullet H_2O + \bullet O \rightarrow H_2O_2$$
$$H\bullet + \bullet OH \rightarrow H_2O$$

Scheme 1.1 – Formation of hydroxyl and hydroperoxyl radicals during thermal dissociation of water.

Due to the transient nature of cavitating bubbles and the rapid speed at which they collapse, it is difficult to directly probe the conditions created. Comparative rate thermometry has been adopted as a technique to estimate the effective temperatures and pressures created during cavitation. A well-documented, competing unimolecular reaction is used, where the rate dependencies on temperature are known[30]. Suslick *et al.*[30] were the first to experimentally determine the effective temperature reached during bubble collapse using the sonochemical ligand substitution of volatile metal carbonyls. The sonochemical reaction rates were compared with the known temperature behaviour for the reactions and revealed two sites of reactivity, with effective temperatures of approximately 5200 K in the core gas phase of the bubble, and up to 1900 K in the initially liquid layer immediately surrounding the bubble[25]. Within the core gas phase are diffuse volatile species that have entered the core during rarefactions. These dissociate into radicals at the high temperatures and pressures within the core, diffusing into the interfacial layer and beyond into the bulk phase. Immediately beyond the gas core is the interfacial layer of liquid, some of which enters the core phase upon implosion (Figure 1.2). The huge temperature gradient created over a short distance and the impact of the collapsing bubble exposes compounds of low

volatility in the surrounding bulk phase to the propagating wave, shock waves from collapse, and radicals passing from the imploding gas core into the bulk[29].

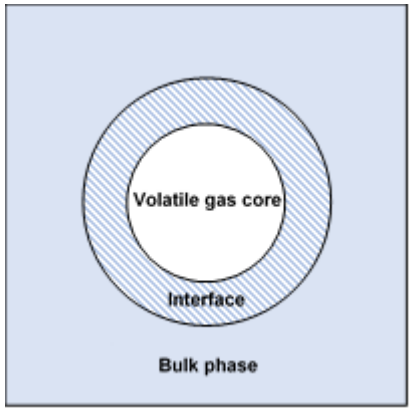

Figure 1.2 – A cavitating bubble immediately prior to collapse. A volatile gas core of high T and P, the site of radical production via dissociation upon collapse. An interfacial region, exposed to less extreme conditions, but with some injection into the gas core upon collapse. A bulk phase of low volatility species exposed to shear forces and radicals leaving the core.

One thermodynamic model that can be used to approximate the conditions during collapse is the calculation of the maximum theoretical temperature within the bubble (T_{max}) from the specific gas/vapour heat ratio and the pressure within the bubble[27].

$$T_{max} = T_0 \left\{ \frac{P_m(\gamma - 1)}{P_v} \right\} \quad (1.1)$$

Where T_0 is the ambient solution temperature, P_m is the bulk liquid pressure, $\gamma = C_p / C_v$ – the specific heat ratio of gas / vapour mixture and P_v is the bubble pressure at maximum size, assumed to equal to the vapour pressure of the bulk liquid. The theoretical T_{max} value is an overestimation, as it assumes the process is adiabatic and does not account for thermal conductivity or energy consumed by gas and vapour decomposition within the core, however it does give an indication of the temperatures reached during cavitation of approximately 6000 K[27].

Sonoluminescence, as with sonochemistry, is derived from acoustic cavitation and further supports the theory of cavitational hot spots[31]. It is the process of converting sound to light and happens during bubble compression in response to the extraordinary force placed upon it. It was first observed by Frenzel and Schultes in 1934 that, when exposed to a high

intensity ultrasonic field, certain liquids would darken immersed photographic plates[32]. This was attributed to the high intensity energy-focusing power of cavitation. A collapsing cavitation bubble can concentrate acoustic energy by a factor of 10^9, turning a sound wave that is centimetres in length into light emitted from a region of atomic dimensions[17]. Analysis of sonoluminescent emissions reveal a sharp emission spike, appearing when the bubble reaches its minimum size during collapse. There are two types of sonoluminescence, single-bubble (SBSL) and multibubble (MBSL).

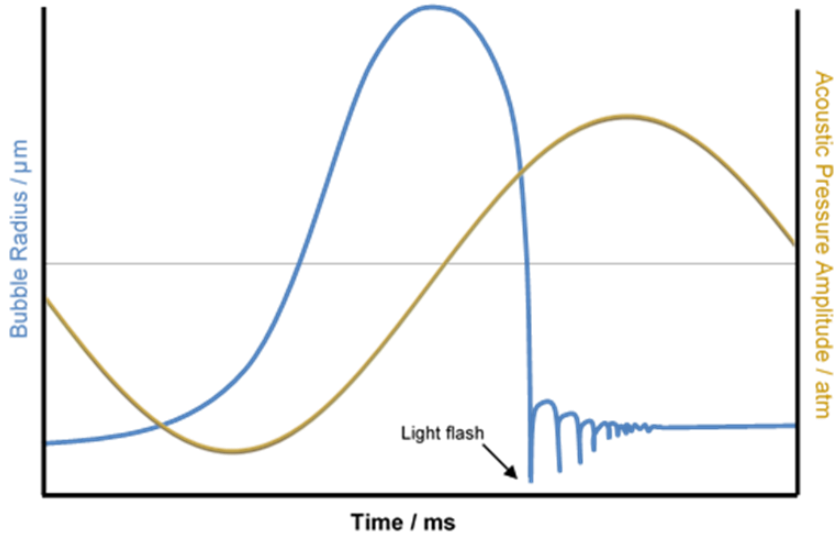

Figure 1.3 – The cycle of a collapsing bubble, showing light emission as a result of increased pressure[33]. Image redrawn from reference model.

Single-bubble systems can be achieved by acoustic levitation of a bubble in a partially degassed liquid, followed by the application of ultrasound to induce large amplitude pulsations and light emission[34]. Figure 1.3 shows the cycle of a collapsing bubble. At low pressure, the bubble experiences rarefaction and increases in size, as the acoustic pressure increases the bubble loses volume dramatically, causing a surge in pressure and a sharp light emission. After collapse, the bubble experiences rapid cycles of smaller rarefaction and compression until it has settled and undergoes the cycle again[33]. The single-bubble model demonstrates the conditions of an ideal adiabatic collapse, however cavitation is a nucleated process, therefore the overwhelming majority of reactions in sonochemistry utilise multibubble systems, also described as a "cavitation cloud". The collapsing bubbles in multibubble systems interact with one another, causing asymmetric collapse and jet formation, thus reducing the energy of each hot spot created relative to a single-bubble

system. Although the "energy per bubble" is far greater during the adiabatic collapse of a single-bubble, the sheer number of bubbles collapsing in a multibubble system produces a much higher net energy, enough to drive a chemical reaction[17].

MBSL in aqueous mediums can be enhanced by the addition of 5-amino-2,3-dihydro-1,4-phthalazinedione (luminol) to water prior to sonication, the enhanced light emission is attributed to the oxidative chemiluminescence of luminol by ●OH radicals, producing a bright blue light which can be used to map the spatial pattern of the multibubble cavitation cloud[35].

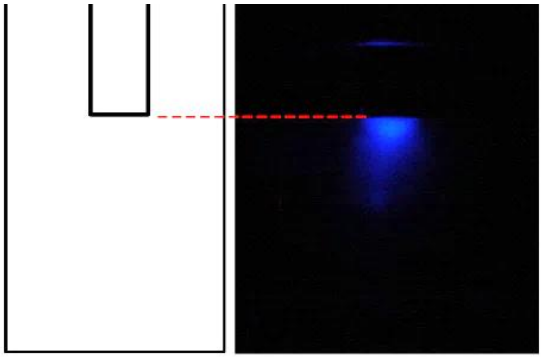

Figure 1.4 – Sonochemiluminescence of an aqueous solution containing luminol 10^{-3} M, pH 11.3 with a typical horn tip[36]. Image adapted from reference.

The Plasma and Electrokinetic Theories

In addition to Hot Spot theory, supported by characterisation and modelling of the conditions during bubble collapse and sonoluminescence, there are other theories that describe the electrical properties of acoustic cavitation[37] and the formation of plasma within the collapsing bubble core[38] as the origin of the sonochemical effects of cavitation.

At the gas-liquid interface of the bubble, species adsorbed to the surface create an electric charge distribution. The movement of the bubbles in the system renews the phase interface, causing short electrical pulses. The "Electrokinetic Theory", described above, can go some way to explain the varying impact cavitation has on reactions in different systems. Margulis[37] hypothesised that the presence of an electric charge distribution in close proximity to a gas/liquid interface affects the stability of the pulsating bubbles, leading to

deformation, collapse and sonoluminescence originating from the electrical discharges. This theory has, however, received considerable criticism as it does not account for the observed sonoluminescence within non-aqueous, non-polar liquids, reported in the literature[39].

Plasma Theory, proposed by Flannigan and Suslick[38], addresses the potential existence of hot opaque plasma cores within a collapsing cavitation bubble. After studying SBSL in low-volatility liquids such as sulphuric acid (H_2SO_4), Flannigan and Suslick discovered what was believed to be conclusive evidence of experimental plasma generation. They stated that the presence of peaks corresponding to molecules, atoms and ions of both the liquid and dissolved noble gases predicts core temperatures up to 20 000 K, ensuring dissociation of all molecules. Although there are three main theories regarding cavitation - hot spot, electrokinetic and plasma - there is no doubt that the origin of each of these sonochemical effects is acoustic cavitation[20].

1.1.2 Applications of Ultrasound

Since Thornycroft's observation[40] of the damaging effects of cavitating bubbles on rotor blades of high-speed submarines as a result of hydrodynamic cavitation, their use as a means to clean the surface of a material has been widely studied and refined. Ultrasonic cleaning baths are now commonplace in many laboratories, dental surgeries and jewellers[20]. Cavitating bubbles interacting in liquids or with a surface lead to asymmetric collapse, unidirectional jet formation and high fluid velocities[40]. Microjets, formed by asymmetric collapse, are the primary cause of bulk-mixing induced by ultrasound. On a surface where dirt and impurities are present, this action can scrub a surface, however too much inertial cavitation can lead to pitting or erosion (Figure 1.5). Naude and Ellis[16] were first to postulate that pitting on a solid surface exposed to ultrasound was a direct result of asymmetric jet formation during bubble collapse.

In a similar vein to ultrasonic cleaning of medical equipment and jewellery, ultrasound has also been employed in the remediation of water[41]. The death of bacteria has been attributed both to the shear forces generated as a result of acoustic waves propagating through the water and the localised heating and free radical formation as a result of cavitation[41].

However, due to the high acoustic energy required, the feasibility of industrial scale-up remains a challenge. Whilst continuous flow systems have been proposed as a means to overcome these issues, they are not without considerable drawbacks including reduced efficiency with respect to benchtop batch methods, probe degradation, or the need for multiple probes and subsequent costly cooling systems, each requiring high energy input[42]. As a result, widely used industrial applications of ultrasound are largely limited to emulsification and mixing processes, such as those used in food processing[43] and the synthesis of paints.

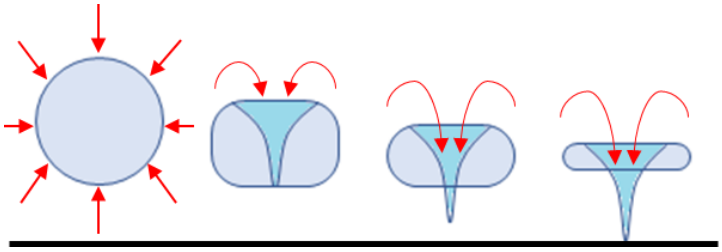

Figure 1.5 – Cavitation bubble collapse and jet formation at a surface.

Ultrasound is a valuable tool in the fields of medicine and biomedical imaging. In therapeutics, significant advances have been made in the use of ultrasound for transdermal drug treatments via sonophoresis, such as in the treatment of rheumatoid arthritis[44] and as a tool for physiotherapy[45]. More recently, ultrasound has been employed as a technique to improve body contouring by localised application of low frequency ultrasound, however, there are conflicting opinions regarding its ability to eliminate cellulite and its success is largely dependent on the acoustic intensity[46]. Malignant tumours of the liver, kidney and prostate have been successfully treated via high intensity focused ultrasound, however exposure limits and tissue cooling rates dictate the limits of treatment[47].

Biomedical imaging is a technique that employs high, non-destructive ultrasonic frequencies. Typically, ultrasound diagnostic imaging equipment operates in the range of 1-15 MHz. Higher frequencies (7-15 MHz) are used to analyse breast tissue, muscle, soft-tissue tumours, and other superficial structures including testes, whereas lower diagnostic frequencies in the range of 1-6 MHz are used to probe the abdomen, vascular system, and brain as well as fetuses and female reproductive organs in the fields of obstetrics and gynecology[48].

The emitted acoustic waves from the ultrasonic probe placed on the skin are scattered and reflected by tissue, blood and bone boundaries. Incoming reflected signals are then collected by the probe to build an image. The machine calculates the distance between a particular boundary and the probe, using the speed of sound in tissue and the time taken for the signal to be returned, to create a 2D image. Machinery has rapidly progressed from capturing course static images to high-resolution real-time digital imaging with significantly reduced signal-to-noise ratios[47]. Although image resolution is compromised at lower frequencies, greater penetration is achieved. The use of microbubble contrast agents has also greatly improved ultrasound image quality, they are largely used intravascularly and enhance the contrast between blood and tissue. Microbubble contrast agents are a form of proteinaceous microsphere and are discussed in more depth in Section 1.2.3.

The most significant application of ultrasound is its use in sonochemistry; the initiation and enhancement of chemical reactions, exploiting the effects of cavitation to yield products via novel reaction pathways. The extreme conditions generated by ultrasound in liquids facilitate the formation of products that cannot be achieved by conventional methods. An example is the formation of unusual iron cluster compounds of $Fe_3(CO)_{12}$ upon sonication of iron pentacarbonyl $Fe(CO)_5$, a product that cannot be generated by treatment with heat or light[40]. Suslick attributed the formation of this compound to the rapid heating and cooling behaviour of ultrasound-induced cavitation, enabling partial carbonyl dissociation and subsequent quenching to yield the unusual cluster.

As well as its use in homogeneous liquid-liquid and heterogeneous liquid-solid systems, ultrasound has also proved useful during the breakdown of alkanes into smaller fragments, known as cracking. It enables the process, usually conducted at temperatures exceeding 500 ^{o}C, to be carried out at room temperature.

Perhaps the most interesting application of sonochemistry, particularly within the scope of this project, is the use of ultrasound and its sonochemical effects as a means to synthesise microscopic proteinaceous capsules, or microspheres. The sonochemical synthesis of microspheres and their wide range of current and potential applications will now be discussed.

1.2 Microspheres – Synthesis, Optimisation and Applications

An important application of sonochemistry is the preparation of biomaterials, most notably the convenient one-pot synthesis of protein microspheres[2]. This project focuses on the use of sonochemical initiation to synthesise biocompatible synthetic polymeric alternatives, with a range of potential applications.

There is often confusion regarding the difference between microspheres, microbubbles, microcapsules and microparticles. Microspheres are micrometre-sized spheres and encompass air-filled microbubbles and non-aqueous and emulsion-filled microcapsules[10]. The characterisation of microparticles is more ambiguous, medical publications define microparticles as membrane vesicles released from different cells[49], whereas others refer to microparticles as an alternative name for microspheres. For the purpose of this project, microspheres refer to microcapsules filled with a liquid phase core, and microbubbles refer to air-filled microbubbles.

1.2.1 Sonochemical Synthesis of Microspheres

The sonochemical synthesis of microspheres is a facile protocol, facilitating the rapid production of microspheres over time scales usually no longer than five minutes[1,7,12,50,51]. The equipment is cost-effective and simple to operate, whilst the method is fast, versatile and environmentally friendly with respect to alternative mechanisms for microsphere synthesis[52], discussed in Section 1.2.2.

Stable microspheres can be easily synthesised by sonication of proteinaceous solutions with high intensity ultrasound[22]. The procedure incorporates the process of emulsification and encapsulation in a "one-pot" sonochemical synthesis (Figure 1.6). The proteinaceous or polymeric solution of the shell species and a non-aqueous encapsulant species are charged to a vial. An ultrasound horn assembly, placed at the oil:water or air:water interface, is used to generate acoustic energy, which disrupts the interface and disperses the non-aqueous phase within the aqueous medium. The solubilised protein then arranges itself around the immiscible droplets in shell self-assembly.

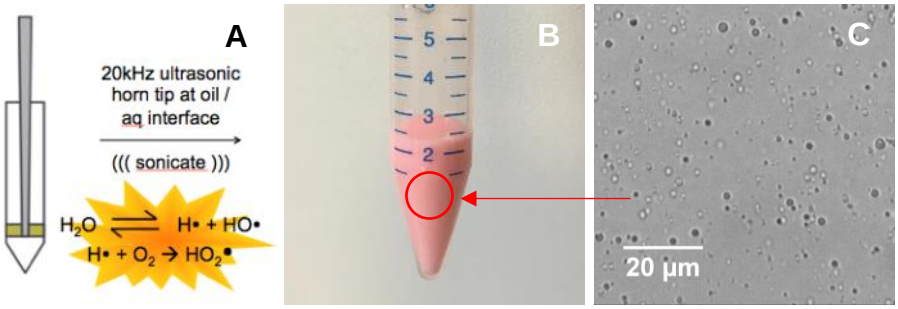

Figure 1.6 – 3 mm horn tip in 15 mL centrifuge tube containing polymer solubilised in buffer with oil layer deposit and horn tip at oil / aq interface (A). Dispersion of Nile Red-saturated tetradecane within thiolated poly(methacrylic acid) microspheres after sonochemical synthesis (B). Micrograph of tetradecane-filled $PMAA_{SH}$ microspheres (C).

Thiol-crosslinked Microspheres

Emulsification by agitation or stirring alone is not enough to form microspheres. During their initial research, Suslick and Grinstaff[1] stated that the successful formation of stable proteinaceous microspheres hinged upon ultrasonic emulsification and cavitation in an oxygen-rich environment to crosslink cysteine-containing proteins. This was demonstrated with the successful formation of thiol-crosslinked bovine serum albumin (BSA) and human serum albumin (HSA)[2] microspheres containing n-dodecane and other hydrophobic liquids, as well as air-filled microbubbles[53]. With the use of radical traps, Suslick and Grinstaff determined that the formation of both hydroxyl and superoxide radicals during cavitation was necessary to produce stable crosslinked protein-shelled microspheres and were able to propose a mechanism for microsphere formation. They deduced that the arrangement of thiol-containing protein aggregates at the interface between dispersed air or oil droplets upon emulsification undergo intermolecular disulphide crosslinking, facilitated by sonochemically-generated superoxide radicals.

Suslick and Grinstaff[1] also demonstrated the case of haemoglobin (Hb) and myoglobin (Mb). Cysteine-containing haemoglobin successfully formed stabilised toluene-filled microspheres, but myoglobin, an analogous protein to Hb but devoid of cysteine residues, was not able to form microspheres. This observation further supported their proposed

mechanism of radically-induced crosslinking in an oxygen-rich environment between thiol functionalities of cysteine-containing proteins.

Ashokkumar *et al.*[3,14] extended the scope to include hen egg-white lysozyme (Figure 1.7), a protein containing intramolecular disulphide linkages. With the use of a reducing agent such as DL-dithiothreitol (DTT), the protein, containing newly exposed sulphydryl groups, can then self-assemble and crosslink in the same way as BSA and HSA proteins during sonication.

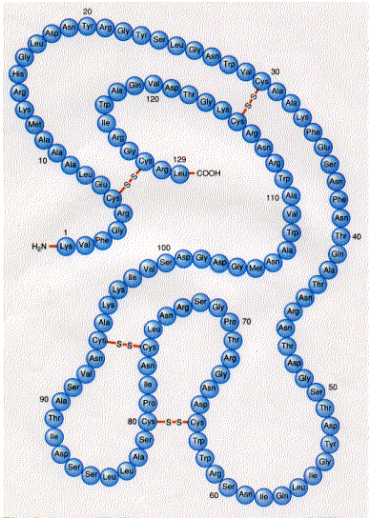

Figure 1.7 – Hen egg-white lysozyme, containing four intermolecular disulphide bridges[54].

As well as proteins, certain thiol-containing biocompatible polymers have also been engineered for use as microsphere shells. Cavalieri *et al.*[10] were first to achieve microsphere synthesis using a "thiol-containing synthetic macromolecule" with thiolated poly(methacrylic acid) ($PMAA_{SH}$). Commercially available PMAA sodium salt was functionalised with cysteamine hydrochloride via a carbodiimide crosslinking reaction to yield the thiolated form $PMAA_{SH}$ with varying degrees of functionalisation from 5-30 % (Scheme 1.2). Microspheres could not be formed in the absence of thiol functionalities, further highlighting the apparent importance of thiol groups for crosslinking and to induce amphiphilicity in the polymer, and reinforcing the mechanism for stable microsphere synthesis proposed by Suslick and Grinstaff[1].

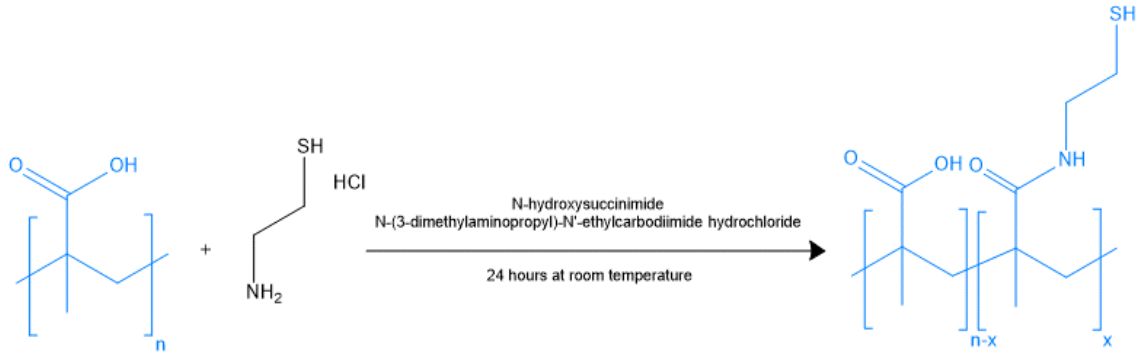

Scheme 1.2 - Carbodiimide cross-coupling functionalisation of Poly(methacrylic acid) (PMAA) with cysteamine hydrochloride to yield thiolate poly(methacrylic acid) ($PMAA_{SH}$) of varying degrees of functionalisation.

Increasing the degree of functionalisation reduces hydrophilicity of the polymer and this in turn impacts the morphology and size distribution of the microspheres and microbubbles[10]. At 10 % functionalisation, a smooth shell surface was observed via scanning electron microscopy (SEM), however when increasing the degree of functionalisation to 30%, the microsphere shell was thicker and the surface appeared rough with free non-crosslinked cysteine residues. This was attributed to the arrangement of polymer aggregates on the sphere surface depending on their degree of functionalisation. Microspheres of 10% functionalisation possess a compact arrangement of crosslinked chains over the sphere surface, and those with shells of 30% functionalised PMAA had increased shell thickness due to more extensive intermolecular cross-linking and a thicker layer of aggregated polymer chains[10].

It is interesting to note that, upon sonication, both perfluorohexane (PFH)-filled microspheres and air-filled microbubbles were formed, yet $PMAA_{SH}$ microbubbles were unable to form in the absence of PFH. It was proposed that PFH evaporation into the gas core stabilises microbubbles by "osmotic stabilisation" due to the reduced solubility of both liquid and gas-phase PFH in water[10,55].

It was reported that PFH-filled microspheres decrease in size with increasing degree of functionalisation from between 1.8 µm and 0.7 µm for 5-30%[10]. This was attributed to the rapid arrangement of $PMAA_{SH}$ around PFH droplets in a surfactant-like manner prior to ultrasound-induced crosslinking, thus preventing coalescence of PFH into larger droplets.

Increasing the degree of functionalisation increases crosslinking likelihood, facilitating rapid stabilisation of smaller droplets[10]. Contrary to the PFH microspheres, microbubbles were larger on average than microspheres, and were shown to increase their average diameter with increasing polymer functionalisation[10]. It was proposed that the increased hydrophobicity of polymers with a higher degree of functionalisation leads to slower diffusion through the aqueous media. Smaller bubbles are quickly overcome with osmotic pressure and rapid dissolution occurs, therefore slowly diffusing polymers are only able to assemble and stabilise larger air bubbles, less susceptible to the shrinking effect of osmotic pressure.

Work continues to incorporate stimuli-responsive blocks within $PMAA_{SH}$ polymeric shell material[6], and is the primary focus of this project. The use of synthetic alternatives to proteins as microsphere shells presents the potential to expand the field and tailor the shell properties and behaviour of microsphere systems. Synthetic polymers for use as microsphere shells are discussed further in Section 1.3.

Microspheres Stabilised by Alternative Interactions

The widely published requirement of cysteine residues for the successful formation of stable microspheres, proposed by Suslick and Grinstaff[2], has since been disproved in recent literature[5,11,12]. In 2002, Avivi and Gedanken[11] first reported the synthesis of streptavidin microspheres containing decanlin. Streptavidin is a protein devoid of thiol residues, yet the microspheres were found to be stable for hours at room temperature and up to one month at 4 ºC. Unlike the successful formation of microspheres employing analogous sulphur-containing avidin as the shell material, whereby Avivi and Gedanken[50] cited free-thiol crosslinking as the mechanism for formation and stability, in the case of streptavidin an alternative mechanism was proposed. Microsphere synthesis could only be achieved in an acidic medium below pH 6, and it was postulated that self-assembly of the protein around the dispersion of oil droplets was driven by the hydrophobic effect, with molecules adopting a more condensed structure at the interface to reduce the interactions between hydrophobic residues and water molecules in the bulk.

The ionised carboxyl groups ($-COO^-$) in a neutral solvent become protonated at an acidic pH, driving the polymer towards hydrophobicity. The preparation of synthetic

poly(glutamic acid) microspheres by Avivi and Gedanken[11], a polymer with carboxyl groups present in each repeat unit of the polymer chain, supports this mechanism of hydrophobic-driven arrangement and stability (Scheme 1.3). Below pH 4.5, stable decanlin-filled microspheres could be formed by a one-pot sonochemical mechanism and stored for up to one month.

Although Dibbern *et al.*[12] have since demonstrated the synthesis of non-thiol crosslinked core-shell microspheres of sodium poly(L-glutamate), they largely disregard Avivi and Gedanken's mechanistic theory[11], claiming core shell microsphere synthesis was "unlikely" due to the hydrophobicity of poly(L-glutamic acid) at low pH. It was inferred that the microspheres generated by Gedanken *et al*. may instead be comprised of a solid matrix structure. Dibbern and coworkers[12] instead attributed the successful synthesis and stability of sodium poly(L-glutamate) core-shell microspheres to multiple intermolecular forces including van der Waals, hydrogen bonding and hydrophobic and ionic interactions. Microspheres remained stable between pH 4.5 and pH 12, and at temperatures up to 60 °C. Dibbern also reported no changes in the MALDI mass spectrum between a sonicated and non-sonicated sample of polymer, a further indication of no covalent crosslinking. Unlike BSA microspheres[2], poly(L-glutamate) microspheres were unaffected by radical scavengers, and were also successfully synthesised in the absence of oxygen[12].

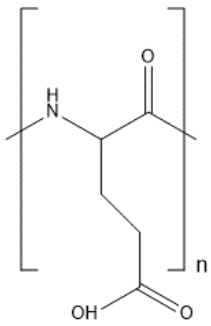

Scheme 1.3 – Poly(L-glutamic acid).

Chitosan microspheres hold great potential as drug delivery vehicles due to the biocompatible nature of the shell material. Chitosan is a non-toxic, naturally-occurring, biodegradable polymer with mucoadhesive properties[5], therefore it exhibits non-specific binding affinity to mucosal membranes. Microsphere synthesis of chitosan-shell

microspheres via sonochemical techniques was first published by Skirtenko *et al.*[5]. Chitosan contains no thiol groups, however the microspheres demonstrated stability within a wide pH range from pH 4-9 at room temperature. Skirtenko[5] attributed this to the formation of imine crosslinks between the deacetylated chitosan chains during sonication. Microsphere stability was also tested at physiological temperature (37 °C) at pH 4.5, 7 and 9. After 7 days, microspheres at pH 9 displayed good stability, yet at neutral pH 7 and acidic pH 4.5 a loss of yield could be observed. Imine bonds display low stability at acidic pH, which would account for the reduced stability of the microspheres at pH 4.5 and 7. Ashokkumar *et al.*[56] have recently prepared crosslinked thiol-functionalised chitosan microspheres encapsulating tetradecane. The functionalised microspheres displayed very similar size distributions to unfunctionalised chitosan spheres prepared using the same sonochemical technique, however, it is possible to tailor the shell thickness of the cross-linked spheres by increasing the degree of thiolation. The mechanical strength of the crosslinked shell, as tested by atomic force microscopy, was found to be almost twice that of the non-crosslinked shell and from this it was inferred that the crosslinked chitosan microspheres would withstand various processing conditions[56]. Although stability with time was not directly measured, assumptions were made regarding the relationship between degree of crosslinking and microsphere stability based upon previous work conducted by Ashokkumar[10].

Shimanovich *et al*. have also demonstrated the sonochemical synthesis of oil-filled DNA[4] and RNA[57] nanospheres. In the case of DNA, the proposed mechanism of stabilisation was attributed to both electrostatic interactions and sonochemically-induced bonding between DNA base pairs. Shimanovich compared the resilience of double-stranded DNA and single-stranded DNA microspheres upon exposure to homogenisation, mechanical pumping and a phenol-chloroform solvent[4]. The double-stranded DNA microspheres remained undisrupted, indicative of covalent bond stability whereas the single-stranded DNA microspheres were destroyed. This was also true in the case of RNA microspheres[57], suggesting that single-stranded DNA and RNA is unable to form the additional stabilising covalent crosslinkers.

Microsphere Morphology

A number of mechanistic variables can determine the morphology of microspheres within a sample, namely acoustic intensity, sonication time and ultrasound frequency, in addition to the encapsulant and shell species.

Han *et al.*[58] published the effect of sonication time and power on the size of silicone oil-filled HSA microspheres generated via one-pot sonochemical synthesis. The mean microsphere size was shown to decrease with sonication time and increasing acoustic power until an equilibrium plateau was achieved. In addition to the variables outlined above, changing the sample volume and reaction vessel can modify the propagation of a wave and impact microsphere size, therefore the trends reported by Han *et al.*[58] are of more significance than the absolute values published. In the same publication, Han observed that inhomogeneous power distribution in a particular vessel increases microsphere size distribution (Figure 1.8). Samples collected immediately below the horn tip (A) and in regions of close proximity to the tip (B) showed smaller microspheres with a narrower polydispersity than those collected from either side of the penetrating horn tip (C). As such, it was proposed that minimising the vessel diameter either side of the horn and inducing circulation would optimise the homogeneity of radical distribution.

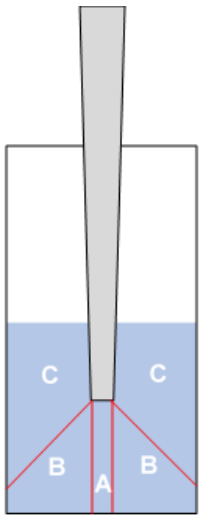

Figure 1.8 – Regions within the reaction vessel in which variations in microsphere size were observed by Han *et al.*[58] A and B = comparable morphologies C = larger, more polydisperse microspheres observed. Image generated from reference model.

Cui *et al*.[52] also cited poor power distribution during sonication as the primary cause of increased size distribution over other synthetic techniques (Section 1.2.2). To fulfil their desired applications as contrast agents or drug delivery vehicles, microspheres must have a smaller diameter than that of blood capillaries (5-10 μm). Cui *et al*.[52] recently compared vegetable oil-filled BSA microspheres prepared by continuous and pulsed sonication mechanisms, reporting size ranges of 0.5-10 μm for continuously sonicated microspheres, and largely monodisperse spheres of less than 2 μm for microspheres synthesised via pulsed ultrasound. It was proposed that the reduction in size and size distribution was caused by an increase in random diffusion within the sample as a result of the intermittent sound wave propagation through the medium. Unlike continuous sonication, which according to Cui experiences "circumfluent" droplet motion in the medium, pulsed ultrasound disrupts this motion, enabling larger vegetable oil droplets to diffuse within close proximity to the horn tip and be further dispersed into smaller droplets. It goes some way to corroborate the data published by Han *et al*.[58] regarding inhomogeneous intensity distribution by improving mixing efficiency during sonication. The pulse-generated microspheres possessed good stability and high dye loading capacity with no leakage over an incubation period of 3 months, demonstrating their potential as drug carriers[52].

Contrary to the size trends with varying sonication time and power published by Han *et al.*[58], Zhou *et al*.[59] reported an increase in microsphere size and size distribution with sonication power and time when preparing air-filled lysozyme microbubbles. Zhou initially proposed that increased cavitation bubble collapse intensity, shear forces and radical production generated at higher sonication power is responsible for more efficient crosslinking of lysozyme around smaller dispersed air bubbles before they succumb to osmotic pressure, however this proposed mechanism instead supports the data published by Han *et al*.[58]. Subsequently, Zhou[59] postulated that, at higher intensities, cavitation bubbles are susceptible to coalescence, and the subsequent reduction in collapse intensity leads to reduce crosslinking efficiency. As a result, larger more stable air bubbles are encapsulated by crosslinked lysozyme whilst smaller bubbles undergo dissolution. This leads to a larger size distribution and a bimodal plot of microsphere sizes, with smaller microspheres generated and encapsulated as expected, and larger microspheres generated as a result of localised cavitation bubble coalescence.

Unsurprisingly, the acoustic frequency of an ultrasonic wave can also impact microsphere morphology and yield. In 2001, Makino *et al*.[60] prepared toluene-filled BSA microspheres at 28 kHz, 45 kHz and 100 kHz at an acoustic intensity of approximately 100 Wcm^{-2}. The highest yield of microspheres was obtained at 28 kHz and was attributed to the increased ultrasonic power and subsequent radical generation relative to 45 kHz, whereby a decrease in yield was observed, and 100 kHz, where no microspheres were generated. The rapid compression and rarefaction of molecules in the path of a propagating wave increases with increasing frequency, reducing the likelihood of overcoming the intermolecular interactions within the fluid and subsequent cavitation[29].

Makino[60] also compared the effect of varying the encapsulant material on microsphere size. Toluene was found to produce smaller microspheres than analogous chloroform-filled BSA microspheres with a narrower size distribution under the same reaction conditions. Toluene is less miscible in water than chloroform, creating a more defined interface with the aqueous phase prior to sonication, and subsequently generating smaller spheres. Soybean oil and peanut oil were also trialled, and the mean size and distribution of these encapsulated BSA microspheres were smaller still. This was attributed to the viscosity of the naturally-occurring oils. Contrary to this, Zhou *et al*.[14] reported an increase in microsphere size and size distribution of viscous sunflower oil-filled lysozyme microspheres relative to tetradecane, dodecane and perfluorohexane. Zhou proposed that additives and impurities present in the naturally occurring oil may compromise the stability of the microemulsion formed during sonication.

The ultimate goal when designing a sonochemical microsphere system is to achieve control over the size and size distribution of a sample. Although modifying the parameters discussed can go some way to refining the mechanism, sonochemical synthesis is inherently non-uniform. Recently, Zhou *et al*.[61] have devised a novel mechanism combining sonochemical and continuous flow-through techniques to synthesise near monodisperse lysozyme microbubbles. A 20 kHz ultrasound horn was designed with a central channel, through which the protein solution is passed and dropped from height into a bulk protein solution, a pump then circulates solution from the bulk back through the horn channel in a continuous flow setup. Sonochemiluminescence images[61] reveal cavitation occurring within the channel at the tip of the horn, as opposed to conventional horn tips which emit from the end of the tip. It was postulated that microbubble synthesis occurs as the protein

solution meets the air interface at the base of the tip. By controlling the exposure of the solution to the cavitating region of the horn and using a flow technique to achieve more uniform exposure of the entire solution, it was possible to achieve an almost monodisperse distribution of microbubbles. The work of Zhou *et al*. certainly demonstrates the potential for simple scale-up of an otherwise restrictive synthetic protocol.

1.2.2 Other Synthetic Protocols for Microsphere Formation

In addition to sonochemical microsphere synthesis, there are a number of other mechanisms commonly used to generate proteinaceous and polymeric microspheres. These include microfluidic techniques, layer-by-layer deposition and emulsification by homogenisation, solvent evaporation and spray drying.

Homogenisation Techniques

It has been previously mentioned in this chapter that manual agitation alone is insufficient mixing to form stable microspheres, high speed homogenisation is an exception to this rule. The high shear forces created by rotor mixing disperse the encapsulant through the bulk medium in tiny droplets[62]. The shell material, such as an amphiphilic polymer, assembles at the A/W or O/W interface, driven by the hydrophobic effect, and will stabilise the droplet in a similar fashion to the self-assembly of streptavidin around sonochemically emulsified droplets[11]. If the shear forces created during homogenisation are sufficient to induce cavitation, a suitably functionalised polymer at the surface may be further stabilised by radical-induced crosslinking.

High-speed homogenisation techniques often go hand in hand with interfacial polymerisation (Figure 1.9). Sun and Deng[63] reported the formation of hollow cross-linked temperature-responsive $PNIPAA_M$-shelled microspheres by homogenisation-facilitated interfacial polymerisation. Firstly, $NIPAA_M$ monomer is solubilised in an aqueous phase, then dispersed in toluene, containing Span 80® non-ionic surfactant (sorbitane monooleate), by homogenisation to yield a W/O emulsion. Redox polymerisation of $PNIPAA_M$ is initiated at the droplet interface by tetraethylenepentamine (TEPA) interfacial

initiator in the aqueous droplets and benzoyl peroxide (BPO) oxidant in the oil phase. Polymerisation must be conducted above the "lower critical solution temperature" of $PNIPAA_M$ (Section 1.3.5) to ensure that the growing polymer chain is neither soluble in the aqueous or oil phase and remains at the interface. The crosslinking agent divinylbenzene (DVB) in the oil phase stabilises the $PNIPAA_M$ shell to generate hollow cross-linked $PNIPAA_M$ microspheres between 1-3 µm with reversible temperature-responsive swelling behaviour.

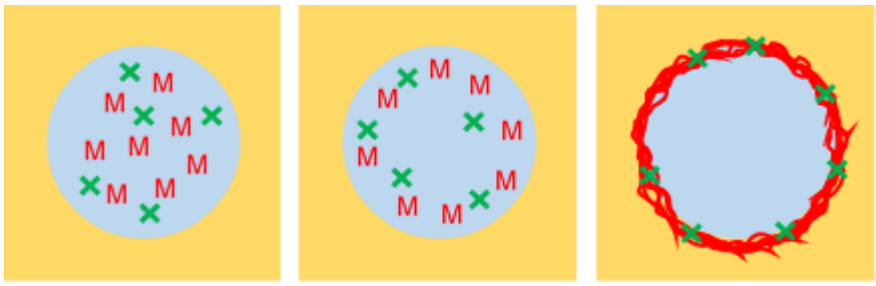

Figure 1.9 – High speed homogenisation with interfacial polymerisation (not to scale). Monomer (red M) and crosslinking agent (green X) in the dispersed aqueous droplet diffuses to the interface and undergo redox-initiated polymerisation to form stable crosslinked-shell microspheres.

Often the shell material is first solubilised in a volatile organic solvent (VOS) and, as emulsification is induced, the VOS partitions into the bulk solution and evaporates, depositing the polymer onto the dispersed oil droplet, so called the solvent evaporation method. O'Donnell and McGinity[64] describe a simple setup, whereby a polymer such as poly(lactic acid) (PLA) is solubilised in a VOS, to which the core material is added and the mixture is charged to a bulk aqueous solution containing emulsifying agents. The emulsion is homogenised until the volatile solvent moves into the bulk aqueous phase and evaporates, leaving a polymer-shelled microsphere which can be collected, washed and dried. The technique is often used in the field of pharmaceuticals. Recently, Sharma *et al*.[65] reported the design of paclitaxel-loaded PLA and PLGA nanospheres via the solvent evaporation mechanism, modifying variables such as aqueous/organic phase ratio and polymer or drug concentration to tailor the nanocapsule morphology and optimise drug loading and release parameters. The technique is straightforward, however it is not without significant risk[64].

The retention of residual VOS impurities, such as chloroform and methylene chloride, within the microspheres poses a concern due to the toxicological threat they pose.

A commonly used homogenisation technique is spray drying. The polymer is solubilised in a VOS, into which a solid encapsulant, ie. a lyophilised drug, is dispersed via homogenisation. Atomisation of the mixture containing the polymer shell species, lyophilised encapsulant and solvent in a stream of heated air causes solvent evaporation and deposition of the polymer shell onto the solid encapsulant. Sizes range from 1-100 µm and are dependent on the conditions during atomisation. Spray drying[66] is a reproducible technique that allows for control over microsphere size and morphology for accurately determined drug loading. However, the extreme conditions generated during synthesis can induce aggregation and denaturation of sensitive species.

Maintaining the activity of the encapsulant throughout the synthetic protocol is a major concern and, although similar, the solvent evaporation technique does not require the harsh conditions imposed by lyophilisation and atomisation, enabling liquid phase encapsulants to be employed[66].

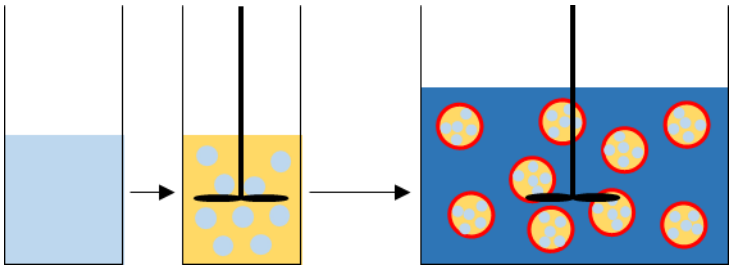

Figure 1.10 – The double emulsion method (not to scale) showing a protein/drug aqueous phase (pale blue) first dispersed in an oil phase (yellow) by homogenisation (black rotor) to yield a W/O emulsion, followed by rapid dispersion in a second aqueous bulk phase (large container, dark blue) containing a PVA stabilising agent (red) to yield a W/O/W emulsion.

Advances have recently been made in the field of sonochemistry to enable the encapsulation of hydrophilic material within microcapsules in W/O emulsions to create stabilised W/O/W double emulsions[7]. However, the double emulsion technique is not a new concept (Figure 1.10). A protein or drug in an aqueous solvent is first dispersed in a bulk oil phase via

homogenisation, and this primary W/O emulsion is then rapidly transferred to a second bulk aqueous phase containing a stabilising agent such as poly(vinyl alcohol) (PVA)[66]. Homogenisation yields a stable W/O/W emulsion of W/O-filled PVA microspheres. Depending on the choice of oil-phase encapsulant and the stability of the system, the oil phase is sometimes then removed via solvent evaporation as with previous techniques to yield a polymeric microsphere containing a hydrophilic polymer or drug.

Layer-by-Layer Deposition

Layer-by-layer (L-b-L) self-assembly is a powerful tool for the synthesis of proteinaceous and polymeric microspheres with precise control over monodispersity and shell thickness. Alternately charged polyelectrolytes are deposited onto a framework by electrostatic interactions (Figure 1.11). The framework can be a sacrificial species[67], or the L-b-L deposition can be used to improve the stability or release kinetics of an existing microsphere system[68]. Shell thickness can be accurately engineered by varying the number of layers deposited, and size control is dependent on the synthetic protocol used to create the framework. Decher *et al*.[69] first reported the deposition of alternating polyelectrolyte layers onto flat silica substrates, before extending the scope to include 3D scaffolds including silica microbeads.

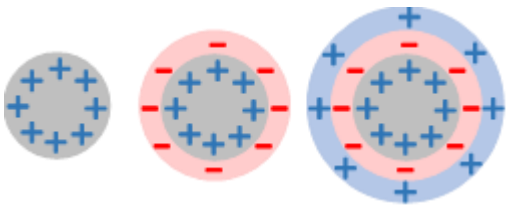

Figure 1.11 – A schematic diagram of alternating layer by layer polyelectrolyte deposition on a silica microbead (grey). The bead is charged and a polyelectrolyte of opposing charge (red ring) is deposited onto the surface of the silica microbead. Layers of alternating charge can be built to achieve desired shell thickness.

As an alternative to the deposition of alternating polyelectrolytes, interactions including hydrogen bonding and disulphide[70] crosslinking have been explored. Kozlovskaya *et al*.[67] deposited alternating hydrogen-bonded poly(N-vinylpyrrolidone) (PVPON) and PMAA

multilayers onto commercially available monodisperse silica nanoparticles (4 μm ± 0.2 μm). Once deposited onto the framework, the PMAA layers are cross-linked by carbodiimide cross-coupling with an ethylenediamine crosslinker and the silica framework is dissolved with dilute hydrogen fluoride solution, yielding a hollow microsphere. Dialysis in pH 8 buffer removes the PVPON layers, leaving hollow cross-linked PMAA microspheres that can be labelled or functionalised as desired. Kozlovskaya[67] also demonstrated a mechanism for labelling of the microspheres by depositing fluoresceinyl-ethylenediamine-labelled PMAA alternately with PVPON in the final three layers of the shell.

Zelikin *et al*.[70] published a similar synthetic protocol for the L-b-L deposition of alternating hydrogen-bonded PVPON and fluorescein isothiocyanate (FITC)-labelled thiolated poly(methacrylic acid) ($PMAA_{SH}$) onto silica microparticles. Hydrogen peroxide was used to cross-link and stabilise the shell, and the silica core was again remove by hydrogen fluoride solution. Zelikin[70] compared the stability of crosslinked PVPON/$PMAA_{SH}$ microspheres and a control sample of non-cross-linked PVPON/PMAA, stabilised solely by hydrogen bonding, by incubation at pH8. Unlike the control sample, the cross-linked capsules retained their stability and were then destroyed with reducing agent DL-dithiothreitol (DTT). To demonstrate drug-loading capabilities[70], unlabelled cross-linked spheres were loaded with labelled protein FITC-transferrin, a glyco-protein found in human blood plasma. Microspheres were stable until exposure to DTT, at which point the multilayers collapsed, releasing the labelled contents.

Although layer-by-layer deposition provides excellent control over shell thickness, and microsphere size if using a commercially available framework, the process is time consuming and labourious. Zelikin and coworkers[70] conducted the deposition of up to five bilayers, with a single layer deposition time of 15 minutes, followed by centrifugation and washing, whilst Kozlovskaya *et al*.[67] deposited up to 40 bilayers onto their silica frameworks, with a total deposition time of 20 hours.

Inkjet Printing and Coaxial Electrohydrodynamic Atomisation (CEHDA)

Inkjet printing is another technique that allows for excellent control over microsphere size. The fluid shell and encapsulant material is drawn into the nozzle from a chamber containing

a piezoelectric crystal[71]. The voltage across the crystal is flipped at a particular frequency, much like the generation of an acoustic wave in sonochemical systems, creating pressure pulses which push the droplet from the tip of the nozzle. This action draws more liquid into the nozzle creating a continuous droplet generation. Droplet size can be controlled by modification of the pulse frequency, allowing for excellent control over size.

The technique has been used by Radulescu *et al.*[72] to prepare anti-tumour drug paclitaxel-loaded poly(lactic-co-glycolic acid) (PLGA) microspheres. The polymer and drug were first solubilised in a VOS, 1,2-dichloroethane, and the resulting mixture was "jetted" into a PVA stabilising solution using pressure-assisted "drop-on-demand" inkjet printing. Evaporation of the VOS facilitated PLGA shell formation around the paclitaxel droplet. The PVA was subsequently removed by washing to yield the paclitaxel-loaded PLGA microspheres. Paclitaxel remained unchanged throughout the synthesis and extraction, and the activity of the extracted drug equaled that of native paclitaxel, demonstrating the viability of the technique for the design of drug delivery vehicles. The microspheres produced were monodisperse, but at 60 μm they were significantly larger than microspheres generated by alternative techniques.

Coaxial Electrohydrodynamic Atomisation (CEDHA) is an interesting technique in which a coaxial jet of two immiscible fluids, or an encapsulant gas phase, are focused into a jet by an applied electric field to form monodisperse core-shell droplets[71]. The two phases are supplied from precision syringe pumps through the coaxially-arranged needles. The encapsulant material, a liquid or gas, passes through the inner needle, whilst the shell material is pumped through the outer needle. The microsphere morphology is controlled by the encapsulant/airflow rate and the flow rate of the shell material. The technique has been used to synthesise phospholipid-coated microbubbles[73], polymer coated microbubbles[74] and liquid-filled microspheres[75].

CEDHA, as with inkjet printing, enables control over droplet size by modifying mechanical settings such as applied frequency, without the need to physically modify the equipment. CEDHA is a facile technique for the synthesis of microbubbles that are stable for a few hours without the need for further processing. Increasing the number of coaxial needles in a system also facilitates the synthesis of multi-layer microbubbles and the potential for multi-layer microspheres[76].

Microfluidics

Microfluidic reactors provide a continuous flow method for microsphere synthesis, generating particles with highly controlled morphologies[71]. The technique can be used to synthesise both hydrophilic- and hydrophobic-encapsulated double emulsion microspheres. Sphere morphology is governed by a number of factors, including the viscosity of the monomer, modification of flow rates, nozzle diameters and the choice of microfluidic medium. These microspheres can be easily tailored for a particular application, depending on their size and morphology.

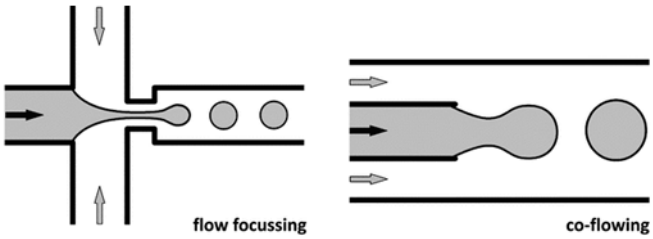

Figure 1.12 – Microfluidic techniques, flow-focusing (left) and co-flowing (right)[77]. Image adapted from reference.

Flow focusing and co-flowing microfluidic systems are two examples of microfluidic reactors (Figure 1.12). An interface is created between two immiscible fluids, and as the encapsulant fluid flows into the bulk phase it segregates into defined droplets that are encapsulated by the shell species in the bulk, much like in CEDHA. Air-filled microbubbles have also been prepared using microfluidic techniques[71], a stream of air enters liquid flow and is focused into a jet. As the gas moves a certain distance from the orifice of the gas stream into the liquid, the interface destabilises and "pinch off" process generates a microbubble within the liquid. Flow-focusing has been employed to generate phospholipid shell microbubbles of 5 μm diameter with a shelf life of ten minutes, as well as nitrogen-filled microbubbles of 1.5 μm diameter with a nine hour shelf life[71,78]. Both demonstrate the potential of microfluidic microbubbles for use as contrast imaging agents, however, in order to achieve small bubbles, very fine channel diameters (approximately 7 μm) are required. The susceptibility of these channels to blockages necessitates costly clean room conditions.

Table 1.1 – A comparison of the main advantages and disadvantages of the techniques for microsphere synthesis.

Technique	Advantages	Disadvantages
Ultrasound	Quick and facile one-pot synthesis Small microsphere sizes with potential for *in vivo* applications (must be ≤ 7 μm) Compatible with many encapsulants Radically-induced covalent crosslinking of shell (confirmed in thiol-containing proteins and polymers) Long term stability and shelf life (many systems stable for months)	Difficult to scale-up technique beyond benchtop Microspheres are not monodisperse Harsh reaction conditions (high shear forces, temperatures and pressure and presence of radicals)
Homogenisation	Radically-induced covalent crosslinking possible if conditions produce radicals Compatible with many shell species and encapsulants Potential for one-pot technique when combined with interfacial polymerisation Good control over size (spray drying) Encapsulation of solid and hydrophilic species possible	High shear forces on mixing or atomisation (spray drying) Use of VOSs Crosslinker usually required to stabilise shells
L-b-L Deposition	Excellent control over size and shell thickness Can have stable crosslinked shell	Time consuming and labour intensive (expensive) Often requires removal of silica framework
Inkjet Printing and CEDHA	Control over size by modification of airflow/encapsulant flow in microbubble/microsphere synthesis Multilayer microspheres possible (CEDHA)	Use of VOSs Hard to achieve small microspheres No covalent shell stabilisation
Microfluidics	Good control over size Small sizes generated (≤ 5 μm)	Short shelf life (hours) No covalent shell stabilisation Very fine channel diameters lead to blockages, requiring expensive clean room conditions

A summary of the advantages and disadvantages of each synthetic technique is shown in Table 1.1. Whilst many of the techniques facilitate the encapsulation of a range of encapsulants within various proteinaceous and polymeric shell species, many require harsh reaction conditions or the use of additional solvents or crosslinkers and lack the stability of those synthesised by the facile one-pot sonochemical method and stabilised by radically-induced crosslinking. Although this technique provides less control over microsphere size, the use of sonochemically-generated microspheres for in vitro applications has been widely researched and successfully demonstrated[13,79–81], highlighting the versatility of the method.

1.2.3 Applications of Sonochemically-produced Microspheres

Microencapsulation[82] is a process whereby materials are trapped within microscopic capsules, namely microspheres. It is a convenient means of converting a liquid to a solid, providing environmental protection to a volatile or delicate encapsulant and controlling the release and administration of the encapsulant. When discussing sonochemically-generated microspheres, the primary core material is always a gas or non-aqueous liquid. Dispersed solids, such as magnetic particles, and aqueous phases within hydrophobic liquid mediums may also be encapsulated[83].

Microspheres as storage and delivery vehicles are widely applicable to a range of potential applications as they can be easily engineered and tailored to optimise their effectiveness. When designing a microsphere system, there are several criteria that must be met[82]. Firstly, the encapsulation efficiency of the synthetic protocol must be high, producing a high yield of microspheres and ensuring optimum incorporation of core species within each microsphere to minimise waste. It is the job of the shell to provide the desired properties of strength, flexibility and impermeability. If the core species is active, the encapsulation method must maintain the biological activity of the encapsulant, as should storage of the microspheres and the chosen release method[66]. During sonochemical preparation, the encapsulant is exposed to the extreme conditions induced by ultrasound, including shear forces, temperature, and radicals produced as a result of cavitation[84]. The process of encapsulation should protect the encapsulant to prevent damage to, or degradation of, the potentially volatile core species. The microspheres should be stable with a known shelf life and non-toxic degradation products, particularly in the case of those with *in vivo* applications. Microsphere size must also be strictly controlled for *in vivo* applications to

ensure that all microspheres meet the size requirements for intravenous injection and free-flowing passage around the blood capillaries (5-10 µm)[52]. When encapsulating a species such as a drug, supplement or flavour, factors such as monodispersity, batch uniformity and optimum loading are of particular importance as the amount of encapsulated drug can correspond to an administered dose when delivered *in vivo*.

Control over release profiles is also of paramount importance in drug delivery as slow release microsphere drug delivery systems have the potential to replace daily-administered systemic therapeutic agents[16] (Figure 1.13). The microsphere release mechanism could be gradual, a controlled zeroth order release to maintain constant drug concentration within the therapeutic range over an extended period of time, or triggered release in response to the needs of the patient. Any deviations from the expected release profile could result in insufficient administration or overdose, therefore an understanding of the precise release profile of a particular system is essential.

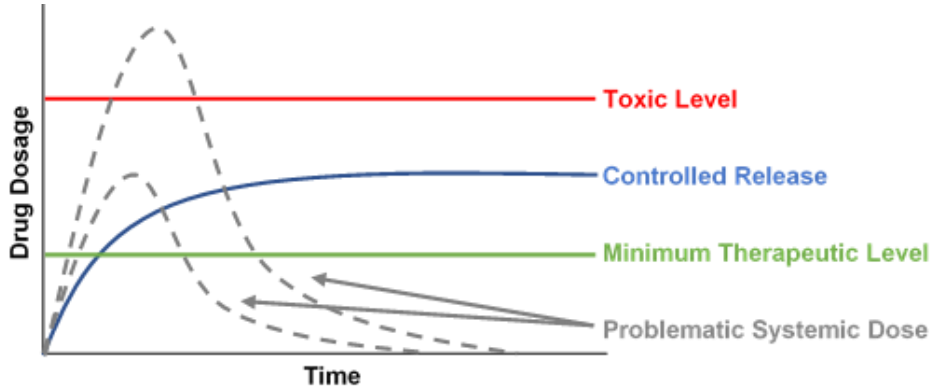

Figure 1.13 – A schematic graph showing the benefit of an ideal system with desirable controlled release of a drug over time, compared to systemic administration[85]. Image generated from reference model.

Factors affecting encapsulant release include the chosen synthetic protocol, the choice of shell material and additional surface functionalities, the choice of encapsulant, microsphere size, and the surrounding environment[86]. The sonochemical preparation of crosslinked proteinaceous microspheres exhibit stability over many months[3,6,10,59]. Release of encapsulants from these microspheres have been successfully triggered by mechanical disruption with high intensity ultrasound[7,14] and chemical disruption of the crosslinked shell

with a reducing agent such as DL-dithiothreitol (DTT)[7]. Ultrasound-induced release holds great potential as a mechanism for releasing the core species from magnetic or surface-functionalised targeted microspheres for localised drug administration or gene delivery[87].

Triggered release by an external stimulus is the most commonly reported method of encapsulant release. In addition to mechanical release by applied ultrasound or release in response to a reductive environment, proteins and polymers can be pH responsive[5], enabling triggered release in certain pH environments within the body and demonstrating some potential for *in vivo* applications.

Temperature-responsive microspheres also demonstrate excellent potential as drug delivery vehicles[6], nutrient carriers in functional foods[43], and agrochemical containers. The stimuli-responsive component is usually in the form of a temperature-responsive polymer incorporated into the shell such as poly(N-isopropylacrylamide) ($PNIPAA_M$), which undergoes a reversible phase transition at its LCST of 31-32 °C[88]. When incorporated in a microsphere shell, this phase transition can cause microsphere collapse and initiate release at a desired location as a result of increasing temperature. Temperature-responsive microspheres synthesised via alternative techniques have been explored[89,90], utilising the responsive behaviour of $PNIPAA_M$, however a sonochemically-generated stimuli-responsive microsphere system containing $PNIPAA_M$ has only recently been investigated[6]. The temperature responsive behaviour of $PNIPAA_M$ is discussed more in Section 1.3.5.

The versatility of microspheres as delivery vehicles is evident when considering the range of species that can be encapsulated. Sonochemically-generated microspheres have a wide range of current and potential applications, exploiting features such as biocompatibility, high mobility, stability, ease of synthetic protocol and flexibility regarding encapsulant, shell species and surface functionality.

Drug Delivery Vehicles and Targeted Therapeutics

One of the most promising applications for sonochemically-produced microspheres is their use as delivery vehicles. There have been many reports in the literature in recent years describing the successful synthesis and administration of drug-filled proteinaceous and polymeric micospheres[9,13,80,91–93], as well as the use of dyes as a model for drug

delivery[7,9,94]. In drug delivery, the increasing complexity and instability of new and innovative therapeutics poses a challenge when determining effective administration. Some drugs are difficult to administer due to certain properties such as high potency or poor solubility. Hydrophobic drugs, for example, will readily precipitate in aqueous media, whereas others may undergo breakdown *in vivo* or be rapidly cleared by the kidneys, requiring high doses or continuous administration. Microsphere drug delivery vehicles have many advantages over traditional methods of administration, including their compatibility with a range of encapsulants, the protection they offer to volatile therapeutics, the ease of administration and their targeting and controlled release potential.

The successful encapsulation of anti-tumour drug Taxol (paclitaxel) within sonochemically-produced BSA microspheres has been reported[91], with a maximum loading capacity of 90 %. Taxol is a hydrophobic drug and is traditionally administered as an emulsion in a parenteral fluid. The need for environmental protection due to its hydrophobicity and toxicity makes it the perfect candidate for encapsulation within microspheres. The drug maintained its biological activity throughout encapsulation, successfully killing mouse multiple myeloma cells upon incubation *in vitro* for 24 hours. The effect of Taxol-loaded microspheres equaled the effectiveness of freshly-prepared Taxol (22-24 % effectiveness at 1.3×10^{-6} M), however it was observed that the drug solvent mesytilene also contributed to cell death. Grinberg *et al*.[91] measured a correlation of increasing cell death with increasing Taxol concentration, confirming the biological activity and effectiveness of the encapsulated Taxol beyond the killing effect of the solvent. Future work includes optimisation with the use of a biocompatible organic solvent to tailor the system for *in vivo* applications.

Avivi and coworkers[13] also employed BSA as a shell material to demonstrate the biological activity of tetracycline (TTCL) upon sonochemical microsphere synthesis, with a maximum loading capacity of 65%. TTCL is a widely used antibiotic, and is relatively stable with respect to varying forms of administration. Avivi[13] attributed the successful encapsulation of a hydrophilic drug within the microspheres to sonochemically-induced partial solubilisation of TTCL in the mesitylene solvent. This was confirmed by the presence of TTCL in mesitylene upon sonication in the absence of BSA shell material. The drug maintained its biological activity during synthesis, with the antimicrobial activity of TTCL microspheres almost equalling that of released TTCL and free TTCL upon treatment of

TTCL-sensitive bacteria strains. This indicates that not only is the biological activity of TTCL unaffected by sonochemical encapsulation, but also that triggered release is not always required to successfully administer the drug[51].

Encapsulation of the hydrophilic anti-cancer drug Gemcitabine within BSA microspheres is achieved by a similar phenomenon to that of TTCL[80]. Sonication improves the solubility of Gemcitabine within dodecane, enabling encapsulation of a hydrophilic material within a hydrophobic core. Grinberg *et al*. reported a loading efficiency of 30 %. Interestingly, no release from the microspheres was observed when stored at 36-37 °C over the course of few days, however upon exposure of the microspheres to renal carcinoma cells (RCC) *in vivo*, significant cell death was observed. Grinberg indicated that this release could be attributed to the possible degradation effect of proteases present in the cell environment.

Grinberg and Gedanken[92] have also generated insulin-loaded starch microspheres containing dodecane. Unlike the TTCL-loaded mechanism of partial solubilisation in the mesitylene core[13], Grinberg[92] defined the structure as a dodecane core surrounded first by insulin, with a starch outer shell stabilised by sonochemically-generated glycosidic crosslinks. It was also proposed that amylase present in the body could readily breakdown the starch outer shell, revealing the insulin core which would subsequently be dissociated by other proteases. The system demonstrates an efficient delivery mechanism for peptide proteins, with a short, facile synthesis, stability in the absence of additional crosslinkers, and a simple release mechanism.

Microspheres have also been explored as potential gene carriers for delivery of DNA[4,95] and RNA[57,96,97] to target cells. DNA uptake within cells is a challenge, due to repulsion between the negatively charged nucleic acid and cell membranes. Encapsulation of DNA and RNA within biodegradable microspheres has many potential benefits, including prevention against degradation, facilitation of uptake into cells in the absence of a transfection agent and the potential for targeting by surface modification. Shimanovich *et al.*[96] have successfully prepared RNA-filled BSA microspheres, between 0.5 μm and 2.5 μm, using a one-pot sonochemical protocol for use as an RNA delivery agent. The sonochemical procedure was not damaging to the RNA structure, and microspheres were stable for up to 5 months. Microspheres were found to spontaneously transfer into U2OS osteosarcoma cells *in vitro*, however, due to the negative charge of the BSA shell[96,98], uptake through the negatively charged cell membrane was poor. Poly (vinyl alcohol)

(PVA) and polyethylenimine (PEI) coatings were trialled to improve transfection and targeting of the microspheres[81]. Confocal microscopy of labelled microspheres revealed a four-fold increase in cell transfection by PVA- and PEI-coated spheres, and Shimanovich[81] attributed this success to the neutralisation of the BSA microsphere shells upon coating. More recently, Rytblat *et al*.[97] have applied the same PEI coating to microspheres with a miRNA antisense shell, neutralising the surface potential from -60.5 mV to 2.1 mV. The microspheres exhibited similar uptake behaviour to the BSA spheres, reducing glioma cell growth by 34.6 % upon transfection into human U87 glioma cells in the absence of a transfection agent.

Targeting capability is a highly desirable feature when designing drug delivery vehicles. Precise administration enables delivery of a required dose to a desired site, whereas systemic delivery leads to inefficient drug administration throughout the whole body. In the case of cancer therapy, administering a sufficient therapeutic concentration to tumourous tissue without significant damage to surrounding healthy tissue poses a serious problem. Anti-cancer drugs possess high toxicity and achieving a balance between tumour cell death and healthy cell toxicity may hinder treatment and cause severe side effects. Encapsulation of these toxic agents within targeting delivery vehicles and accumulation of the drug via uptake into target cells may enable the use of higher therapeutic concentrations, increasing tumour cell death via controlled drug release whilst minimising systemic distribution and subsequent toxicity.

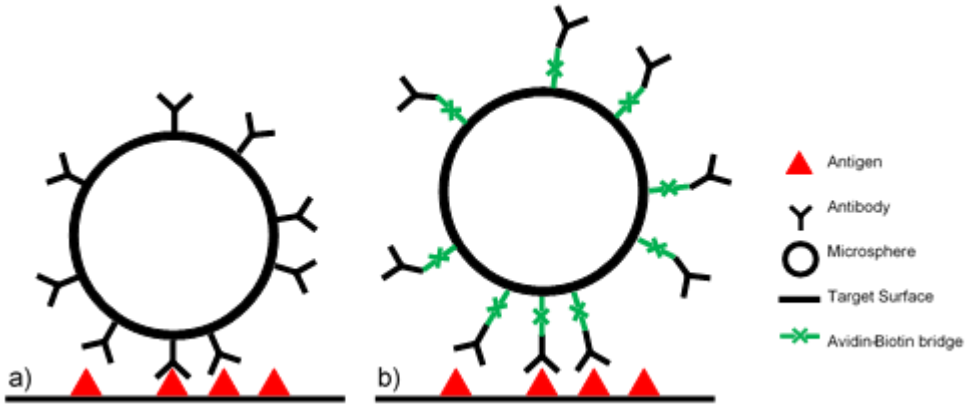

Figure 1.14 – Attaching ligands to a microbubble surface via direct anchor ligand attachment (left) or the use of an avidin-biotin bridge (right). Image generated from reference model[99].

Introducing targeting capabilities into a microsphere system may be achieved by encapsulation, surface modification, or functionalisation of the shell species pre- or post-synthesis[9,10,56,100]. The method functionality incorporation is largely dependent on the species being attached[99], certain delicate ligands such as antibodies may not survive the harsh conditions of sonochemical synthesis, therefore are bound post-synthesis. There are multiple methods for ligand attachment, both covalent and non-covalent (Figure 1.14). An active group can be incorporated within the shell species prior to microsphere synthesis, onto which a ligand can be attached post-synthesis. One non-covalent method that is often used during the initial stages of research is attachment of a ligand via an avidin-biotin binding protein pair, one of the strongest known ligand-protein interactions[50]. Although a convenient mechanism for ligand attachment, it is preferable to avoid the introduction of unnecessary foreign proteins and instead opt for a direct anchor-ligand covalent attachment for enhanced stability[99].

Toublan and coworkers[98] have designed a microsphere system to target integrin receptors which overexpress in tumour cells. The surface of sonochemically-generated vegetable oil-filled BSA microspheres were functionalised by layer-by-layer (L-b-L) electrostatic adhesion of integrin-targeting tripeptides. BSA microspheres contain numerous ionisable groups in the microsphere shell. Toublan[98] reported that, at pH 7, BSA carries a net charge of -17, originating from 185 counterions from acidic and basic residues. In a typical microsphere of 2 μm there are approximately 10^6 BSA proteins crosslinked across the surface, therefore the negatively charged proteinaceous microspheres are perfect for electrostatic adhesion. Tripeptide RGD (argenine-glycine-aspartic acid) motifs can be recognised by integrin receptors and were integrated into peptides with positively charged lysine residues as anchors. The polycationic peptides were then deposited onto the negatively charged microsphere surface. The targeting ability of the microspheres was confirmed by *in vitro* binding of labelled RGD-modified microspheres to human colon tumour cells[98].

The encapsulation of solid species within sonochemically-generated microspheres has enabled the development of delivery vehicles capable of targeted release in response to an applied magnetic field. Avivi *et al*.[83] synthesised magnetic iron oxide (Fe_2O_3) microspheres by encapsulating iron pentacarbonyl ($Fe(CO)_5$) dispersed in decane within BSA microspheres via the one-pot sonochemical protocol. Avivi reported that iron

pentacarbonyl within the vicinity of cavitating bubbles undergoes decomposition and oxidation reactions to form iron oxide, this was confirmed by the absence of signals in the carbonyl region of the microsphere infrared (IR) spectrum. More recently, Wu *et al.*[93] have extended the scope, successfully synthesised drug-loaded magnetic microspheres via a sonochemical protocol. Tetracycline (TTCL) and hydrophobic ferrofluids (Fe_3O_4) were incorporated within BSA microspheres, exhibiting magnetic behaviour and biological activity upon synthesis. As observed by Avivi *et al.*[13], TTCL could be successfully administered *in vitro* without the need for a release mechanism. Wu[93] attributed this to the low density of the BSA shell, in comparison to other shell materials, allowing for slow liquid exchange and controlled TTCL release.

Most recently in 2017, Cui *et al.*[9] have designed a multi stimuli-responsive folic acid-functionalised chitosan smart delivery vehicle for the targeted delivery and triggered release of hydrophobic drugs. The targeting folic acid (FA) and fluorescent tag Rhodamine B isothiocyanate (RITC) were coupled to the chitosan polymer prior to microsphere synthesis. Oleic acid-modified iron oxide nanoparticles and Coumarin 6 (C6) green fluorescent hydrophobic dye as a drug model were then dispersed in soybean oil and encapsulated within thiolated FA/RITC-labelled chitosan microspheres. Cui *et al*. observed a green fluorescent core and red fluorescent shell in CLSM images of C6-loaded FA/RITC-labelled microspheres, confirming successful encapsulation of the dye. Incubation of the microspheres *in vitro*, within HeLa cervical cancer cells containing folate-receptors, revealed enhanced uptake of FA/RITC-labelled C6-loaded chitosan microspheres over C6-loaded chitosan microspheres, demonstrating the importance of the FA functionality[9]. Although no direct analysis of the effect of magnetic targeting on uptake was reported, it is clear that the multifunctionality of the microsphere system will improve both regional targeting and localised uptake.

In addition to proteins, natural and synthetic polymeric microspheres have been investigated as drug delivery vehicles. Cavalieri *et al.*[10] have demonstrated the uptake of hydrophobic doxorubicin, a fluorescent anti-cancer agent, within thiolated poly(methacrylic acid) microspheres post synthesis. The drug was incubated with a microsphere suspension overnight, followed by washing to remove residual doxorubicin in the bulk. CLSM was used to qualitatively observe the uptake of doxorubicin into the microspheres. Applied sonication *in vitro* led to microsphere collapse, demonstrating a

potential release mechanism for the drug-loaded contents, however it was also proposed that glutathione, an intracellular reducing agent, may provide an alternative mechanism for payload release by reduction of crosslinked disulphide bridges within the microsphere shell

When designing microsphere systems for *in vivo* applications it is important to consider their degradation pathways and excretion from the body to ensure there is no risk of exposure to, or accumulation of, toxic degradants. Both biodegradable microspheres and those that undergo triggered release must, upon administering their payload, be removed. Such products are likely to enter the circulation and may lead to tissue deposition, accumulation, and subsequent toxicity. The long term toxicological evolution of the system must be considered, particularly when designing a controlled release system which will persist in the body, or if administration of the microspheres is likely to continue for a long period of time[66].

Microbubble Contrast Agents in Diagnostic Imaging

Ultrasound as a diagnostic imaging tool is widely used due to the relatively inexpensive equipment, its efficiency and portability. A high frequency acoustic signal penetrates the body from an ultrasonic probe placed upon the skin, and the variations in intensity and time of the reflected signals create a 2D image. In the past, differentiation between various soft tissue and blood vessel signals posed a challenge due to their similar densities and resultant indistinguishable scattering intensities. Gas-filled microbubble contrast agent (MBCAs) are biocompatible particulate materials that strongly scatter acoustic waves, passing through the circulatory system as an intravascular contrast media. Their effectiveness is not only a result of the large change in density across the microbubble surface, but also due to their behaviour in response to an acoustic signal. Gases are far more compressible than tissue and at their resonant frequency the microbubbles oscillate readily in response to a propagating wave. In doing so they reflect a far stronger signal than red blood cells, thus greatly enhancing the vascular signal relative to local tissue[101]. A microbubble is unable to diffuse from blood vessels, therefore can be used as blood pool markers and tracers, enhancing the ultrasound signal of highly vascularised organs and tissue. Initial investigations have been conducted into the relationship between the degree of

vascularisation and malignancy of renal, breast and prostate lesions by use of microbubble contrast agents to map the lesion vascularity[101,102].

The success of MBCAs is dependent on their shell material and the gas contained within, whether air or a gas-phase perfluorocarbon. To enable passage through even the smallest capillaries, such as those across the lung bed, microbubbles must be no larger than 7 μm in diameter. Stability is also of great importance when designing contrast agents, they should be stable enough to persist in the bloodstream for several minutes to allow time for enhanced imaging to occur[101]. Albunex® was the first FDA-approved, commercially available MBCA produced sonochemically, consisting of crosslinked HSA shells surrounding a gas bubble. Due to the short lifetime of Albunex®, as a result of rapid diffusion of air from the core[103], subsequent "second generation" MBCAs such as sonochemically-generated Optison™ and Sonovue® were produced, containing gaseous perfluorocarbon cores. Their enhanced stability was attributed to the low solubility of the core species[99].

Targeted microbubbles can greatly enhance diagnostic imaging by localised accumulation of a high microbubble concentration at a desired location. Korpanty *et al.*[104] have successfully incorporated avidin into sonochemically-generated albumin and dextrose-shell microbubbles, onto which biotinylated monoclonal antibodies targeting endoglin can be conjugated. Endoglin is an endothelial glycoprotein responsible for blood vessel angiogenesis. In small, immature tumours, endoglin is excessively overexpressed as new blood vessels are rapidly generated to perfuse the tumour[105]. By targeting this tumour angiogenesis marker with MBCAs, there is the potential to quantify endoglin production as a prognostic tool.

Clinical ultrasound and magnetic resonance imaging (MRI), provide complementary imaging to improve analytical accuracy without the damaging ionising radiation of x-rays[106]. Due to the possibility of hybrid imaging in the future, magnetic gas-filled microspheres incorporating superparamagnetic iron oxide nanoparticles (SPIONS)[106] serve not only as a means to target a location for enhanced ultrasound imaging due to their magnetic shell and echogenic nature, but also to enhance MRI images due to the superparamagnetic behaviour of the nanoparticles.

Fluorine ^{19}F is widely used in MRI to enhance signals due to its 100 % abundance. It is mostly present in the body as solid fluoride in bones and teeth, therefore there are no competing signals during imaging. Perfluorocarbons (PFCs) are non-toxic, biocompatible molecules that provide a source of high fluorine concentration, however due to their poor solubility in aqueous mediums, they are usually administered in the form of an emulsion or encapsulated within microspheres[107]. The use of sonochemically-generated fluorocarbon microspheres to enhance MRI signals was first proposed by Webb *et al.*[108]. Perfluorononane-filled BSA microspheres were prepared via a sonochemical protocol. Due to the high encapsulation efficiency of sonochemically-generated PFC microspheres over conventional PFC emulsions, Webb reported a six-fold increase in the volume of PFC that can be administered per unit injection volume and an observed increase of up to 300 % in the signal-to-noise ratio.

Topical Delivery

Some targeted drug delivery vehicles, classed as bioadhesive microspheres, are designed with mucoadhesive or cytoadhesive properties[79,109,110]. The desirable properties of bioadhesive polymers include improved surface to volume ratio exposure to the tissue, and prolonged contact of the microspheres with the mucosal layer. Bioadhesive microspheres have the potential for a range of applications including topical administration of ocular drugs[110].

Another example of topical delivery is the potential immobilisation of drug-loaded microspheres into bandages. Microspheres have been successfully immobilised onto fabrics[111,112] via a simple sonochemical protocol. Gouveia[111] successfully immobilised antimicrobial BSA microspheres onto a range of fabric substrates to create novel antimicrobial bandages. The cysteine antimicrobial species maintained biological activity throughout encapsulation, killing microbes such as staphylococcus aureus *in vitro*. This report demonstrates the huge potential for controlled-release antimicrobial wound dressings and other textile-based biodelivery systems for topical administration.

Other Applications

The utilisation of biocompatible microspheres as delivery vehicles extends beyond their applications in therapeutics. In recent years, the desire for people to lead a healthier lifestyle has led to an increased consumer awareness of the benefits of certain foodstuffs and the subsequent development of so called "functional foods" that are augmented with ingredients to improve their nutritional value[113]. Simple addition of ingredients such as vitamins and minerals may compromise taste, texture and aroma, as well as risk rapid degradation by oxidation. Microencapsulation offers a solution to facilitate nutrient delivery whilst masking unappealing flavours and odours and protecting the nutrient against processing and packaging. Although not widely reported in the literature, the concept mirrors that of therapeutic delivery systems[14,114], with a simple sonochemical protocol, targeting via surface functionalisation, and controlled delivery[43].

In the field of durable fragrances, Tzhayik *et al.*[115] demonstrated the successful encapsulation of the fragrant oil amyl acetate within sonochemically-generated BSA microspheres. The microspheres achieved an encapsulation efficiency of approximately 97 % and were stable at both room temperature at 4 °C for six months in a sealed container. The controlled release duration at 25 °C and 15 °C was 23 and 40 hours respectively. The plotted data revealed a slope with two distinct release rates. The first between 0-10 hours was described as the initial loss in mass corresponding to evaporation of both amyl acetate as well as residual bulk aqueous phase. Beyond 10 hours Tzhayik described the release rate slope as almost equal to that of pure amyl acetate, and attributed this to the collapse of BSA microspheres as a result of no surrounding moisture. Not only can amyl acetate pass easily through the BSA shell[93], but Tzhayik proposed that the high surface tension of amyl acetate leads to poor adsorption of BSA at the interface during sonication, creating weak shells that readily collapse upon amyl acetate release[115].

Prior to this report, Shimanovich *et al.*[112] demonstrated the immobilisation of proteinaceous microspheres onto cotton and polyester fabrics. The half-life stability of the bonded microspheres at ambient temperature was 5 months, and microspheres were also found to withstand washing cycles at 40 °C. If combined, fragrant microspheres immobilised onto fabrics have the potential to be utilised as slow release fragrances. Alternative approaches to fragrance microencapsulation and immobilisation onto textiles have been explored[116,117] however their effect is relatively short lived. The additional stability of sonochemical

crosslinking in a one-pot encapsulation and immobilisation technique may facilitate a more long-term release mechanism.

Although there are currently no publications regarding the use of sonochemically-generated microspheres for agrochemical applications, agrochemical-loaded microspheres synthesised by other mechanisms, including those with thermoresponsive characteristics, are detailed in the literature[118,119]. Adaptation of sonochemical synthetic mechanisms could tailor the proteinaceous or polymeric microsphere systems to suit agrochemical applications, particularly those with stimuli-responsive or bioadhesive capabilities.

1.3 RAFT Polymerisation

When synthesising sonochemically-generated microspheres, employing a synthetic polymer as the shell species in place of a naturally-occurring proteins[10–12], consideration must made for the appropriate mechanistic protocol with which to synthesise the shell material. This project is concerned with RAFT polymerisation as a protocol for the synthesis of poly(methacrylic acid) (PMAA) and PMAA-based block copolymers for use as shell material in the sonochemical synthesis of polymeric microspheres. The scope is extended to include the incorporation of poly(N-isopropylacrylamide)-based thermoresponsive polymer blocks, with an aim to generate stimuli-responsive microspheres capable of releasing their payload in response increasing temperature.

Radical polymerisations are the most widely used, versatile technique for the polymerisation of unsaturated monomers[120]. The polymer chain grows by the sequential addition of unsaturated monomer units to a terminal active site at the end of the propagating chain. The radical attacks the double bond of the monomer, causing homolytic cleavage. Some examples of unsaturated monomers are shown in Scheme 1.4.

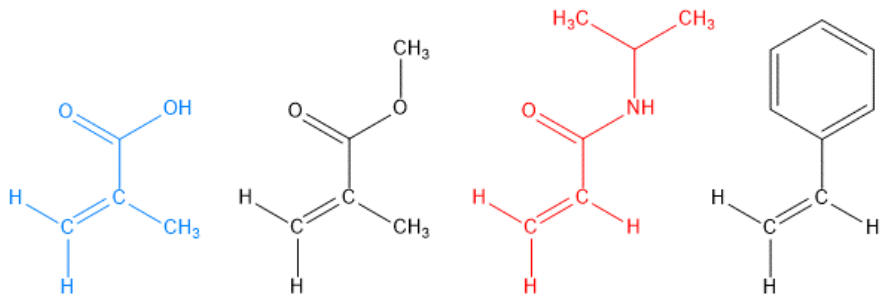

Scheme 1.4 – Unsaturated monomers (from left to right): methacrylic acid (MAA), methyl methacrylate (MMA) N-isopropylacrylamide ($NIPA_M$) and styrene. Those that are colour coded are done so for easy recognition in upcoming chapters.

Since the 1980s, approximately half of all polymers produced commercially have been prepared by free-radical polymerisation[121]. Common applications of these polymers include paints, adhesives, plastics, rubbers and specialist clinical applications[122]. Free-radical polymerisation was traditionally perceived as an inherently uncontrollable mechanism that would continue until its natural conclusion, either by consumption of the radical initiator or monomer. Upon the discovery of new mechanisms for "controlled radical polymerisation" (CRP), with agents to mediate chain propagation, polymers with well-defined architectures and narrow polydispersities can be generated. The dynamic equilibrium established between a propagating radical and a dormant species is the essence of CRP mechanisms. There are several methods of controlled radical polymerisation that utilise this equilibrium, including RAFT polymerisation, atom transfer radical polymerisation (ATRP) and nitroxide-mediated radical polymerisation (NMP)[123].

1.3.1 RAFT – A Synthetic Route to Well-defined Polymers

The mechanism for radical polymerisations can be subdivided into three stages; initiation, propagation and termination[120]. Chain polymerisations that have no mechanism for termination are often termed "living polymerisations"; the active sites at the chain end remain and can propagate further polymerisation reactions on the addition of more monomer under appropriate reaction conditions. If the rate of initiation greatly exceeds the rate of propagation, a living polymerisation will propagate chains at a constant rate,

producing polymers of known architecture with controlled molecular weights and narrow size distributions, or polydispersities. Living polymerisation also offers strict control over block copolymer architecture by the subsequent addition of monomers to produce well-defined block copolymers that cannot be readily synthesised by alternative methodologies.

Reversible addition-fragmentation chain-transfer radical polymerisation (RAFT) is a versatile technique for the controlled radical polymerisation of living polymers. To achieve control, the reaction employs a mediating chain transfer agent (or RAFT agent) in the form of a dithioester, trithiocarbonate, xanthate or dithiocarbamate to generate a dynamic equilibrium of reversible chain transfer with a propagating chain radical. The utilisation of thiocarbonylthio compounds as chain transfer agents was first discovered in 1998 by researchers at CSIRO Australia[124]. RAFT differs from other controlled radical polymerisation techniques due to its compatibility with a wide range of monomers and reaction conditions, making it a facile technique for polymer synthesis.

The RAFT Mechanism

RAFT, unlike ATRP and NMP, is largely analogous to conventional radical polymerisation[125]. As with conventional free radical polymerisation, radicals must first be generated. This is usually achieved by the thermal decomposition of azo compounds such as azobisisobutyronitrile (AIBN) or 4,4'-azobis(4-cyanovaleric acid) (ACP), which readily decompose at commonly employed reaction temperatures (Scheme 1.5). Alternatively photoinitiators may be employed[126], further demonstrating the versatility of the technique.

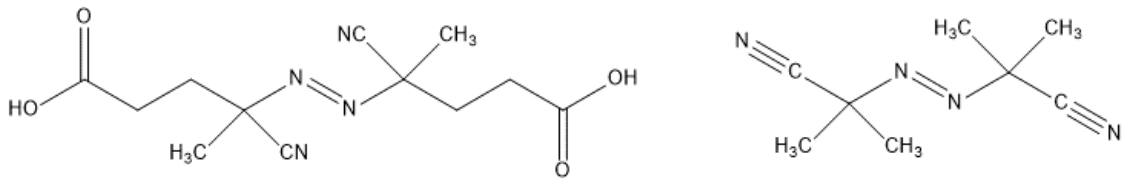

Scheme 1.5 – Azobisisobutyronitrile (AIBN) (left) and 4,4'-Azobis(4-cyanovaleric acid) (ACP) (right) initiators.

Scheme 1.6 shows the general mechanism for RAFT polymerisation[127]. Firstly, the radical initiator undergoes cleavage, and initial interactions between the initiator-derived radicals and monomer yield propagating oligomers. Due to the high transfer constants of RAFT agents, propagation via chain transfer quickly overrides radical-induced propagation in the "pre-equilibrium", whereby the propagating radical interacts with the RAFT agent (1) to form an intermediate radical (2). The intermediate radical then fragments, yielding the polymeric dithioester compound (3) and the R• radical leaving group. The ejected R• radical reacts with further monomer units to form a new propagating radical in a re-initiation step. In an ideal RAFT polymerisation, initiation and the pre-equilibrium steps are rapid and the large majority of polymer chains are therefore R• radical-initiated and mediated by the RAFT equilibrium as opposed to initiator-initiated. To ensure that this is the primary mechanism and to minimise side reactions, the RAFT agent is used in excess of the initiator. The main equilibrium is responsible for the control over polydispersity, ensuring all chains propagate at equal rates. A rapid equilibrium occurs between the propagating radicals P_m• and P_n• and the dormant polymeric dithioesters (3a) and (3b), mediated by the cleavage of a stable intermediate radical adduct (4). Once completed, the majority of polymers retain their RAFT functionality and can either be isolated as a final product or employed as a macroRAFT agent to facilitate block copolymerisations[128].

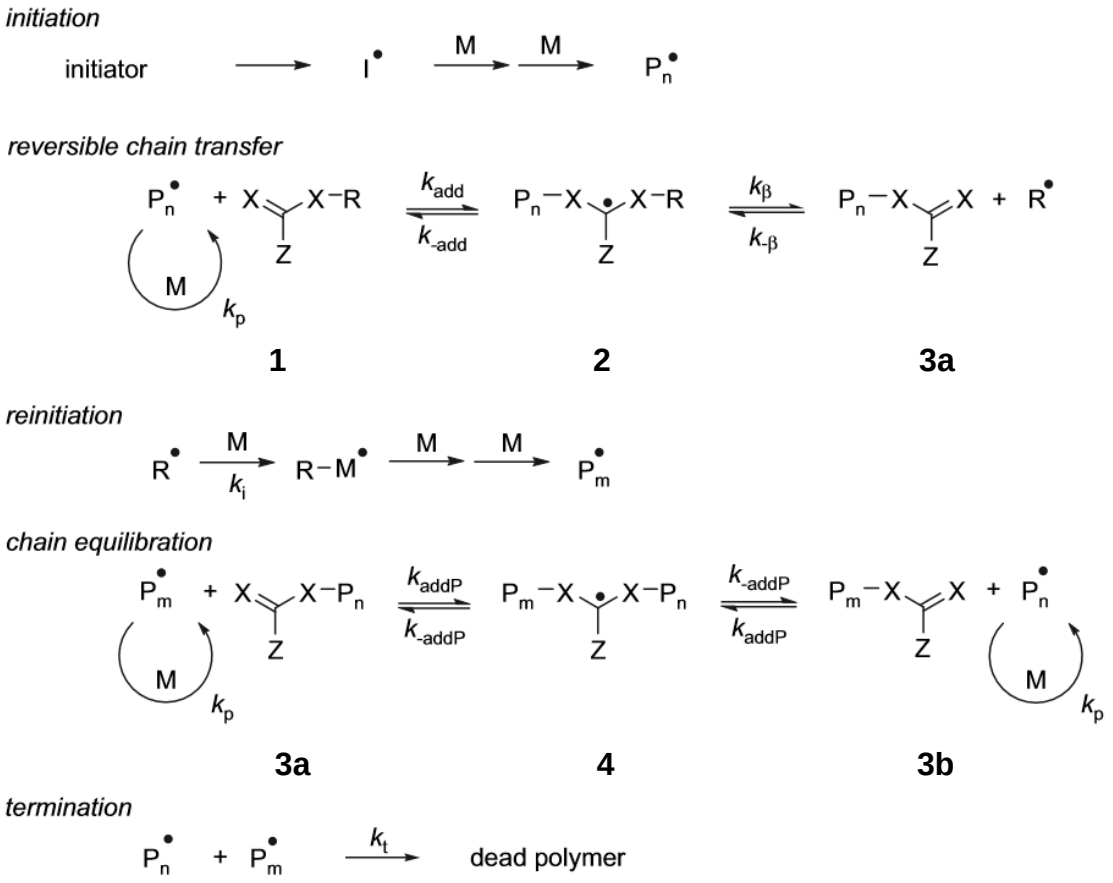

Scheme 1.6 – A general mechanism for RAFT polymerisation, in the case of thiocarbonylthio RAFT agents, X=S, (Z and R as before)[128]. Image adapted from reference.

Worthy of note is a feature exclusive to RAFT polymerisation. The product of the chain transfer equilibrium is itself a chain transfer agent, retaining the dithioester moiety at the end of the polymer chains. The synthesised "macroRAFT" agent should possess a comparable activity to the precursor RAFT agent, and the precursor and macroRAFT agent should differ only in their molecular weights. It is this that confers the living characteristics of this particular radical polymerisation and enables chain extension.

Due to the nature of the reaction mechanism, a small number of undesirable non-RAFT mediated reactions may occur, such as termination by combination or disproportionation. Some chains may also propagate via conventional radical polymerisation, which could greatly affect the polydispersity of a sample[125]. To maintain the living character of the polymer and to ensure that polymer chains retain their RAFT end groups, these reactions

must be minimised. Optimising the reaction conditions and finding a suitable RAFT agent to complement the choice of monomer goes a long way to perfect the living characteristics of a polymerisation.

$$C_{tr} = \frac{k_{tr}}{k_p} \tag{1.2}$$

$$k_{tr} = k_{add}\phi = k_{add}\left(\frac{k_\beta}{k_{-add}+k_\beta}\right) \tag{1.3}$$

The properties of a RAFT agent can be defined by its transfer coefficient C_{tr} (Equation 1.2), where k_{tr} is the rate constant for radical addition (Equation 1.3), and k_p is the rate constant of monomer propagation[129]. ϕ is the partition coefficient and indicates the preference for intermediate radicals (2) or (4) to fragment into products or to return to the starting materials. Effective RAFT agents (2) with an efficient R• leaving group should favour formation of the propagating radical, therefore ϕ should be greater than 0.5. In an ideal pre-equilibrium, the reverse reaction, C_{-tr}, should equal zero as intermediate (2) should be driven to (3a) by the ejected R• leaving group and should not revert to the reformation of the original RAFT agent (1). On the other hand, during the main equilibrium the symmetrical intermediate radical (4) should possess the ideal degree of stability/instability towards fragmentation of either the P_n or P_m chains in equal probability. C_{tr} should therefore equal the reverse C_{-tr}, and ϕ will be approximately 0.5[129]. As such, bimolecular termination of the two propagating radicals makes an insignificant contribution and the majority of chains should retain their RAFT agent end group-functionality.

An ideal reaction can therefore be described by Equation 1.4, whereby $\overline{x}_n$ is the number average degree of polymerisation, c is the fractional monomer conversion, $[M]_0$ is the initial monomer concentration and $[RAFT]_0$ is the initial RAFT concentration. The number average degree of polymerisation should increase linearly with c, assuming the RAFT agent efficiency is 100 %. The expected number average molecular weight (M_n) can then be calculated theoretically by application of Equation 1.4 to Equation 1.5, where M_0 is the molecular weight of the monomer[124,130].

$$\overline{x}_n = \frac{c[M]_0}{[RAFT]_0} \tag{1.4}$$

$$M_{n_{theoretical}} = \overline{x}_n M_0 \tag{1.5}$$

If the RAFT agent behaves in an ideal fashion, the kinetics of RAFT polymerisation should be similar to those of conventional radical polymerisations. Moad *et al*.[127,131] reported half order kinetics with respect to the initiator, as in conventional radical polymerisation, and zero order kinetics with respect to the RAFT agent. The rate constant is largely independent of the RAFT agent concentration in a reaction[132], as demonstrated by Moad in the radical polymerisation of methyl methacrylate (MMA) at increasing RAFT agent concentrations. As with all models, there are deviations from the ideal, such as rate retardation when using high RAFT agent concentrations, or for monomers with a high propagation rate (k_p). In this case, substituting the RAFT agent may diminish retardation when used at elevated concentrations with a particular monomer[133].

RAFT Agent Design

The impact of a chain transfer agent on the kinetics of RAFT polymerisation emphasises the importance of employing a suitable RAFT agent and the subsequent impact on reaction kinetics. The two most important features of the RAFT agent are the R and Z groups (Scheme 1.7).

The choice of Z group functionality on a RAFT agent modifies the rate of addition to, and fragmentation of, the intermediate radical adducts in both the pre-equilibrium and main RAFT equilibrium. Dithiocarbamates and xanthanates exhibit a much lower reactivity with respect to radical addition than dithioesters and trithiocarbamates; this is primarily due to the presence of a lone pair adjacent to the C=S double bond. Resonance creates zwitterionic forms, reducing the double bond character of the C=S bond and therefore stabilising the RAFT agent against radical addition and ejection of the R group[129].

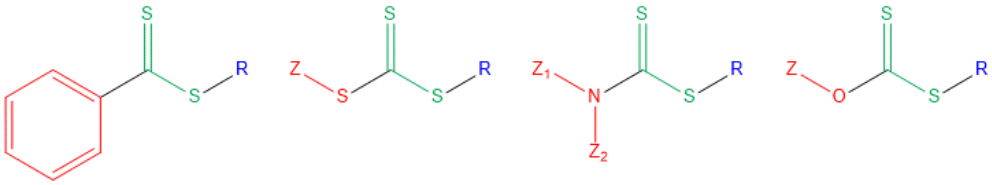

Scheme 1.7 – The four main classes of RAFT agent, from left to right: Dithiobenzoates (a type of dithioester), trithiocarbamates, dithiocarbamates and xanthanates. Regions shown in red represent the Z group, the thiocarbonylthio group is highlighted in green, and the R leaving group is shown in blue.

The presence of an electron-withdrawing Z group can greatly enhance the transfer constant (k_{tr}) by stabilising the adjacent radical upon formation of the intermediate adduct. Too stable, however, and the susceptibility of side reactions with the intermediate radical increases as the rate of fragmentation is retarded.

There is a strong relationship between the stability of the Z group and the activity of the chosen monomer, and they can be subdivided into two categories depending on the activity of the terminal radical[129]. More active monomers (MAMs) possess a double bond that is conjugated either to an aromatic ring, such as styrene, or a carbonyl group like those found in acrylates (Scheme 1.4). In less active monomers (LAMs), the double bond is usually adjacent to a saturated carbon, oxygen, or nitrogen lone pair. The terminal radical of MAMs are less reactive with respect to radical addition (k_{add}) but make good homolytic leaving groups, therefore a more active RAFT agent is required with an electron-withdrawing Z group, such as a dithioester. Propagating radicals possessing a LAM terminal, on the other hand, have a high k_{add} and require a less active RAFT agent to prevent stabilisation of the intermediate radical and subsequent retardation by slow fragmentation. Figure 1.15 shows the reactivity of RAFT agents with respect to their Z-group functionalities.

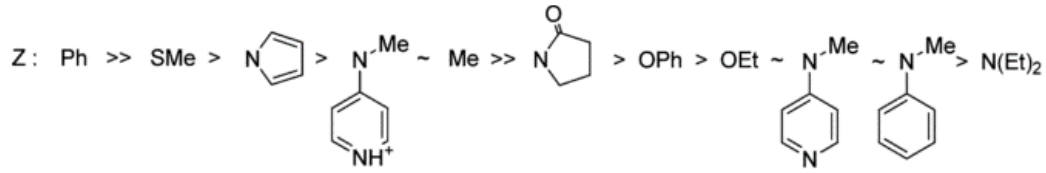

Figure 1.15 – The reactivity of various RAFT agent Z groups[129]. Left = high transfer constants, suitable with MAMs, right = lower transfer constants, suitable with LAMs. Image adapted from reference.

The role of the R group in a RAFT agent is to efficiently cleave from the intermediate radical (2) in the pre-equilibrium to yield an R• radical, capable of efficiently re-initiating propagation. As such the R group must be a more favourable homolytic leaving group than P_n• to prevent the reformation of pre-equilibrium starting products (1). The behaviour of the R group therefore largely determines the partition coefficient (ϕ) for a particular reaction. Factors affecting radical stability include the structure of the R group, whether primary, secondary or tertiary, and the behaviour of any substituents. Moad *et al.*[129] described a general increase in transfer coefficient with increasing carbon functionalisation from primary through to tertiary R groups due to resonance stabilisation. As with Z group functionalities, it was observed that electron-withdrawing groups on the R group also drive partitioning of the R• radical due to their delocalisation capabilities. Figure 1.16 shows the trend in partition coefficients of R leaving groups, from electron-withdrawing and tertiary leaving groups with high fragmentation rates, to secondary and primary leaving groups with low fragmentation rates but rapid reinitiation rates.

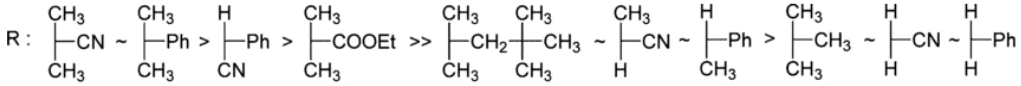

Figure 1.16 - The reactivity of various RAFT agent R groups[129]. Left = high transfer coefficients and high fragmentation rate, right = lower transfer coefficients and low fragmentation rate. Image adapted from reference.

Once the R group has left the intermediate, the newly formed R• radical must be able to reinitiate polymerisation at a rate exceeding that of propagation ($k_i > k_p$), analogous to conventional radical polymerisation. In doing so, the R• radical will be consumed only by the main polymerisation reaction as opposed to undesirable side reactions that could broaden the polydispersity of the final product. As mentioned above, monomers with a particularly high propagation rate constant (k_p) can inflict rate retardation if the rate of reinitiation by the R• radical does not exceed the rate of propagation. Propagating monomers with a high k_p therefore require a primary or secondary R• radical that is not stabilised by tertiary resonance to ensure $k_i > k_p$ and achieve good control over the reaction.

1.3.2 Comparing Controlled Radical Polymerisation Techniques

Contrary to conventional radical polymerisation or competing CRP techniques, which require highly controlled reaction conditions, RAFT polymerisation is highly versatile as it can be easily implemented and is compatible with a range of monomers and reaction conditions. RAFT polymerisations have been successfully conducted in aqueous solutions[134], emulsions[135,136], suspension[137], and under exposure to oxygen[138], which is highly unusual in radical polymerisation systems[124].

Unlike ATRP and NMP, RAFT has also displayed excellent tolerance for unprotected monomer functionalities including -OH and -COOH functional groups, thus avoiding the additional experimentation, loss of product and costs associated with protection and deprotection[139]. Matyjaszewski *et al.*[140] described the challenge of polymerising acrylic and methacrylic acid monomers by ATRP due to the tendency for monomers to form metal carboxylates with the metal complexes employed to catalyse the reaction.

The one feature that unites all methods of CRP is the dynamic equilibrium created between a propagating radical and a mediating species. The benefit of CRP over conventional radical polymerisation is the ability of this mediating species to control the molecular weight and polydispersity of the final product by managing the rate of propagation after rapid initiation. There are two main mechanistic pathways employed in order to establish this equilibrium, either via reversible termination, as is the case in ATRP and NMP, or by reversible transfer, as occurs in RAFT polymerisation.

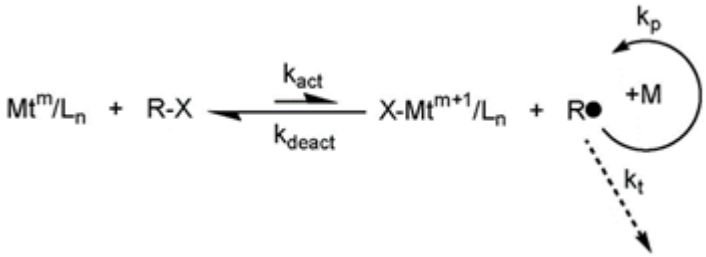

Scheme 1.8 – A schematic of ATRP, whereby Mt/L_n = the transition metal ligand complex, $X\text{-}Mt/L_n$ = the transition metal halide complex, R = the alkyl radical and subsequent propagating radical[141].

ATRP depends upon a metal halide ligand complex to catalyse the reaction and exert control over the chain growth. The transient radical is first formed rapidly by cleavage of the R-X bond of an alkyl halide initiator by a low oxidation state transition metal complex (MtL_n) to yield the radical R•, and a transition metal halide complex ($MtXL_n$)[142]. R• then propagates the monomer, mediated by halide transition between the metal halide complex and the propagating radical (Scheme 1.8). The mechanism ensures chain growth is controlled by trapping the propagating radical in a cycle of reversible termination reactions, termed the persistent radical effect (PRE). As the reaction progresses, the number of side termination reactions (k_t) greatly diminishes due to the high rate of coupling between the propagating radical and X, and the equilibrium is driven towards the formation of the dormant halide-capped polymer chain ($k_{deact} >> k_{act}$). ATRP transition metal catalysts are most compatible with styrenes, acrylates, methacrylates and other MAMs that form relatively stable radicals[140], however certain monomer functionalities may require protection prior to synthesis as previously mentioned. NMP works in much the same way as ATRP, except the reaction utilises alkoxyamines (general structure $R^1\text{-O-}NR^2R^3$) as both the initiating species (R^1•) and to employ control over propagation as the persistent radical (•$O\text{-}NR^2R^3$). Whilst suitable for the polymerisation of styrene and styrene-based copolymers, the rate of NMP polymerisations is often very slow due to strong, covalent alkoxyamine bonds shifting the equilibrium in favour of the dormant species[142].

Although each technique offers its own benefits and comes with its own limitations, a choice between CRP protocols must primarily be driven by suitability of the mechanism for the chosen monomer. Within the scope of this project, RAFT polymerisation was

deemed the most sensible mechanistic option as its compatibility with acid-functionalised and acrylamide-based monomers far exceeds that of ATRP or NMP.

1.3.3 Block Copolymerisation

Prior to the discovery of RAFT polymerisation as a synthetic route to well-defined polymers, the use of other CRP techniques to synthesise block copolymers was largely limited by their poor compatibility with a broad range of monomers and stringent reaction conditions[143]. Matyjaszewski *et al.*[144] reported the use of both RAFT polymerisation and ATRP to synthesise poly(vinyl acetate)-based block copolymers due to the incompatibility of ATRP with highly reactive vinyl acetate radicals.

The preparation of block copolymers by RAFT polymerisation serves as a means to synthesise polymers with a variety properties independent from those of the component homopolymers[145]. The diverse applications for block copolymers include surfactants, dispersants, surface modifiers such as those found in paints, and most importantly, within the scope of this project, drug delivery vehicles.

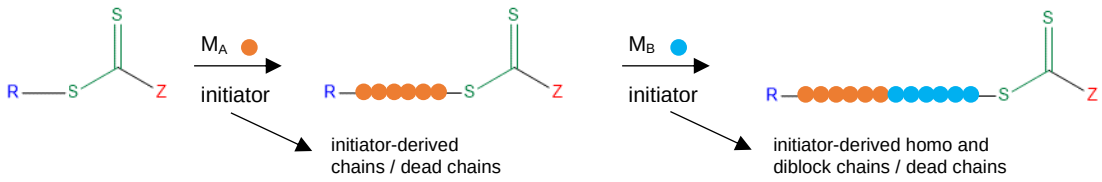

Scheme 1.9–RAFT diblock copolymerisation with a monofunctional RAFT agent.

The simplest approach to block copolymerisation is by subsequent sequential homopolymerisation[145], as shown in Scheme 1.9. The first monomer is synthesised by RAFT polymerisation to yield a homopolymer of desired length, retaining the RAFT functionality at the chain ends. After work-up and characterisation, the homopolymer then assumes the role of macroRAFT agent for subsequent addition of the second monomer to

yield an AB diblock copolymer. For polymerisation to be successful, the RAFT agent, initiator and chosen solvent must be compatible with both monomers. The functionalities of the RAFT agent must employ adequate control over each of the propagating radicals to prevent polydispersity of either the macroRAFT agent or second block[145], as such the macroRAFT agent must possess a comparable activity to its precursor.

The order in which monomers are copolymerised subsequently in a block copolymer can be of great importance, particularly as the initial homopolymeric block serves as the macroRAFT agent onto which the second monomer propagates. Monomers that produce stable tertiary radicals such as methacrylates and methacrylamides should be polymerised first as they possess good leaving group ability, maintaining the activity of the precursor RAFT agent. Propagating radicals with a relatively stable secondary structure such as styrenes, acrylamides and acrylates may then be introduced, followed by highly reactive secondary propagating radicals such as vinyl esters. This is a common limitation across all forms of CRP and does somewhat restrict the range of block copolymers that may be generated by dictating the order of block addition, however there are mechanisms that have been investigated to overcome these limitations.

More recently, alternative "universal" RAFT agents, such as stimuli-responsive "switchable" agents, have been trialled. Moad *et al.*[129] have designed switchable RAFT agents, whereby the electron-withdrawing capability of the Z group can be increased in the presence of a strong protic acid, making it suitable for both LAMs and MAMs. The switchable RAFT agents were designed with an aim to facilitate the efficient block copolymerisation of poly(LAM)-poly(MAM) block copolymers, and have proved successful in the RAFT polymerisation of LAMs in the "unswitched" form and MAMs in protonated "switched" form.

Multi-functional RAFT agents have greatly expanded the range of possible architectures for block copolymers. Trithiocarbonates, for example, can either possess monofunctinality or di-functionality if both the Z- and R- groups are identical substituents[146]. Mayadunne *et al.*[146] reported the successful synthesis of polystyrene-block-poly(n-butyl acrylate)-block polystyrene in a two-step reaction using a difunctional trithiocarbonate RAFT agent. Although limiting the architecture to an ABA structure, as opposed to ABA or ABC that can be achieved by a sequential three-step mechanism with a monofunctional RAFT agent, it is certainly an efficient process to achieve triblock ABA copolymers of known molecular

weights. The scope has also been extended further to include more complex architectures such as ABA star and graft block copolymers[147]. Z-linked and R-linked multifunctional dithioesters also offer a similar result. R-linked block polymers offer increased stability as hydrolysis of the thiocarbonylthio end group does not compromise the structure of the polymer. In Z-linked polymers, however, removal of the thiocarbonylthio functionality cleaves the polymer.

The term "click" chemistry describes a rapid, high yielding reaction between two functional groups with high selectivity under mild reaction conditions. In 2011, Webster *et al.*[148] devised a novel system for the application of click chemistry to the synthesis of block copolymers. Each of the copolymers were synthesised using two independent polymerisation techniques, and were subsequently bound to one another by a simple yet highly efficient click reaction. Azide-terminated poly(tert butyl methacrylate) (ptBMA), synthesised by ATRP and end-functionalised with sodium azide, was reacted with RAFT-synthesised poly(butyl acrylate) containing a terminal propargyl group to yield the block copolymer. The azide and propargyl groups react in a 1,3-dipolar cycloaddition in the presence of a copper catalyst to form a linking triazole ring. The technique was applied to a range of polymer combinations and enables two relatively incompatible monomers to be copolymerised that may not be successfully polymerised via subsequent sequential block copolymerisation.

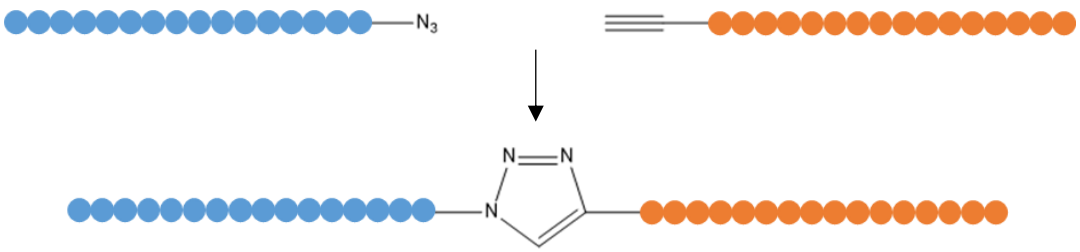

Figure 1.17 – Polymers synthesised by various techniques with an azide terminus (blue) and propargyl terminus (orange) incorporated into a block copolymer by click chemistry[148]. Image redrawn from reference model.

1.3.4 Poly(methacrylic acid) (PMAA)

As discussed in Section 1.2, biocompatible drug delivery vehicles are of particular interest in the field of therapeutics as a means to transport and administer highly potent and unstable drugs whilst maintaining their biological activity. This project focuses on the design and synthesis of biocompatible polymers and block copolymers, namely poly(methacrylic acid) (PMAA) and poly(N-isopropylacrylamide) ($PNIPAA_M$), by RAFT polymerisation for use as a synthetic alternative to proteinaceous microsphere shells.

Poly(methacrylic acid) is a biocompatible synthetic polymer[149] that has recently been employed as polymeric shell material in the sonochemical synthesis of PFC-filled microspheres[10], as described previously. The polymer was chosen due to the ease with which it can be synthesised and functionalised to enable sonochemically-induced crosslinking of the polymer chains during microsphere synthesis, in behaviour analogous to that of cysteine-containing proteins.

To be characterised as biocompatible, a material must display no systemic toxicity, cause no immunogenic or thrombogenic response, trigger minimal allergic reaction or irritation, and must be non-carcinogenic. The material must also exhibit sufficient stability in the physiological medium in order to fulfil their function and, if necessary, elicit a biological response[150]. Although naturally-derived biocompatible polymers and proteins possess inherent biocompatibility and biological activity, largely due to their abundance within the structural tissues of living organisms, they cannot undergo the same degree of modification as synthetically-engineered polymers. Biocompatible synthetic polymers can be synthesised by controlled radical polymerisation (CRP) techniques with predetermined architectures, known molecular weights and narrow polydispersities. They can also be readily functionalised, labelled, and modified post-synthesis to fulfil for a particular function[66].

RAFT Polymerisation of Methacrylic Acid

There are very few reports in the literature of the direct polymerisation of poly(methacrylic acid) by RAFT polymerisation. PMAA polymerisations employing a dithiobenzoate RAFT agent have been successfully conducted in methanol[151,152] and dioxane[153], but publications

usually describe polymerisation of the tert butyl methacrylate monomer (tBMA) by RAFT polymerisation, followed by deprotection of the acid by hydrolysis to yield PMAA[6,154].

Yang and Cheng[151] were the first to report the RAFT polymerisation of methacrylic acid with a dithiobenzoate RAFT agent, commercially available S-(thiobenzoyl)thioglycolic acid (CMDB) as seen in Scheme 1.10, to yield poly(methacrylic acid) with controlled molecular weights and narrow polydispersities. Prior to this, PMAA had only been incorporated via RAFT as a second chain in a block copolymer[143], or as one of two monomers in a random copolymer with methyl methacrylate[155].

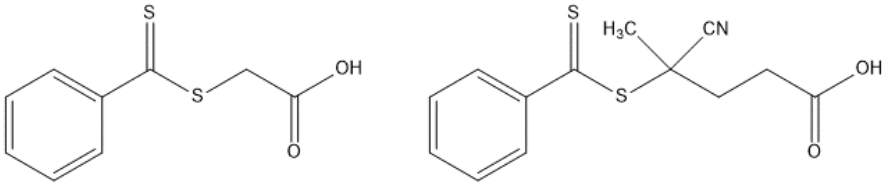

Scheme 1.10 – Two dithiobenzoate RAFT agents. S-(Thiobenzoyl)thioglycolic acid (primary R leaving group) (left). 4-cyanopentanoic acid dithiobenzoate (tertiary R leaving group) (right).

Apparent first-order kinetics were observed, characteristic of both an ideal RAFT polymerisation and free radical polymerisation. Many of the chains retained their RAFT agent functionality, facilitating block copolymerisation reactions as a macro RAFT agent. Yang and Cheng did report a period of induction at the start of the polymerisation, and attributed this to the slow fragmentation of the primary R leaving group ($\bullet CH_2CH_3COOH$) and subsequently slow reinitiation step (k_i) and low transfer constant (k_{tr}). In order to improve the rate of chain transfer, Pelet and Putnam[152] substituted a tertiary R group for the primary R group of CMDB in the form of 4-cyanopentanoic acid dithiobenzoate (CPADB) (Scheme 1.10). The polymerisation displayed the same first order kinetics of an ideal RAFT polymerisation and a short induction period was still observed within the first two hours of polymerisation, likely due to the stability of the tertiary radical ejected with respect to reinitiation. The correlation between theoretical M_n values and experimental M_n data was closer for CPADB-mediated polymerisation than CMDB-mediated polymerisation. This indicates that, as expected, the tertiary radical of CPADB ($\bullet C(CN)(CH_3)CH_2CH_2COOH$) is readily ejected from the RAFT agent intermediate radical

to reinitiate propagation, reducing the likelihood of initial propagation in the absence of RAFT-agent mediation[151,152].

Nejad *et al.*[153] also utilised CPADB for the polymerisation of PMAA oligomers in 1,4-dioxane. However, Nejad noted the formation of dithiobenzoic acid as a side product, giving rise to an increase in polydispersity and a bimodal size exclusion chromatography (SEC) distribution. When increasing the degree of polymerisation to yield polymers of higher molecular weight, a monomodal distribution upon SEC analysis could be observed. It was therefore concluded that the extent of side product contamination was low, unless generating polymers of low molecular weight.

Trithiocarbonate RAFT agents have also been investigated, most recently by Chaduc *et al*. in the RAFT polymerisation of PMAA in water[134]. The polymerisation exhibited enhanced reaction kinetics and conversion rates compared to equivalent reactions conducted in methanol and dioxane. A period of inhibition was observed with all reactions, and this was attributed to the low chain transfer ability of the 4-thiothiopropylsulphanyl pentanoic acid RAFT agent, likely due to the poor stability of the intermediate radical.

1.3.5 Poly(N-isopropylacrylamide) (PNIPAA$_M$)

Poly(N-isopropylacrylamide) (PNIPAA$_M$) is a polymer that is often employed as a drug delivery vehicle in the field of therapeutics due to its stimuli-responsive behaviour. The polymer exhibits a lower critical solution temperature (LCST) upon heating beyond a transition temperature of approximately 30-35 °C[151,156,157], collapsing from a hydrophilic coil structure to a hydrophobic globular aggregate[151]. The transition is reversible and, once cooled below the phase transition temperature, PNIPAA$_M$ returns to its extended, water soluble state.

According to Schild[157], the earliest known publication describing the LCST of poly(N-isopropylacrylamide) comes from a commercial brochure by the American Cyanamid Company in 1963[158], the brochure reports a gradual change in solubility with increasing temperature to potential users. It was Scarpa *et al.*[159] who, in 1967, first reported the now characteristic sharp change in solubility of a polymeric PNIPAA$_M$ solution at 31 ^oC.

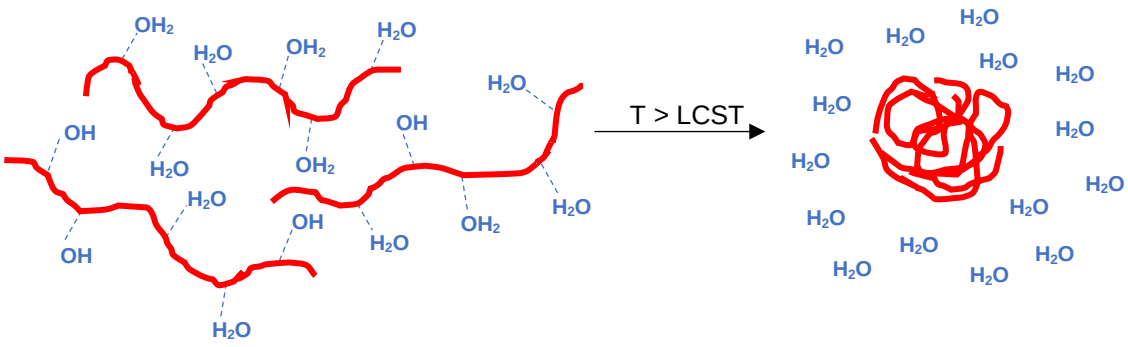

Figure 1.18 – PNIPAA$_M$ chains below the LCST interact with water via hydrogen bonds. On heating, the chains collapse to exclude water, leading to an increase in disorder of the water molecules.

Below its LCST, PNIPAA$_M$ is completely miscible with water and appears as a homogenous solution[85]. The polymer exists in the medium as isolated polymer chains, ordered into a coil structure to reduce exposure of the hydrophobic isopropyl groups to water (Figure 1.18). The reorientation and organisation of water molecules results in a fall of entropy (ΔS)[157]. As the temperature of the solution increases, the entropic term dominates the exothermic enthalpy of solution (ΔH), leading to a positive Gibbs free energy (ΔG). The change in polymer miscibility occurs at the LCST because it is entropically favourable. It is the increase in disorder, and change in entropy, as a result of unbound water molecules that drives PNIPAA$_M$ to undergo a coil-to-globule transition at the LCST (Equation 1.6). Beyond the LCST, the solution becomes cloudy as a result of precipitation, hence the commonly used terminology "cloud point".

$$\Delta G = \Delta H - T\Delta S \qquad (1.6)$$

Pelton[160] argued that although PNIPAA$_M$ undergoes a phase transition at the LCST, it should not be described as truly hydrophilic or hydrophobic. Below the LCST, the polymer displays amphiphilic character, such as lowering the surface tension of water, as a result of the hydrophobic isopropyl groups. Beyond the LCST, the collapsed aggregates retain a high percentage of water, and therefore cannot be described as truly hydrophobic. The terms were described as misleading, and do not accurately characterise the behaviour of the polymer[160]. "Miscible" and "immiscible" defines the two phases more accurately.

The LCST can be modified to suit particular applications. An LCST of 31 °C is not too far from that of physiological body temperature (37 °C), further highlighting the suitability of $PNIPAA_M$ for *in vivo* release applications with little modification required[161]. Factors reported to impact the LCST of $PNIPAA_M$ include molecular weight, pH, concentration[162], tacticity[163], and the introduction of copolymers. The copolymerisation of $PNIPAA_M$ with hydrophobic or hydrophilic comonomers has the potential to cause the biggest deviation from the characteristic LCST, depending on the percentage incorporated with $NIPAA_M$ during copolymerisation[164], however there is some disparity amongst authors as to which other factors actually affect the LCST, namely the effect of molecular weight.

There are two schools of thought regarding the effect of molecular weight on LCST. Data published by Fujishige *et al.*[88] shows that the LCST is largely independent of molecular weight or concentration. Polymers with molecular weights varying from 50-8400 kDa were studied, and a sharp transition in transmittance upon analysis by UV/Vis spectroscopy was observed at 31 °C for all samples. The same independence was observed when measuring the LCST of 8400 kDa $PNIPAA_M$ solutions of increasing concentration. The only observed difference in samples of increasing concentration was a corresponding increase in sample opacity beyond the LCST. The findings of Furyk *et al.*[165] also demonstrated that, above 50 kDa, factors such as molecular weight and polydispersity have little effect on the LCST and cited changes in end group structure as the cause of any variations in cloud point of low molecular weight polymers. Schild and Tirrell[166], on the other hand, reported an inverse relationship between molecular weight and LCST of low molecular weight polymers by calorimetric techniques. They attributed the observations made by Fujishige to the high molecular weights of the polymers measured, whereas at lower molecular weights the effect of chain length may be more significant, however no further explanation for the observed effects were proposed.

It is widely reported in the literature that LCST modification in $PNIPAA_M$ can be achieved by copolymerisation of $NIPAA_M$ with more hydrophilic or hydrophobic monomers[85,156,167,168]. Feil *et al.*[167] have copolymerised poly($NIPAA_M$-co-BMA-co-X), whereby X represents either hydrophobic butyl methacrylate (BMA), hydrophilic acrylamide (AAm), acrylic acid (AAc) or (diethylamino)-ethyl methacrylate (DEAEMA). The LCST of the copolymer increased linearly from 28 °C with an increasing percentage of hydrophilic monomer incorporation from 0-20 %, thus demonstrating the versatility of

LCST modification. Abraham *et al.*[169] generated copolymers of $NIPAA_M$ with hydrophobic methyl methacrylate (MMA) by free radical copolymerisation. The measured LCST of the copolymer was 29 °C, and the ratio of $NIPAA_M$:MMA was 95:5, further demonstrating the sensitivity of the LCST with respect to copolymerisation. More recently, in 2016, Shieh *et al.*[170] reported the increase in the measured LCST of temperature- and pH-responsive P($NIPAA_M$-acrylic acid(AAc)) copolymers at increasing pH between pH 3.0 and 4.5 via UV/Vis.

The effect of pH, concentration, and both block copolymerisation and copolymerisation on the measured LCST of $PNIPAA_M$-containing polymers, synthesised during the course of this project, is discussed further in Chapter 3.

RAFT Polymerisation of N-isopropylacrylamide

Ganachaud *et al.*[130] first reported the synthesis of $PNIPAA_M$ by RAFT polymerisation, utilising dithiobenzoates with primary and tertiary R groups in benzene and 1,4-dioxane respectively. The polymerisations exhibited first order kinetics with a good correlation between theoretical and experimental M_n values, regardless of the choice of R group or solvent. Yang and Cheng[151] have since polymerised $NIPAA_M$ with the dithiobenzoate S-(thiobenzoyl)thioglycolic acid (CMDB) (Scheme 1.10). A small induction period was observed, as with the polymerisation of PMAA under almost identical conditions, and was attributed once again to the behaviour of the RAFT agent (Section 1.3.4). As a result, there was some disparity between the theoretical and experimental M_n values due to some initial propagation in the absence of RAFT agent mediation. The $PNIPAA_M$ macroRAFT agent underwent successful chain extension by block copolymerisation with PMAA, and both the homo and diblock polymers exhibited an LCST at 31 °C. It is interesting to note that block copolymerisation does not affect the LCST of $PNIPAA_M$, and it is only when the chain is disrupted by the presence of intermittent comonomers that the transition temperature changes[151].

Poly(N-isopropylacrylamide) in Drug Delivery

Although there are no reports in the literature of sonochemically-generated hollow $PNIPAA_M$ microspheres, the use of $PNIPAA_M$ as a drug carrier has been widely investigated. Fundueanu *et al*.[161] have reported thermoresponsive release of vitamin B12 from N(isopropylacrylamide)-co-methacrylic acid-co-methyl methacrylate microspheres prepared by solvent evaporation techniques. Yoshida *et al*.[171] generated crosslinked $PNIPAA_M$ hydrogels that collapsed reversibly upon heating, rapidly releasing the contents immobilised within. Hoffman *et al*.[172] have also utilised the temperature-responsive behaviour of $PNIPAA_M$ in the design of drug delivery vehicles. Dual temperature and pH responsive P($NIPAA_M$-co-acrylic acid (AAc))-streptavidin conjugates were immobilised onto magnetic microparticles for pH controlled binding of biotin to streptavidin and thermo-responsive triggered release. The incorporation of acrylic acid both modified the LCST to that of physiological body temperature (37 ^oC) and introduced a pH responsive component.

1.4 Chapter Summary

Whilst the use of proteins as microsphere shell material has been widely researched and the mechanisms of their sonochemical formation, stability and release well characterised, synthetic alternatives have yet to attract the same attention in the field. The need for further control over microsphere morphology, targeting and release behaviour, in order for microspheres to be considered a viable option for controlled drug delivery, calls for an alternative to naturally-occurring proteins as shell species.

The work carried out during the course of this project provides a contribution to the field by employing polymers and stimuli-responsive block copolymers, synthesised by RAFT polymerisation, as alternative shell material with an aim to achieve control over microsphere size and release behaviour by modifying the polymer molecular weight, composition or degree of functionalisation. By introducing thermoresponsive poly(N-isopropylacrylamide), the scope is extended to attempt controlled release in response to an increase in temperature.

2 Experimental Methods

All reagents were purchased from Sigma Aldrich and used as supplied unless otherwise stated.

Experiments requiring sonication during the course of this study were conducted using a Sonics and Materials VC600 high intensity ultrasonic processor (23 kHz and 600 W maximum power output) connected to a horn with a 3 mm microtip attachment.

All ^{1}H NMR spectra were collected using a Bruker Avance 300 MHz spectrometer. Deuterated methanol-d^4 was chosen as the deuterated solvent unless otherwise stated.

DOSY NMR experiments were conducted on a Bruker Avance 400 MHz spectrometer and processed using the Bruker Topspin software. Acquisition was conducted using an "ledbpgp2s" pulse program. The acquisition parameters are as follows: gradient strength was measured in 16 steps between 5 and 95 % of the total gradient strength (gradient pulse length = 1.5 ms and relaxation delay = 5 s). To avoid measurement disruption by convection within the sample, the temperature probe and gas flow was turned off and measurements were conducted at a set temperature of 298 K. Temperature dependent DOSY NMR analysis was also conducted on the Bruker Avance 400 MHz spectrometer.

An Agilent 8453 spectrophotometer was used for UV/Vis analysis. Fourier Transform Infrared Spectroscopy (FT-IR) was conducted using a Perkin Elmer FT-IR spectrometer, fitted with a PIKE MIRacle ATR (attenuated total reflectance) attachment.

Dynamic Light Scattering measurements were conducted using a Malvern Nano-S Zetasizer with a non-invasive backscatter measurement angle of 173 º.

Optical Microscopy images were taken with a Canon EOS 500D fitted with an optical microscope viewpoint adaptor. The camera was connected to a Brunel microscope, fitted with a PL Fluotar 40x/0.70 objective optical zoom lens. ImageJ software (version 1.42q) was used to process micrographs.

Confocal microscopy was conducted on a Zeiss LSM 510 META Confocal Microscope. Fluorescence of the aqueous probe 5,6-carboxyfluorescein was detected by an argon laser with an excitation of 488 nm and an emission band pass of 505-530 nm. Nile Red

fluorescence was detected using a HeNe laser with an excitation of 543 nm and an emission long pass of ≥560 nm. A Plan-Apochromat microscope lens was used with a 63x/1.4 oil Ph3 objective.

2.1 Chapter 3 - RAFT Polymerisation

The following experiments (2.1.1-2.1.5) aim to produce polymers with 100 repeat units of monomer. Other experiments were conducted varying the ratio of monomer to RAFT agent to create polymers of different molecular weight (Table 2.1, Table 2.2 and Table 2.3), and are discussed in Chapter 3.

Prior to use, methacrylic acid (MAA) and methyl methacrylate (MMA) were purified by passing through inhibitor remover columns to remove 250 ppm monomethyl ether hydroquinone (MEHQ) (Sigma Aldrich). All other reagents were used as received from the supplier without further processing and purification. All glassware was dried in an oven prior to use.

2.1.1 Poly(methacrylic acid) (PMAA)

In a typical procedure, 10.00 g (116.16 mmol) MAA (99 %) was charged to a dry 250 mL round-bottomed flask with 40 mL methanol (≥ 99 %). Once fully solubilised, 0.25 g (1.16 mmol) S-(thiobenzoyl)thioglycolic acid (CMDB) (99 %) RAFT agent and 0.07 g (0.23 mmol) 4,4'-Azobis(4-cyanovaleric acid) (ACP) (≥ 98 %) initiator were added to the reaction vessel. The reagents were purged with nitrogen gas for 30 minutes prior to three cycles of freeze-pump-thaw to degas the reaction. The reaction was then sealed under nitrogen, wrapped in foil to exclude ambient light and left to stir for 24 hours at 60 °C.

After this time, the reaction mixture was dissolved in the minimum volume of methanol to reduce the viscosity before dropwise addition to ice-cold diethyl ether anti-solvent. The precipitate was then filtered by vacuum filtration and dried in an oven overnight at 60 °C.

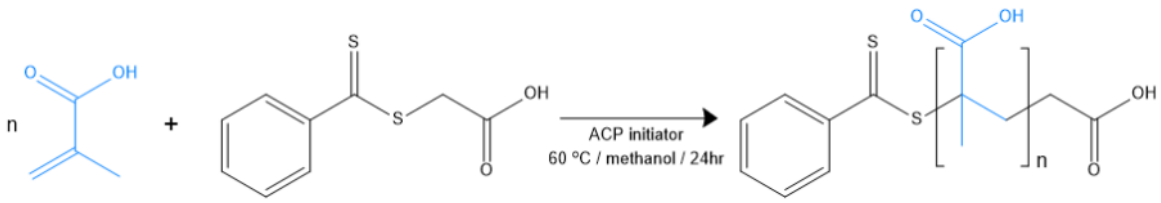

Scheme 2.1 – RAFT polymerisation of methacrylic acid with S-(thiobenzoyl)thioglycolic acid).

Table 2.1 – Molecular weights of monomer, CMDB and ACP for RAFT polymerisation of methacrylic acid.

Polymer Name	MAA / g	MAA / mol	CMDB / g	CMDB / mmol	ACP / g	ACP / mmol
$PMAA_{(100)}$	10.00	0.12	0.25	1.16	0.07	0.23
$PMAA_{(75)}$	7.50	0.09	0.25	1.16	0.07	0.23
$PMAA_{(50)}$	5.00	0.06	0.25	1.16	0.07	0.23
$PMAA_{(25)}$	2.50	0.03	0.25	1.16	0.07	0.23

2.1.2 Poly(N-isopropylacrylamide) ($PNIPAA_M$)

10.00 g (88.37 mmol) $NIPAA_M$ (≥ 99 %) was dissolved in 40 mL 1,4-dioxane (99.8 %) in a round-bottomed flask with 0.19 g (0.88 mmol) CMDB RAFT agent and 0.05 g (0.18 mmol) ACP. The experiment was conducted as described in Experiment 2.1.1. The reaction was left to proceed under nitrogen for 64 hours at 60 °C. After this time, a minimum volume of methanol was added and the polymer was recovered by precipitation from ice-cold diethyl ether and drying overnight at 60 °C.

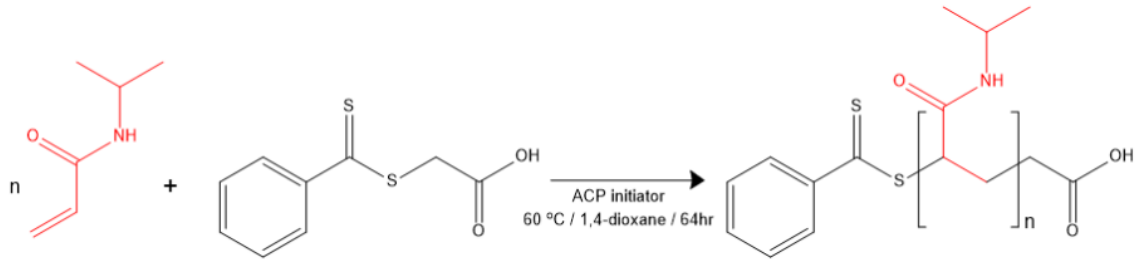

Scheme 2.2 - RAFT polymerisation of N-isopropylacrylamide with S-(thiobenzoyl)thioglycolic acid).

2.1.3 Diblock Copolymerisation of PMAA-PNIPAA$_M$

In a typical block copolymerisation, 2.00 g (17.67 mmol) NIPAA$_M$ was solubilised in 20 mL methanol with 1.56 g (0.18 mmol) PMAA macroRAFT agent (Experiment 2.1.1) and 10.10 mg (0.04 mmol) ACP in a round-bottomed flask. All other conditions are as previously described in Experiment 2.1.2.

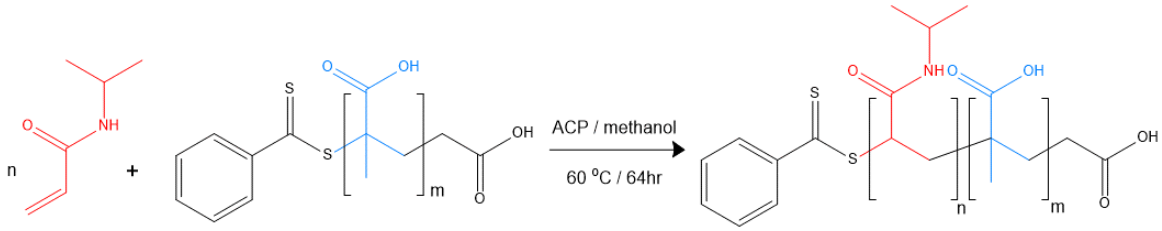

Scheme 2.3 - RAFT block copolymerisation of (N-isopropylacrylamide) (NIPAA$_M$) with PMAA macroRAFT agent (Experiment 2.1.1) to yield PMAA-PNIPAA$_M$.

Table 2.2 - Molecular weights of NIPAA$_M$, macroRAFT and ACP for RAFT block copolymerisation of NIPAA$_M$ with PMAA.

Polymer Name	NIPAA$_M$ / g	NIPAA$_M$ / mmol	macroRAFT / g	macroRAFT / mmol	ACP / g	ACP / mmol
PMAA$_{(100)}$-PNIPAA$_{M(100)}$	2.00	17.67	1.56	0.18	0.01	0.04
PMAA$_{(75)}$-PNIPAA$_{M(100)}$	2.00	17.67	1.57	0.24	0.01	0.05
PMAA$_{(50)}$-PNIPAA$_{M(100)}$	2.00	17.67	1.60	0.35	0.02	0.07
PMAA$_{(25)}$-PNIPAA$_{M(100)}$	2.00	17.67	1.67	0.71	0.04	0.14

2.1.4 Triblock Copolymerisation of PMAA-PNIPAA$_M$-PMAA

1.00 g (11.62 mmol) MAA monomer was added to a round-bottomed flask containing 20 mL methanol. 2.10 g (0.12 mmol) PMAA-PNIPAA$_M$ macroRAFT agent (based on a diblock copolymer of PMAA$_{(100)}$-PNIPAA$_{M(100)}$ with a RAFT agent end group) was charged to the vessel along with 6.70 mg (0.03 mmol) ACP. All other conditions are as described in Experiment 2.1.1.

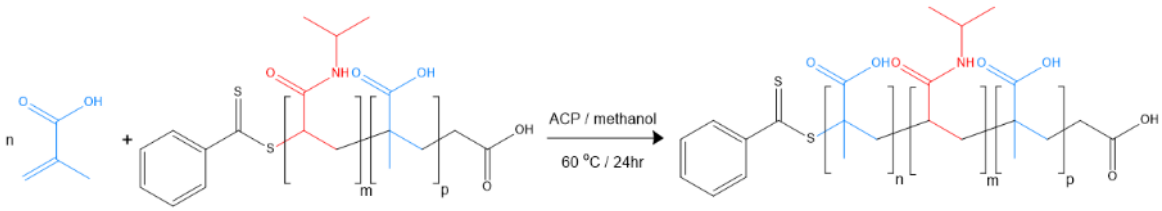

Scheme 2.4 - RAFT block copolymerisation of methacrylic acid (MAA) with PMAA-PNIPAA$_M$ macroRAFT agent (Experiment 2.1.3) to yield PMAA-PNIPAA$_M$-PMAA.

Table 2.3 - Molecular weights of NIPAA$_M$, macroRAFT and ACP for RAFT block copolymerisation of methacrylic acid with PMAA-PNIPAA$_M$.

Polymer Name	MAA / g	MAA / mmol	macroRAFT / g	macroRAFT / mmol	ACP / g	ACP / mmol
PMAA$_{(100)}$-PNIPAA$_{M(100)}$-PMAA$_{(100)}$	1.00	11.75	2.10	0.12	0.01	0.03
PMAA$_{(75)}$-PNIPAA$_{M(100)}$-PMAA$_{(75)}$	0.75	8.71	2.10	0.12	0.01	0.03
PMAA$_{(50)}$-PNIPAA$_{M(100)}$-PMAA$_{(50)}$	0.50	5.81	2.10	0.12	0.01	0.03
PMAA$_{(25)}$-PNIPAA$_{M(100)}$-PMAA$_{(25)}$	0.25	2.90	2.10	0.12	0.01	0.03

2.1.5 Sequential Copolymerisation of PMAA-PNIPAA$_M$-PMAA

5.00 g (58.08 mmol) MAA was solubilised in 60 mL methanol in a two-neck round-bottomed flask. 0.12 g (0.58 mmol) CMDB RAFT agent and 0.03 g (0.12 mmol) ACP initiator were both charged to the flask and the reaction was purged with nitrogen for 30 minutes. The reaction was then degassed by three cycles of freeze-pump-thaw on a Schlenk line to fully degas the reaction. Due to the presence of a Suba-Seal® in the second neck of the flask, the reaction was not sealed under nitrogen, but rather a positive pressure of nitrogen was maintained in the flask for the duration of the reaction via the Schlenk line with a syringe needle outlet. A larger volume of solvent was used to prevent the reaction drying out under nitrogen flow. As with previous experiments, the vessel was wrapped in foil and left to stir for 24 hours at 60 °C.

6.5633 g (49.77 mmol) NIPAA$_M$ monomer, solubilised in 10 mL methanol and purged under nitrogen gas for 30 minutes, was charged to the main reaction vessel via a nitrogen-purged syringe. The reaction was then left to proceed for a further 64 hours at 60 °C.

After this time, a purged solution of 5.00 g (50.08 mmol) MAA in 10 mL methanol, was added using a nitrogen-purged syringe, and the reaction was left to react for a final 24 hours at 60 °C. The work-up protocol was conducted as previously described.

2.1.6 RAFT Copolymerisation of P(MMA-co-NIPAA$_M$)

After passing through an inhibitor remover column, 0.25 g (2.50 mmol) MMA (≥ 99 %) was charged to a round bottomed flask containing 4.75 g (41.98 mmol) NIPAA$_M$, 0.01 g (0.05 mmol) CMDB and 2.80 mg (0.01 mmol) ACP initiator in 30 mL 1,4-dioxane. As with previous polymerisations, the reaction was purged with nitrogen for 30 minutes, followed by three cycles of freeze-pump-thaw. The reaction was then sealed under nitrogen, wrapped in foil and left to proceed at 60 °C for 9 hours.

After this time, the reaction was stopped. Due to the considerable amount of monomer still present in the reaction mixture, the volume of 1,4-dioxane was first reduced by rotary evaporation prior to dropwise addition to diethyl ether. The fine precipitate formed a

viscous layer upon precipitation, which was dried under vacuum and ground into a fine powder. The polymer was then dried in an oven at 60 °C overnight to remove residual diethyl ether.

2.1.7 Diblock Copolymerisation of PMAA-(MMA-co-NIPAA$_M$)

0.25 g (2.50 mmol) MMA, 4.75 g (41.98 mmol) NIPAA$_M$, 0.40 g (0.05 mmol) PMAA macroRAFT agent (Experiment 2.1.1) and 2.80 mg (0.01 mmol) ACP were charged to a round bottomed flask containing 40 mL methanol. The reaction was purged with nitrogen for 30 minutes, followed by three cycles of freeze-pump-thaw. The reaction was then conducted as described in Experiment 2.1.6.

2.1.8 Esterification of Poly(methacrylic acid)

In a typical experiment, 0.88 g (0.10 mmol, 1 unit mmol MAA) PMAA$_{(100)}$ was dissolved in 3 mL dimethyl sulphoxide (DMSO) (VWR, ≥ 99.9 % ultrapure), to which 0.126 mL (1.60 mmol) 1,1,3,3-tetramethylguanidine (99 %) and 0.10 mL (1.10 mmol) methyl iodide (99.5 %) was added. The reaction mixture was stirred for 2 hours at room temperature, after which time the reaction was neutralised with a minimum volume of 1 M acetic acid (99.5 %). The reaction was precipitated into methanol, collected via vacuum filtration and dried in an oven overnight at 60 °C.

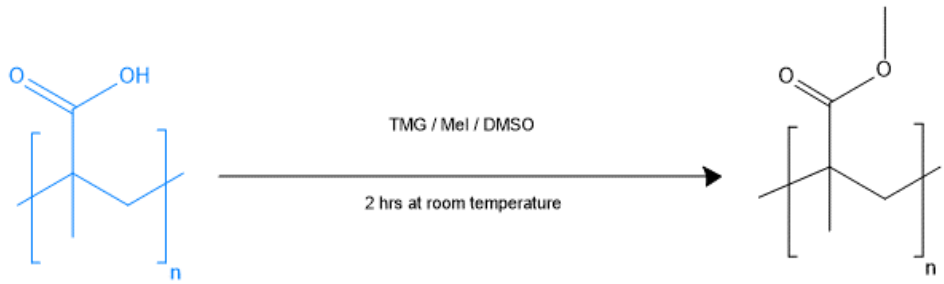

Scheme 2.5 – Esterification of PMAA to yield PMMA.

For molecular weight comparison, the diffusion coefficients of poly(methyl methacrylate) (PMMA) standards (Polymer laboratories Ltd) were conducted by DOSY NMR spectroscopy.

Table 2.4 – Molecular weights and measured diffusion coefficients in deuterated chloroform ($CDCl_3$) for PMMA standards, purchased from Polymer Laboratories Ltd.

Polymer Name	M_w/M_n	MW g/mol	D ($x10^{-10}$) m^2/s
PMMA 1	1.05	6500	3.60
PMMA 2	1.09	21600	1.10
PMMA 3	1.07	60000	1.00
PMMA 4	1.10	107000	0.62
PMMA 5	1.11	330000	0.29

2.1.9 LCST Determination

To measure the LCSTs of the polymers synthesised, 100 mM and 50 mM solutions in pH 7.2 (25 ^oC) potassium phosphate buffer (diluted from concentrate) were prepared. The approximate temperature range for the LCST of each polymer was determined by placing 5 mL of the sample into a glass vial and placing it on a IKA RET hotplate set to 35 °C. As the temperature of the sample within the vial increased, monitored by the hotplate contact thermometer, a visible change in the appearance of the sample from clear and colourless to cloudy could be observed.

In addition to visual determination of the approximate LCST range, UV/Vis Spectrophotometry, Dynamic Light Scattering and DOSY NMR Spectroscopy were used to determine the LCST of each polymer.

UV/Vis Spectrophotometry

1 mL of the 100 mM solution of each polymer was inserted into a quartz cuvette with a path length of 1 cm. Prior to sample analysis, a blank measurement of water was conducted on the spectrophotometer using the same cuvette. A measurement was also conducted prior to heating as a control. The cuvette containing the sample was then held in a water bath set

to 70 °C and remained there until the sample had equilibrated in temperature. Temperature was measured using a thermocouple probe. The cuvette was then returned to the spectrophotometer and the temperature probe was held in the top of the sample so as not to interfere with the absorbance measurements. Once the temperature of the sample had dropped to 40 °C measurements were taken at 1 degree intervals until the sample cooled to 28 °C. This measurement range was lowered for MMA-containing polymers.

Dynamic Light Scattering

1 mL of 50 mM polymer in solution was filtered through a Whatman GD/X PTFE syringe filter (0.45 μm pore size) and approximately 40 μL was charged to a Malvern ZEN0040 disposable cuvette. The cuvette was then inserted into the Zetasizer and a trend programme was conducted for analysis of the polymer LCST with 5 measurements taken at 1ºC intervals between 27 and 38 °C and an equilibration time of 120 s between each temperature. The temperature range was modified for MMA-containing polymers.

In the case of $PNIPAA_M$, 50 mM solutions of polymer in pH 4.0 (phthalate), pH 7.2 (phosphate) and pH 9.8 (borate) buffers (all Fisher Scientific) were also prepared. 40 μL of the solution was filtered and charged to a Malvern ZEN0040 disposable cuvette for analysis.

DOSY NMR Spectroscopy

As a final supporting method for LCST determination, polymers were solubilised in 1mL of deuterated water (D_2O) (99.8 %) to give a sample of 1 mM concentration for analysis. Measurements were taken at 1 °C intervals between 28 °C and 40 °C.

2.1.10 Effect of pH on Polymer Solubility

Four 50 mM solutions of each synthesised polymer were prepared in water. The solutions were then treated with hydrochloric acid (37 %) and sodium hydroxide (prepared from

pellets, ≥ 98 %) to prepare acidic solutions of pH 4 and 6 and basic solutions of pH 8 and 10 respectively. The pH was measured using a Mettler Toledo SevenCompact pH meter. The samples were briefly agitated and any changes in the solutions appearance were observed visually.

2.1.11 Thiolation of PMAA-containing Polymers

0.15 g (0.02 mmol / 1.74 unit mmol MAA) PMAA (Experiment 2.1.1) was charged to a clean 100 mL round bottomed flask containing 20 mL pH 7.2 (25 °C) phosphate buffer solution. 0.10 g (0.53 mmol) N-(3-dimethylaminopropyl)-N'-ethylcarbodiimide hydrochloride (EDAC) (≥ 98 %) and 0.06 g (0.53 mmol) N-hydroxysuccinimide (NHS) (98 %) were then added to the flask and the reaction was left to stir for 15 minutes. After this time, 0.06 g (0.53 mmol) cysteamine hydrochloride (C.HCl) (≥ 98 %) was charged to the reaction which was then sealed with parafilm to prevent contamination and left to stir for a further 24 hours at room temperature.

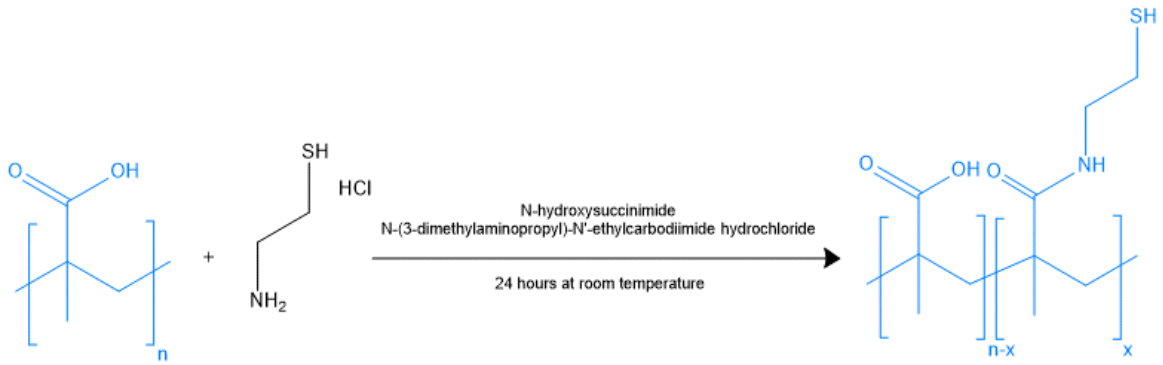

Scheme 2.6 – Thiolation of poly(methacrylic acid) with cysteamine hydrochloride to yield $PMAA_{SH}$ with x % functionalisation of carboxylic acid side chains.

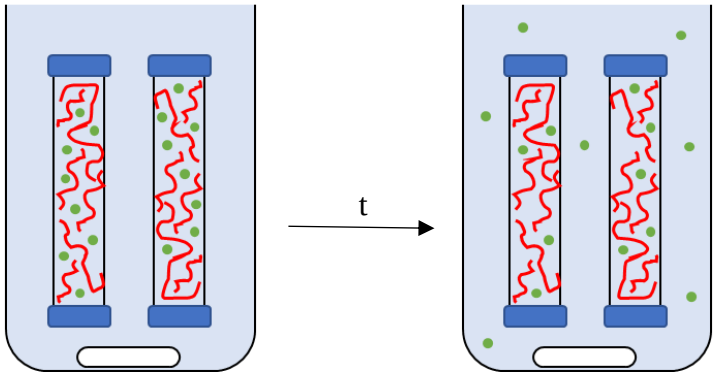

Figure 2.1 – Schematic of dialysation and the passage of small particles (green) (below the molecular weight cut off (MWCO) of the dialysis tubing) through the dialysis membrane into the bulk phase. Larger particles (red) above the MWCO are trapped within the tubing and the concentration of small impurities (green) within the tubing decreases with time, t.

Once complete, the reaction mixture was charged to lengths of dialysis tubing (Sigma Aldrich, benzoylated, 2000 MWCO) to wash the functionalised polymer by dialysation for four days (Figure 2.1). The bulk phase of deionised water was replaced hourly for the first three hours of dialysation, followed by every 10-12 hours to maintain a high concentration gradient. The polymer in solution was then transferred to small glass vials and frozen. The samples were then placed into a SP Scientific Benchtop Pro freeze dryer to dry the polymer by lyophilisation.

In all thiolation reactions of PMAA-containing polymers and block copolymers, the amount of MAA repeat units within the polymer were kept consistent at 1.74 unit mmol MAA. All other reaction conditions remained the same.

Table 2.5 – Thiolation of PMAA-containing polymers with cysteamine hydrochloride.

Polymer Name	Mass of Polymer / g	Polymer / mmol	MAA / unit mmol	C. HCl / g	C. HCl / mmol
$PMAA_{(100)}$	0.15	0.02	1.74	0.06	0.53
$PMAA_{(75)}$	0.15	0.02	1.74	0.06	0.53
$PMAA_{(50)}$	0.16	0.04	1.74	0.06	0.53
$PMAA_{(25)}$	0.16	0.07	1.74	0.06	0.53
$PMAA_{(100)}$-$PNIPAA_{M(100)}$	0.35	0.02	1.74	0.06	0.53
$PMAA_{(75)}$-$PNIPAA_{M(100)}$	0.42	0.02	1.74	0.06	0.53
$PMAA_{(50)}$-$PNIPAA_{M(100)}$	0.55	0.04	1.74	0.06	0.53
$PMAA_{(25)}$-$PNIPAA_{M(100)}$	0.95	0.07	1.74	0.06	0.53
$PMAA_{(100)}$-$PNIPAA_{M(100)}$-$PMAA_{(100)}$	0.25	0.01	1.74	0.06	0.53
$PMAA_{(75)}$-$PNIPAA_{M(100)}$-$PMAA_{(75)}$	0.28	0.01	1.74	0.06	0.53
$PMAA_{(50)}$-$PNIPAA_{M(100)}$-$PMAA_{(50)}$	0.35	0.02	1.74	0.06	0.53
$PMAA_{(25)}$-$PNIPAA_{M(100)}$-$PMAA_{(25)}$	0.55	0.03	1.74	0.06	0.53
$PMAA_{(100)}$-(MMA-co-$NIPAA_{M}$)	0.35	0.02	1.74	0.06	0.53

The thiolation experiment was also conducted using 0.48 g commercially available Poly(methacrylic acid sodium salt) solution (30 % wt. in H_2O, av. M_n approx. 5,400, av. M_w approx. 9,500 by GPC) and 20-80 mg (0.18-0.70 mmol) C. HCl to determine the effect of degree of functionalisation on microsphere morphology.

2.2 Chapter 4 - Sonochemical Microsphere Synthesis

Polymers prepared in Sections 2.1 were employed for the sonochemical preparation of polymeric microspheres. All commercial reagents were used as supplied unless otherwise stated.

2.2.1 Calibration of Ultrasound Horn by Calorimetry

100.00 g of deionised water was measured into a 150 mL beaker and the water was equilibrated to ambient room temperature. The 3 mm horn microtip was placed in the centre of the beaker at mid-depth and a thermocouple was submerged to the same depth, equidistant from the horn tip and beaker wall (Figure 2.2). The mass of water was then sonicated at an arbitrary power level for 5 minutes and the increase in temperature – as a result of dissipated heat from the horn tip – was monitored.

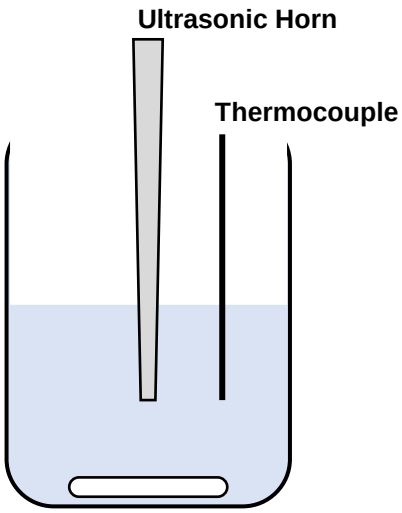

Figure 2.2 – Calorimetry experimental setup, with the thermocouple probe equidistant from the horn tip and the flask wall.

The intensity of power dissipated from the 3mm horn can be determined using Equation 2.1, whereby power output as a function of the horn tip surface area is calculated.

$$I = \frac{mc\delta T}{\delta t} / SA \quad (2.1)$$

Where I = intensity / Wcm^{-2}, m = mass / g, c = specific heat capacity of water (4.184 $J/g/K$[173]), T= temperature / K, t = time / s and SA = surface area of the horn tip / cm^2. The surface area of the 3 mm horn tip was calculated from the tip diameter, which was accurately measured by microscopy against a scale bar. Three measurements at each power value were taken, and an average power output and intensity calculated from these measurements. The calculated intensities are shown in Table 2.6 and the accompanying arbitrary power values were selected for all forthcoming sonochemical experiments unless otherwise stated.

The experiment was repeated using the 1 cm horn tip, the same experimental protocol was applied and the results can be seen in Table 2.7.

Table 2.6 - Calorimetry data measuring power dissipated from the ultrasonic generator with a 3 mm horn tip.

Power Level	Heat Generated / J	Power Output / W	Intensity / Wcm^{-2}	St. Dev. in Intensity
1	910 ± 20	3.03	43 ± 1	0.93
2	2128 ± 20	7.09	100 ± 1	0.93
3	3402 ± 34	11.34	160 ± 2	1.62
4	4634 ± 20	15.45	219 ± 1	0.93

Table 2.7 - Calorimetry data for power dissipated from the ultrasonic generator with a 1 cm horn tip.

Power Level	Heat Generated / J	Power Output / W	Intensity / Wcm^{-2}	St. Dev. in Intensity
1	2184 ± 34	7.28	9.2 ± 0.2	0.15
2	2982 ± 34	9.94	12.7 ± 0.2	0.15
3	4144 ± 40	13.81	17.6 ± 0.2	0.17
4	5348 ± 40	17.83	22.7 ± 0.2	0.17

2.2.2 Fricke Dosimetry

A 5 mmol dm^{-3} solution of iron (II) sulphate heptahydrate (≥ 99 %) in 5 mmol dm^{-3} sulphuric acid (diluted from concentrate ≥ 99.9 %) was prepared in a 1 L volumetric flask. A sample was taken for analysis by UV/Vis Spectroscopy and charged to a 1 cm quartz cuvette. 100 mL of the dosimeter was then charged to a clean dry 150 mL jacketed flask with a constant flow of water to maintain a constant temperature of 21.2 ± 0.8 ºC. The ultrasound horn tip was placed into the centre of the water within the flask, and a thermocouple probe was placed at the same depth, equidistant from the horn tip and the side of the flask (Figure 2.3). Prior to sonication a sample was removed for analysis by UV/Vis Spectroscopy. The sample was sonicated for 5 minutes, after which time a sample was removed from the reaction vessel for analysis by UV/Vis Spectroscopy. The sample was returned to the vessel after each measurement to maintain a constant reaction volume. The dosimeter was sonicated for a total of 60 minutes in 5 minute intervals and a change in absorbance was monitored by UV/Vis Spectroscopy.

To quantify the concentration of oxidising radicals produced by the dosimeter, solutions of known known iron (III) chloride hexahydrate (Fe^{3+}) concentrations were prepared (Figure 2.4) and a graph of the measured absorbance with increasing concentration at 295 nm was plotted. Application of the Beer-Lambert law (Equation (2.2)) enables the determination of the molar extinction coefficient, ε = 381.08 mol dm^3 cm^{-1} at 295 nm.

$$A = \varepsilon c l \tag{2.2}$$

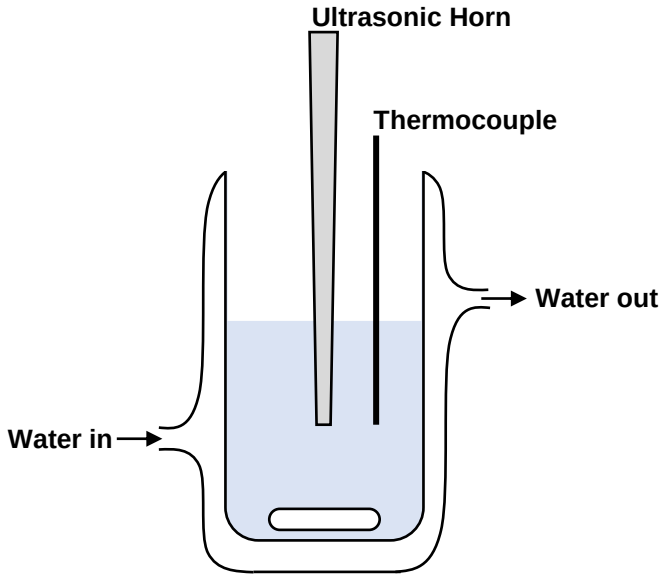

Figure 2.3 – Fricke dosimeter experimental setup, with the thermocouple probe equidistant from the horn tip and the wall of the jacketed flask.

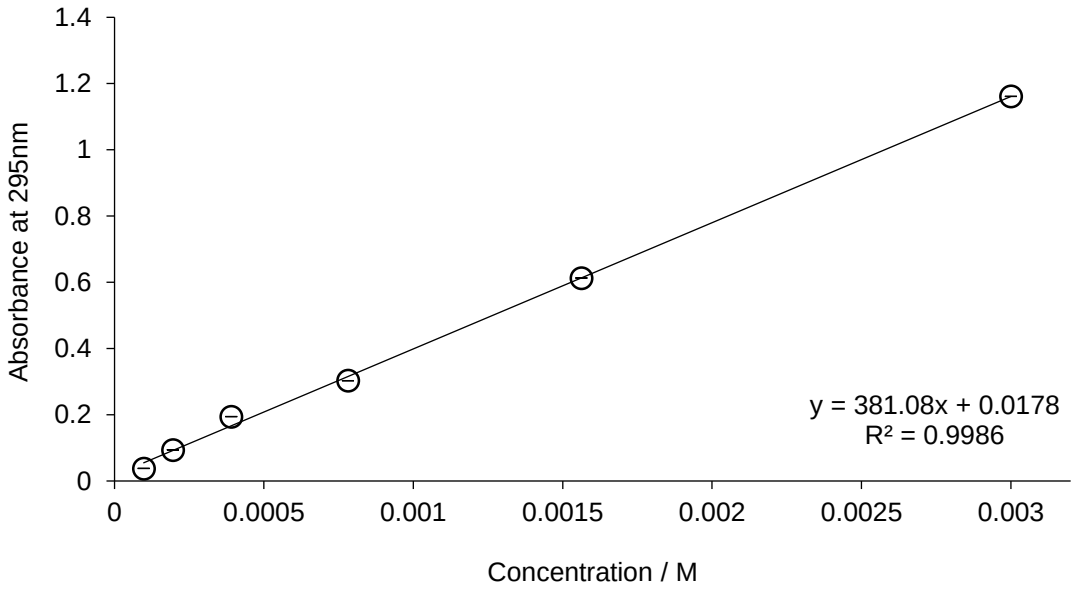

Figure 2.4 – Beer-Lambert plot for Fe^{3+} at increasing concentrations (Wavelength = 295 nm). Measurements were conducted in triplicate.

2.2.3 Air-filled Lysozyme Microbubbles

0.05 mg of lysozyme (from chicken egg white, ≥ 90%) was solubilised by agitation in 1 mL pH 8 tris acetate buffer (diluted from concentrate) in a 15 mL centrifuge tube and left to stand for 1 hour. Following this, 0.03 mg DL-dithiothreitol (DTT) (≥ 99 %) was added and the mixture was lightly agitated for 2 minutes at ambient room temperature. The 3 mm horn tip was placed at the air:water interface and the reaction mixture was sonicated at a chosen power output for between 10 and 60 s.

Once sonicated, the sample was made up to 14 mL in the centrifuge tube with deionised water and the sample was left to stand overnight to allow the microspheres to settle at the top of the tube.

2.2.4 Tetradecane-filled Lysozyme Microspheres

0.05 g of lysozyme was accurately weighed and charged to 1 mL pH 8 tris acetate buffer in a 15 mL centrifuge tube. The tube was left to stand for 1 hour, after which time 0.03 g DTT was added. During the two minutes prior to sonication, 100 μL tetradecane (≥ 99%) was deposited on top of the aqueous layer using a Finnpipette™. The 3 mm horn tip was placed at the oil:water interface and the reaction mixture was sonicated at a chosen power output for between 10 and 60 s. Samples were then made up to 14 mL with deionised water and left to stand overnight.

2.2.5 Oil-filled Polymeric Microspheres

For each experiment conducted, the concentration of thiolated poly(methacrylic acid) within the polymeric and block copolymer solutions was maintained at 5 mg (PMAA) / mL in an effort to minimise variables by keeping the number of thiol units in each sample consistent. The preparation of 5 mg (PMAA) / mL $PMAA_{SH(100)}$ in pH 8 tris acetate buffer is described as an example.

10.20 mg (1.2 x 10^{-3} mmol) of $PMAA_{SH(100)}$ was charged to 2 mL pH 8 tris acetate buffer in a 15 mL plastic centrifuge tube. Once fully solubilised overnight, 100 μL tetradecane was deposited onto the aqueous layer and the 3mm horn tip was placed at the oil:water interface. The sample was sonicated at a chosen power output for between 10 and 300 s.

In addition to the use of thiolated polymers, the synthesis of microspheres employing non-thiolated shell species was attempted. 5 mg (PMAA) /mL solutions of non-functionalised polymer in pH 8 tris acetate buffer were sonicated with 100 μL tetradecane as described above. In the case of $PNIPAA_M$ and MMA-co-$NIPAA_M$, 5 mg / mL of each polymer was employed.

To facilitate analysis by LSCM, experiments were repeated encapsulating Nile Red-saturated tetradecane (technical grade), and to enable analysis by UV/Vis spectroscopy, microspheres containing Sudan III-saturated tetradecane (Sigma Aldrich) were prepared as outlined above. To prepare the fluorescent-labelled tetradecane liquids, saturated solutions were prepared, followed by using a Whatman GD/X PTFE syringe filter (0.45 μm pore size) syringe filter.

Experiments were also repeated for the encapsulation of non-aqueous tetradecafluorohexane (PFH), soybean oil and vegetable oil (Sainsbury's), conducted at 100 Wcm^{-2} for 60 s.

2.2.6 Optimisation of Water-in-Tetradecane Emulsions

Water-in-tetradecane emulsions with Span 80® nonionic surfactant were prepared via sonochemical agitation for encapsulation within polymeric microspheres. In order to produce a stable emulsion suitable for encapsulation, a range of experiments were conducted to optimise the conditions. Variables included the concentration of sodium chloride (99 %) in the aqueous phase, modifying the ratio of the aqueous to oil phases, adjusting the percentage of Span 80® solubilised in tetradecane, and altering the sonication power and time during synthesis.

A chosen wt % Span 80® was solubilised in a volume of tetradecane. A total of 1 mL of aqueous and oil phase media was charged to a 15 mL centrifuge tube, the 3 mm horn tip of

the sonicator was placed at the oil:aq interface and the sample was sonicated at a chosen power output for between 10 and 900 s. To avoid overheating, the centrifuge tube was suspended in an ice bath during sonication.

The optimised conditions are as follows: 4 w/w % Span 80® in tetradecane, a 40:60 ratio of 1 M NaCl $_{(aq)}$:oil phase, with a sonication time / power of 60 s and 100 Wcm^{-2}.

Experiments varying the surfactant concentration were also conducted for the optimisation of 1M NaCl-in-olive oil (Sigma Aldrich) emulsions, stabilised with Span 20® non-ionic surfactant (Sigma Aldrich). The optimised conditions are as follows: 5 w/w % Span 20® in olive oil and a 10:90 ratio of 1 M NaCl $_{(aq)}$:oil phase, all other conditions were consistent with water-in-tetradecane emulsions.

2.2.7 Dynamic Light Scattering of Emulsions

A sample of prepared emulsion was diluted ten-fold into bulk 4 w/w % Span 80®-in-tetradecane, matching the continuous phase of the initial emulsion, to achieve a final aqueous fraction of 4 w/w % in tetradecane.

0.80 mL of the diluted sample was then charged to a 3.50 mL quartz cuvette via a syringe adapted with a Whatman GD/X PTFE syringe filter (0.45 µm pore size) to remove impurities and dust from the sample. Scattering measurements were conducted at 25 ºC with a 120 s equilibration time and five measurements were recorded for each sample.

2.2.8 Monitoring the Phase Separation of Emulsions

Emulsion samples were prepared as per the experimental protocol in Experiment 2.2.6 with increasing aq:tetradecane ratios between 10 and 50 % and increasing Span 80® concentrations between 0 and 6 %. The emulsions were sonicated at 100 Wcm^{-2} for 5 minutes and any observed partitioning of the aqueous phase was measured after 24 hours by extraction of the phase-separated aqueous layer.

2.2.9 Water-in-Tetradecane Emulsion-filled Microspheres

2 mL of 5 mg (PMAA) / mL chosen thiolated polymer in pH 8 tris acetate buffer was prepared in a 15 mL plastic centrifuge tube as in Experiment 2.2.5. Once fully solubilised overnight, 100 µL freshly prepared emulsion (Experiment 2.2.6) was deposited onto the aqueous layer and the microspheres were prepared as described in Experiment 2.2.5.

The experiment was repeated with fluorescent labels for analysis by LSCM to confirm encapsulation of both the aqueous and lypophilic phases. Nile Red®-soaked tetradecane was employed as an alternative oil phase and 5,6-carboxyfluorescein (≥ 97 %) was charged to 1M NaCl $_{(aq)}$ for use as the alternative aqueous phase.

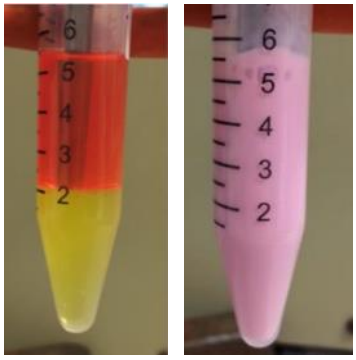

Figure 2.5 – 5,6-carboxyfluorescein-labelled 1M NaCl $_{(aq)}$ (yellow) and Nile Red®-labelled tetradecane (red) prior to sonication with the 3 mm horn tip at the oil:water interface (left) and after sonication at 100 Wcm^{-2} for 60 s (right).

Experiments were also conducted for the encapsulation of 1M NaCl-in-olive oil emulsions. 100 µL of the emulsion (Experiment 2.2.6) was deposited onto the aqueous buffer phase, and the sample was sonicated at 100 Wcm^{-2} for 30 s. The experiment was repeated with 5,6-carboxyfluorescein-saturated 1M NaCl for analysis by laser scanning confocal microscopy.

2.2.10 Microsphere Synthesis in the Absence of Oxygen

A sample of thiolated polymer in buffer with 100 μL tetradecane was prepared as per Experiment 2.2.5. Prior to sonication, the horn was placed at the oil:water interface, the horn and tube were sealed with Parafilm® to exclude oxygen and the reaction was purged by bubbling nitrogen via a syringe inlet and outlet for ten minutes. Approximately two minutes prior to sonication the syringe was lifted out of the liquid to allow the two phases to re-equilibrate and the nitrogen continued to flow gently over the top of the reaction mixture. The reaction was sonicated at 100 Wcm^{-2} for 60 s and the sample was made up to 14 mL with deionised water.

2.2.11 Tert-butanol Radical Trapping

Lysozyme and $PMAA_{SH}$ microspheres were prepared as described in Experiments 2.2.4 and 2.2.5 respectively. Immediately prior to sonication, between 10-200 μL tert-butanol was charged to the reactions and the samples were sonicated at 100 Wcm^{-2} for 60 s. The samples were made up to 14 mL in the centrifuge tube with deionised water.

2.2.12 The Effect of Sonication on Polymer Morphology

2 mL of 5 mg (PMAA) /mL non-functionalised polymers in pH 8 tris acetate buffer were sonicated in the absence of an encapsulant at 100 Wcm^{-2} for 60 s. Samples were then dried in an oven and the dried polymer was analysed by FT-IR spectroscopy.

2.3 Chapter 5 - Encapsulation and Release

Experiments were conducted in order to quantify the encapsulation efficiency of tetradecane-filled microspheres and release behaviour of synthetic polymeric-shelled microspheres prepared in Section 2.2.

2.3.1 Microscopy

To facilitate the analysis of the microsphere sizes and sample size distribution by optical microscopy, a small volume of washed microspheres was removed from the top fraction of the sample tube and placed onto a glass microscope slide. The droplet was covered by a glass coverslip and the sample was imaged and analysed using ImageJ processing software.

In order to determine successful encapsulation by observed fluorophore-loading 0.3 mL of microsphere dispersion was removed from the top fraction of microsphere samples prepared in Section 2.2, diluted in 3 mL deionised water and left to stand for 1 hour. A small volume of microspheres was once again removed from the top fraction of the diluted sample and placed onto a glass microscope slide. A glass coverslip was placed onto the droplet, the samples was then sealed and imaged by LCSM.

Temperature-dependent release from stimuli-responsive microspheres was also analysed by both optical and confocal microscopy.

2.3.2 Encapsulation Efficiency

Sudan III-saturated tetradecane-filled polymeric microspheres were prepared as described in Experiment 2.2.5. Once synthesised, a layer of 2 mL isopropyl myristate (IPM) was deposited onto the undiluted microsphere emulsion. The reaction was manually agitated to partition unencapsulated Sudan III-soaked tetradecane into the IPM layer.

UV/Vis spectroscopy was used as a technique to determine the percentage of tetradecane encapsulated within microspheres, relative to a control sample of 0 % encapsulation. The concentrations of Sudan III present in the IPM phase during encapsulation efficiency and release experiments were quantified by comparison against the linear calibration of Sudan III absorbance standards in IPM at a chosen wavelength of 480 nm. The released concentration can be determined from Equation 2.2, where $\varepsilon = 0.0267$ μmol dm^3 cm^{-1} (Figure 2.6).

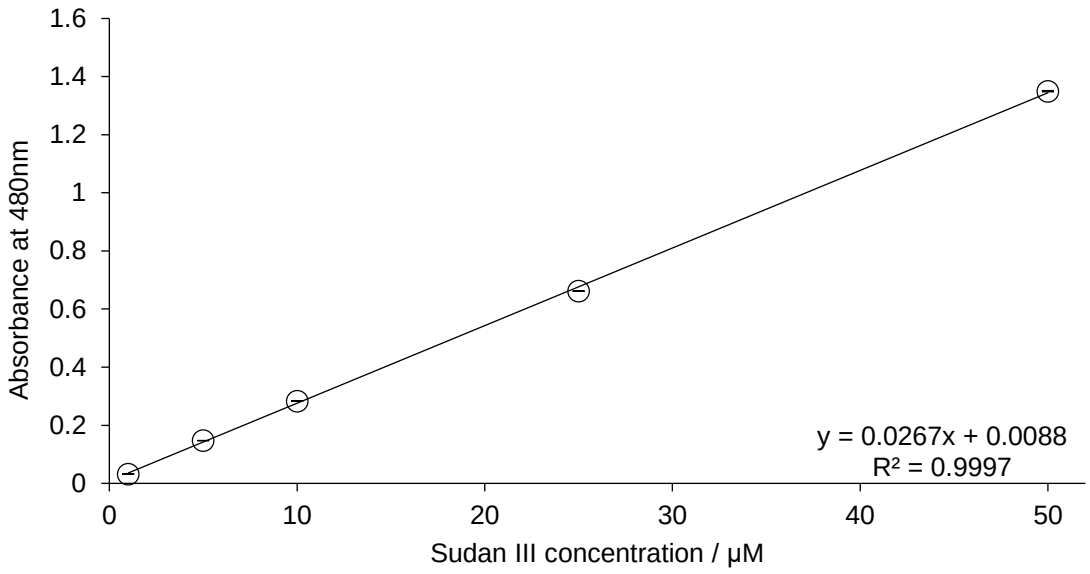

Figure 2.6 – Absorbance calibration plot for Sudan III in Isopropyl Myristate at increasing concentration (Wavelength = 480 nm). Measurements were conducted in triplicate.

2.3.3 Breakdown of Microspheres by Sonication

Undiluted microsphere samples were subjected to sonochemical disruption for 5 minutes at 219 Wcm^{-2}. 2 mL IPM was then deposited onto the dispersion and the samples were gently agitated. After equilibration of the two phases, a sample was taken from the IPM layer for analysis by UV/Vis spectrophotometry.

2.3.4 Breakdown of Microspheres by pH Modification

Sudan III-saturated tetradecane-filled microspheres were synthesised as per the method outlined in Experiment 2.2.5. After synthesis, the undiluted microsphere samples were either acidified to pH 1 by the addition of HCl or alkalised to pH 13 by NaOH. Samples were then left to incubate at room temperature for one hour, after which time UV/Vis analysis of released encapsulant into 2 mL IPM was conducted as previously described. Where possible, samples were also examined by optical microscopy.

2.3.5 Breakdown of Microspheres by DTT

Sudan III-saturated tetradecane-filled microspheres were treated with 0.12 g DTT and manually agitated. Samples were examined by optical microscopy after 1 hour and 24 hours. Microspheres were prepared as previously described, after which time 0.12 g DTT was charged to the undiluted microsphere sample and the sample was manually agitated. 2 mL IPM was deposited onto the microsphere phase, and DTT-triggered release was observed by release of Sudan III-soaked tetradecane into IPM.

2.3.6 Sudan III Release from Thermoresponsive Microspheres

Sudan III-soaked tetradecane-filled microspheres were prepared as previously described and layered with 2 mL IPM. An absorbance measurement was recorded prior to heating to negate unencapsulated tetradecane from the release measurement. The sample was then heated beyond the LCST of the particular microsphere system and left to incubate for 24 hours, after which time samples were gently agitated to ensure complete partitioning of any released tetradecane into the IPM layer. Aliquots were then drawn from the IPM layer to observe the temperature-triggered release of tetradecane from the prepared microspheres. After analysis, the aliquot was returned to the sample to maintain a constant IPM volume. Samples were left to incubate for a further 24 hours, and the analytical process was repeated.

2.3.7 NaCl Release from Thermoresponsive Microspheres

Emulsion-filled microspheres were prepared as detailed in Experiment 2.2.9, substituting a 5M NaCl solution for the 1M NaCl aqueous phase. After sonication, the undiluted microsphere dispersions (2 mL) were transferred into two 1.5 mL microcuvettes containing a dialysis membrane window (Sigma Aldrich, benzoylated, 2000 MWCO), which were then inserted into 50 mL centrifuge tubes containing 20 mL deionised water. The samples were heated to 40 ºC in a water bath and conductivity measurements were taken from the bulk deionised water using a Mettler Toledo SevenCompact conductivity meter. As a control, the conductivity of samples stored at room temperature for 48 hours were also measured, and the difference in sample conductivity of the bulk solution as a function of heating was calculated. A sample of 100 µL 40:60 5M NaCl-in-tetradecane emulsion with 2 mL pH 8 tris acetate buffer in two 1 mL microcuvettes, stored at 40 ºC for 48 hours, was employed as a control to mimic 100 % release. The conductivity of 2 mL pH 8 tris acetate buffer in 20 mL deionised water was measured as a second control. A calibration graph of measured conductivity with increasing NaCl concentration is shown in Figure 2.7.

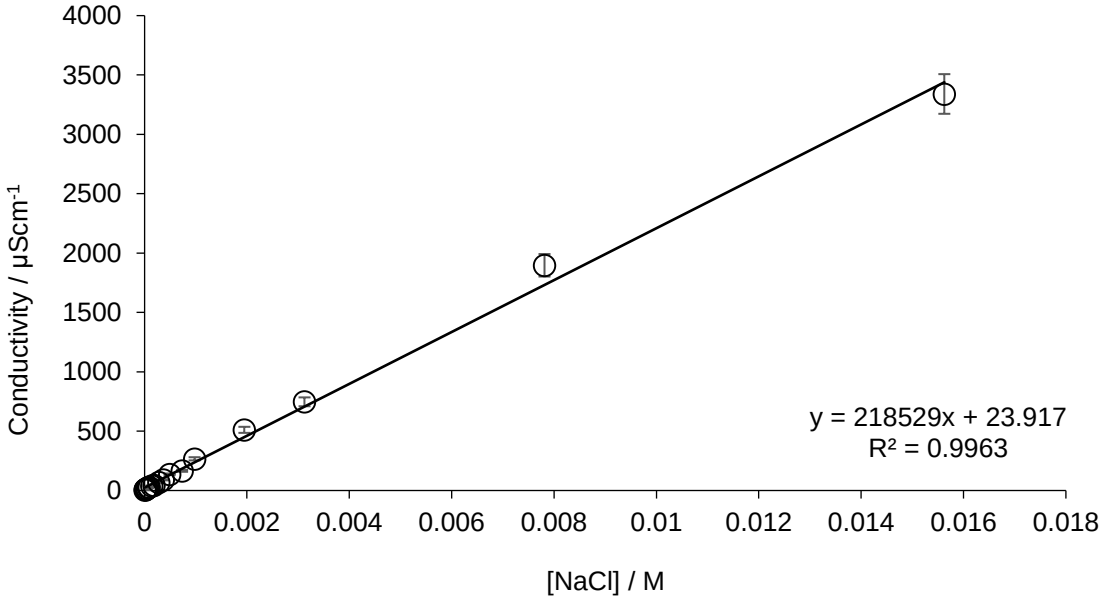

Figure 2.7 – Calibration plot for NaCl in deionised water. Measurements were conducted in triplicate.

3 RAFT Polymerisation

Reversible Addition-Fragmentation Chain Transfer polymerisation, or RAFT, is a well-established "living polymerisation" technique for the synthesis of well-defined polymers with controlled molecular weights and narrow polydispersities. Moad *et al.*[124] were the first to discover this technique in 1998, and many have since adopted and adapted the protocol[125] due to its compatibility with a range of different monomers and varying reaction conditions. This chapter reports the synthesis of biocompatible polymers and block copolymers, incorporating thermoresponsive poly(N-isopropylacrylamide) and LCST-modified MMA-NIPAA$_M$, for use as shell species in the sonochemical synthesis of novel thermoresponsive polymeric microspheres as smart delivery vehicles.

3.1 Poly(methacrylic acid) (PMAA)

Poly(methacrylic acid) of varying chain lengths was synthesised using the protocol outlined in Experiment 2.1.1 (Scheme 2.1). The reaction progress was monitored by NMR in order to establish the rate of reaction. The PMAA synthesised was then functionalised for microsphere synthesis or employed as a macroRAFT agent in the synthesis of di- and triblock copolymers for use as microsphere shells.

^{1}H NMR spectra of each of the final PMAA products (Figure 3.1) reveal a characteristic peak at 1.0-1.3 ppm (a) corresponding to the methyl group of the polymer backbone and another at 1.7-2.2 ppm representative of the CH_2 group in the polymer backbone (b). Integration of these peaks confirms a 2:3 ratio of the two hydrogen environments, as expected[174,154]. The absence of vinylic signals at 5.7 ppm and 6.2 ppm indicates high conversion and an absence of any residual monomer in the isolated product. It was not possible to confirm the presence of RAFT agent end groups by proton NMR, the spectrum of which possesses a peak at 3.3 ppm corresponding to the methylene group adjacent to the dithiocarbonate (c). Upon polymerisation, the R leaving group containing the methylene functionality reinitiates polymerisation, becoming a chain end group bound to the methylene group of the methacrylic acid monomer, therefore a shift in the signal to within

the regions of the MAA CH_2 group may be observed. Propionic acid (CH_3CH_2COOH) possesses a CH_2 group in proximity to a carboxylic acid functionality, analogous to that of the CMDB R end group. Spectra of propionic acid in the literature[175,176] show the methylene signal appearing between 2.1-2.4 ppm. Due to the very low signal intensity relative to those corresponding to MAA repeat units, the RAFT agent signals were not clearly visible, however it is possible that the asymmetric hump on the left-hand side of the polymer methylene signal may correspond to the small RAFT agent peak. Polymers were dried in an oven once isolated to remove solvent and anti-solvent traces, however some remnants of solvent impurities are indicated in the spectrum.

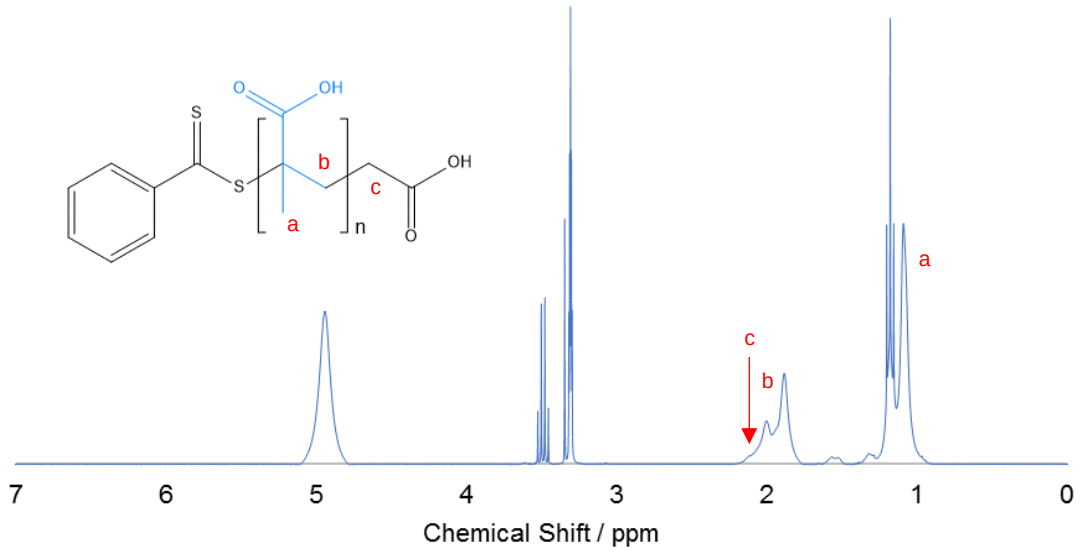

Figure 3.1- 1H NMR of Poly(methacrylic acid) in deuterated methanol (MeOD) (1 mM). a – CH_3 in PMAA backbone, b – CH_2 in PMAA backbone, c – CH_2 adjacent to dithiocarbonate of end group.

Due to the low target molecular weights of PMAA homopolymers synthesised during this project (no greater than 9 kDa), CMDB was deemed the more suitable RAFT agent. Yang and Cheng[151] demonstrated the compatibility of CMDB with both MAA and $NIPAA_M$ monomers, yielding homopolymers and block copolymers with narrow molecular weight dispersities of less than 1.5. The undesirable dithiobenzoic acid formation upon polymerisation of MAA with CPADB, observed by Nejad *et al.*[153], was more significant when synthesising polymers of low molecular weight due to the increased [CPADB]:[MAA] ratio, therefore was deemed less suitable. Yang and Cheng[151] reported

no undesirable side reactions and this was also evident in the size exclusion chromatographs, which indicated no secondary peaks[151].

Table 3.1 – Conversion and rate values for PMAA, synthesised with CMDB RAFT agent and ACP.

Polymer Name	Conversion % (NMR)	Rate Constant k_p (10^{-6}) / s^{-1}	Reaction Rate Rp (10^{-6}) / Ms^{-1}
$PMAA_{(100)}$	90 ± 2	27 ± 2	2.9 ± 0.2
$PMAA_{(75)}$	92 ± 3	27 ± 2	2.2 ± 0.2
$PMAA_{(50)}$	91 ± 2	27 ± 2	1.4 ± 0.1
$PMAA_{(25)}$	91 ± 1	28 ± 1	0.7 ± 0.0

Table 3.1 outlines the conversion data for PMAA homopolymers, synthesised with various target chain lengths. The percentage conversion for each polymer was calculated from the ^{1}H NMR integral peak heights corresponding to MAA monomer vinylic signals at t=24 hr and t=0 hr. The rate constants, k_p, and rate, R_p, were determined from application of Equations 3.1 and 3.2 to the conversion graphs. A linear conversion as a function of time implies first order kinetics[141], indicating that the concentration of the propagating radical, [P*], remains constant during the reaction.

$$R_p = -\frac{d[M]}{dt} = k_p[P*][M] \quad (3.1)$$

$$\ln\frac{[M]_0}{[M]} = k_p[P*]t = k_p^{add}t \quad (3.2)$$

Comparison of the reaction rate data reveals an increase in rate with increasing [MAA]:[CMDB] ratio, as observed by Pelet and Putnam[152] during the synthesis of high molecular weight PMAA polymers by RAFT polymerisation. The rate constants for PMAA homopolymers remained consistent between samples, contrary to the observed increase with decreasing molecular weight reported by Pelet and Putnam. However, the rate constant is dependent on mechanistic conditions such as temperature and therefore should remain constant between samples conducted under the same reaction conditions. Figure 3.2 shows the conversion of monomer to polymer for $PMAA_{(100)}$. A percentage

conversion of 90 % after 24 hours was calculated using Equation 3.3. Integral heights of the monomer peaks at 5.7 and 6.2 ppm were measured to monitor the conversion of monomer as a function of time. Due to the linear conversion observed, the rate constant of $PMAA_{(100)}$ was therefore calculated from the slope of the graph to be $k_p = 0.0956\ h^{-1} = 2.7 \times 10^{-5} \pm 0.2\ s^{-1}$ from which the rate was calculated as $R_p = 2.9 \times 10^{-6} \pm 0.2\ Ms^{-1}$.

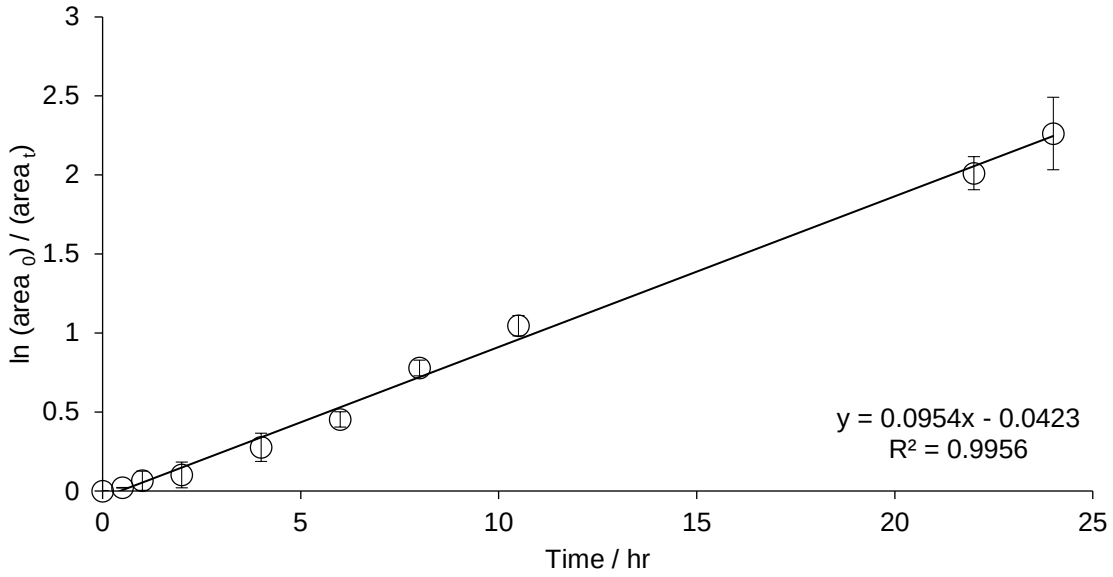

Figure 3.2 – $PMAA_{(100)}$ NMR conversion monitored by change in monomer integral area as a function of time (1 mM in MeOD). Experiments were conducted in triplicate.

$$\% \text{ Conversion} = 100 - \left[\left(\frac{\text{M height}_t}{\text{M height}_0}\right) \times 100\right] \quad (3.3)$$

If the chosen RAFT agent does not behave optimally, modifying other conditions such as initiator concentration and reaction time can go some way to compensate for this. Due to the reported slow fragmentation of the RAFT agent[151], a ratio of 1:0.20 [CMDB]:[ACP] was chosen to minimise the initiator-derived chains whilst not greatly inhibiting reaction progress. An extended reaction time of up to 24 hours was employed to improve the conversion whilst achieving greater control[151].

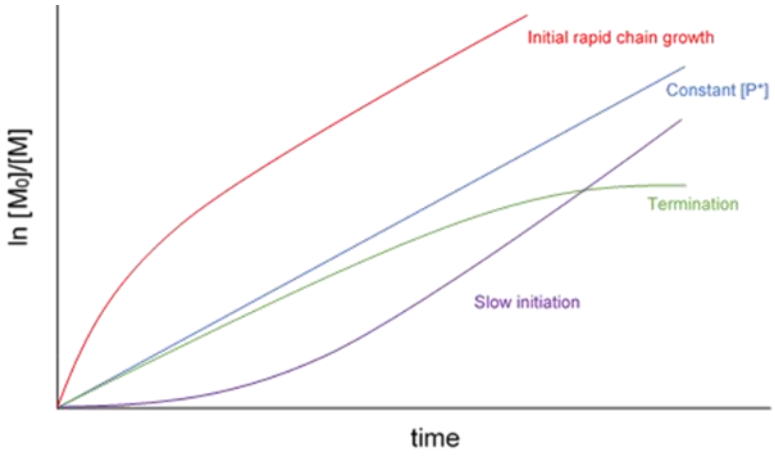

Figure 3.3 – The dependence of monomer concentration on time.

Monitoring the loss of monomer does not directly reveal whether the reaction was initially propagated from initiator-derived chains or RAFT-mediated chain growth, but the linear relationship between loss of monomer peak height with time would suggest that, contrary to the observations of Yang and Cheng[151], the reaction did not demonstrate rapid monomer consumption via initiator-mediated polymerisation (Figure 3.3). This demonstrates good compatibility between the RAFT agent and monomer.

Diffusion-Ordered NMR Spectroscopy (DOSY) was used to determine whether polymerisation of homo and block copolymers synthesised via RAFT polymerisation was successful. DOSY separates the NMR signals of different species within a sample depending on the diffusion coefficient of the sample through the medium[177]. Molecules are "spatially labelled"[178], then measured again after diffusion time Δ to determine the velocity of their motion through the solvent medium; this is known as pulsed field gradient NMR spectroscopy. A diffusion profile is obtained by increasing the magnitude of the field gradient (g), leading to faster molecular diffusion and reduced signal strength. Smaller molecules move faster, leading to faster attenuation and greater loss of signal intensity. Equation 3.4 shows the relationship between peak intensity (I), and diffusion coefficient (D), where γ is the gyromagnetic constant of the nucleus under observation and δ represents the gradient duration. Once plotted, the slope of $\ln(I/I_0)$ against g^2 affords the diffusion coefficient, D for the molecule.

$$I = I_0 e^{-D\gamma^2 g^2 \delta^2 \left(\Delta - \frac{\delta}{3}\right)} \quad (3.4)$$

Smaller molecules, such as residual monomer or solvents, will diffuse through the medium much faster than larger molecules, and the spectral pattern of the DOSY spectrum will show distinct regions at different diffusion coefficients. Secondary spectral signals within the region of polymeric diffusion coefficient values, on the other hand, can indicate polydispersity, indicative of some initiator-derived chains as well as RAFT-derived chains.

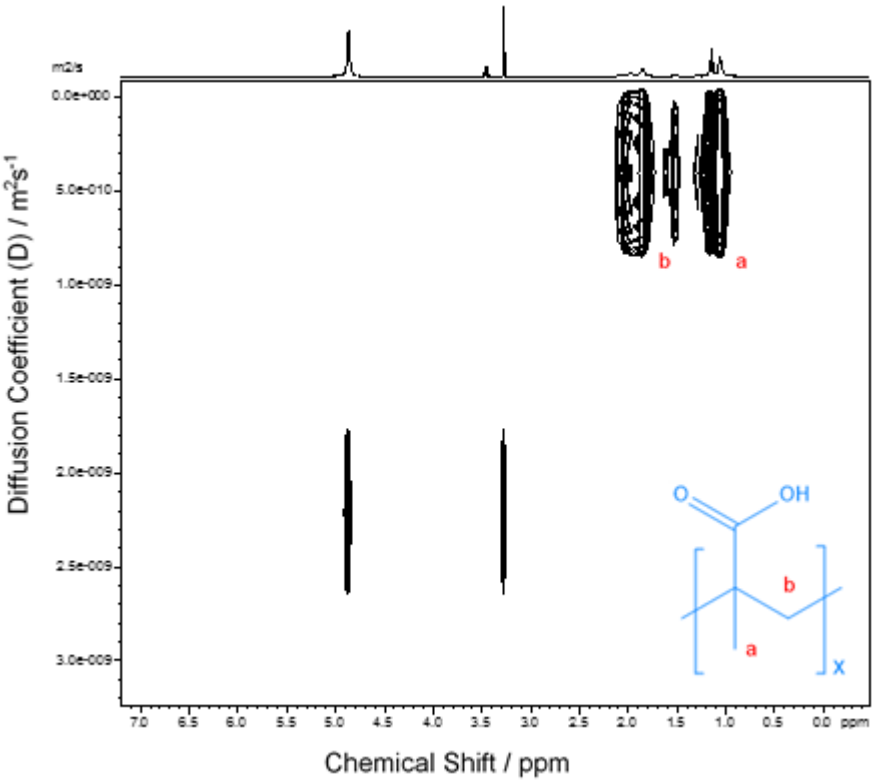

Figure 3.4 – DOSY NMR Spectrum of $PMAA_{(100)}$ in MeOD (1 mM).

The DOSY NMR spectrum of $PMAA_{(100)}$ is shown in Figure 3.4. There is a distinct signal at 1.0-2.3 ppm, characteristic of PMAA ^{1}H NMR signals. The absence of diffusion peaks at 5.7 and 6.2 ppm indicates that no residual monomer is present in the final product and the spectral patterns at 3.3 and 5.0 ppm correspond to the deuterated methanol solvent. The diffusion coefficient (D) for the polymer is 4.8 x 10^{-10} m^2s^{-1}. Comparison of the natural log of homopolymer diffusion coefficients with increasing molecular weight reveal a linear relationship whereby ln(D) is inversely proportional to $\ln(MW_{PMAA})$, as expected, and can

be seen in Figure 3.25. The linear relationship is also indicative of a controlled system whereby modification of the [M]:[CTA] ratio generates polymers of varying molecular weights with controlled architectures.

In order to approximate the molecular weight of poly(methacrylic acid) homopolymers synthesised during the course of this project, the diffusion coefficients of esterified polymers (Experiment 2.1.8) were compared against those of commercially available standards, as shown in Figure 3.5. Assuming complete esterification, as reported by Li *et al.*[179], diffusion coefficients of the synthesised PMMA polymers were first fitted to the slope of analytical standards to approximate their molecular weights. The degree of polymerisation (DP) was then determined by deducting the molecular weight of CMBD and applying Equation 3.5, whereby MW_{PMMA} is the measured molecular weight of PMMA and M_0 is the molecular weight of the monomer MMA. It was then possible to approximate the molecular weight of the PMAA polymers by multiplying the degree of polymerisation by the molecular weight of MAA monomer.

$$\mathrm{DP} = \frac{\mathrm{MW_{PMMA}}}{\mathrm{M_0}} \qquad (3.5)$$

The measured molecular weights in Table 3.2 are largely comparable to the calculated target molecular weights for the homopolymers, the biggest deviation occurring for $PMAA_{(100)}$. It demonstrates a linear dependence on [MAA]:[CMDB] and that it is possible to control the molecular weight by modifying the concentration of monomer relative to the RAFT agent concentration. It also demonstrates the viability of comparative DOSY NMR as a technique to approximate the degree of polymerisation of PMAA in the absence of techniques such as GPC.

GPC may provide a more comprehensive analysis of the reaction conversion and differentiation between calculated and experimental number average molecular weight (M_n) values, however the tetrahydrofuran (THF) solvent system used in the available GPC equipment at the University does not facilitate the analysis of PMAA and its block copolymers.

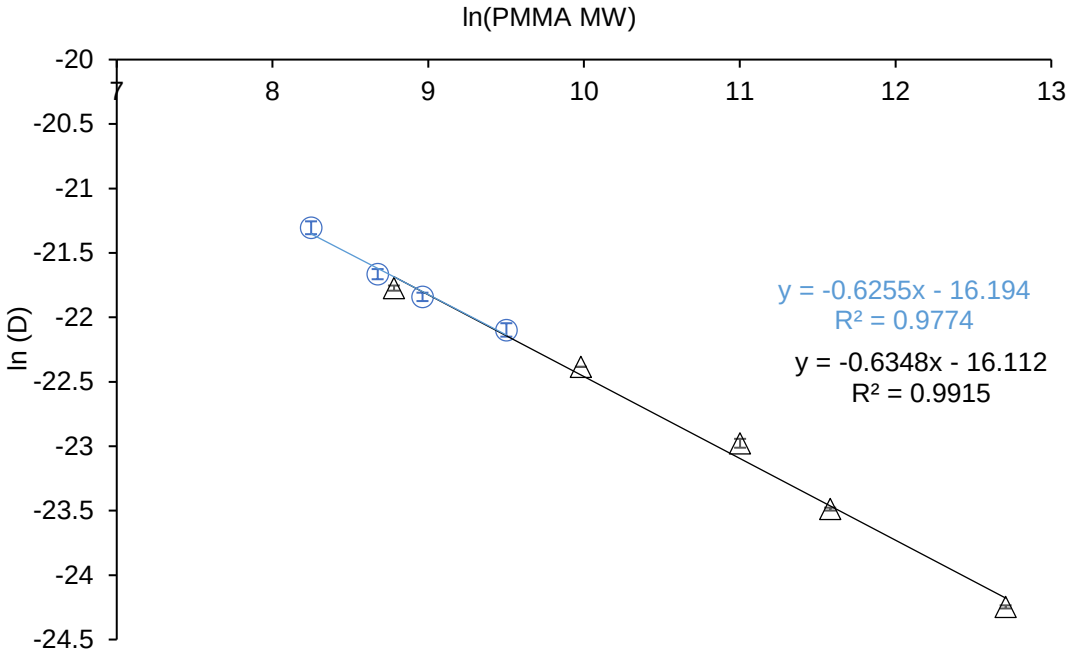

Figure 3.5 – The diffusion coefficients of synthesised PMMA (blue) (esterified PMAA) and PMMA standards (black). Measurements were conducted in triplicate.

Table 3.2 – Diffusion coefficient data for PMMA, synthesised from PMAA homopolymers, and calculation of PMAA molecular weight from PMMA molecular weight.

Polymer Name	D_{PMAA} / x10^{-10} m^{2}s^{-1}	D_{PMMA} / x10^{-10} m^{2}s^{-1}	MW PMMA (NMR)	DP	PMAA MW (NMR)	PMAA MW (calc.)
$PMAA_{(100)}$	2.9	2.5	13400 ± 900	131 ± 9	11500 ± 800	8821.29
$PMAA_{(75)}$	3.6	3.3	7700 ± 400	76 ± 5	6600 ± 300	6669.04
$PMAA_{(50)}$	5.1	3.9	5800 ± 400	56 ± 4	5000 ± 300	4516.79
$PMAA_{(25)}$	7.4	5.6	3800 ± 300	36 ± 2	3200 ± 250	2364.54

3.2 Poly(N-isopropylacrylamide) (PNIPAA$_M$)

Poly(N-isopropylacrylamide) (PNIPAA$_M$) was synthesised, as per the experimental protocol outlined in Experiment 2.1.2 (Scheme 2.2), to determine the stimuli-responsive behaviour of the polymer prior to incorporation within PMAA-based block copolymers. Conversion of the monomer after 64 hours was calculated as 85 ± 3 % from integration of the depleting monomer peaks at 5.7 ppm and 6.2 ppm against time (Figure 3.6).

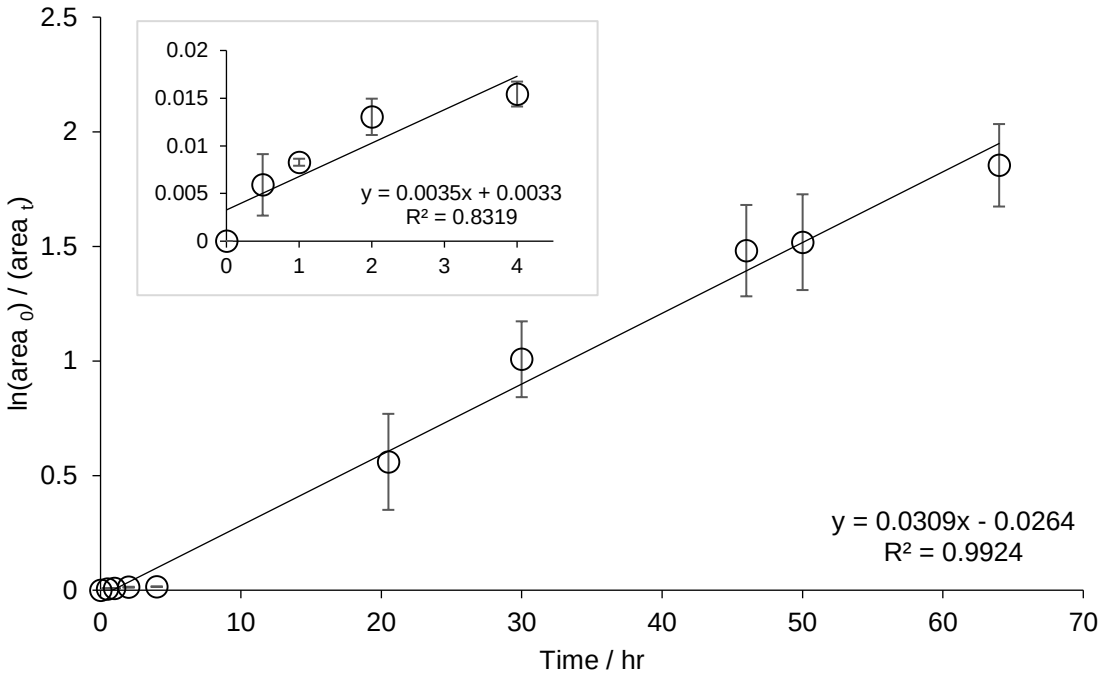

Figure 3.6 – PNIPAA$_{M(100)}$ conversion monitored by NMR of monomer integral height as a function of time (1 mM in MeOD). Initial conversion highlighted in insert. Experiments were conducted in triplicate.

As observed by Yang and Cheng[151], and contrary to the data obtained for PMAA, the conversion graph reveals a short period of inhibition in the early stages of the reaction, as highlighted in the initial rate insert of Figure 3.6. Slow fragmentation of the intermediate radical adduct in the pre equilibrium of RAFT polymerisation leads to an R• radical deficit and subsequently slow monomer propagation (Scheme 1.6), which would explain the delayed incorporation of NIPAA$_M$ monomer into the reaction. Once more CMDB is recruited into the reaction and RAFT-mediated propagation occurs, a linear relationship

characteristic of living polymerisation and a constant number of propagating chains was observed, indicative of retention of the RAFT end group functionality. The rate constant was measured as 8.7 x 10^{-6} ± 0.7 s^{-1} and rate of reaction was calculated as 6.4 x 10^{-7} ± 0.5 Ms^{-1}. Although both conducted at the same temperature of 60 ºC, the rate of reaction is slower than of a comparable PMAA RAFT polymerisation (Table 3.1), likely due to the formation of tertiary MAA radicals and the compatibility between methacrylate MAMs and active dithioester RAFT agents (Section 1.3.1)[129].

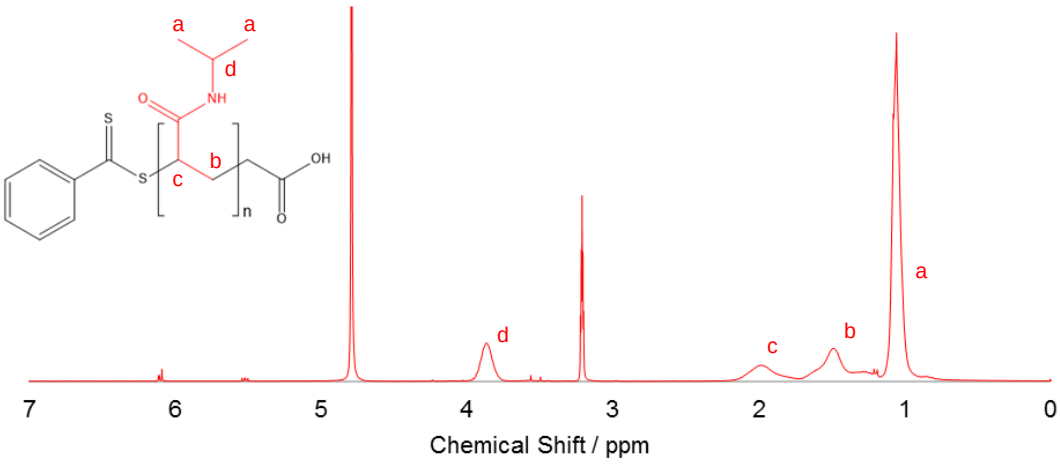

Figure 3.7 – ^{1}H NMR of Poly(N-isopropylacrylamide)$_{(100)}$ in MeOD (1 mM). a – CH_3 of $PNIPAA_M$ isopropyl groups, b – CH_2 in $PNIPAA_M$ backbone, c – CH of $PNIPAA_M$ backbone, d – CH of $PNIPAA_M$ side chain.

The negligible residual peaks at 5.7 ppm and 6.2 ppm in Figure 3.7, representative of monomeric vinyl environments, and the presence of corresponding peaks upfield at 1.3-1.7 ppm and 1.8-2.0 ppm confirm polymerisation. There is a characteristic $PNIPAA_M$ peak at 3.8 ppm (d) corresponding to the R_3CH group in the polymer, deshielded by its proximity to a tertiary amine. The peak assignments are in agreement with published values for the polymer[151].

As described in Chapter 1, and widely published in the literature[151,157,180,181], $PNIPAA_M$ has an LCST of 31-32 °C. Various factors including concentration and copolymerisation can reportedly influence this temperature, and a range of techniques were utilised to confirm the LCST of each polymer synthesised (Experiment 2.1.9).

The cloud point was first measured visually on heating a $PNIPAA_M$ solution through the LCST. Phosphate buffer was chosen to model the buffer system that operates within the cytoplasm of all cells, with a comparable pH to blood of 7.2[182]. Figure 3.8 shows the change in appearance of the solution below and above the LCST. The polymer transitions from the extended miscible state to the coiled immiscible state, causing the solution to change from clear and colourless to cloudy beyond 31 ºC.

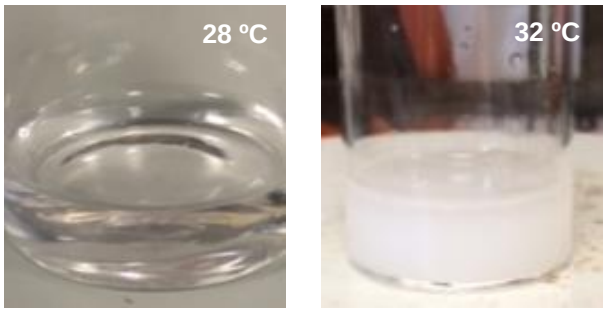

Figure 3.8 – The reversible transition of 100 mM $PNIPAA_M$ in solution from clear and colourless to cloudy beyond the LCST of 31 ºC.

To determine the accurate transition temperature for each synthesised polymer, a combination of UV/Vis spectrophotometry, dynamic light scattering and diffusion-ordered NMR spectroscopy was utilised. UV/Vis has previously been adopted as a simple technique to quantify the cloud point of $PNIPAA_M$-based polymers and nanoparticles[88,170]. Figure 3.9 shows the change in UV / Vis absorbance of $PNIPAA_M$ samples at three different concentrations with decreasing temperature. Samples were heated and the absorption was monitored at 1 ºC intervals as they cooled. Fujishige *et al.*[88] demonstrated negligible hysteresis of $PNIPAA_M$ homopolymers upon cooling via UV/Vis, with the LCST of the polymer on cooling mirroring the LCST when heated. The measured LCST of 31 °C, taken from the point at which the absorbance reaches a minimum and plateaus, is consistent amongst all samples, in agreement with the findings of Fujishige *et al*[88]. Whilst in the collapsed globular phase above the LCST, the absorbance remains consistent, then prior to dissolution of the polymer chains between 36-33 ºC there is a slight increase in absorption, before a sharp drop is observed between 33-31 ºC. It was postulated that during this phase, the aggregated globules begin to break apart into smaller particles, temporarily increasing the opacity of the solution. Other techniques may confirm whether this is in fact the case,

and globular $PNIPAA_M$ continues to aggregate beyond the LCST in an entropically-favoured exclusion of water molecules.

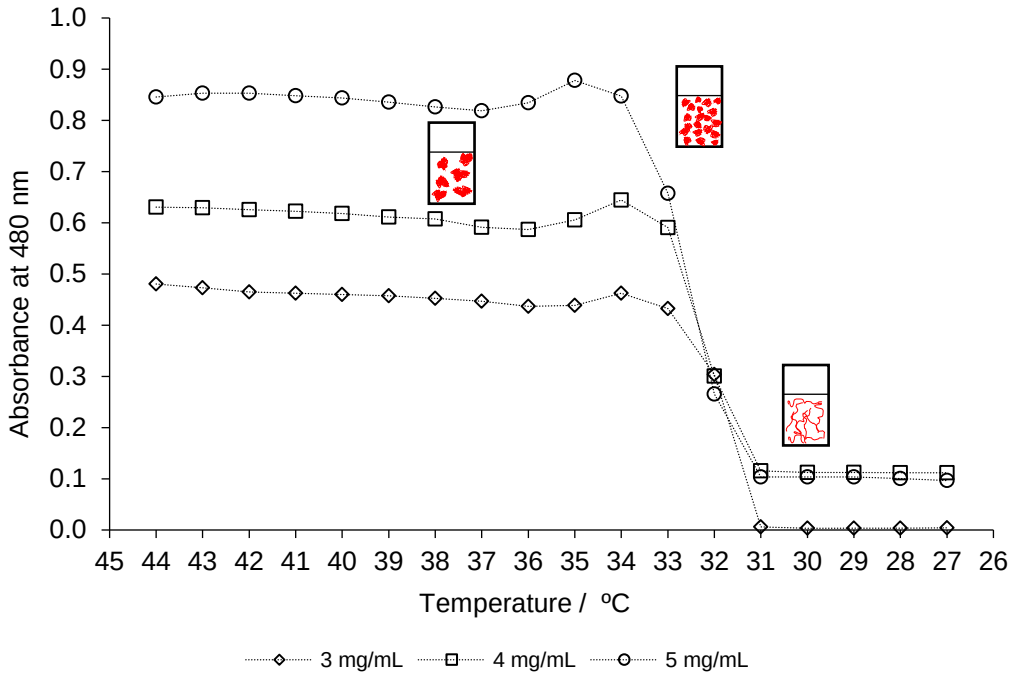

Figure 3.9 – UV/Vis absorbance data of $PNIPAA_{M(100)}$ solutions of increasing concentration to determine the effect of concentration on LCST. Samples were heated to 50 ºC and measurements were taken at 1 ºC intervals between 44 ºC and 27 ºC on cooling under ambient conditions. Diagrams depict large aggregated globules above the LCST, breakdown into smaller aggregates prior to dissolution on cooling, and miscible chains below the LCST. Measurements were conducted in triplicate.

UV/Vis Spectrophotometry certainly provides quantitative data regarding the cloud point of a sample, but should not be used alone to confirm an LCST as the manual measurements are open to interpretation[157]. Dynamic Light Scattering (DLS) was used to corroborate the LCST by measuring the change in hydrodynamic radii of the collapsing polymer.

DLS data in Figure 3.10 shows a clear change in the Z-average diameter of the polymer at 31 ºC as it collapses to the globular conformation. Between 24-30 ºC, the polymer exists as free chains in the solution, denoted by small hydrodynamic diameters of less than 50 nm. At 31 ºC, the polymers collapse and immediately begin to aggregate in order to exclude water. An equilibration time of 120 s at each temperature interval accounts for the jump in

Z-average diameter due to the almost immediate phase transition behaviour at 31 °C. An increase in polydispersity can be observed as a result of the degree to which globules have aggregated. The measured values were in agreement with values published by Malvern[183] and the LCST was corroborated by the increase in size distribution of particles by volume at 31 °C (Figure 3.11). At 30 °C (green peak), the polymers as individual chains each occupy a smaller volume in the sample vial than the aggregating particles at 31 °C (amber peak) as the polymer begins to collapse out of solution. By 33 °C the polymer has fully collapsed and aggregated, denoted by the sharp single peak (red).

Although they lie beyond the recommended upper size limit for the zetasizer of 10000 nm (10 µm)[184], the data reveals a further increase in Z-average diameter beyond the LCST at 34 °C. It is possible that the continued globule growth is due to further aggregation of collapsed polymer chains to increase the entropy of the system, driven by the number of unbound water molecules. This is in agreement with the UV/Vis absorbance data for the polymer, which indicates further aggregation by a slight reduction in sample opacity beyond 34 °C.

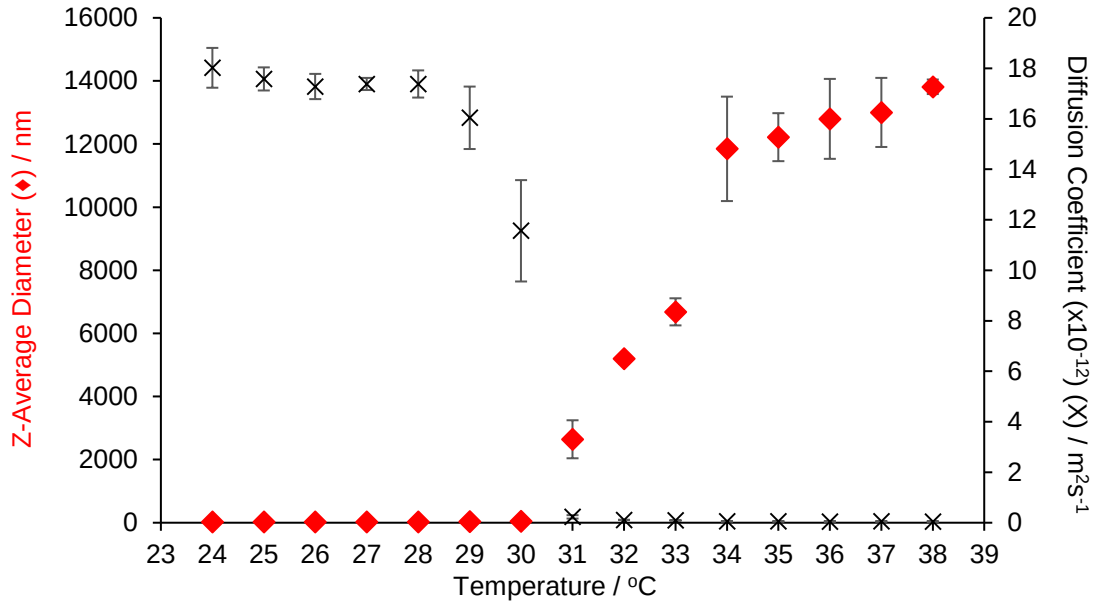

Figure 3.10 – Monitoring the change in Z-average diameter (♦) of PNIPAA$_{M(100)}$ in pH 7.2 phosphate buffer (50 mM) in DLS measurements made with increasing temperature reveals a clear change at 31 °C. Measurements were conducted in quintuplicate.

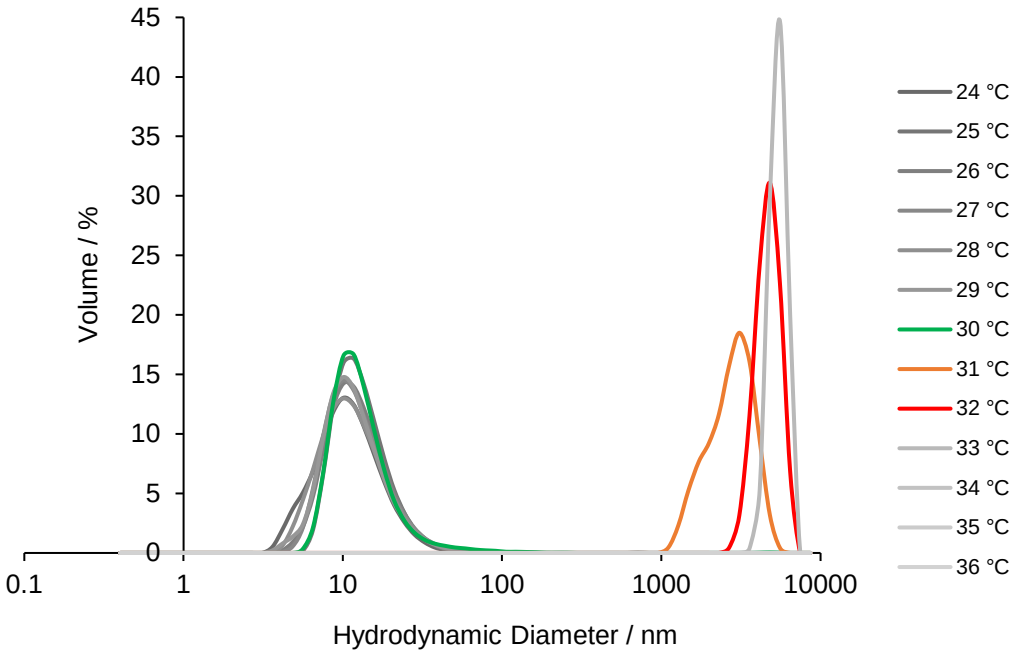

Figure 3.11 – Size distribution by volume for PNIPAA$_{M(100)}$, the temperature immediately prior to the LCST is highlighted in green, followed by the LCST of 31 °C in amber.

Dynamic light scattering assumes analysed particles are spherical, however in practice this is not always the case. The hydrodynamic radius is calculated as the size of an equivalent hypothetical hard sphere with the same translational diffusion coefficient as the particle being analysed[185]. The Stokes Einstein equation[186] (Equation 3.6) describes the inverse relationship between hydrodynamic radius and diffusion coefficient. As the Z-average diameter (and hence R_H) of the collapsing PNIPAA$_M$ polymer increases beyond the LCST, the diffusion coefficient drops as velocity of the Brownian motion slows (Figure 3.10).

Table 3.3 shows the diffusion coefficients and hydrodynamic radii of PNIPAA$_{M(100)}$ at increasing temperature, highlighting the inverse relationship between diffusion coefficient and hydrodynamic radii. It is interesting to note that the diffusion coefficient of the polymer begins to change at a lower temperature than that of the Z-average diameter. This shows that the polymer is responding to the change in temperature and modifying its interaction with the surrounding water molecules prior to the observed cloud point, leading to a decrease in D.

Table 3.3 – Diffusion coefficients (D) and hydrodynamic radii (R_H) of $PNIPAA_{M(100)}$ (50 mM in pH 7.2 phosphate buffer) with increasing temperature. R_H values obtained experimentally in quintuplicate by dynamic light scattering, from which St. Dev. in R_H and D values were calculated using the Stokes Einstein equation.

T / °C	D (x 10^{-12}) / m^2s^{-1}	R_H / nm	St. Dev. in R_H
24	18.0	13.3	1.2
25	17.6	14.0	0.7
26	17.3	14.6	0.9
27	17.4	14.9	0.4
28	17.4	15.3	1.0
29	16.0	17.0	2.5
30	11.6	24.2	8.7
31	0.2	1237.4	658.1
32	0.1	2592.6	147.5
33	0.1	3328.4	429.4
34	0.1	5798.3	2110.4
35	0.1	6083.2	760.4
36	0.1	6338.8	1266.8
37	0.1	6451.5	1094.6
38	0.1	6883.7	402.9

$$R_H = \frac{k_B T}{6\pi\eta D} \qquad (3.6)$$

DLS was also used to measure the effect of varying solution pH on the LCST of $PNIPAA_M$ homopolymers (Figure 3.12). Polymers were dissolved in water and three separate buffer solutions at pH 4 (phthalate), 7.2 (phosphate) and 9.8 (borate), and the LCST was measured at 1 °C intervals as described in Section 2.1.9. The LCST remained consistent between samples at 31 °C, however the size of the collapsed globules beyond the LCST increased with increasing pH. Although the effect of ion concentration on the LCST of $PNIPAA_M$ solutions has been previously reported by Zhang *et al.*[181], whereby increasing anion concentration led to a decrease in LCST, there are no reports in the literature that address the pH-dependent aggregation behaviour of $PNIPAA_M$ beyond the LCST.

It is possible that the presence of certain buffer ions in solution may determine the extent of aggregation depending on the degree to which ions can "salt out" the polymer, increasing the effective polymer concentration in the "free" bulk and increasing the extent of aggregation. Alternatively, the increased aggregate size may simply be a result of pH-

dependent water retention within the aggregates. The comparable measurements observed for $PNIPAA_M$ in deionised water (pH 7.1) and pH 7.2 phosphate buffer would indicate that the aggregation is pH driven as opposed to a result of ion concentration, but the precise explanation for this observation is unknown.

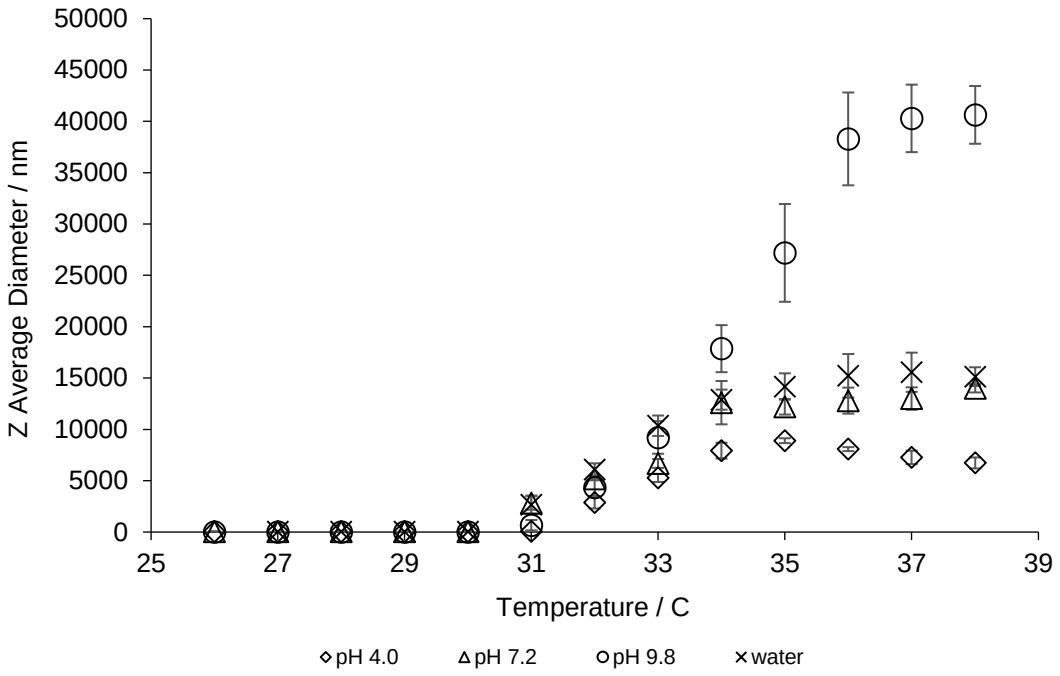

Figure 3.12 – Determining the effect of solution pH upon the LCST of $PNIPAA_{M(100)}$ homopolymers (50 mM). Measurements were conducted in quintuplicate.

Analogous to dynamic light scattering is diffusion-ordered NMR spectroscopy (DOSY)[187]. Both techniques utilise the Stokes Einstein equation to determine the hydrodynamic radii of particles (Equation 3.6). As demonstrated by DLS, $PNIPAA_M$ changes its conformation and R_H value beyond the LCST, therefore DOSY NMR was trialled as a technique to corroborate this data and monitor the change in diffusion coefficient with temperature.

Contrary to the expected outcome explained by the Stokes Einstein equation and demonstrated by DLS, where R_H is proportional to T, it is clear that as the polymer undergoes a transition at the LCST, the diffusion coefficient of the polymer increases and the R_H decreases during DOSY analysis (Figure 3.13 and Table 3.4).

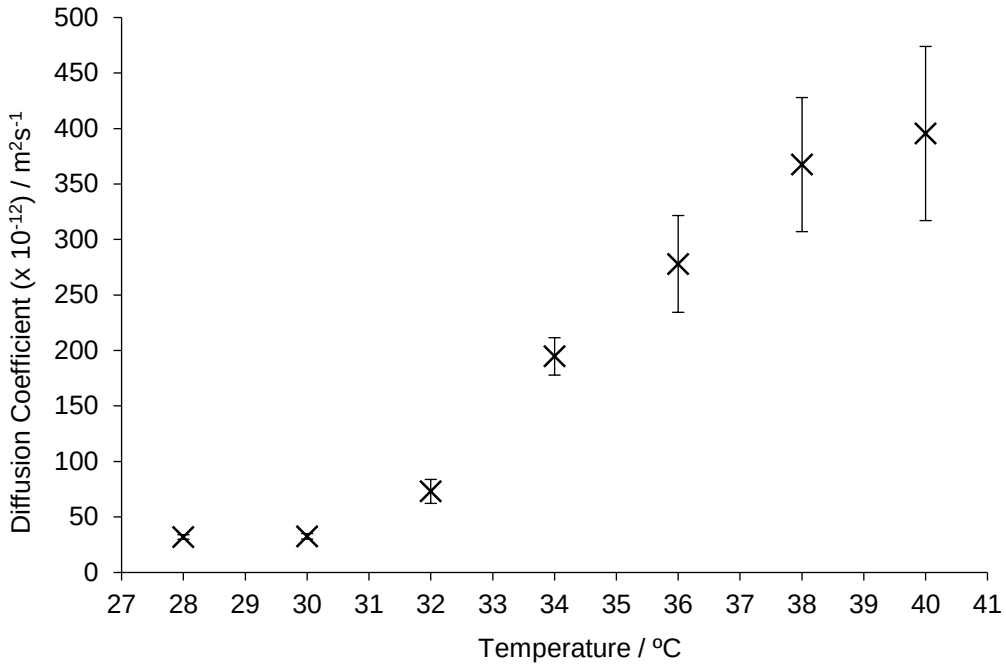

Figure 3.13 – Monitoring the change in diffusion coefficient of $PNIPAA_{M(100)}$ in D_2O (1mM) via DOSY NMR. Measurements were conducted in triplicate.

Table 3.4 – DOSY NMR diffusion coefficient (D) and hydrodynamic radius (R_H) data for $PNIPAA_{M(100)}$ in D_2O (1 mM). D values obtained experimentally by DOSY NMR spectroscopy, from which R_H values were calculated using the Stokes Einstein equation.

T / ºC	D (x 10^{-12}) / m^2s^{-1}	R_H / nm
28	3.20E-11	8.51
30	3.26E-11	8.79
32	7.31E-11	4.12
34	1.95E-10	1.62
36	2.78E-10	1.18
38	3.86E-10	0.92
40	3.96E-10	0.88

One condition of NMR spectroscopy is that the sample must be fully soluble in the selected deuterated solvent. Solid particles can distort the magnetic field homogeneity of a sample, leading to broad peaks and indistinct spectra[188] as observed in Figure 3.14. The DOSY diffusion signals begins to broaden at 32 ºC, indicative of phase separation and the presence of solid $PNIPAA_M$ in the sample.

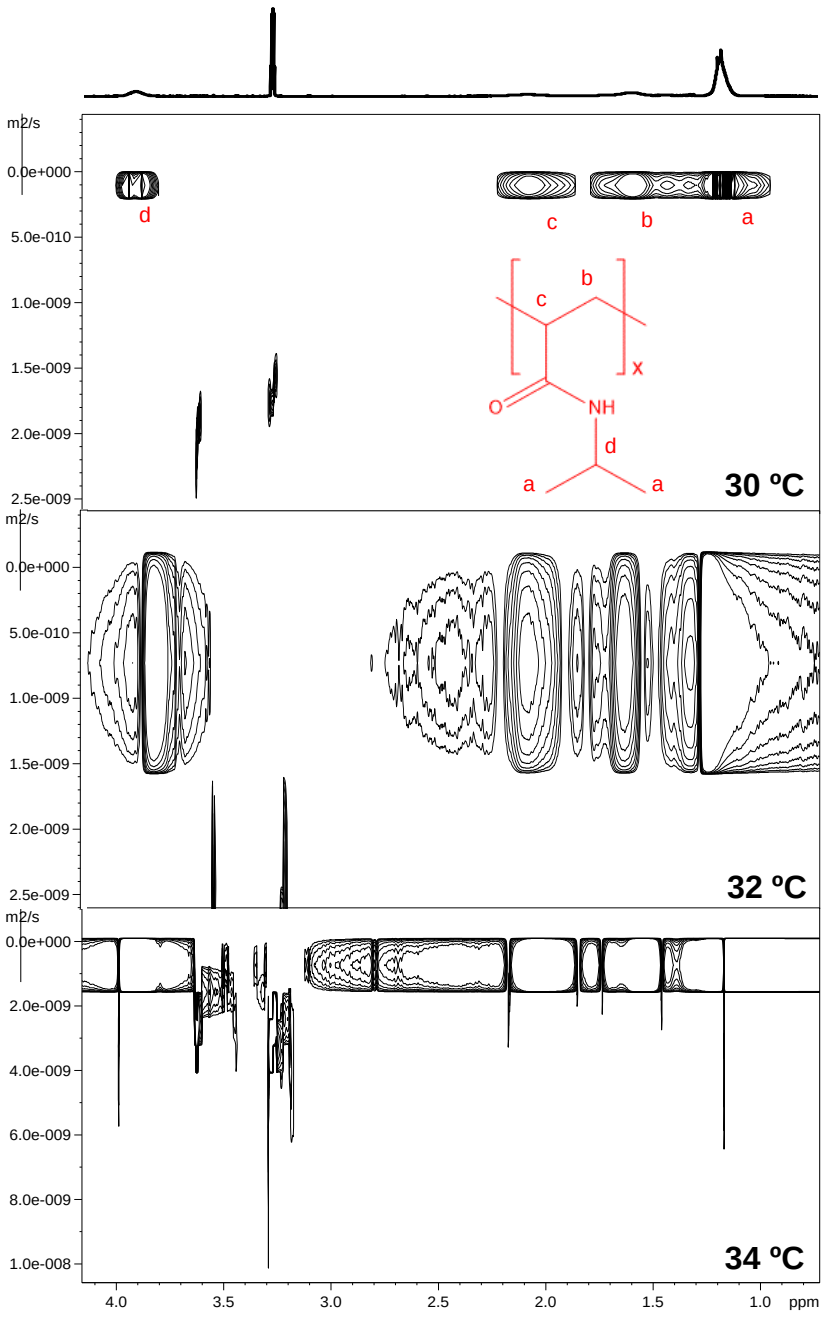

Figure 3.14 – DOSY NMR spectrum of $PNIPAA_{M(100)}$ in deuterated methanol D_2O (1 mM) with increasing temperature. Note the increase in Y axis scale of the spectrum at 34 ºC.

DOSY NMR provides a quantitative value for the LCST by revealing a change in D, but the data should not be used to gain accurate measurements of the diffusion coefficient or subsequent calculation of the hydrodynamic radius beyond the LCST due to the presence of solid impurities. Diffusion coefficients and calculated R_H of DOSY NMR and DLS data (Table 3.3) below the LCST should also not be directly compared to one another, as measurements are dependent on both sample concentration, as a result of increased sample viscosity and intermolecular interactions between polymer chains, and the choice of solvent. Consequently, DLS was deemed the more appropriate technique to quantify the LCST and the behaviour of collapsing and aggregating thermoresponsive polymers.

Once the compatibility of RAFT polymerisation employing CMDB had been demonstrated for the RAFT-mediated propagation of both PMAA and $PNIPAA_M$ homopolymers, exhibiting a good relationship between the calculated and experimental molecular weights by NMR, the next step was to employ poly(methacrylic acid) as a macroRAFT agent to form thermoresponsive di- and triblock copolymers.

3.3 PMAA-$PNIPAA_M$

Chain extension of poly(methacrylic acid) with poly(N-isopropylacrylamide) was conducted to facilitate the formation of stimuli-responsive polymer-shelled microspheres by incorporation of thermoresponsive $PNIPAA_M$. It has been shown previously that thiolated $PMAA_{SH}$ microspheres will successfully form[10], but as yet there are no publications in the literature detailing the sonochemical generation of a thermoresponsive polymeric microsphere system, aside from preliminary investigations conducted at the University of Bath[6]. It was initially proposed, based on the findings of Cavalieri *et al.*[10], that PMAA-based polymers would only form microsphere shells in the presence of thiolated $PMAA_{SH}$ moieties. Therefore, the copolymerisation of $PNIPAA_M$ with PMAA was initially thought to be required to facilitate disulphide crosslinking and form stable thermoresponsive microspheres.

The homopolymer of PMAA was first synthesised as a macroRAFT agent and isolated prior to diblock copolymerisation with $NIPAA_M$ to avoid contamination by the primary monomer, MAA (Experiment 2.1.1).

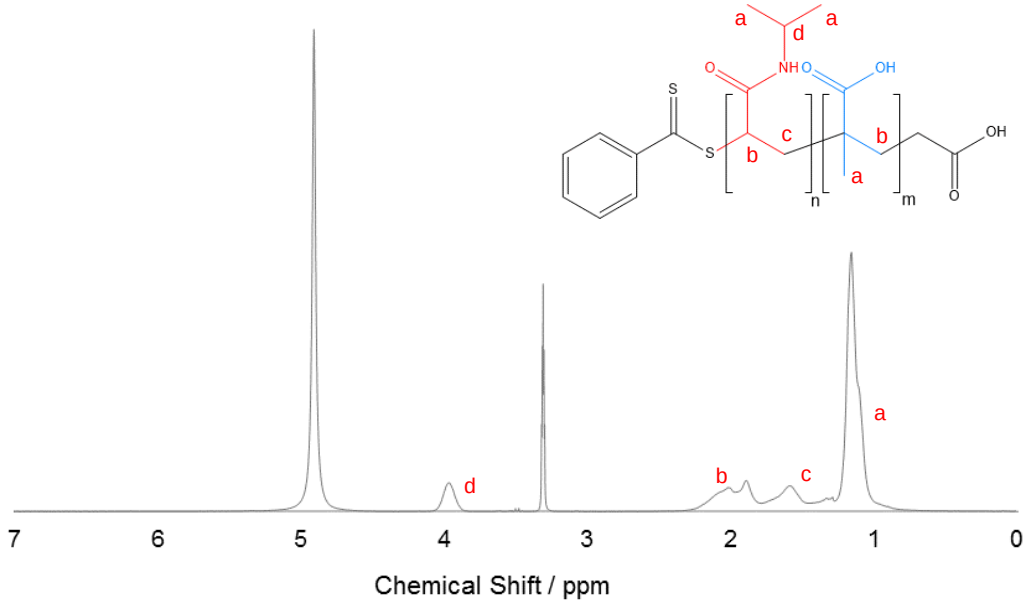

Figure 3.15 – ^{1}H NMR of PMAA$_{(100)}$-PNIPAA$_{M(100)}$ in MeOD (1 mM). a – CH$_3$ in PMAA backbone and CH$_3$ in PNIPAA$_M$ isopropyl groups, b – CH$_2$ in PMAA backbone and CH in PNIPAA$_M$ backbone, c – CH$_2$ in PNIPAA$_M$ backbone, d – CH in PNIPAA$_M$ side group.

Once the PMAA macroRAFT homopolymer had been fully characterised, the diblock copolymer was synthesised via the experimental protocol outlined in Experiment 2.1.3 (Scheme 2.3). The 1H NMR spectrum (Figure 3.15) reveals additional peaks, relative to the PMAA macroRAFT agent (Figure 3.1), at 1.6-1.8 ppm (c), representative of the methylene group in the polymer backbone and 3.8-4.0 ppm (d), characteristic of the R_3CH environment of the PNIPAA$_M$ isopropyl group. Contrary to the PNIPAA$_M$ homopolymer NMR spectrum (Figure 3.7), integration of the peak at 1.8-2.2 ppm reveals hydrogen environments corresponding to both PMAA (CH_2 of backbone) and PNIPAA$_M$ (1H of backbone). This is also true of the peak at 1.0-1.2 ppm, representative of the isopropyl methyl groups in PNIPAA$_M$ and the methyl group in the backbone of PMAA.

The conversion from monomer and macroRAFT agent to diblock copolymer was monitored using ^{1}H NMR as a function of time, as shown in Figure 3.16 and Table 3.5.

Table 3.5 – Molar ratios and conversion data for $PNIPAA_{M(100)}$ block addition to PMAA macroRAFT agents by RAFT polymerisation. Conversion values obtained in triplicate, from which k_p and R_p values were values were calculated.

Polymer Name	Conversion % (NMR)	Rate Constant k_p (10^{-6}) / s^{-1}	Reaction Rate Rp (10^{-7}) / Ms^{-1}
$PMAA_{(100)}$-$PNIPAA_{M(100)}$	97 ± 1	17 ± 2	2.7 ± 0.3
$PMAA_{(75)}$-$PNIPAA_{M(100)}$	89 ± 5	14 ± 4	2.2 ± 0.2
$PMAA_{(50)}$-$PNIPAA_{M(100)}$	92 ± 2	16 ± 8	2.5 ± 0.9
$PMAA_{(25)}$-$PNIPAA_{M(100)}$	94 ± 3	13 ± 1	2.1 ± 0.1

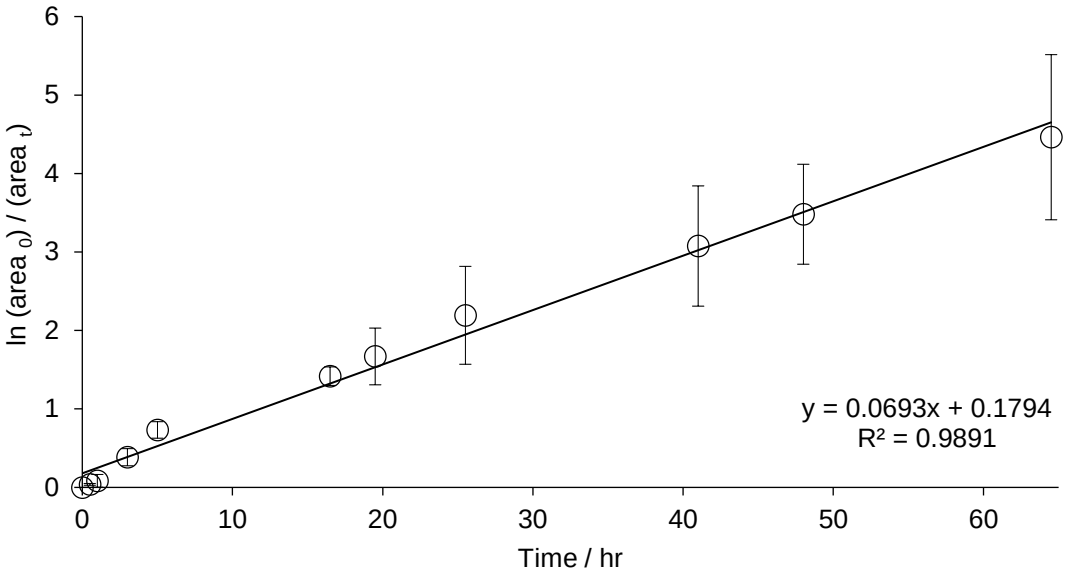

Figure 3.16 – The conversion of $PMAA_{(100)}$-$PNIPAA_{M(100)}$ diblock copolymerisation via ^1H NMR spectroscopy in MeOD (1 mM) as a function of time. Experiments were conducted in triplicate.

The rate constant (k_p) for the polymerisation of $PMAA_{(100)}$-$PNIPAA_{M(100)}$ was measured as 0.0693 h^{-1} = 1.7 x 10^{-5} s^{-1}. The rate was therefore calculated to be 2.7 x 10^{-7} Ms^{-1}. As observed by Ganachaud *et al.*[130], in addition to the choice of RAFT agent, the rate of reaction can be modified by adjusting the [M]:[CTA] ratio, the [CTA]:[initiator] ratio, and the choice of solvent and reaction conditions, therefore reaction rates are highly specific to a particular reaction. A comparison of the rate constant is instead more indicative of the behaviour of a particular reaction.

The measured rate constant (k_p) for monomer propagation is considerably higher than that of the $PNIPAA_M$ homopolymerisation, this is likely due to the excellent initial R leaving group ability of the macroRAFT agent in the pre-equilibrium, relative to CMDB, and the ready formation of tertiary terminal methacrylic acid R• radicals, combined with the relative instability of the secondary propagating acrylamide structure.

When conducting block copolymerisation reactions, there is a risk of competing side reactions such as initiator-initiated homopolymerisation of the second monomer. DOSY NMR was used to determine whether any side reactions had occurred by analysis of the diffusion peaks of hydrogen environments corresponding to $PNIPAA_M$ and PMAA. Secondary diffusion coefficient peaks in the spectrum, corresponding to $PNIPAA_M$-specific peaks, would reveal the presence of residual homopolymeric $PNIPAA_M$. On the other hand, no relationship in the diffusion coefficient values for PMAA-specific and $PNIPAA_M$-specific peaks would imply no chain extension via block copolymerisation has occurred. Either of these spectral anomalies could indicate poor RAFT agent end-group retention of the macroRAFT homopolymer.

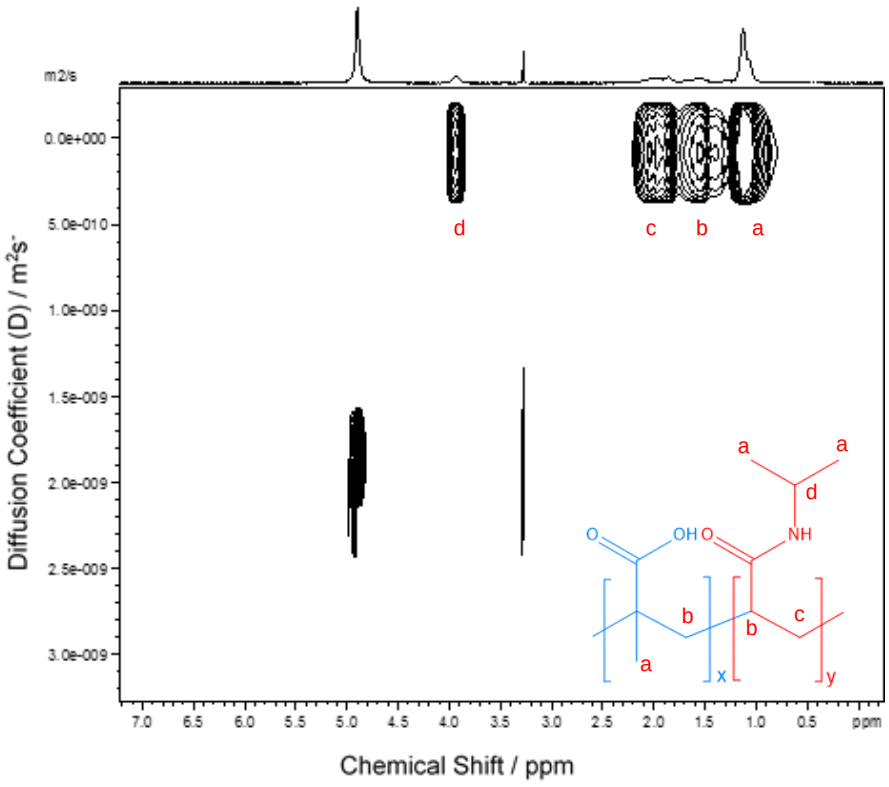

Figure 3.17 – DOSY NMR spectrum of diblock $PMAA_{(100)}$-$PNIPAA_{M(100)}$ (1 mM in MeOD).

The single spectral pattern, excluding solvent signals at 3.3 and 5.0 ppm, and shared diffusion coefficients of PMAA and $PNIPAA_M$-specific peaks denotes the formation of diblock $PMAA_{(100)}$-$PNIPAA_{M(100)}$ (Figure 3.17). The diffusion coefficient of the diblock copolymer is smaller than that of the macroRAFT agent at 1.3 x 10^{-10} m^2s^{-1}, a further indication of successful chain extension. For comparison, Figure 3.18 demonstrates the expected spectral pattern of an unsuccessful chain extension of $PMAA_{(25)}$-$PNIPAA_{M(100)}$. Vinylic signals at 5.7 and 6.2 ppm (e and f) and the monomeric R_3CH signal at 3.8 ppm (d), with a diffusion coefficient of 1.7 x 10^{-9} m^2s^{-1}, correspond to $NIPAA_M$ monomer that has not been incorporated into the reaction. The polymeric diffusion peak at 3.8 ppm, however, is indicative of a degree of successful chain extension.

A comparison of the diffusion coefficients for both the di- and triblock copolymers is made in Section 3.4.

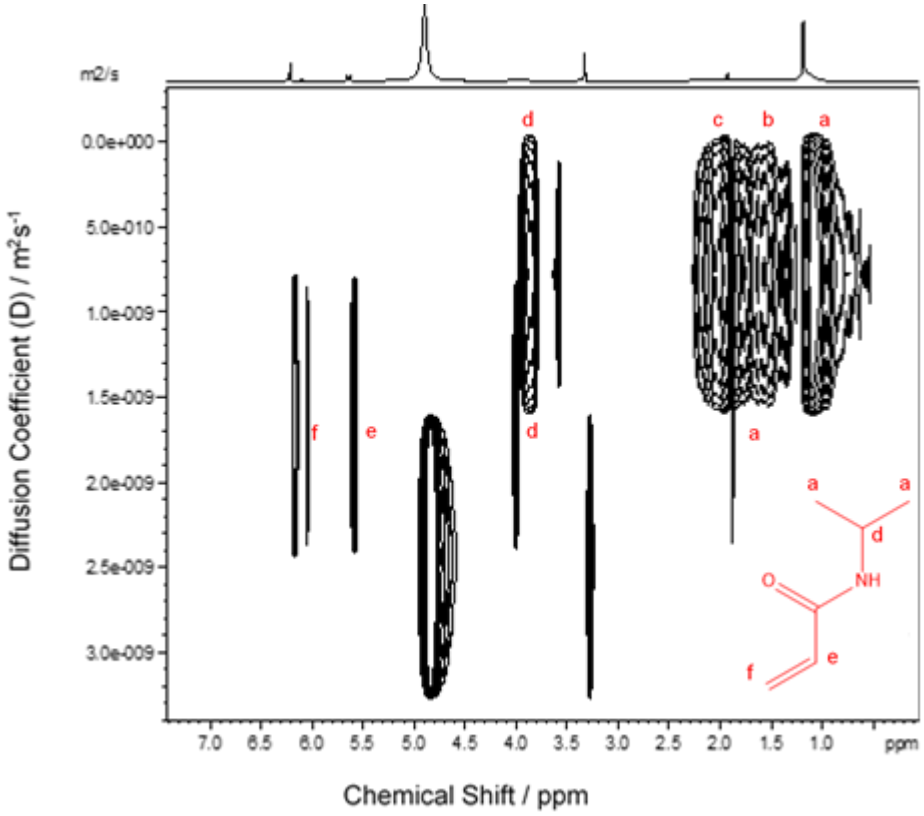

Figure 3.18 – DOSY NMR of a largely unsuccessful diblock copolymerisation of $PMAA_{(25)}$-$PNIPAA_{M(100)}$.

Analysis of PMAA-PNIPAA$_M$ diblock copolymers by DLS reveals that the incorporation of PNIPAA$_M$ into diblock copolymers with hydrophilic poly(methacrylic acid) does not influence the LCST of the PNIPAA$_M$ block (Figure 3.19). The polymer block retains the thermoresponsive behaviour of the homopolymer, undergoing the characteristic change at 31 °C. This is in agreement with data published by Yang and Cheng[151], who report no change in the DSC endotherm LCST values of diblock PNIPAA$_M$-PMAA and triblock PNIPAA$_M$-PMAA-PNIPAA$_M$ with respect to the homopolymer. Tang *et al.*[189] have also observed no change in the characteristic transition temperature of PNIPAA$_M$ blocks when copolymerised with hydrophobic PMMA, indicating that the thermoresponsive behaviour of PNIPAA$_M$ is largely independent of the alternate polymer block. Polymers that demonstrate thermoresponsive capabilities at this temperature are valuable for potential *in vivo* applications. The ability to form block copolymers without compromising the LCST improves their functionality and range of potential applications.

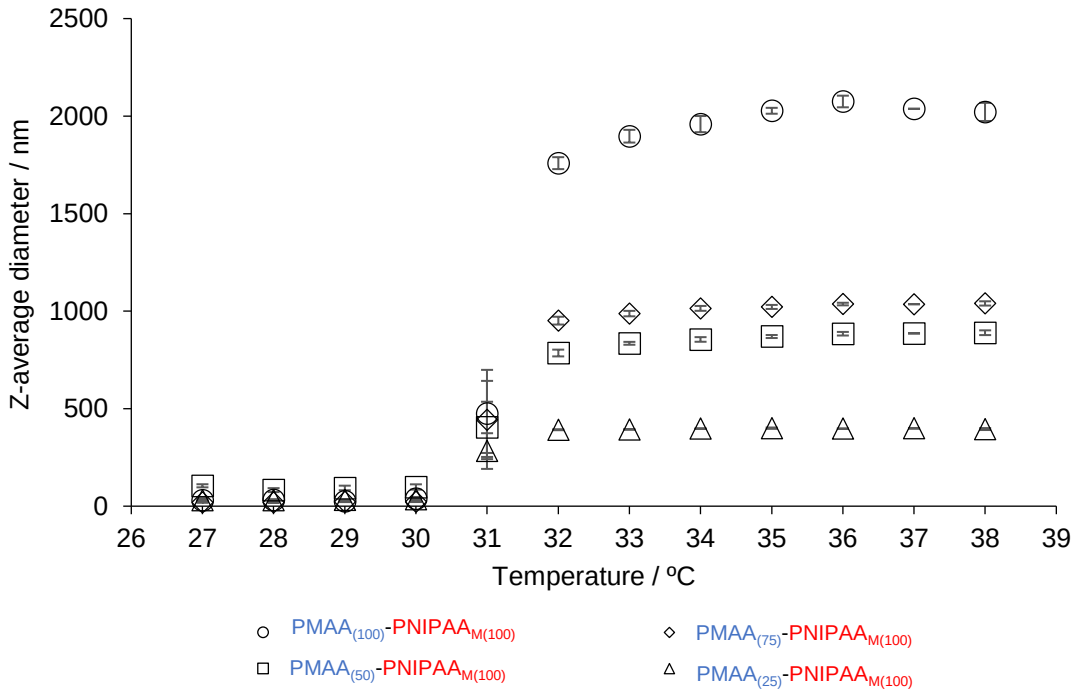

Figure 3.19 – Z-average diameters of PMAA-PNIPAA$_M$ diblock copolymer chains in pH 7.2 phosphate buffer (50 mM). Measurements were conducted in quintuplicate.

Due to the increased molecular weights of the diblock copolymers relative to the $PNIPAA_{M(100)}$ homopolymer, it was initially proposed that the Z-average diameters of the collapsed globules would be larger than those of $PNIPAA_M$, Figure 3.19 demonstrates that this is not the case. Collapsed diblock PMAA-$PNIPAA_M$ globules reach approximately 1700 nm at 32 °C, as opposed to $PNIPAA_{M(100)}$ (Figure 3.10) where the Z-average diameter of globules at 32 °C is almost 6000 nm. It was subsequently proposed that the hydrophilic PMAA component of the block copolymer, which does not undergo a thermoresponsive transition, in some way inhibits maximum water exclusion by extensive aggregation, therefore preventing the formation of larger globules. Varying the molecular weight of the PMAA component within the copolymer does, however, affect the measured Z-average diameter of the collapsed globule when comparing two diblock copolymers of increasing PMAA:$PNIPAA_M$ ratio (Figure 3.19). This would imply that, upon collapse, polymer chains adopt a "core-shell" structure (Figure 3.20). The polymer becomes amphiphilic, and the hydrophobic $PNIPAA_M$ forms the core whilst the hydrophilic PMAA chains extend into the solvent. Increasing the PMAA molecular weight therefore increases the chain length extending into the bulk phase, thus increasing the globule size between block copolymers of increasing PMAA chain length.

Beyond 32 °C, the block copolymers show very little change in Z-average diameter with increasing temperature, whereas the $PNIPAA_M$ homopolymer (Figure 3.10) continues to aggregate to exclude the maximum amount of water and further increase the disorder of the system, as shown by the continued increase in Z-average diameter beyond the LCST. This can be observed in the increasing Z-average diameter measurements at temperatures beyond the LCST. Feijen *et al.*[190] observed similar behaviour when heating block copolymers of $PNIPAA_M$ and poly(ethylene glycol) (PEG) beyond the LCST of $PNIPAA_M$ and described their intended application as stimuli-responsive drug delivery vehicles, with the potential to initiate release by applied localised hypothermia. On the other hand, Papadakis *et al.*[191] utilised the hydrophilic behaviour of $PNIPAA_M$ below the LCST to synthesise ABA block copolymer core shell microspheres of PS-$PNIPAA_M$-PS that become completely hydrophobic and collapse beyond the LCST.

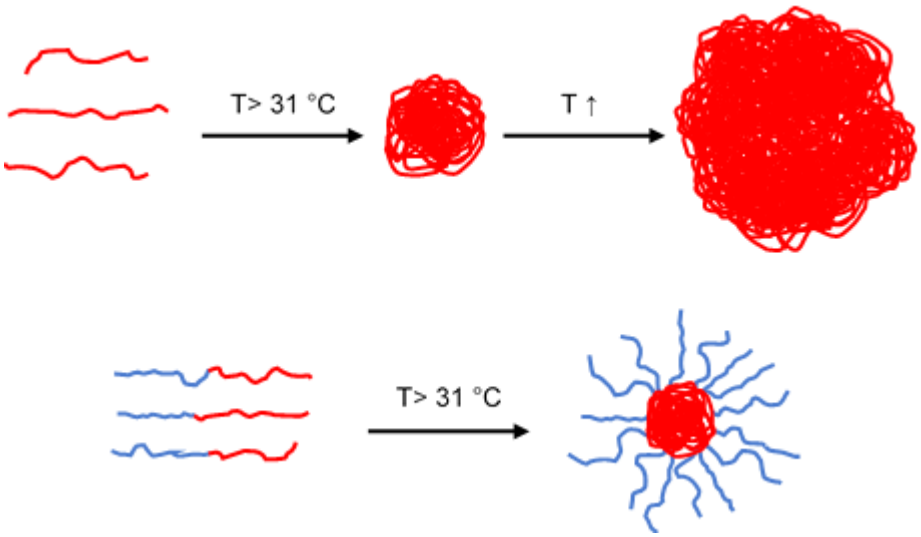

Figure 3.20 – A diagram representing the proposed structure of collapsing PNIPAA$_M$ and diblock PMAA-PNIPAA$_M$ copolymer globules beyond the LCST. (Blue regions = PMAA, red regions = PNIPAA$_M$).

UV/Vis spectroscopy data supports the cloud point measurements conducted by DLS (Figure 3.21). It reveals a change in the sample absorbance that levels at 31 °C. Contrary to the absorbance data for the PNIPAA$_M$ homopolymer, the UV/Vis data for the block copolymers do not show the same slight increase in absorbance measurements between 35-33 °C prior to the sharp drop immediately above the LCST on cooling. Further supporting the theory that the block copolymers only undergo a degree of aggregation beyond the LCST, however remain in small aggregated "core-shell" structures and do not undergo extensive aggregation.

There is no observed correlation between the diblock copolymer molecular weight and the measured absorbance, and this was again attributed to the hydrophilic nature of the PMAA blocks within the copolymers. Only the PMAA block length changes between diblock copolymer samples, and as these blocks are not involved in thermoresponsive collapse. Hydrophilic PMAA chains extending from the aggregated PNIPAA$_M$ core will not contribute to the increased sample absorbance above the LCST, therefore any change in absorbance is dependent upon the small collapsed PNIPAA$_M$ core. The homopolymer sample concentration is half that of the block copolymer sample for analysis, this was necessary due to very low absorbance readings when comparing block copolymer samples of the same concentration as the PNIPAA$_M$ homopolymer.

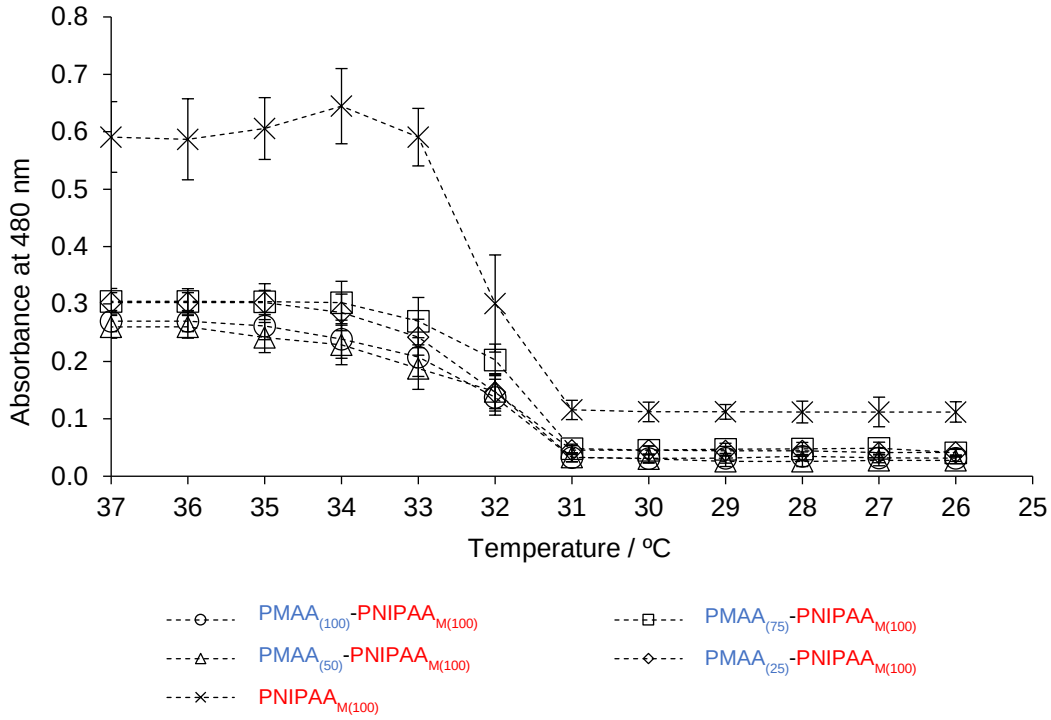

Figure 3.21– A comparison of the UV/Vis absorbance data of $PNIPAA_M$ homopolymer (4 mg/mL) and diblock PMAA-$PNIPAA_M$ copolymers (8 mg/mL). Samples were heated to 50 ºC and measurements were taken at 1 ºC intervals between 37 ºC and 26 ºC on cooling under ambient conditions. Measurements were conducted in triplicate.

3.4 PMAA-$PNIPAA_M$-PMAA

Triblock PMAA-$PNIPAA_M$-PMAA was generated as per the protocol outlined in Experiment 2.1.4. The initial reasoning behind further chain extension was to prevent potential localisation of the PMAA and $PNIPAA_M$ chains into regions within the microsphere shell. It was postulated that regions of crosslinked $PMAA_{SH}$ and non-crosslinked $PNIPAA_M$ would destabilise the shell and increase susceptibility to degradation. Successful chain extension also demonstrates the potential of the diblock macroRAFT agent to facilitate the formation of ABC triblock copolymers, increasing functionality and possible applications.

Once fully characterised, the diblock copolymer was employed as the macroRAFT agent for triblock chain extension. The monofunctionality of the initial CMDB RAFT agent ensures chain extension proceeds via monomer addition to the radical R• terminal of the most recently polymerised block (Scheme 1.6).

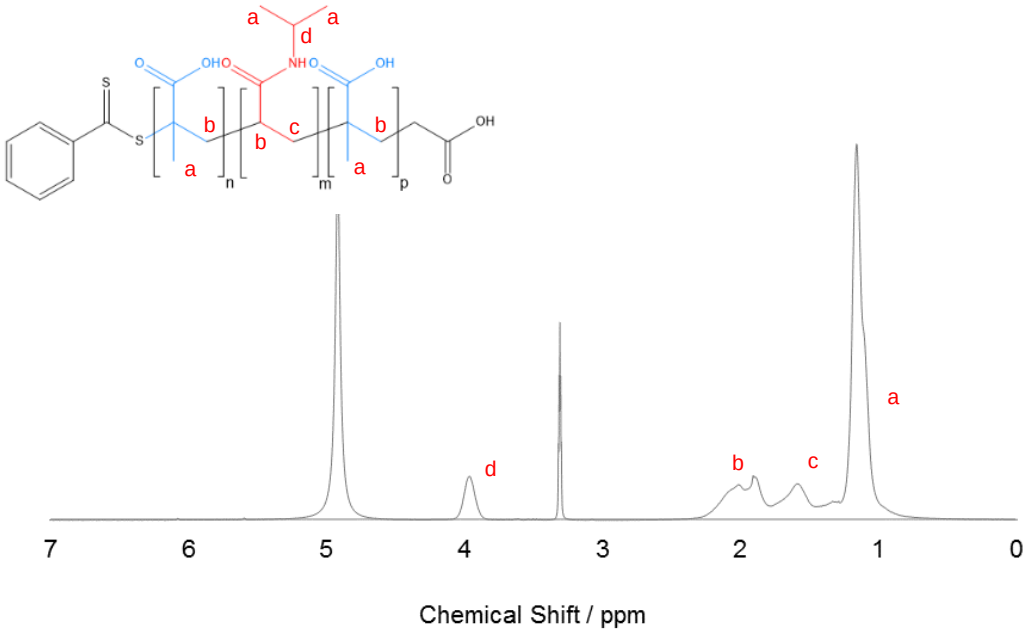

Figure 3.22 – ^{1}H NMR of PMAA$_{(100)}$-PNIPAA$_{M(100)}$-PMAA$_{(100)}$. 1 mM in MeOD. a – CH$_3$ in PMAA backbone and CH$_3$ in PNIPAA$_M$ isopropyl groups, b – CH$_2$ in PMAA backbone and CH in PNIPAA$_M$ backbone, c – CH$_2$ in PNIPAA$_M$ backbone, d – CH in PNIPAA$_M$ side group.

^{1}H NMR of PMAA$_{(100)}$-PNIPAA$_{M(100)}$-PMAA$_{(100)}$ (Figure 3.22) reveals a clean polymer with no remnants of residual monomer and an approximate 2:1 ratio for PMAA-specific and PNIPAA$_M$-specific peaks upon measurement of the integrals. Although analysis of the integral area goes some way to demonstrate triblock formation, it alone does not confirm successful chain extension.

Table 3.6 - Molar ratios and conversion data for the block chain extension of macroRAFT PMAA-PNIPAA$_M$ with MAA.

Polymer Name	Conversion % (NMR)	Rate Constant k_p (10^{-6}) / s^{-1}	Reaction Rate Rp (10^{-7}) / Ms^{-1}
PMAA$_{(100)}$-PNIPAA$_{M(100)}$-PMAA$_{(100)}$	60 ± 7	9 ± 1	0.6 ± 0.2
PMAA$_{(75)}$-PNIPAA$_{M(100)}$-PMAA$_{(75)}$	55 ± 12	9 ± 1	0.4 ± 0.1
PMAA$_{(50)}$-PNIPAA$_{M(100)}$ -PMAA$_{(50)}$	50 ± 15	8 ± 3	0.2 ± 0.1
PMAA$_{(25)}$-PNIPAA$_{M(100)}$ -PMAA$_{(25)}$	53 ± 8	9 ± 2	0.1 ± 0.1

As with the homopolymeric PMAA and diblock PMAA-PNIPAA$_M$ macroRAFT agents, conversions of the triblock copolymers were monitored by ^{1}H NMR (Figure 3.23 and Table 3.6). The rate of reaction increases with increasing [MAA]:[macroRAFT] ratio, as observed with the homopolymer rates (Table 3.1)[152] and the rate constant remains unchanged. The reaction largely adheres to the linear living characteristics of both the homopolymerisation and diblock copolymerisations, however there are deviations from the ideal and the reported conversion yields, calculated from the loss of monomer peak integrals, are considerably lower than that of the homopolymers and diblock copolymers. This is largely due to the poor suitability of the macroRAFT agent, which possesses the secondary R leaving group of a terminal N-isopropylacrylamide repeat unit, to efficiently polymerise the stable tertiary methacrylic acid propagating radicals. The intermediate radical is more likely to cleave in favour of the more stable leaving group in the pre-equilibrium, inhibiting chain growth (Section 1.3.3). The slow propagation constant and reaction rate relative to its precursors are also likely a result of the size and mobility of the R leaving group.

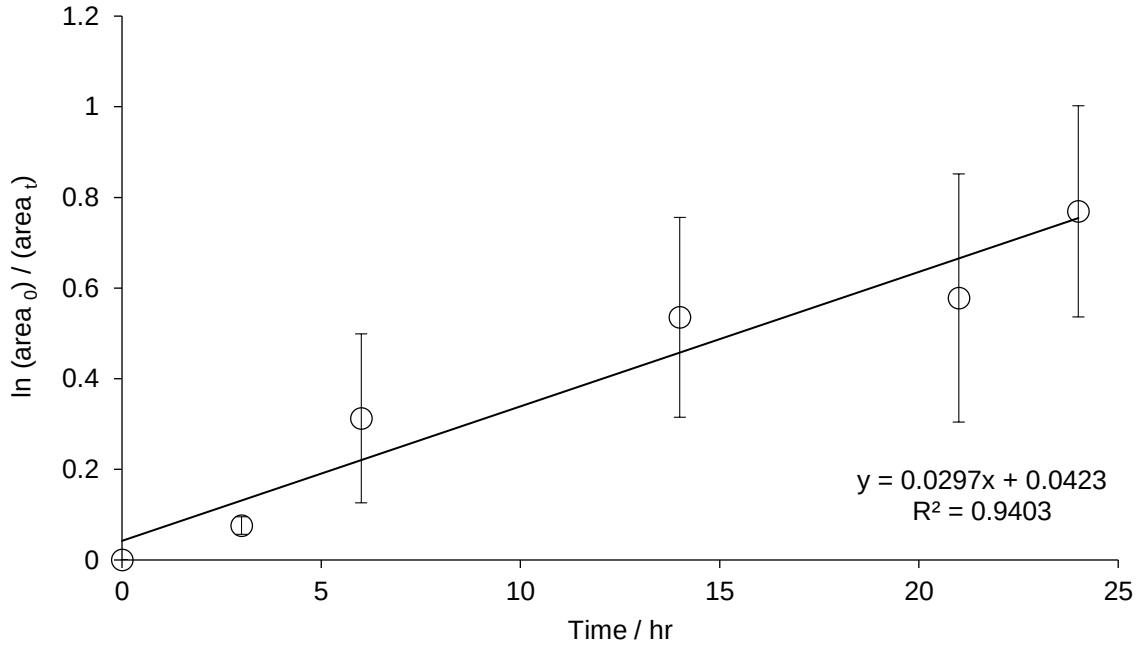

Figure 3.23 – Conversion of triblock copolymerisation of PMAA(100)-PNIPAA$_{M(100)}$-PMAA$_{(100)}$ monitored by ^{1}H NMR in MeOD. Experiments were conducted in triplicate.

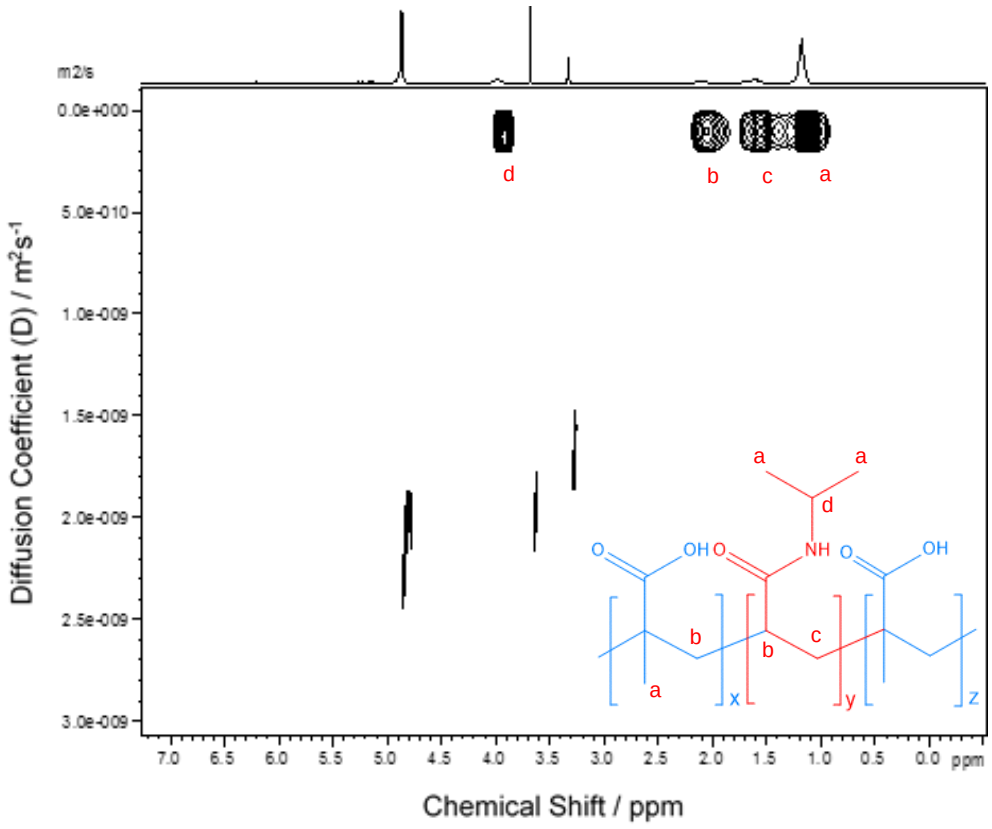

Figure 3.24 – DOSY NMR spectrum of triblock $PMAA_{(100)}$-$PNIPAA_{M(100)}$-$PMAA_{(100)}$ (1 mM in MeOD).

DOSY NMR was once again used to confirm successful polymerisation and determine the presence of residual monomer or side reaction products such as homopolymeric PMAA, synthesised by simple radical polymerisation during the reaction. Figure 3.24 shows the DOSY NMR spectrum of the triblock copolymer $PMAA_{(100)}$-$PNIPAA_{M(100)}$-$PMAA_{(100)}$. The absence of secondary diffusion peaks, excluding those belonging to the solvents, implies that no significant side reactions, including radical homopolymerisation of PMAA, have occurred. The diffusion coefficient is lower than that of the homo and diblock copolymers at 2.0×10^{-11} m^2s^{-1}, again indicative of successful chain extension.

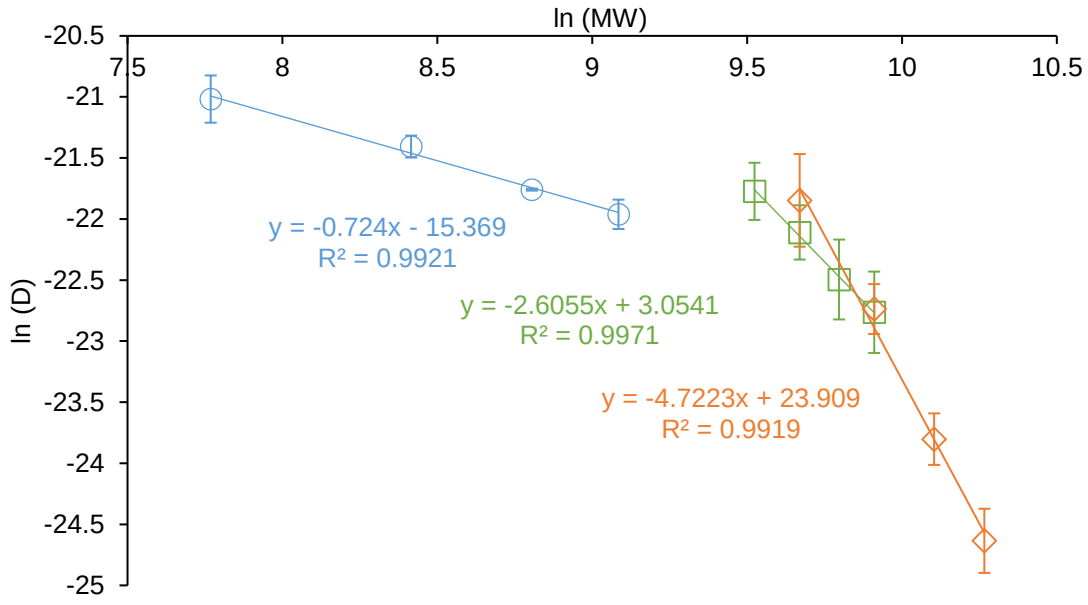

Figure 3.25 – A comparison of the polymer diffusion coefficients for homo- (A) (blue) di- (AB) (green) and triblock (ABA) (orange) copolymers of PMAA (A block) and PNIPAAm (B block) with increasing PMAA molecular weight (1 mM in MeOD). All measurements were conducted in triplicate.

Table 3.7 – The diffusion coefficients of di- and triblock AB and ABA PMAA (A) and $PNIPAA_M$ (B) block copolymers.

Polymer Name	Target Calculated M/W / g/mol	D (x 10^{-10}) / m^2s^{-1}
$PMAA_{(25)}$-$PNIPAA_{M(100)}$	13700	3.5 ± 1.3
$PMAA_{(50)}$-$PNIPAA_{M(100)}$	15800	2.5 ± 1.2
$PMAA_{(75)}$-$PNIPAA_{M(100)}$	18000	1.7 ± 1.4
$PMAA_{(100)}$-$PNIPAA_{M(100)}$	20100	1.3 ± 1.4
$PMAA_{(25)}$-$PNIPAA_{M(100)}$ -$PMAA_{(25)}$	15800	3.3 ± 1.5
$PMAA_{(50)}$-$PNIPAA_{M(100)}$ -$PMAA_{(50)}$	20100	1.3 ± 1.2
$PMAA_{(75)}$-$PNIPAA_{M(100)}$-$PMAA_{(75)}$	24400	0.5 ± 1.2
$PMAA_{(100)}$-$PNIPAA_{M(100)}$-$PMAA_{(100)}$	28700	0.2 ± 1.3

When comparing the diffusion coefficient values for all synthesised polymers against their calculated molecular weights, an inverse linear relationship can be observed (Figure 3.25). The strong linear correlation implies that by varying the [M]:[CTA] ratio it is possible to tailor the degree of polymerisation to fit the slope. The di- and triblock copolymers exhibit a different slope to that of the PMAA homopolymers, which would indicate that the copolymer interacts differently with the solvent under an applied field. Zhang and Peppas[192] have reported intermolecular hydrogen bonding between $PNIPAA_M$ and PMAA in interpenetrating polymer networks and, more recently, Mukherji *et al.*[193] have demonstrated the preferential binding of $PNIPAA_M$ to deuterated methanol (MeOD) in cosolvent systems, particularly between the isopropyl side chains.

As with the homo and diblock precursors, LCST determination of triblock copolymers was conducted via DLS. Figure 3.26 compares the LCST of di- and triblock copolymers with increasing PMAA chain length. The graph not only demonstrates that the collapsed block copolymers containing larger PMAA blocks possess larger Z-average diameters, but also that Z-average diameter is largely independent of whether the polymer is a di- or tri-block, and is instead dependent on PMAA chain length. Triblock PMAA-$PNIPAA_M$-PMAA polymers have a similar Z-average diameter to their macroRAFT precursors beyond the LCST. This further supports the core-shell theory discussed in Section 3.3, whereby the PMAA blocks extend from the central collapsed aggregated $PNIPAA_M$ globule.

Approximation of the homopolymeric molecular weights of the PMAA precursors, by DOSY NMR of esterified PMMA, revealed that $PMAA_{(100)}$ actually has a degree of polymerisation of approximately 130, whilst $PMAA_{(50)}$ is formed of approximately 56 repeat units. It is therefore interesting to observe that the Z-average diameters of collapsed $PMAA_{(100)}$ di- and triblock copolymers beyond the LCST are approximately twice the diameter of those containing $PMAA_{(50)}$.

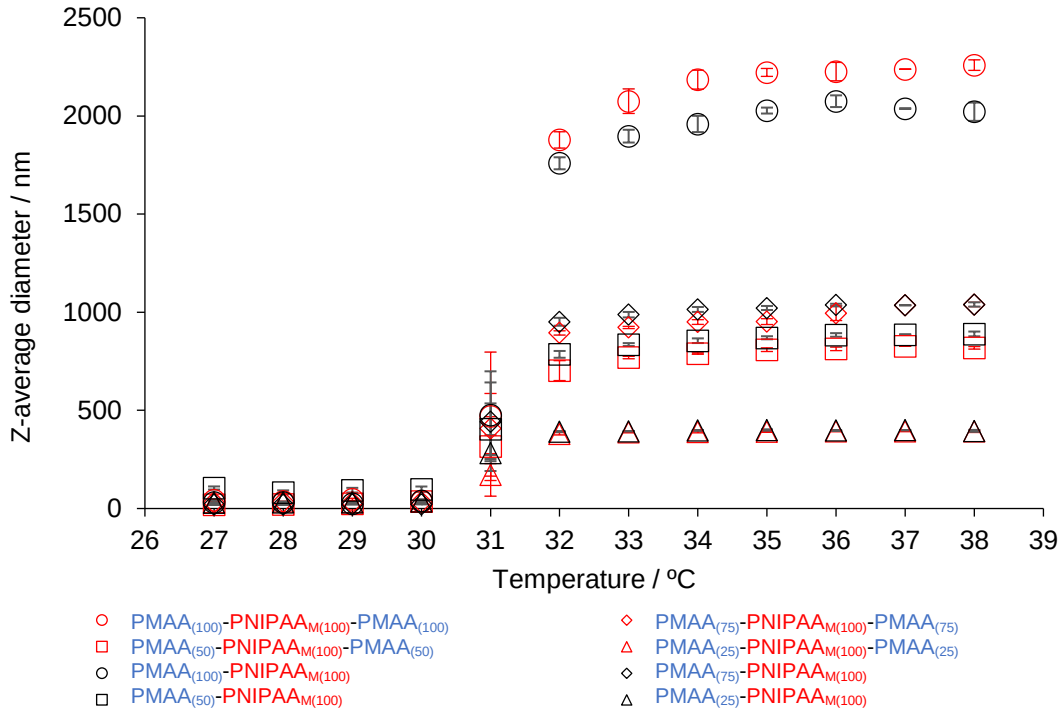

Figure 3.26 - A comparison of the Z-average diameters of diblock and triblock copolymer chains of increasing PMAA:PNIPAA$_M$ ratio beyond the LCST (50 mM). Measurements were conducted in quintuplicate.

UV/Vis was once again employed to corroborate the LCST values measured by DLS. Figure 3.27 compares triblock PMAA-PNIPAA$_M$-PMAA copolymers with PNIPAA$_{M(100)}$. The behaviour of the triblock is very similar to that of the diblock precursor, albeit with a more gradual dissolution of the polymer chains as the temperature decreases prior to the LCST, which could be attributed to the presence of more hydrophilic PMAA blocks relative to PNIPAA$_M$ blocks. It has already been shown that block copolymerisation of thermoresponsive PNIPAA$_M$ with PMAA does not affect the LCST of the polymer. This is also true here, however at temperatures above the LCST the high concentration of hydrophilic PMAA chains, relative to PNIPAA$_M$, appear to slow the rate of dissolution. The presence of more PMAA chains in the triblock core-shell aggregates may induce mild hysteresis, whereby the rate of aggregation, shown by DLS to be unaffected by the addition of a third hydrophilic PMAA block, does not equal the rate of dissolution.

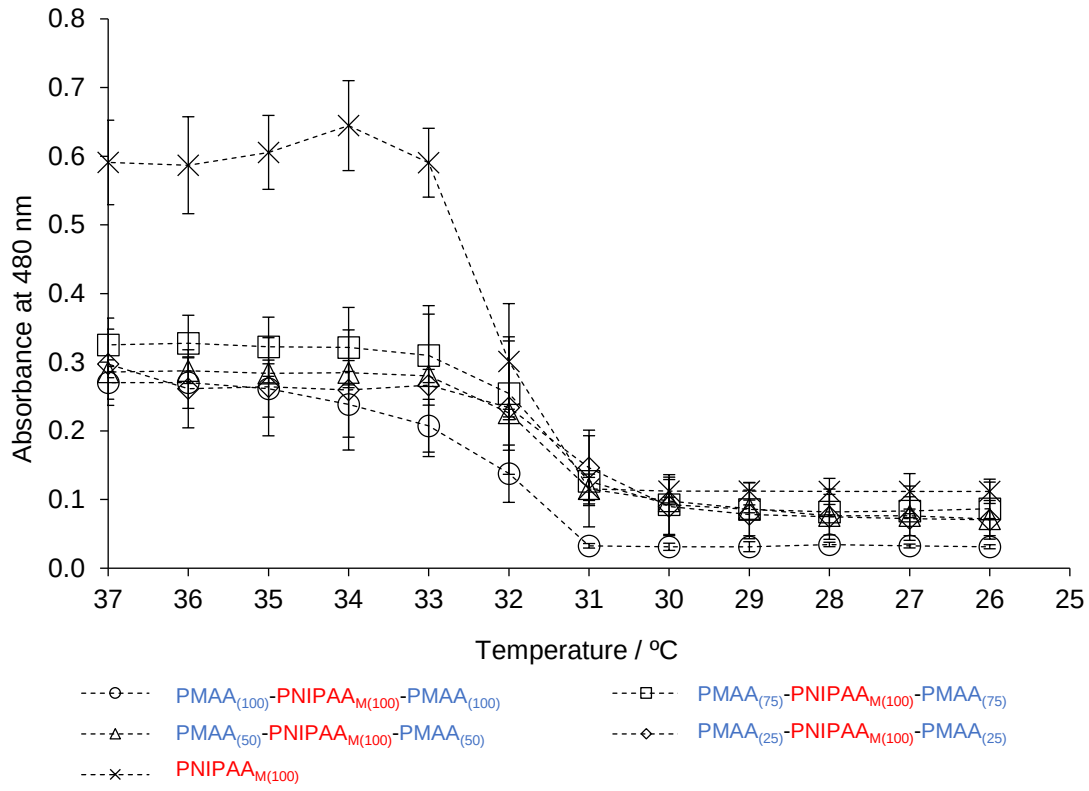

Figure 3.27 – A comparison of the UV/Vis absorbance data of $PNIPAA_{M(100)}$ (4 mg/mL) and triblock $PMAA\text{-}PNIPAA_{M}\text{-}PMAA$ copolymers in pH 7.2 phosphate buffer (8 mg/mL) Measurements conducted in triplicate.

In addition to copolymerisation reactions in which each macroRAFT agent was isolated and characterised prior to subsequent block addition, "one-pot" block copolymerisation was conducted with an aim to determine the suitability for sequential preparation. Ideally, one-pot block copolymerisation is a facile and inexpensive way to prepare block copolymers, greatly reducing reaction times and loss of product during multiple isolations and characterisations. However, there are many limitations including monomer reactivity, solvent solubility and the introduction of impurities into an otherwise sealed system[194]. When conducting sequential one-pot block copolymerisations, there is also an increased risk of "block contamination" (Figure 3.28), as residual monomer present in the solvent upon the addition of the second or third monomer may then copolymerise and be present in the next block. In very high molecular weight polymers this minimal contamination may not pose an issue as the block will largely retain its character, but in relatively low molecular weight polymers such as these, clearly defined blocks ensure that the desired behaviour of

stimuli-responsive $PNIPAA_M$ is not modified in any way by random copolymerisation with hydrophilic MAA repeat units. Given the high conversion values observed for block copolymers synthesised via subsequent RAFT polymerisation, it was proposed that, if conducted successfully with minimal contamination, there would be little block contamination via sequential methods.

Figure 3.28 – A diagram comparing an ideal sequential block copolymerisation (top) with a less ideal product containing block contamination (bottom), caused by the presence of residual monomer due to poor conversion.

Guerrero-Sanchez *et al.*[194,195] successfully prepared block copolymers of methacrylate-based monomers via RAFT polymerisation using an automated parallel synthesiser system, achieving less than 15% contamination of the initial monomer presenting in subsequent blocks. The experimental protocol adopted during this project follows the same concept, but in a more rudimentary one-pot design. The reaction proceeds under nitrogen flow in a 250 mL two-necked round-bottomed flask and degassed monomer is injected into the system at desired intervals, as prescribed by the conversion data for the subsequent block copolymerisations, to build the block copolymer. Analysis of the ^1H NMR spectrum for the polymer, analogous to that of the subsequently polymerised triblock copolymer (Figure 3.22), reveals approximately 21 % contamination of the final product with monomeric residues, indicative of 79 % conversion. The spectrum does not, however, expose the presence of homopolymeric contaminants, therefore DOSY NMR was once again employed to determine successful chain extension.

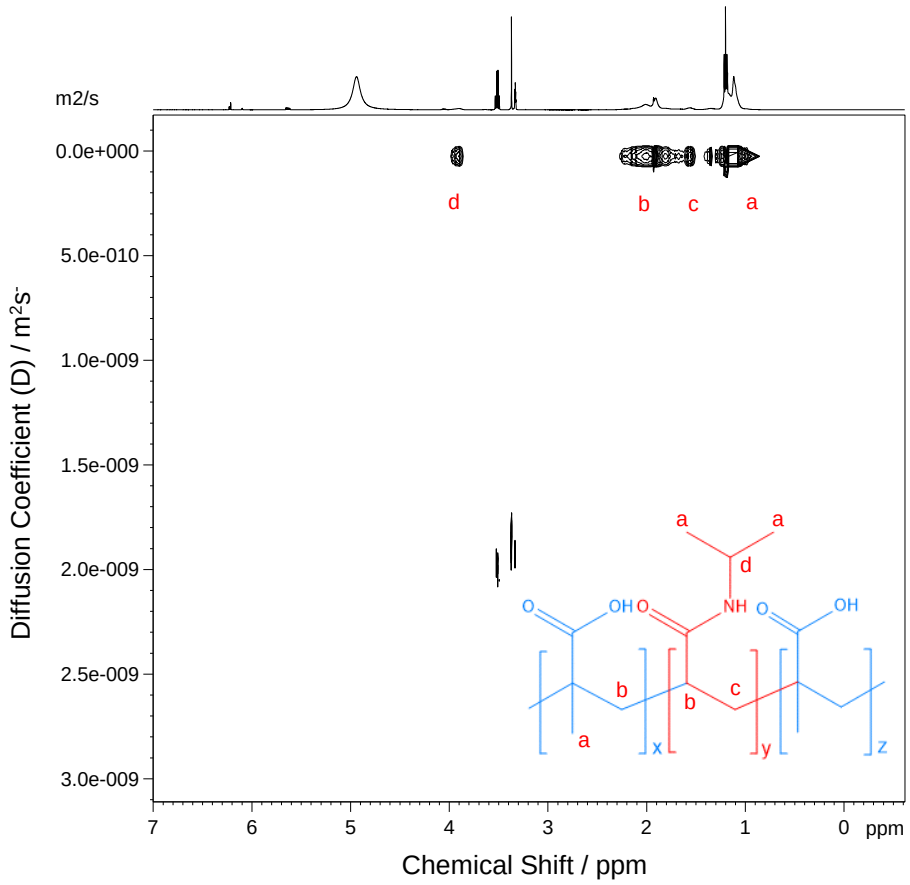

Figure 3.29 – DOSY NMR spectrum of sequential triblock $PMAA_{(100)}$-$PNIPAA_{M(100)}$-$PMAA_{(100)}$ (1mM in MeOD).

It was assumed that there may be some homopolymeric contamination of PMAA, generated by free radical polymerisation, due to the stability of the diblock macroRAFT agent with respect to cleavage in the pre-equilibrium and the presence of monomer residues in the ^1H NMR spectrum. However, the DOSY spectrum of the final product (Figure 3.29) reveals no homopolymeric contamination, characterised by the single spectral pattern and diffusion coefficient of both PMAA and $PNIPAA_M$-specific peaks. Monomer contamination in the ^1H NMR spectrum is therefore likely due to the relatively poor RAFT agent compatibility of the diblock macroRAFT agent towards addition of the final PMAA block. The diffusion coefficient is also comparable to that of $PMAA_{(100)}$-$PNIPAA_{M(100)}$-$PMAA_{(100)}$ copolymerised by subsequent block copolymerisation at 3.7×10^{-11} m^2s^{-1}. It is a promising result and further investigation may facilitate rapid, reproducible block copolymer preparation, improving the efficiency of an otherwise extensive protocol.

3.5 Modifying the LCST

$NIPAA_M$ was copolymerised with hydrophobic methyl methacrylate in an attempt to modify the LCST by RAFT polymerisation. Due to the controlled nature of RAFT polymerisation, and the differing polymerisation rate constants of PMMA and $PNIPAA_M$ (46.5 x 10^{-6} s^{-1} and 8.7 x 10^{-6} s^{-1} respectively in 1,4-dioxane with CMDB and ACP), the reaction was designed with a 95:5 initial feed ratio of [$NIPAA_M$]:[MMA]. Moad *et al.*[128] proposed that the conventional limitations of copolymerisation, such as differing reaction rates, pose less of a concern in RAFT polymerisation as copolymer composition remains largely homogeneous with respect to propagation. However, at low molecular weights the effect of R group specificity as a result of compatibility may influence the composition. The MMA repeat units were therefore present in small enough quantities to randomly copolymerise with the far higher concentration of $NIPAA_M$ repeat units rather than preferentially homopolymerising due to their compatibility with dithiobenzoate RAFT agents. The reaction was also monitored and stopped after approximately 10% conversion to prevent the formation of a $PNIPAA_M$ tail block in the eventuality that MMA distribution throughout the copolymer was not homogeneous (Figure 3.30). A large block of $PNIPAA_M$ homopolymer may confer characteristic thermoresponsive behaviour upon the polymer, overriding the modified LCST of the copolymer region.

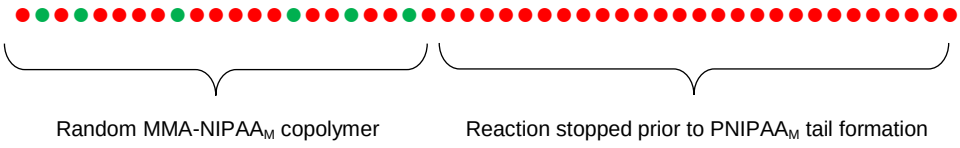

Figure 3.30 – Schematic of P(MMA-co-$NIPAA_M$) copolymerisation. Reaction stopped prior to formation of $PNIPAA_M$ tail block.

Due to the overlap of MMA and $NIPAA_M$-specific monomer peaks, the conversion was monitored by the loss of monomer peak heights of both MMA and $NIPAA_M$ by NMR (Figure 3.31). After 9 hours an approximate conversion of 11-13 % was achieved, determined by integration of the monomeric peak heights between 5.7-6.5 ppm (Figure 3.32), and the reaction was stopped. The initial rate constant (k_p) for monomer consumption is far higher than for homopolymeric $PNIPAA_M$ (3.19×10^{-6} s^{-1} and 9.7×10^{-7} s^{-1} respectively). This would suggest that, contrary to the period of initial inhibition observed upon polymerisation of $NIPAA_M$ with CMDB[151] (Figure 3.6), the monomers are rapidly consumed into the reaction and propagated, much like the observed behaviour of PMAA polymerisation. MAMs such as methacrylates are highly compatible with dithioester RAFT agents, and the addition of a small percentage of methyl methacrylate may increase the rate of monomer consumption due to the intermittent presence of a readily dissociating tertiary R leaving group upon the equilibrium of the propagating chain.

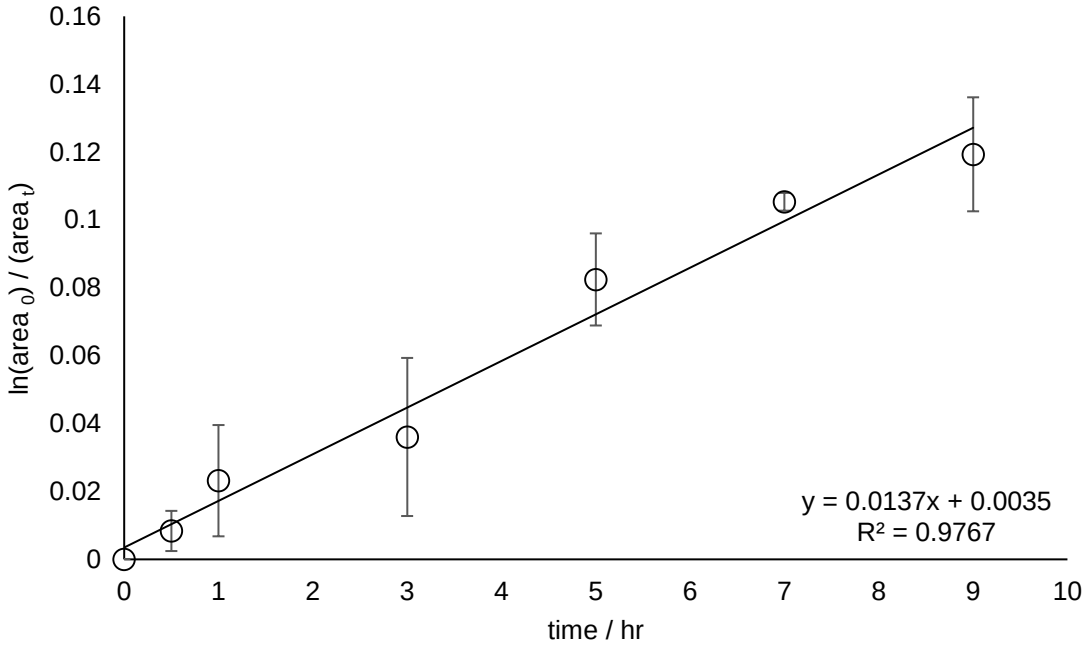

Figure 3.31 – Monitoring the conversion of P(MMA-co-$NIPAA_M$) by ^1H NMR. Experiments were performed in triplicate.

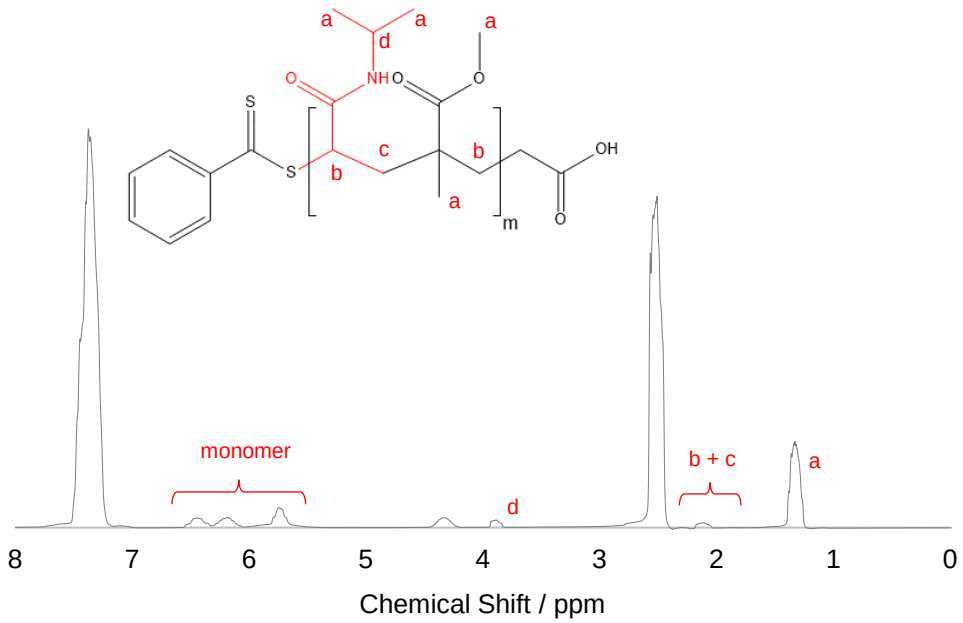

Figure 3.32 – ^{1}H NMR of P(MMA-co-NIPAA$_M$) at 12 % conversion ($CDCl_3$). a – CH_3 in PMMA methyl and PNIPAA$_M$ isopropyl groups, b – CH_2 in PMMA backbone and CH in PNIPAA$_M$ backbone, c – CH_2 in PNIPAA$_M$ backbone, d – CH in PNIPAA$_M$ side group.

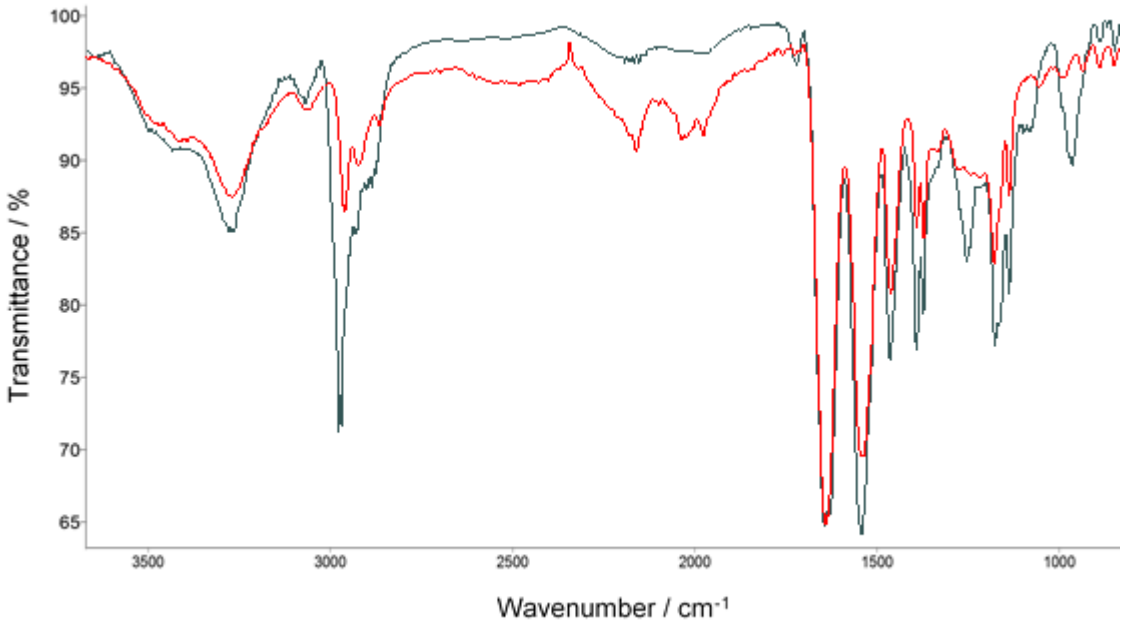

Figure 3.33 – FT-IR spectra of PNIPAA$_{M(100)}$ (red) and P(MMA-co-NIPAA$_M$) (black).

Analysis of the FT-IR spectrum of P(MMA-co-NIPAA$_M$) (black) and comparison with the spectrum of PNIPAA$_M$ (red) further confirms successful copolymerisation of the two monomers (Figure 3.33). The weak two banded signal of the copolymer spectrum at 1100 cm^{-1}, absent on the homopolymer spectrum, represents the C-O bond of the methacrylate ester functionality and the single peak at 1250 cm^{-1} corresponds to the sp^3 carbon bending signal of the MMA methyl group in the backbone. In addition, the small peak at 1750 cm^{-1} is characteristic of an acid carbonyl signal.

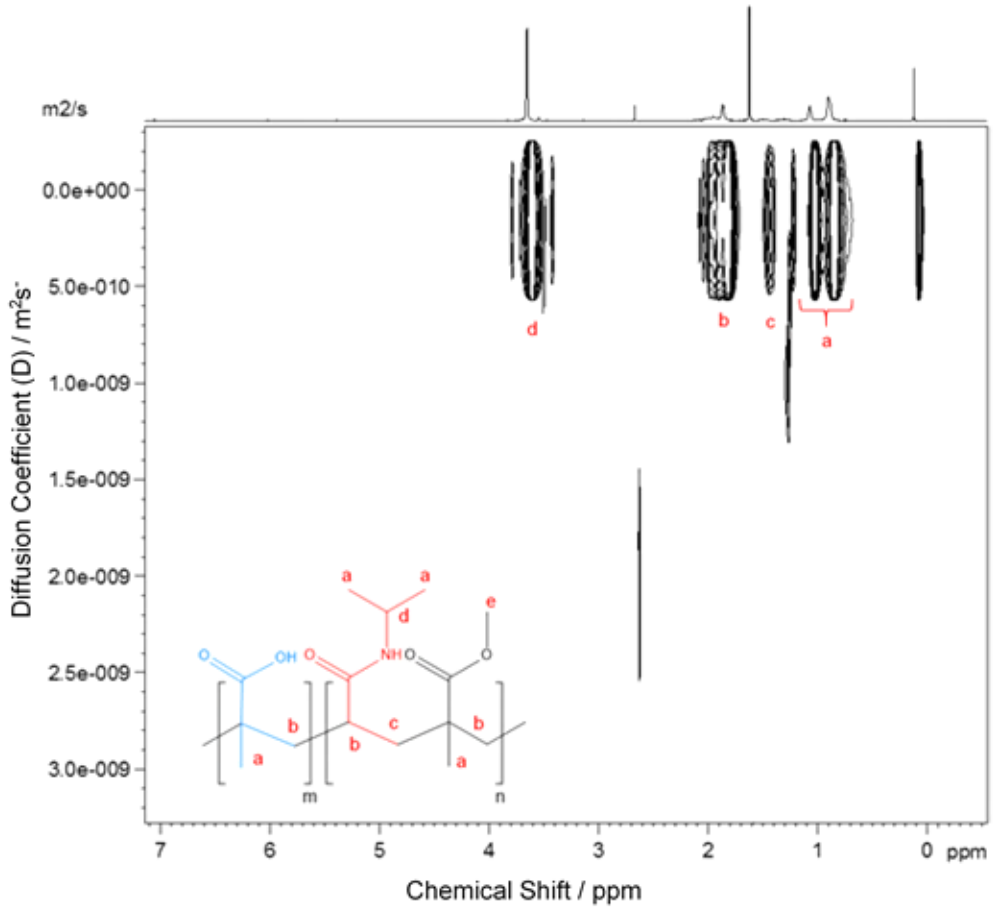

Figure 3.34 – DOSY NMR spectrum of PMAA$_{(100)}$-P(MMA-co-NIPAA$_M$) (1mM in D$_2$O).

Figure 3.34 shows the DOSY NMR spectrum for the block copolymerised $PMAA_{(100)}$-P(MMA-co-$NIPAA_M$). The peaks corresponding to PMAA and copolymerised $NIPAA_M$ can be seen to have the same diffusion coefficient, of 1.0×10^{-10} m^2s^{-1}. It was not possible, however, to differentiate MMA-specific peaks within the spectrum, therefore measurements of the LCST proved valuable in confirming successful MMA incorporation.

DLS analysis of the polymers reveal a distinctive shift in the LCST to 28 °C of P(MMA-co-$NIPAA_M$) and diblock $PMAA_{(100)}$-(MMA-co-$NIPAA_M$) (Figure 3.35 and Figure 3.36) from that of homopolymeric $PNIPAA_M$ and $PNIPAA_M$-containing block copolymers (Figure 3.26). This shift in transition temperature is indicative of random distribution of MMA repeat units throughout the polymer, as opposed to localisation into blocks or independent homopolymerisation. As with $PNIPAA_M$ (Figure 3.10), the Z-average diameter of the collapsed P(MMA-co-$NIPAA_M$) globules continues to grow as the temperature increases and the polymer globules aggregate to further exclude water. The block copolymer of $PMAA_{(100)}$-(MMA-co-$NIPAA_M$), however, exhibits the same behaviour as that of the other diblock PMAA-$PNIPAA_M$ copolymers, indicative of core-shell globules (Figure 3.35). $PMAA_{(100)}$-P(MMA-co-$NIPAA_M$) also exhibits a comparable Z-average diameter beyond the LCST to that of $PMAA_{(100)}$-$PNIPAA_{M(100)}$, further confirming that the behaviour of LCST-modified block copolymers is analogous to that of $PNIPAA_M$-containing block copolymers, albeit with a lower transition temperature.

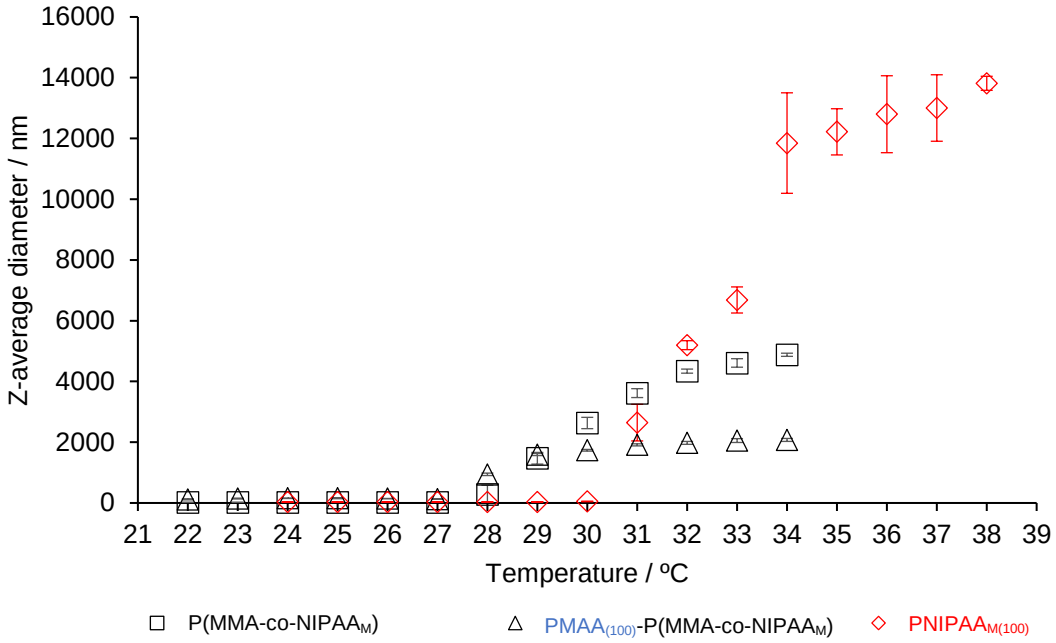

Figure 3.35 - The change in Z-average diameter of P(MMA-co-NIPAA$_M$) (feed ratio 5:95) and PMAA-P(MMA-co-NIPAA$_M$) (feed ratio 5:95) in pH 7.2 phosphate buffer (50 mM) with increasing temperature. Measurements conducted in quintuplicate.

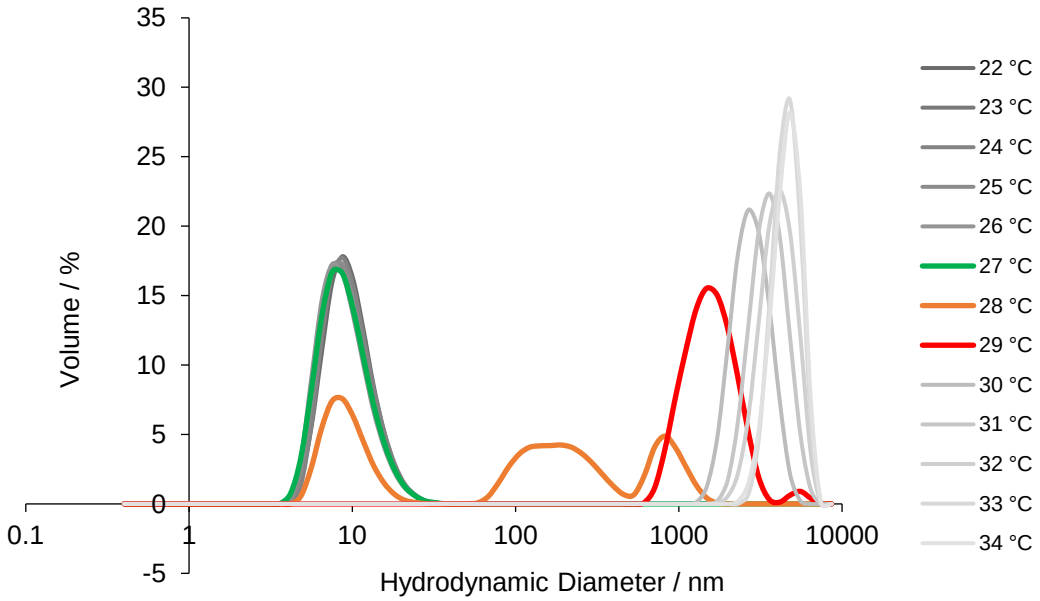

Figure 3.36 – Size distribution by volume for P(MMA-co-NIPAA$_M$) (feed ratio 5:95), the temperature immediately prior to the transition is highlighted in green, followed by the LCST of 28 ºC in amber and the collapsing globular polymer is shown in red.

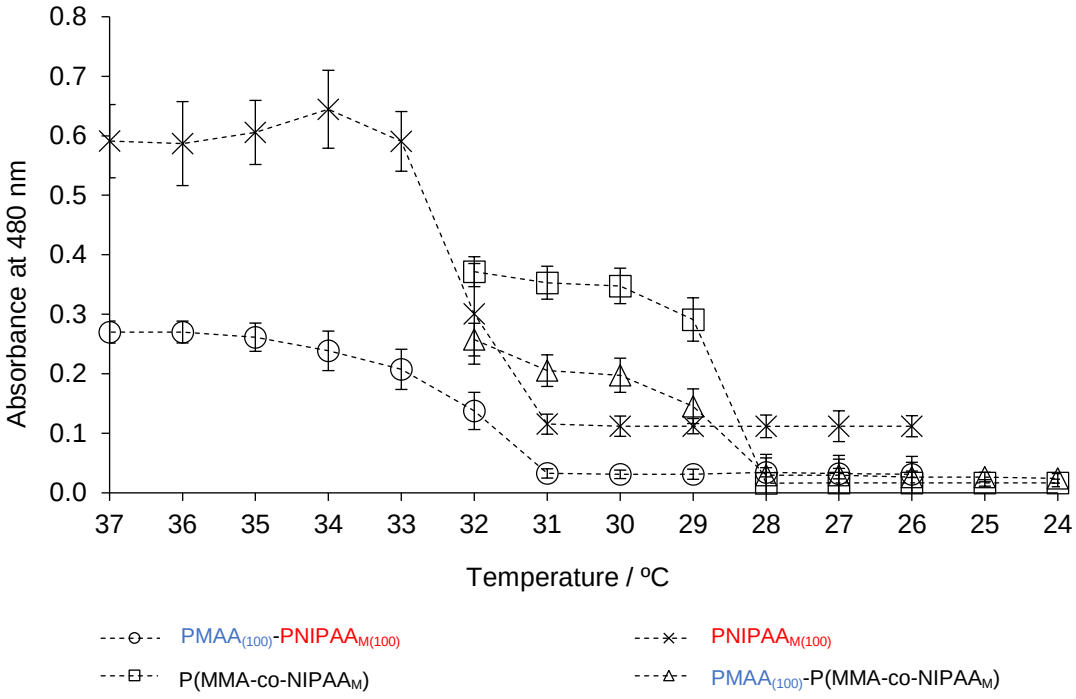

Figure 3.37 – UV/Vis absorption data of $PNIPAA_{M(100)}$, $P(MMA\text{-}co\text{-}NIPAA_M)$ (feed ratio 5:95) (both 4 mg/mL), $PMAA_{(100)}$-$PNIPAA_{M(100)}$ and $PMAA_{(100)}$-$(MMA\text{-}co\text{-}NIPAA_M)$ (feed ratio 5:95) (both 8 mg/mL). Measurements conducted in triplicate.

As with previous polymers, the change in measured absorbance with decreasing temperature indicates a loss of sample opacity at 28 °C, corroborating the transition temperature values obtained by DLS (Figure 3.37). The MMA-containing copolymers largely mimic the behaviour of their $PNIPAA_M$ counterparts. A sharp transition can be observed for $P(MMA\text{-}co\text{-}NIPAA_M)$, analogous to that of $PNIPAA_M$ (Figure 3.9) whilst the presence of a PMAA block leads to a gradual loss of absorbance from 2-3 °C above the measured LCST. As previously discussed, this is likely a result of hydrophilic PMAA disrupting the core shell aggregate structures prior to the measured LCST of 28 °C.

Modification of the LCST in this way further widens the scope of potential applications for thermoresponsive polymers, namely in their use as polymeric drug delivery vehicles, discussed further in Chapter 5.

3.6 Thiolation of Polymers

The use of synthetic macromolecules as a means to generate microspheres via a sonochemical protocol has received little attention in the literature, with many focusing instead on the use of readily-available proteins. Cavalieri *et al.*[10] were the first to report the use of synthetic polymers. A percentage of the acid moieties of PMAA were thiolated with cysteamine hydrochloride in a carbodiimide crosslinking reaction to yield thiolated $PMAA_{SH}$ in order to mimic the behaviour of thiol-containing proteins[2,14] under the influence of ultrasound, forming microspheres stabilised by radically-induced disulphide crosslinking[2]. Although the need for thiol functionalities in certain systems has since been disproved[11,12], Cavalieri[10] reported no stable microsphere formation when preparing perfluorohexane (PFH)-filled PMAA microspheres in the absence of thiol moieties and cited the requirement of radically-induced disulphide crosslinkers to form microspheres in this particular system.

To enable a comparison between the behaviour of functionalised and non-functionalised PMAA-based polymers upon sonication, those prepared as described in Section 2.1 were thiolated to yield chains with a degree of -SH functionalisation. The hydrophilicity of PMAA is dependent upon its carboxylic acid functionalities, therefore overfunctionalisation ultimately decreases the polymer solubility. A degree of functionalisation of the MAA repeats units was targeted at approximately 30% to maintain hydrophilicity whilst ensuring sufficient crosslinking. The reaction proceeds via a carbodiimide crosslinking reaction (Figure 3.38) to yield the thiolated polymer (4).

In a typical carbodiimide crosslinking reaction, the carboxylic acid, in this case of the MAA repeat units, is activated by conjugation with N-(dimethylaminopropyl)-N'-ethylcarbodiimide (EDAC) (1) to form an O-acylisourea intermediate (2), this can easily undergo nucleophilic attack by the primary amine of cysteamine hydrochloride to yield the thiol substituted MAA repeat unit (4) and an isourea by product. The intermediate O-acylisourea is unstable with respect to hydrolysis in aqueous solutions, therefore N-hydroxysuccinimide (NHS) is often employed to substitute the O-acylisourea for an NHS-ester (3), which is far more stable and may be isolated if required. Nucleophilic attack by the primary amine then occurs as previously described[196].

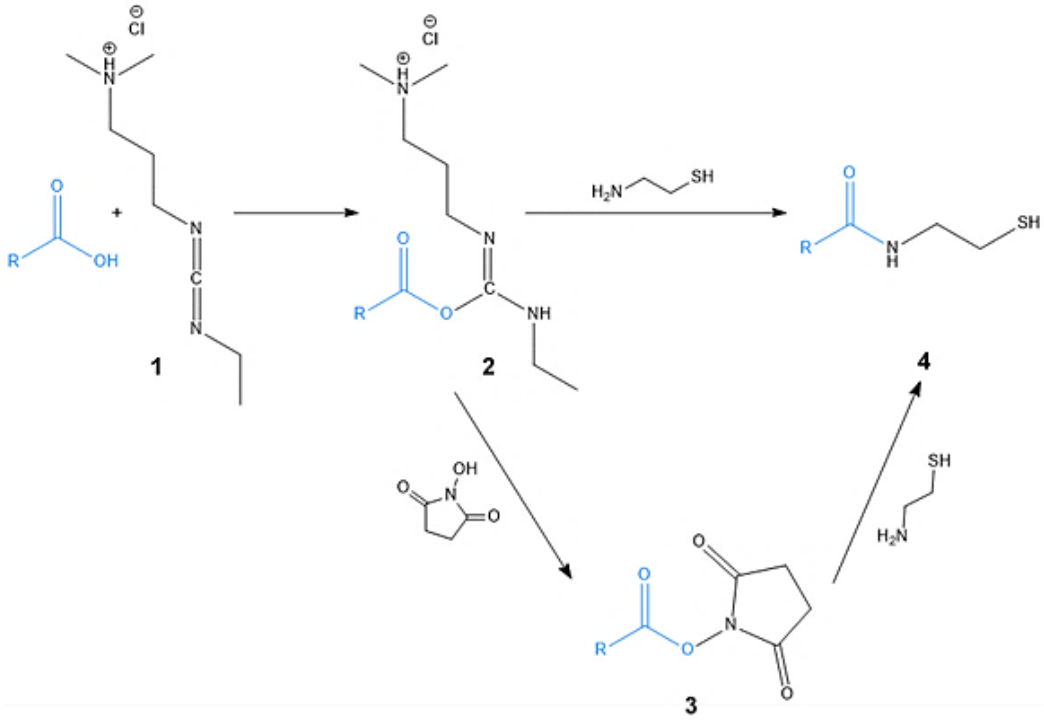

Figure 3.38 – Functionalisation of a carboxylic acid (blue) by carbodiimide crosslinking with N-(dimethylaminopropyl)-N'-ethylcarbodiimide (1), N-hydroxysuccinimide (3) and cysteamine hydrochloride (4).

To tailor the degree of functionalisation of PMAA-based polymers by cysteamine hydrochloride, the number of moles of MAA repeat units of each polymer were first calculated, and a percentage of cysteamine hydrochloride was subsequently charged to the reaction. The delay of 15 minutes prior to addition of the primary amine was to ensure that the O-acylisourea intermediate had been substituted to form the stable NHS-ester. Although direct attack by the primary amine upon intermediate (2) is possible as previously described, the low concentration of cysteamine hydrochloride used exposes the unstable intermediate to hydrolysis.

Table 3.8 – The degree of thiolation of PMAA blocks within polymers synthesised as described in Section 2.1. Thiolation experiments were conducted in triplicate, from which an average degree of thiolation was determined.

Polymer Name	Degree of Thiolation of PMAA (^{1}H NMR)
$PMAA_{SH(25)}$	28 ± 2
$PMAA_{SH(50)}$	27 ± 1
$PMAA_{SH(75)}$	29 ± 1
$PMAA_{SH(100)}$	28 ± 1
$PMAA_{SH(25)}$-$PNIPAA_{M(100)}$	29 ± 2
$PMAA_{SH(50)}$-$PNIPAA_{M(100)}$	30 ± 1
$PMAA_{SH(75)}$-$PNIPAA_{M(100)}$	28 ± 3
$PMAA_{SH(100)}$-$PNIPAA_{M(100)}$	27 ± 2
$PMAA_{SH(25)}$-$PNIPAA_{M(100)}$ -$PMAA_{SH(25)}$	31 ± 1
$PMAA_{SH(50)}$-$PNIPAA_{M(100)}$ -$PMAA_{SH(50)}$	27 ± 4
$PMAA_{SH(75)}$-$PNIPAA_{M(100)}$-$PMAA_{SH(75)}$	28 ± 2
$PMAA_{SH(100)}$-$PNIPAA_{M(100)}$-$PMAA_{SH(100)}$	28 ± 3

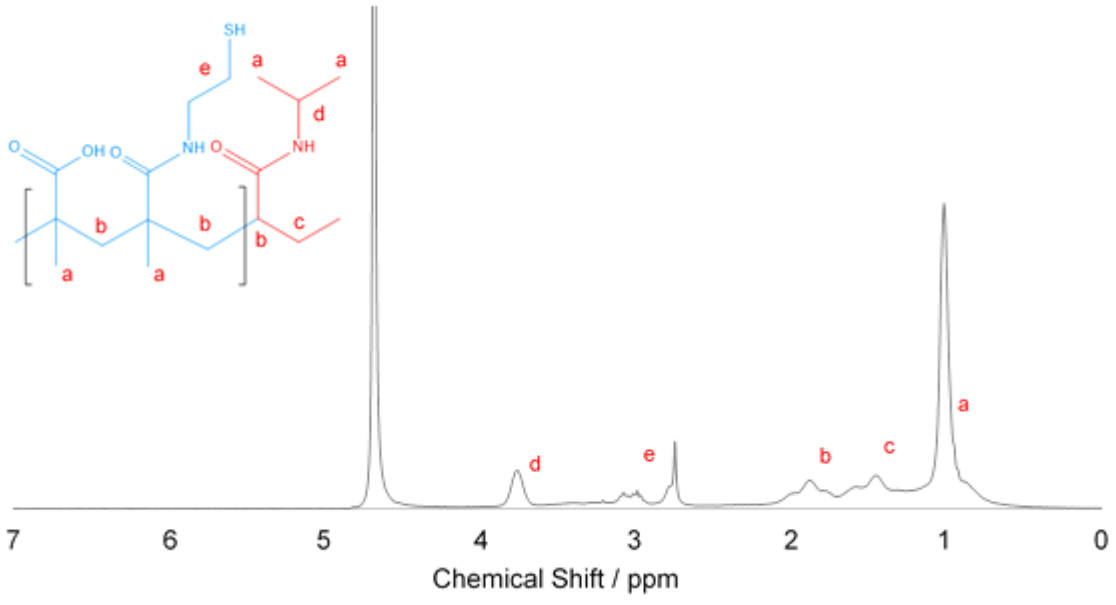

Figure 3.39 – ^{1}H NMR of thiolated $PMAA_{SH(100)}$-$PNIPAA_{M(100)}$. Integration of functional peak heights reveals 29 % thiolation of MAA repeat units (1 mM in MeOD). Peaks a – d as before, e - CH_2 groups in functionalised side group of $PMAA_{SH}$.

The degree of functionalisation of PMAA blocks was determined by integration of cysteamine hydrochloride-specific peaks at 3.0-3.1 ppm (e) as a percentage of the methyl integrals of the PMAA backbone at 1.0 ppm, an example of which is shown in Figure 3.39 for $PMAA_{SH(100)}$-$PNIPAA_{M(100)}$. For $PMAA_{SH}$ homopolymers, 28 ± 2 % thiolation was achieved. Diblock copolymers exhibited approximately 28 ± 3 % functionalisation of the PMAA block and in the triblock $PMAA_{SH}$-$PNIPAA_{M}$-$PMAA_{SH}$ copolymers 27 ± 5 % functionalisation was achieved (Table 3.8). It must be noted that the maximum degree of functionalisation of MAA repeats units permissible by the reaction parameters was 30.3 %.

Fourier transform infra-red spectroscopy was employed as a technique to corroborate the ^{1}H NMR data and confirm successful functionalisation. The FT-IR spectra for thiolated $PMAA_{SH}$ (black) and non-thiolated PMAA (black) is shown in Figure 3.40. The band corresponding to thiol SH functionalities at 2600-2550 cm^{-1} is notoriously weak[197]. It is therefore not possible to distinguish between the two analogues from this signal alone. The signal corresponding to the carbonyl of the carboxylic acid at 1700 cm^{-1} is shifted upfield slightly in the thiolated polymer due to the proximity of the functionalised repeat unit carbonyls to the NH group of the thiol functionality[198]. The carbonyl becomes part of an amide R-CONH-R^{1} as opposed to that of the MAA carboxylic acid R-COOH. The asymmetry of the peak on the left-hand side is indicative of signal overlap with the MAA carbonyl signal.

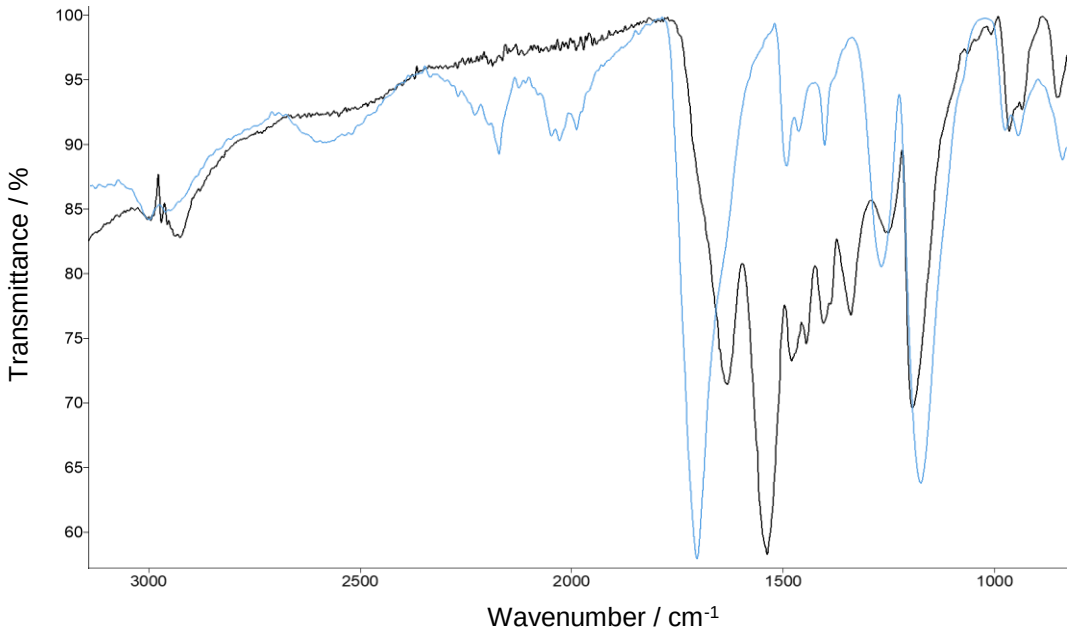

Figure 3.40 – FT-IR spectra of $PMAA_{(100)}$ (blue) and functionalised $PMAA_{SH(100)}$ (black).

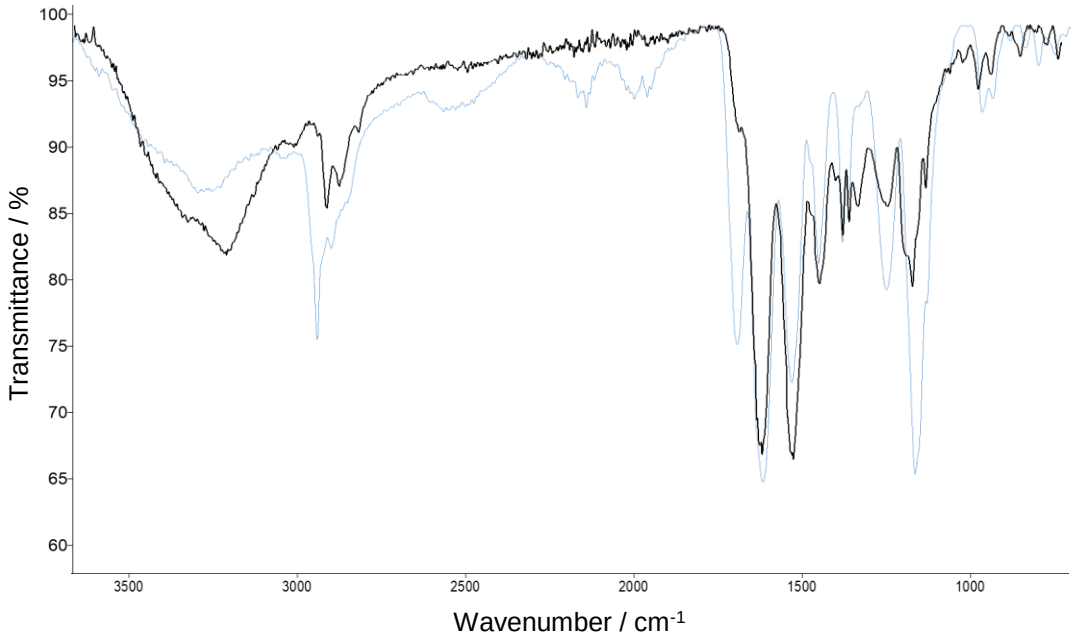

Figure 3.41 - FT-IR spectra of $PMAA_{(100)}$-$PNIPAA_{M(100)}$ (blue) and functionalised $PMAA_{SH(100)}$-$PNIPAA_{M(100)}$ (black).

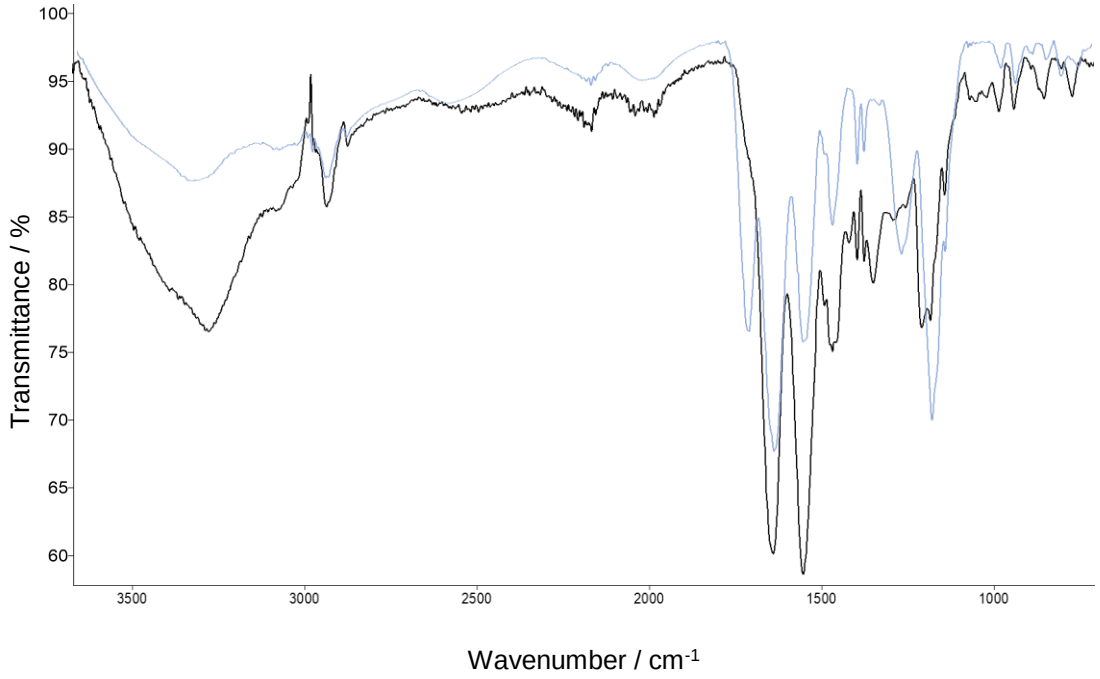

Figure 3.42 - FT-IR spectra of $PMAA_{(100)}$-$PNIPAA_{M(100)}$-$PMAA_{(100)}$ (blue) and functionalised $PMAA_{SH(100)}$-$PNIPAA_{M(100)}$ (black).

FT-IR spectra of the native and thiolated di- and triblock copolymers, and of the LCST-modified diblock copolymer, also indicate successful functionalisation, characterised by shifting of the carbonyl peak as a result of a percentage of carbonyls bonding to cysteamine hydrochloride to form a secondary amide (Figure 3.41, Figure 3.42 and Figure 3.43). It is interesting to note that, in the block copolymers, the shifted carbonyl peak now overlaps the carbonyl peak found in N-isopropylacrylamide, whereby the carbonyl is bonded to the secondary amine carrying the isopropyl moiety. The twin peak at 1200-1300 cm^{-1} corresponding to the C-O stretch of PMAA carboxylic acid functionalities is also reduced in the functionalised spectra, as with the homopolymer (Figure 3.40). The secondary amine bending signal at 1550 cm^{-1} is now also present in the non-functionalised polymer due to the presence of a secondary amine in the $NIPAA_M$ repeat units. The decrease in transmittance of the secondary NH stretching signal of $PNIPAA_M$ and the thiol functionalised MAA repeat units at >3300 cm^{-1} is due to the presence of an overlapping residual water signal in the functionalised samples.

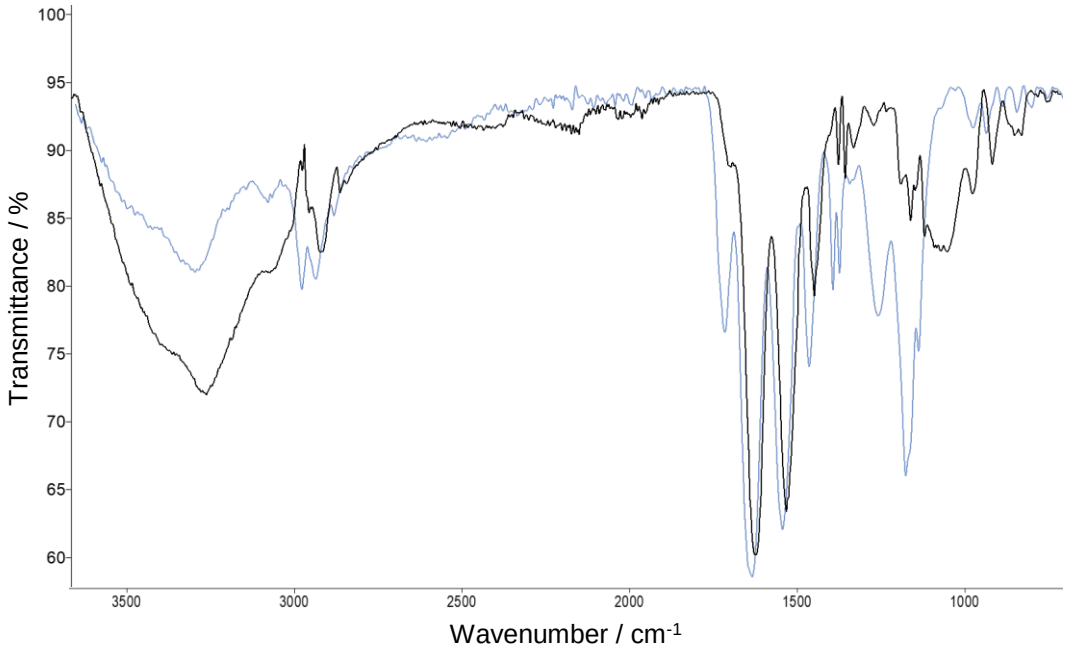

Figure 3.43 - FT-IR spectra of $PMAA_{(100)}$-(MMA-co-$NIPAA_M$) (blue) and functionalised $PMAA_{SH(100)}$-(MMA-co-$NIPAA_{M(100)}$) (black).

The polymers were washed by dialysis after thiolation to ensure that no residual short chain impurities, such as unreacted cysteamine hydrochloride, remained as contaminants. DOSY NMR was subsequently employed as a technique to confirm that the ^1H signals for the cysteamine thiol moieties correspond to those of the functionalised polymer, an example of which is shown in Figure 3.44 for $PMAA_{SH(100)}$-$PNIPAA_{(100)}$-$PMAA_{SH(100)}$. The diffusion peak at 3 ppm corresponds to the two CH_2 groups of the cysteamine hydrochloride and exhibits the same diffusion coefficient as the polymeric signals of 0.3 x 10^{-10} m^2s^{-1}.

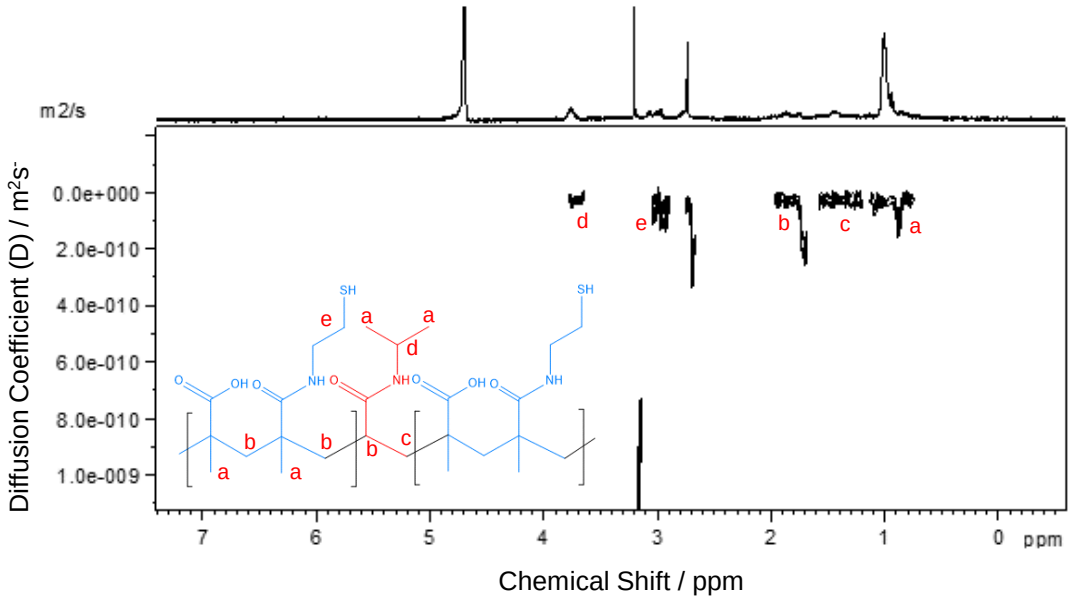

Figure 3.44 – ^{1}H DOSY NMR spectrum of PMAA$_{SH(100)}$-PNIPAA$_{(100)}$-PMAA$_{SH(100)}$ in D$_2$O (1 mM).

The stimuli-responsive behaviour of thiolated PMAA-based block copolymers containing PNIPAA$_M$ was measured by UV/Vis spectrophotometry to determine whether the effect of thiolation had modified the transition temperature of the polymers. As expected, the measured values in Figure 3.45, comparing thiolated and non thiolated PMAA$_{(100)}$-containing block copolymers as an exemplar, reveal no change in the LCST of thiolated block copolymers with respect to their non-functionalised precursors (Figure 3.27 and Figure 3.37). It is interesting to note upon analysis of the DLS data (Figure 3.46) beyond the LCST that aggregates containing thiolated PMAA$_{SH}$ moieties do not quite reach the size of their non-thiolated counterparts, particularly in the case of PMAA$_{SH}$-(MMA-co-NIPAA$_M$). It has already been acknowledged that block copolymers form core-shell aggregates upon collapse, and the data would suggest that the presence of hydrophobic thiol functionalities in the PMAA blocks leads to more folded chains extending from the hydrophobic PNIPAA$_M$ core in order to localise thiol regions within the chain (Figure 3.47). The effect of this folding on polymers below the LCST is not significant enough to affect the observed Z-average diameter as chains are moving freely through the medium and interacting with one another and the solvent. It is only upon the organisation of chains into core-shell aggregates to increase the entropy of the overall system that this folding effect can be observed. It is for this reason that care must be taken not to overfunctionalise the

chains as insufficient carboxylic acid moieties within a chain leads to hydrophobicity. Cavalieri *et al.*[10] describe the balance between achieving stability through extensive crosslinking and the risk of polymer hydrophobicity through overfunctionalisation. A target percentage thiolation of 30 % was chosen as, in the block copolymers that comprise of only 20 % PMAA such as $PMAA_{(25)}$-$PNIPAA_{M(100)}$, that equates to an overall degree of functionalisation of 6 %, still within the range investigated by Cavalieri *et al.* in PMAA homopolymers.

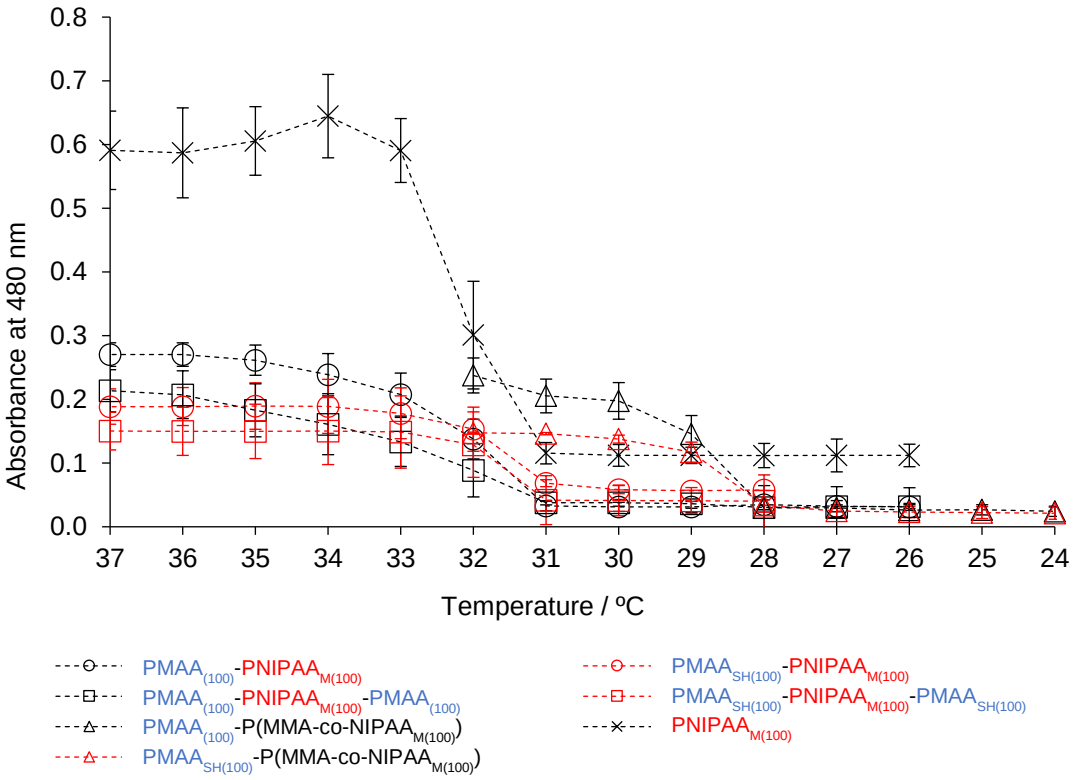

Figure 3.45 – UV/Vis absorbance data of thiolated (red) and non-thiolated (black) PMAA-based stimuli-responsive block copolymers (8 mg/mL) and $PNIPAA_M$ (4 mg/mL). Measurements conducted in triplicate.

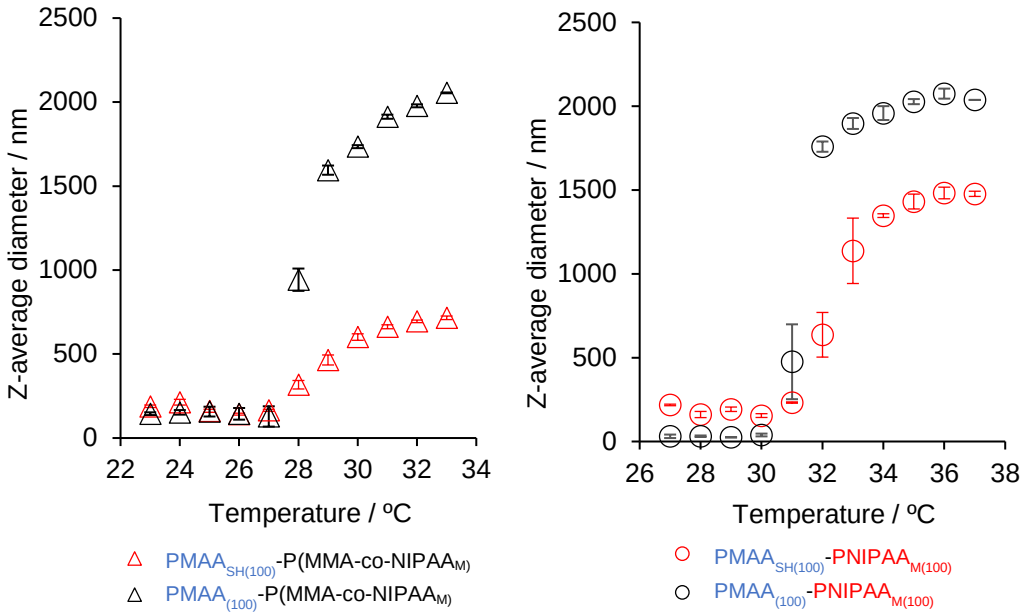

Figure 3.46 – Monitoring the change in Z-average diameter of thiolated (red) and non-thiolated (black) PMAA$_{SH(100)}$-PNIPAA$_M$ and PMAA$_{SH(100)}$-(MMA-co-NIPAA$_M$) in pH 7.2 phosphate buffer with increasing temperature (50 mM). All measurements were conducted in quintuplicate.

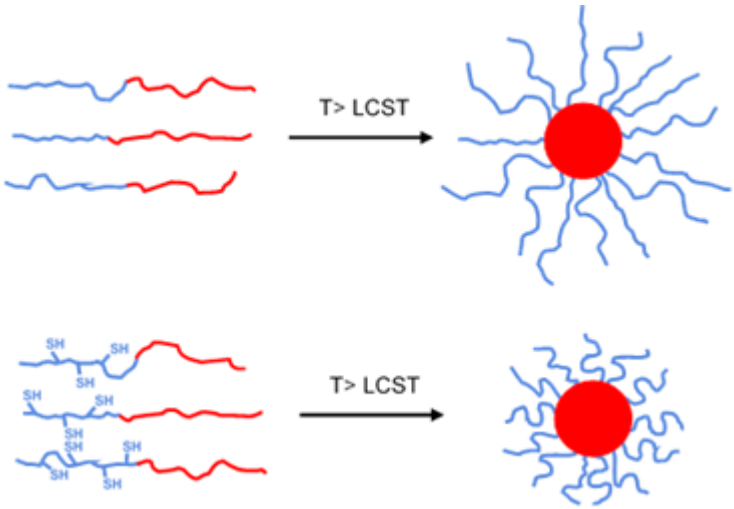

Figure 3.47 – Proposed contracted core-shell structure of stimuli-responsive PMAA$_{SH}$-based block copolymers as a result of localised chain folding. Not to scale.

3.7 The Effect of pH on Polymer Solubility

The carboxylic acid functionalities of poly(methacrylic acid) will readily deprotonate at a solution pH above the pKa of the polymer at 5.5[192] (Equation 3.7). It is this ionisation that is responsible for the inherent solubility of PMAA in polar solvents including water and methanol. To confirm that the behaviour of polymers generated during the course of this project exhibit the same solubility parameters as those reported in the literature, two solutions of polymer in water were acidified and alkalised with hydrochloric acid and sodium hydroxide respectively.

$$RCOOH \rightleftharpoons H^+ + RCOO^- \quad (3.7)$$

As expected, upon acidification to pH 4 PMAA homopolymers and their functionalised analogues were insoluble due to protonation of all ionised carboxylic acid functionalities (Figure 3.48). The same could also be observed for native and thiolated block copolymeric PMAA-PNIPAA$_M$ and triblock PMAA-PNIPAA$_M$-PMAA copolymers. PNIPAA$_M$ is not inherently pH responsive due to a lack of ionisable functionalities, therefore PNIPAA$_M$ and P(MMA-co-NIPAA$_M$) did not exhibit the same insolubility at low pH.

Figure 3.48 – pH solubility of PMAA$_{(100)}$ (A), PNIPAA$_{M(100)}$ (B), PMAA$_{(100)}$-PNIPAA$_{M(100)}$ (C) and PMAA$_{(100)}$-PNIPAA$_{M(100)}$-PMAA$_{(100)}$ (D) in solutions of pH 4,6,8 and 10.

Whilst this project focuses on the thermoresponsive behaviour of these block copolymers for their use as thermoresponsive delivery vehicles, it is interesting to observe their dual-stimuli responsiveness at a pH below the pKa of PMAA, and may facilitate their use for more diverse applications as delivery vehicles in the future.

3.8 Chapter Summary

In this chapter, the synthesis of PMAA polymers and di- and triblock copolymers incorporating thermoresponsive poly(N-isopropylacrylamide) has been demonstrated, exhibiting an LCST characteristic of that of homopolymeric $PNIPAA_M$ at 31 ºC. Modification of the LCST to 28 ºC was also achieved by copolymerisation of $NIPAA_M$ with hydrophobic methyl methacrylate, in order to generate microspheres with an alternative release temperature.

The polymers were designed with varying PMAA block lengths in order to determine the effect of PMAA block length on microsphere morphology and potential release behaviour of the microspheres. It was possible to estimate the molecular weights of the PMAA homopolymers by esterification to yield PMMA and comparative DOSY NMR against commercially available standards of known molecular weight. The chosen RAFT agent CMDB was shown to confer good control over the polymerisations, with a linear relationship observed between ln(MW) and ln(D), however due to the incompatibility of the polymers with GPC, it was not possible to quantify the molecular weight and polydispersity of each polymer.

Following their synthesis, both the thiolated and non-thiolated polymers were employed as shell material in the sonochemical synthesis of synthetic polymeric microspheres, as discussed in Chapter 4.

4 Sonochemical Microsphere Synthesis

The versatility of sonochemically-generated microsphere systems, with respect to the range of shell materials and encapsulants that can be employed, make them attractive storage and delivery vehicles for a range of applications. The formation of microspheres from proteins lacking thiol functionalities have demonstrated the alternative interactions that can stabilise sonochemically-generated microspheres and, more recently, synthetic alternatives have been explored to broaden the range of shell materials and potential applications.

This chapter reports the generation of polymer-shelled microspheres, containing both hydrophobic and hydrophilic encapsulants, utilising the polymers and thiol-functionalised polymers synthesised in Chapter 3.

4.1 Optimisation of Sonochemically-generated Microspheres

In order to design an efficient system and tailor the conditions for sonochemical microsphere synthesis, a range of optimisation reactions and stability measurements were conducted. These included characterisation of the ultrasonic processor, determination of the effects of mechanistic variables upon microsphere morphology, and optimisation of the encapsulant species.

4.1.1 Characterisation of the Ultrasonic Processor

Sonochemically-generated crosslinking of thiol moieties during microsphere synthesis is a process that exploits radical generation as a result of ultrasonic cavitation. As such, the ultrasonic processor system was characterised both to gain an understanding of the acoustic power, and to measure successful radical generation.

In order to determine the power output of the ultrasonic horn setup and acoustic intensity generated from the horn tip, calorimetry was employed (Experiment 2.2.1). Calorimetry measures the power and intensity of the ultrasonic generator as a function of heat transfer

into a medium of known mass and heat capacity, as shown in Equation 2.1. The measured intensities for the processor, fitted with a 3mm horn tip, are displayed in Table 2.6 and the change in temperature with respect to time at arbitrary power settings 2 and 4 of the equipment are shown in Figure 4.1. During this project, power setting P=2 was employed as the chosen power for microsphere synthesis, and P=4 was utilised for sonochemical microsphere disruption. It is clear that, as the acoustic power is increased, the heat transferred to the surrounding water increases at a greater rate. Each experiment was conducted in triplicate and a reproducible linear relationship can be observed.

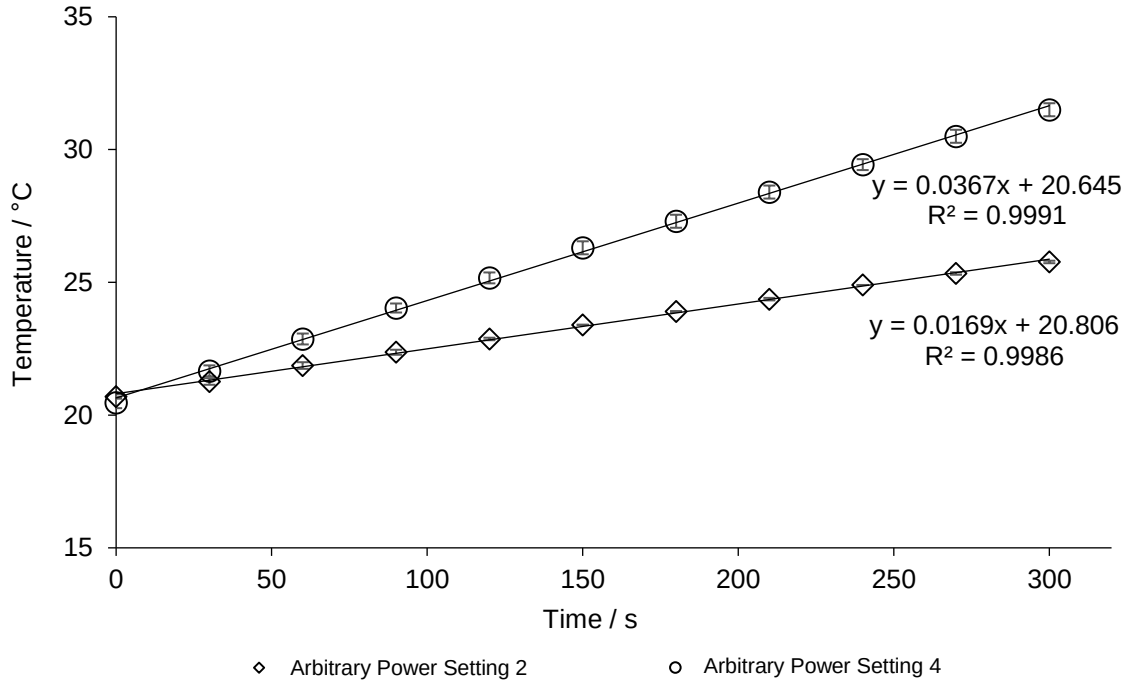

Figure 4.1 – Change in temperature with increasing sonication at arbitrary power settings 2 and 4 for the VC600 Processor, fitted with a 3 mm horn tip. Experiments conducted in triplicate, error bars indicate standard deviation in temperature.

The ultrasonic power and intensity for the 3 mm horn tip at P=2 were measured as 7.09 W and 100 ± 1 Wcm^{-2} respectively, and at P=4 were 15.45 W and 219 ± 1 Wcm^{-2}.

Chemical dosimetry was employed to estimate the radical production of the system during sonication. Radical production can be measured with the use of a Fricke dosimeter by monitoring a drop in the UV/Vis absorbance of a peak associated with Fe^{2+} and a corresponding increase in the Fe^{3+} peak, which denotes the radical-induced oxidation of

Fe^{2+} to Fe^{3+} (Equations 4.1-4.3)[199]. Fricke dosimeters were prepared as outlined in Experiment 2.2.2, and samples were taken at 5 minute intervals for analysis by UV/Vis spectroscopy. An increase in absorbance of the Fe^{3+} signal at 295 nm was measured, from which the change in concentration of Fe^{3+} was calculated (Figure 2.4).

$$Fe^{2+} + \bullet OH + H^+ \rightarrow Fe^{3+} + H_2O \quad (4.1)$$

$$Fe^{2+} + HO_2 \bullet + H^+ \rightarrow Fe^{3+} + H_2O_2 \quad (4.2)$$

$$Fe^{2+} + H_2O_2 + H^+ \rightarrow Fe^{3+} + \bullet OH + H_2O \quad (4.3)$$

The G value denotes the energy-specific yield of a sonochemical system. It can be used to approximate the number of moles of radicals generated during sonication by monitoring the change in concentration of Fe^{3+} with time[199]. Fe^{2+} is oxidised to Fe^{3+} by •OH radicals, generated as a result of sonication (Equation 4.1), however in an oxygen rich system H^+ is scavenged by O_2, which facilitates further oxidation of Fe^{2+} to Fe^{3+}. An equation to determine the G value of Fe^{3+} is therefore displayed as shown below in Equation 4.4, whereby one sonochemically-generated •OH radical yields one Fe^{3+}, one molecule of hydrogen peroxide generates two Fe^{3+}, and one superoxide radical yields three Fe^{3+} molecules[200]. All microsphere samples prepared throughout this project were sonicated in a system open to the air unless otherwise stated, therefore application of Equation 4.4 was used to approximate the number of radicals generated by sonication in the presence of oxygen.

$$G(Fe^{3+})_{O_2} = G(\bullet OH) + 2G(H_2O_2) + 3G(HO_2 \bullet) \quad (4.4)$$

According to Figure 4.2, the calculated concentration of radicals generated by the 3 mm horn tip after sonication of the dosimeter for 60 minutes at 100 Wcm^{-2} was approximately 112 $\mu moldm^{-3}$, which correlates to a G value of 4.4 x 10^{-9} $molJ^{-1}$ at 7.09 W input power and an approximate radical concentration of 2 $\mu moldm^{-3}$ generated during a typical reaction of 60s. In the absence of oxygen, the G value was approximated solely as a result of •OH concentration to be 7.3 x 10^{-10} $molJ^{-1}$. To enable a comparison, the 1 cm horn tip achieved an approximate radical concentration of 385 $\mu moldm^{-3}$ after 60 minutes, corresponding to a G value of 1.1 x 10^{-8} $molJ^{-1}$ at the same applied frequency and 9.94 W input power (Figure 4.3) and an approximate radical concentration of 6 $\mu moldm^{-3}$ generated after 60 s. In the absence of oxygen, this was approximated to be 1.8 x 10^{-9} $molJ^{-1}$.

Although the intensity of the 3 mm horn tip at the same arbitrary power far exceeds that of the 1 cm horn tip (100 Wcm^{-2} and 13 Wcm^{-2} respectively), the measured power output for the 1 cm horn tip is greater, hence the disparity in measured radical production. The smaller 3 mm horn tips are not designed for samples beyond 15 mL, whereas the 1 cm horn tip will effectively process a solution up to 250 mL far more rapidly and effectively than a microtip[201]. No samples prepared for sonication during the course of this project exceeded 3 mL, therefore the 3 mm horn tip was chosen due to its compatibility with systems of small volume.

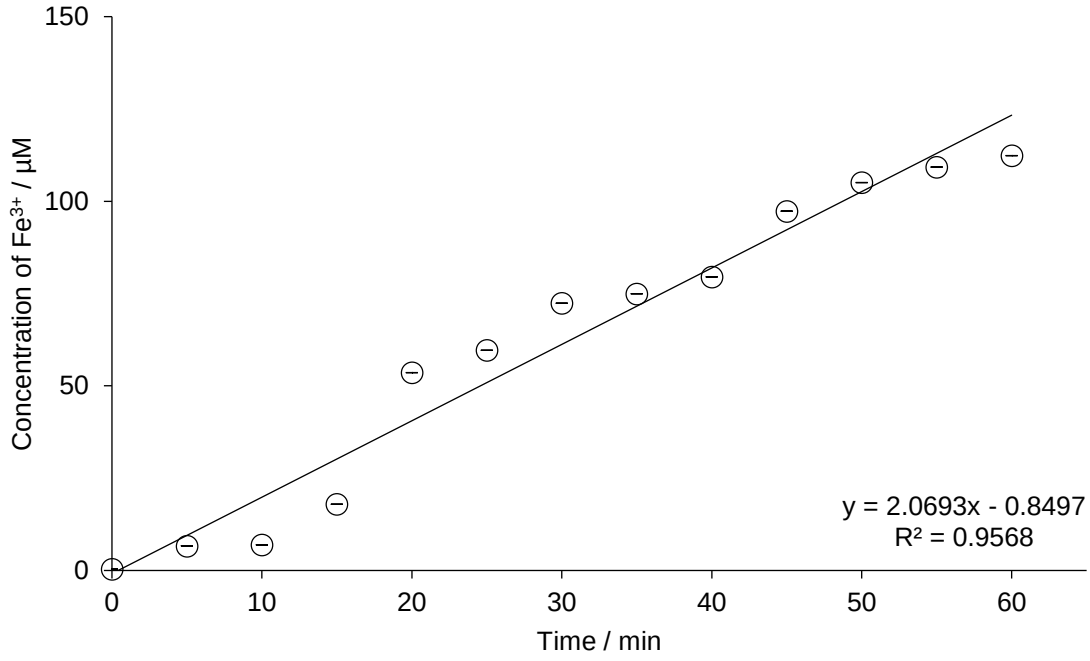

Figure 4.2 – Fricke Dosimetry of the 3 mm horn tip at arbitrary power P=2 (100 Wcm^{-2}). Measurements of Fe^{3+} concentration conducted in triplicate.

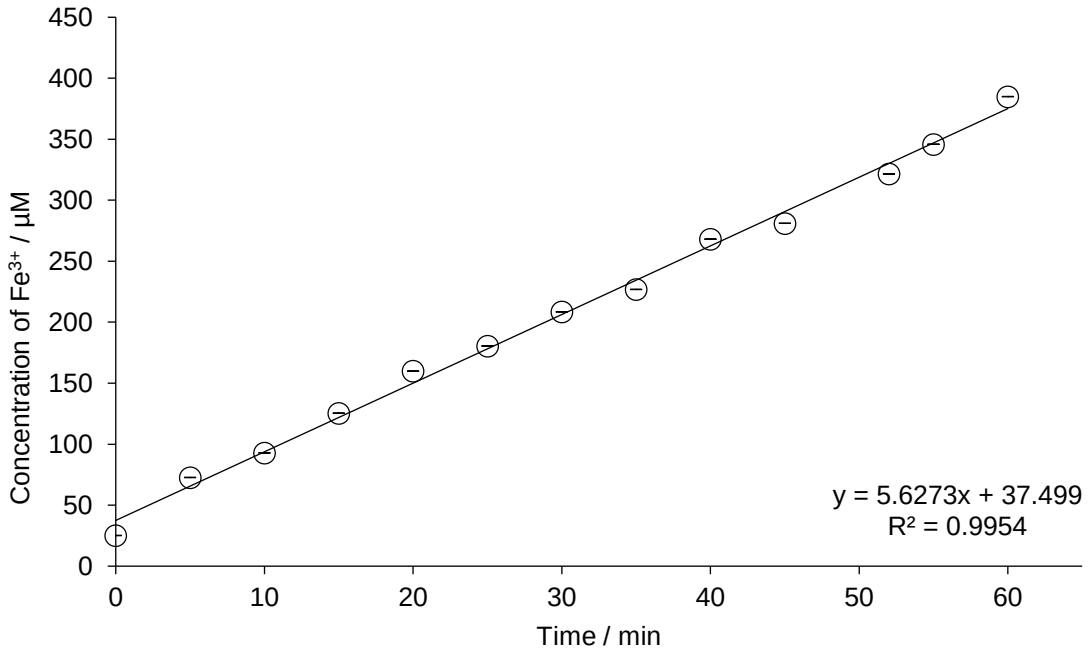

Figure 4.3 – Fricke Dosimetry of the 1 cm horn tip at arbitrary power P=4 (13 Wcm^{-2}). Measurements of Fe^{3+} concentration conducted in triplicate.

4.1.2 Effect of Sonication Time and Power on Microsphere Size

It was important to first observe the effects of mechanistic variables, ie. the ultrasonic intensity and the sonication duration, upon microsphere size to optimise the conditions for the preparation of small microspheres (below the size limit for *in vivo* applications of 7 µm) with narrow polydispersities. The sonochemical synthesis of thiolated $PMAA_{SH}$ microspheres has been previously reported, therefore a solution of 28 % functionalised $PMAA_{SH(100)}$ (Experiment 2.1.11) was employed to conduct this initial investigation. 2 mL of the solution was charged to a 14 mL centrifuge tube, onto which a layer of 100 µL tetradecane was deposited. The horn tip was placed at the oil:aq interface to optimise initial mixing, however contrary to previous publications[1,7,10], the horn was moved into the centre of the volume of liquid after initial dispersion of the oil phase to prevent foaming and introduction of air into the sample, increasing the sample polydispersity (Figure 4.4).

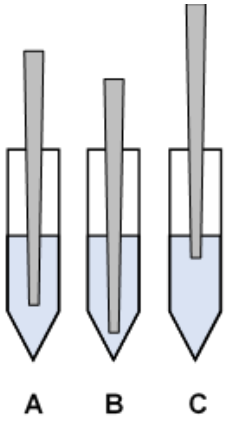

Figure 4.4 – Correct positioning of the horn tip (A) to optimise mixing and prevent poor circulation (B) or foaming (C)[201]. Image redrawn from reference model.

Micrographs of the samples of sonochemically-prepared $PMAA_{SH}$ microspheres, sonicated for 60 s at arbitrary power settings 2 and 4, are shown in Figure 4.5. Visually it would appear that the microspheres generated at P=4 possess a larger average diameter and size distribution than those prepared at P=2, in agreement with the observations of Zhou *et al*.[59]. To further characterise their size and size distribution, ImageJ processing software was used. Samples were prepared in triplicate, and each sample slide was imaged at three random locations. The processing software was used to determine the microsphere diameters in each region and averages were taken to calculate the distribution of microsphere diameters across a particular sample.

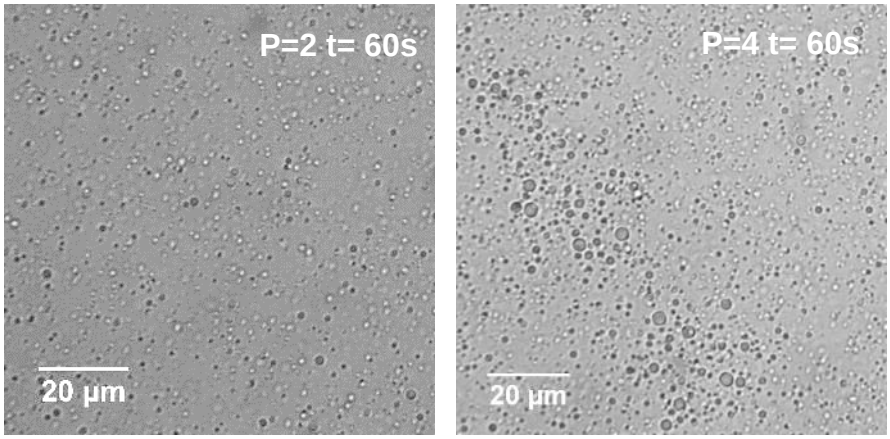

Figure 4.5 – One-pot sonochemical synthesis of tetradecane-filled $PMAA_{SH(100)}$ microspheres at P=2 (100 Wcm^{-2}) and P=4 (219 Wcm^{-2}) for 60 s.

It must be noted that ImageJ processes the images by determining the difference in contrast between the microsphere core and shell. The differentiation between the shell and core, as well as the bulk phase, is enhanced by a colour contrast image, as shown in the ImageJ image of $PMAA_{SH(25)}$ in Figure 4.6. The program measures the diameter of each complete red sphere in the colour contrast image, differentiating the circular microspheres from the bulk phase. However, the software therefore measures the diameter of the core as opposed to the diameter of the entire microsphere. The analysis is limited by the image quality and as such very small particles, or those not within a particular plane of focus, may not be measured. The optical slice of the images is approximately 1 µm, therefore this limitation will only apply to microspheres and particulate matter of less than 1 µm in diameter. The software does, however, give a good indication of the effect of experimental variables on the size distribution and average diameter of microspheres.

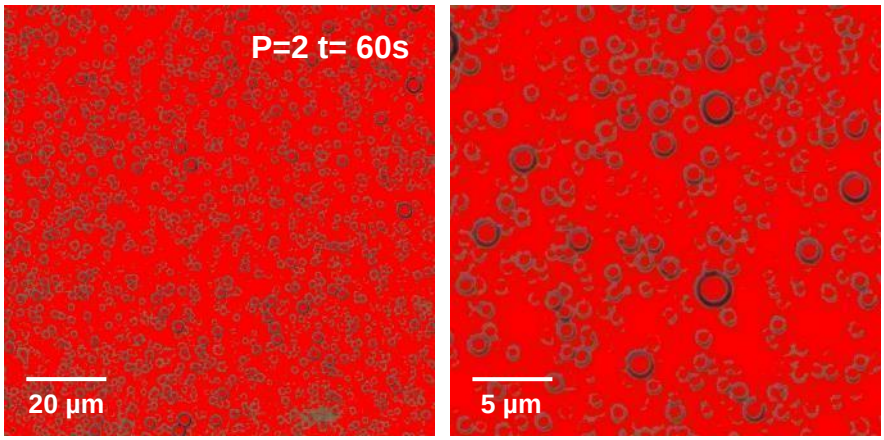

Figure 4.6 – ImageJ contrast image of $PMAA_{SH(25)}$ (left), sonicated at 100 Wcm^{-2} and an enlarged region of the image to highlight the contrast between microsphere core and shell (right). $PMAA_{SH(25)}$ shown as exemplar as microspheres are larger and differentiation in contrast between microsphere interior and shell is clearer and more defined for demonstration.

Figure 4.7 shows the average diameter and size distributions of $PMAA_{SH}$ microspheres, sonicated at P=2 and P=4 for increasing durations. Samples sonicated at 100 Wcm^{-2} (white) possess a smaller average diameter than those sonicated at 219 Wcm^{-2} (grey), and all microspheres are within the acceptable limits for intravenous *in vivo* applications. Both power settings reveal an initial drop in microsphere diameter with increasing sonication time, and this was attributed to the increased emulsification with time, leading to smaller

dispersion droplets and the prolonged generation of radicals able to cross-link the free thiol residues and stabilise the microsphere shells[58]. Beyond this, the average diameter begins to increase again, likely due to the introduction of air into the system as a result of aggressive mixing. The introduction of air into the system causes foaming, poor mixing and a reduction in cavitation efficiency. At the higher acoustic intensity, mixing is more aggressive, and the likelihood of air introduction into the system is increased. As a result, the consequences of foaming, including an increase in the microsphere mean diameter, can be observed between 30 and 60 s compared with 60 and 300 s at P=2.

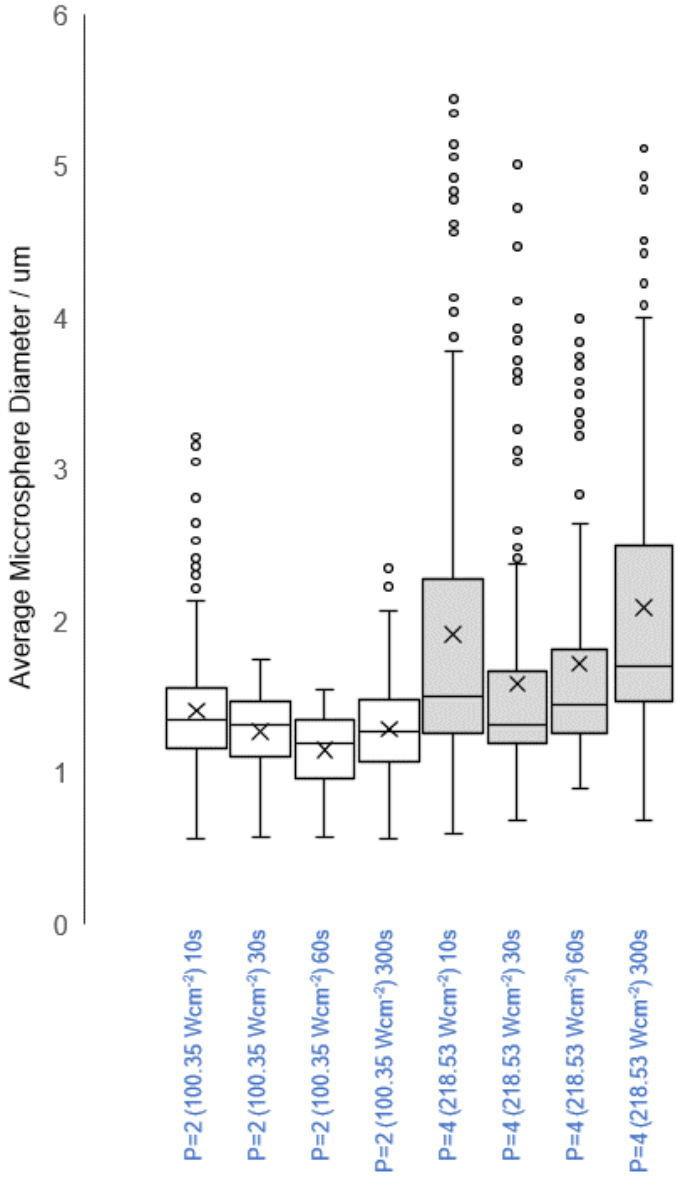

Figure 4.7 – The effect of sonication power and duration on the average diameter and size distribution of $PMAA_{SH(100)}$ microspheres. 100 Wcm^{-2} (white) and 219 Wcm^{-2} (grey). The mean diameter is indicated by a cross. The box defines the upper and lower quartiles, whilst the whiskers define the 5 and 95 percentiles. Additional points represent outliers.

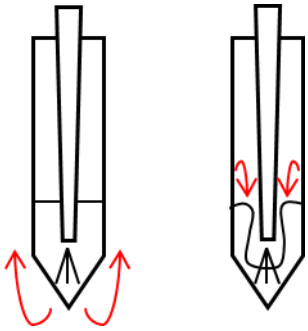

Figure 4.8 – Observed air introduction into a system. As acoustic waves begin to pass through the liquid, they disrupt the solution and the bulk immediately below the horn tip moves, allowing air introduction into the system.

At lower intensities and with correct horn tip placement, the initial liquid displacement is quickly rectified and efficient sonochemical mixing occurs. However, if the intensity is high and the horn tip remains close to the air:emulsion interface after initial placement at the oil:aq interface (B) (Figure 4.4), air is introduced into the system and foaming is observed, as depicted in Figure 4.8.

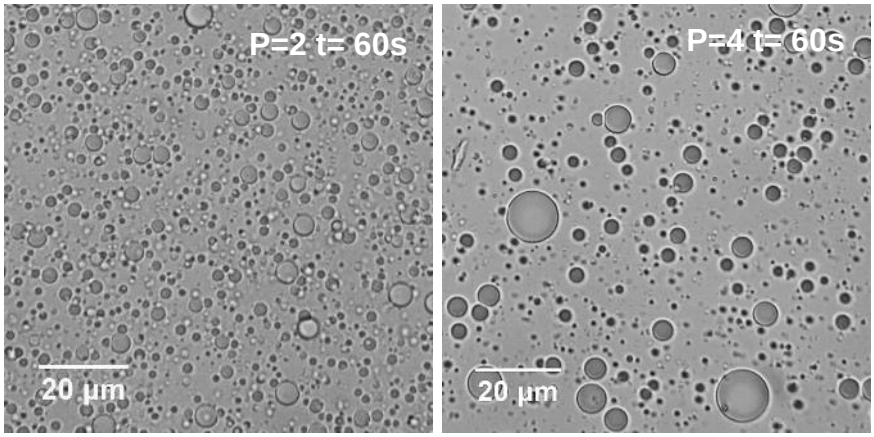

Figure 4.9 - Sonochemical synthesis of tetradecane-filled $PMAA_{SH(100)}$-$PNIPAA_{M(100)}$ microspheres at P=2 (100 Wcm^{-2}) and P=4 (219 Wcm^{-2}) for 60 s.

Based upon the size distribution data, the optimised conditions for microsphere preparation were determined as 100 Wcm^{-2} and 60 s. Unless imaged and measured for a particular stability or release experiment, microspheres were washed in deionised water and imaged after 24 hours to allow microspheres to settle at the top of the sample tube.

Comparable behaviour was also observed for block copolymeric systems prepared under the same reaction conditions, although the observed average diameter and polydispersity of all samples were larger than those of the homopolymeric microspheres (Figure 4.9 and Table 4.1).

Table 4.1 – The size distributions of tetradecane-filled $PMAA_{SH}$, $PMAA_{SH}$-$PNIPAA_{M}$ and $PMAA_{SH}$-$PNIPAA_{M}$-$PMAA_{SH}$ microspheres sonicated for 60 s at 100 Wcm^{-2} and 219 Wcm^{-2}. Three samples were imaged, from which three regions were analysed at random to yield size distribution data.

Shell Material	Microsphere Size / μm (100 Wcm^{-2})	Microsphere Size / μm (219 Wcm^{-2})
$PMAA_{SH(25)}$	1.26 ± 0.22	1.81 ± 0.70
$PMAA_{SH(50)}$	1.18 ± 0.32	1.85 ± 0.63
$PMAA_{SH(75)}$	1.19 ± 0.18	1.76 ± 0.66
$PMAA_{SH(100)}$	1.15 ± 0.25	1.72 ± 0.77
$PMAA_{SH(25)}$-$PNIPAA_{M}$	2.12 ± 1.03	3.09 ± 2.87
$PMAA_{SH(50)}$-$PNIPAA_{M}$	1.66 ± 1.05	3.03 ± 2.19
$PMAA_{SH(75)}$-$PNIPAA_{M}$	1.61 ± 0.84	2.74 ± 1.53
$PMAA_{SH(100)}$-$PNIPAA_{M}$	1.45 ± 0.47	2.25 ± 1.31
$PMAA_{SH(25)}$-$PNIPAA_{M}$-$PMAA_{SH(25)}$	1.86 ± 0.98	2.81 ± 1.29
$PMAA_{SH(50)}$-$PNIPAA_{M}$-$PMAA_{SH(50)}$	1.88 ± 0.74	2.33 ± 1.55
$PMAA_{SH(75)}$-$PNIPAA_{M}$-$PMAA_{SH(75)}$	1.40 ± 0.91	2.47 ± 1.16
$PMAA_{SH(100)}$-$PNIPAA_{M}$-$PMAA_{SH(100)}$	1.36 ± 0.33	2.07 ± 1.02

Modifying the molecular weight of homopolymeric $PMAA_{SH}$ had little effect on the average diameter and size distribution of microspheres, as shown in Table 4.1. The concentration of MAA repeat units in each sample was maintained. All PMAA blocks within each of the synthesised polymers possessed approximately 30 % functionalisation and a concentration 5 mg (PMAA) / mL was employed for all microsphere syntheses, therefore the only variable between samples was the polymer chain lengths.

When comparing the block copolymers, however, the size of microspheres increased on average as the percentage of PMAA within the polymer decreased. Diblock $PMAA_{SH(25)}$-$PNIPAA_{M(100)}$ microspheres, containing approximately 20 % PMAA with an overall degree of thiolation of 6 %, produced the largest microspheres of all thiol crosslinked samples. Figure 4.10 shows the increase in size distribution between $PMAA_{SH(100)}$-$PNIPAA_{M(100)}$ and $PMAA_{SH(25)}$-$PNIPAA_{M(100)}$, sonicated at 100 Wcm^{-1} for 60s.

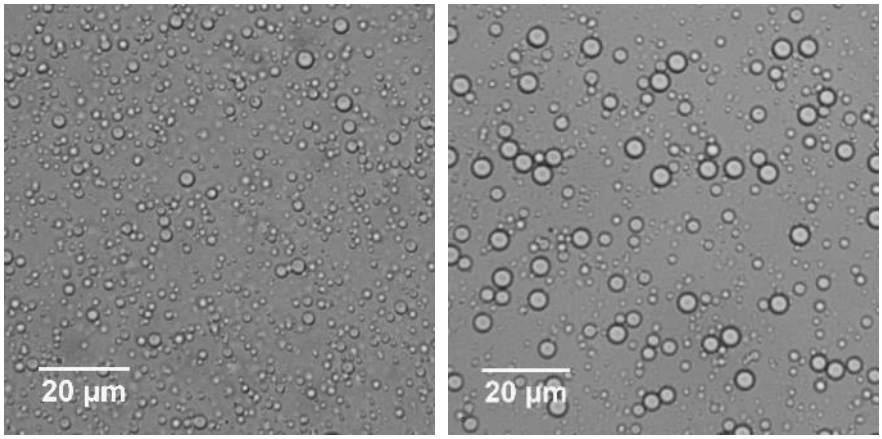

Figure 4.10 – The effect of PMAA percentage on the size and size distribution of $PMAA_{SH(100)}$-$PNIPAA_{M(100)}$ (left) and $PMAA_{SH(25)}$-$PNIPAA_{M(100)}$ (right).

The inverse relationship between PMAA percentage within the block copolymers and increasing average diameter may be attributed to a reduction in degree of functionalisation of the polymer, approximately 15 % and 6 % respectively. The observed relationship correlates with values reported in Table 4.1 and previously published data for $PMAA_{SH}$[10]. The effect of modifying the degree of thiolation within homopolymers of the equal chain length was investigated to determine the importance of the degree of thiolation on microsphere morphology.

4.1.3 The Effect of Degree of Thiolation

$PMAA_{SH}$ microspheres employing poly(methacrylic acid) with increasing degrees of thiolation were synthesised to determine its effect on microsphere size. Cavalieri *et al.*[10] observed a drop in the average diameter and size distribution of microspheres generated with $PMAA_{SH}$ shells of increasing thiol functionalities. During sonication, the oil is first dispersed in the buffer solution and the amphiphilic polymer arranges itself at the interface. Cavalieri reported that thiolated polymers with a higher degree of functionalisation have an increased availability of free -SH groups available to undergo radically-induced crosslinking, thus forming a stable, heavily crosslinked shell more rapidly than those of polymers possessing fewer thiol functionalities. The thickness of microsphere shells also reportedly increases with increasing thiolation.

When preparing samples for analysis to determine the effects of modifying the degree of functionalisation upon microsphere morphology, the degree of thiolation was the single variable as the same mass of a commercially available polymer with varying degrees of thiolation was employed.

Table 4.2 - The size distributions of tetradecane-filled $PMAA_{SH}$ microspheres (from PMAA sodium salt) with increasing degrees of functionalisation, sonicated for 60 s at 100 Wcm^{-2}. Three samples were imaged, from which three regions were analysed at random to yield size distribution data.

Degree of Functionalisation / %	Microsphere Size / μm (100 Wcm^{-2})
0	1.62 ± 0.71
10	1.58 ± 0.56
20	1.44 ± 0.51
30	1.19 ± 0.27
40	1.42 ± 0.26

Table 4.2 shows the impact of increasing the degree of functionalisation of MAA repeat units within a polymer upon the diameter and size distribution of tetradecane-filled $PMAA_{SH}$ microspheres. As observed by Cavalieri *et al.*[10] the microsphere diameter decreases with increasing functionalisation percentage. However, at 40 % functionalisation the polymer in solution appeared slightly cloudy, indicative of reduced solubility due to loss of acid moieties. A target percentage functionalisation of MAA repeat units of 30 % was subsequently chosen for PMAA homopolymers and PMAA-based block copolymers, largely due to the presence of non-thiol containing $PNIPAA_M$ reducing the degree of thiolation of the polymer in its entirety.

The most interesting observation to note in Table 4.2 is the successful formation of microspheres in the absence of any thiol functionalities. According to Cavalieri *et al.*[10] the successful sonochemical synthesis of poly(methacrylic acid)-shelled microspheres is dependent upon a degree of thiolation of the polymer, and subsequent sonochemically-induced crosslinking of the thiol functionalities. Contrary to these findings, sonication of analogous samples of unfunctionalised and functionalised PMAA polymers, layered with 100 µL tetradecane, yielded microspheres with seemingly comparable morphologies. The microspheres remained stable overnight, and it was therefore pertinent to investigate further to gain an understanding of the interactions stabilising the non-thiol functionalised microspheres. The synthesis and stability of non-thiol functionalised microspheres is discussed in Section 4.1.6.

4.1.4 Lysozyme Microspheres

Lysozyme microbubbles and microspheres were generated in order to compare the synthetic microspheres with a known protein-shelled system[3,14]. Lysozyme contains intermolecular disulphide crosslinks that reportedly require reduction prior to sonication to enable new sonochemically-induced disulphide crosslinks to form. 30 mg of reducing agent DL-dithiothreitol (DTT) was therefore added to the reaction two minutes prior to sonication to reduce the disulphide linkages.

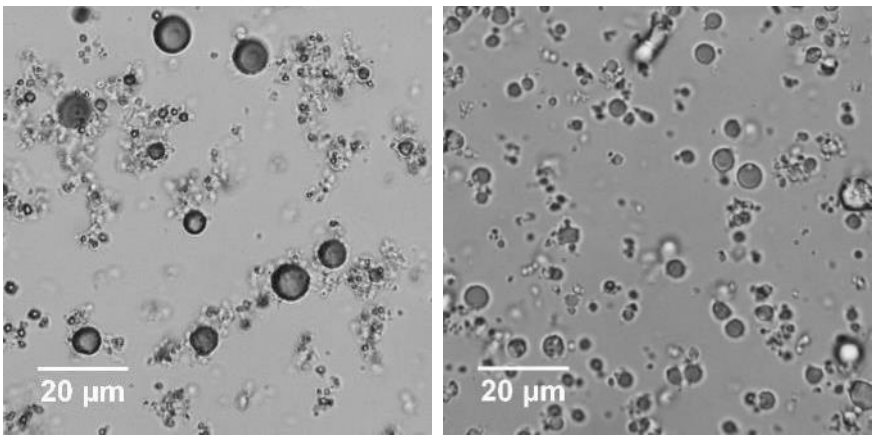

Figure 4.11 – Air-filled lysozyme microbubbles (left) and tetradecane-filled lysozyme microspheres (right), sonicated at 100 Wcm^{-2} for 60s (unwashed).

The average diameter of the microbubbles and tetradecane-filled microspheres were 3.75 ± 1.87 µm and 2.41 ± 1.19 µm respectively, larger than those of the synthetic-shelled polymers. The micrographs reveal a considerable amount of debris amongst the discrete microspheres, not present in the synthetic polymer-shelled analogues (Figure 4.11). Although the cause of the debris is not known, it is likely a result of proteinaceous impurities present within the naturally-occurring lysozyme.

To confirm the presence of radically-induced disulphide crosslinking upon the successful formation of lysozyme microspheres, a number of reactions were conducted including the use of a radical scavenger and sonication in the absence of oxygen. The results of these are discussed in Section 4.1.5 upon comparison with synthetic analogues.

4.1.5 Evidence of Sonochemically-induced Crosslinking

To better understand why non-thiolated poly(methacrylic acid) is able to form microspheres, samples were prepared by simple homogenisation using a vortex mixer. Samples of PMAA and PMAA$_{SH}$ of increasing thiolation were prepared as per the experimental protocol outlined in Experiment 2.2.5, and 100 µL tetradecane was deposited onto the buffer layer. The sample was then agitated by using a Grant Bio PV-1 vortex mixer for five minutes. Although visible mixing was observed in all samples, phase

separation was almost immediate and, upon imaging, no microspheres were present on the micrograph.

Suslick reported the importance of superoxide radicals to the successful sonochemical formation of thiol-crosslinked microspheres[2,22]. To corroborate this, both thiolated and non-thiolated PMAA samples were prepared under nitrogen (Experiment 2.2.10) and compared against a known system of lysozyme microspheres. Hydroxyl radicals will still be generated by sonolysis of water (Equation 4.1), yet the highly diminished availability of oxygen as a result of purging will prevent the reaction of oxygen with H^+ to yield superoxide radicals and hydrogen peroxide (Equation 4.2).

To achieve an oxygen-devoid atmosphere, 2 mL of the polymer in buffer was layered with 100 µL tetradecane, the 3 mm horn tip was placed at the oil:water interface and the reaction was sealed to the air. The reaction was then purged with nitrogen for 10 minutes, after which time the purging syringe was moved into the void above the reaction mixture to allow the interface to reestablish prior to sonication at 100 Wcm^{-2} for 60 s.

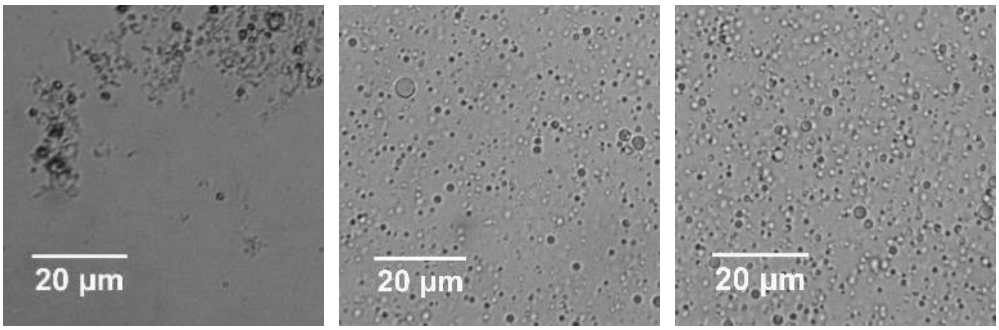

Figure 4.12 – Sonochemical microsphere synthesis under nitrogen. From left to right: Tetradecane-filled lysozyme microspheres, tetradecane-filled $PMAA_{SH(100)}$ microspheres, and tetradecane-filled $PMAA_{(100)}$ microspheres.

Figure 4.12 shows the effect of nitrogen purging during the synthesis of sonochemically-generated tetradecane-filled microspheres. No lysozyme microspheres were generated, indicating that the successful formation of lysozyme microspheres is dependent upon the generation of superoxide radicals. Although no discrete microspheres were observed, regions of what appeared to be polymer aggregates were dispersed throughout, as shown.

Contrary to previous publications[6], $PMAA_{SH}$ microspheres were formed in the absence of O_2, yet analysis of their size and size distributions reveal an average diameter comparable with that of non-functionalised PMAA microspheres of 1.64 ± 0.32 μm (Table 4.2). This would suggest that the interactions stabilising the microspheres are not those of the superoxide-induced disulphide crosslinks, but instead are interactions between the carboxylic acid groups analogous to those in non-thiolated PMAA. Dibbern *et al.*[12] also observed microspheres upon the sonochemical synthesis of poly(L-glutamate) microspheres in the absence of O_2, indicative of stabilisation by an •OH-induced crosslinking mechanism or non-covalent stabilisation.

To substantiate this data and determine whether the interactions between non-thiolated PMAA are radically-induced, samples were sonicated in the presence of a radical scavenger. Tert-butanol was employed (Experiment 2.2.11) as it targets •OH radicals, therefore radicals generated by sonolysis of water and secondary radicals generated in the presence of oxygen would, theoretically, be scavenged. Equations 4.5 and 4.6 show the reaction of •OH with tert-butanol to yield 2,5-dimethylhexane-2,5-diol, the major product of tert-butanol sonication[202].

Increasing concentrations of tert-butanol were added immediately prior to sonication, equating to 8, 39, and 78 μM when added to the 2 mL of protein or polymer solution, exceeding the approximate radical concentration of 2 μM generated during 60 s sonication as estimated by Fricke dosimetry.

A drop in the yield of microspheres was observed for both thiolated microspheres and their non-thiolated analogues, an example of which is shown in Figure 4.13. Although the yield of microspheres was suppressed at increasing tert-butanol concentrations, microspheres were still present on the micrographs after incubation. Tauber *et al.*[202] found that, at the elevated temperatures within a collapsing bubble, the scavenging capability of tert-butanol may be suppressed by a side decomposition reaction of tert-butanol into isobutene and water (Equation 4.7).

$$\bullet OH\ (H\bullet) + (CH_3)_3COH \rightarrow H_2O + \bullet CH_2C(CH_3)_2OH \quad (4.5)$$

$$2\ \bullet CH_2C(CH_3)_2OH \rightarrow [CH_2C(CH_3)_2OH]_2 \quad (4.6)$$

$$(CH_3)_3COH \rightarrow H_2O + CH_2C(CH_3)_2 \quad (4.7)$$

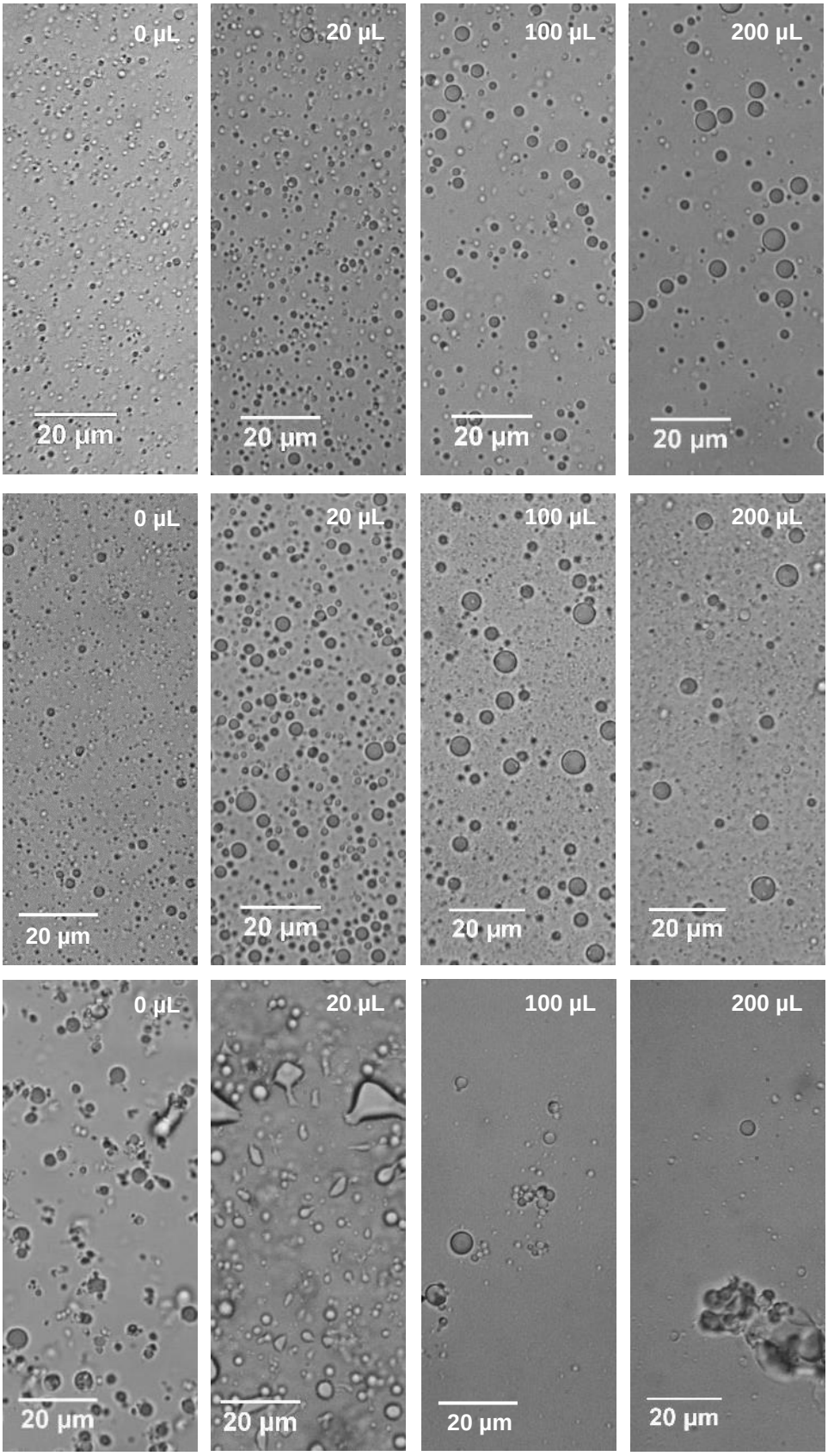

Figure 4.13 – Tetradecane-filled $PMAA_{SH(100)}$ (top row), $PMAA_{(100)}$ (middle row) and lysozyme (bottom row) microspheres sonicated at 100 Wcm^{-2} for 60 s with increasing tert-butanol aliquots.

An increase in microsphere diameter can also be observed, likely due to the diminished radical availability of both •OH and superoxide radicals, reducing the likelihood of sonochemical crosslinking mechanisms and delaying polymer stabilisation of the interface prior to initial droplet coalescence. For lysozyme microsphere preparations, however, the yield dropped dramatically in samples treated with 20 µL and completely disabled microsphere production at a concentration of 100 µL. This would suggest that, whilst lysozyme microspheres are dependent on radically-induced crosslinking, there may be secondary non-covalent interactions stabilising the synthetic polymeric microspheres in the absence of disulphide linkages.

4.1.6 Microspheres in the Absence of Thiol Functionalities

In order to further explore the findings reported in Table 4.2, samples of both functionalised and non-functionalised PMAA-based polymers were prepared in pH 8 tris acetate buffer (5 mg (PMAA)/mL) and sonicated at 100 Wcm^{-2} for 60 s. Upon analysis of microsphere diameters with ImageJ processing software, it was found that the average microsphere diameter and range of microsphere sizes are comparable for both thiolated and non-thiolated microspheres.

An example of the effect of functionalisation on the average size and size distribution of homopolymeric $PMAA_{(75)}$ and $PMAA_{(75)}$ and $PNIPAA_{M(100)}$ di- and triblock copolymers is shown in Figure 4.14. The plots show that microspheres with functionalised polymer shells are, on average, smaller than their non-functionalised analogues with narrower size distributions, in agreement with the initial findings published in Table 4.2. Cavalieri *et al.*[10] reported that $PMAA_{SH}$ behaves as an emulsifier during microsphere formation. The amphiphilic behaviour of the polymer is responsible for the arrangement of the polymer at the interface, whilst the rapid cross-linking facilitates both immediate stability with respect to phase separation and enables long term stability due to the intermolecular covalent crosslinking across the shell surface. It could therefore be assumed that hydrophilic PMAA in the absence of thiol functionalities would not arrange itself in the same fashion at the interface, yet the sonochemical synthesis of non-thiol-functionalised polymers has been achieved (Section 1.2.1).

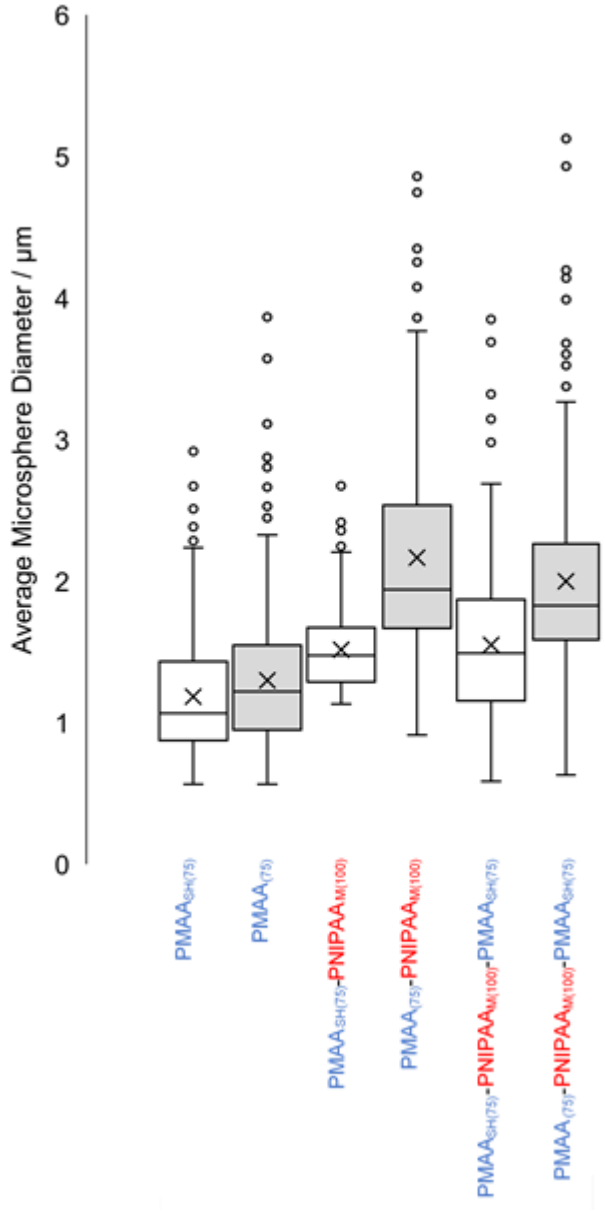

Figure 4.14 – A comparison of the average diameter and size distributions of tetradecane-filled $PMAA_{SH(75)}$ shell (white) and $PMAA_{(75)}$ shell (grey) microspheres, sonicated at 100 Wcm^{-2} for 60 s. The mean diameter is indicated by a cross, and the midline within the box represents the median diameter. The box defines the upper and lower quartiles, whilst the whiskers define the 5 and 95 percentiles. Additional points represent outliers.

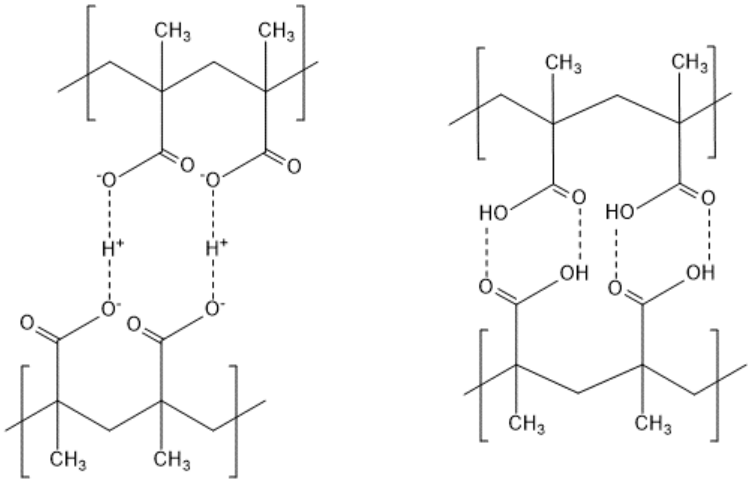

Scheme 4.1 – The proposed interactions for the stabilisation of PMAA microspheres in the absence of sonochemically-induced crosslinking. Ion pair interactions (left) and hydrogen bonding (right).

Gedanken *et al.*[11] postulated a combined process of sonochemically-induced partial denaturation and the hydrophobic effect as the reason for the formation of stable streptavidin microspheres, a protein containing amine and hydroxyl functionalities but lacking thiol-containing cysteine residues, as previously discussed in Section 1.2.1. The stabilisation of non-thiol containing poly(glutamic acid) (Scheme 4.1) microspheres is instead reportedly due to hydrogen bonding of the carboxylic acid functionalities and the formation of ion pairs (RCO_2^-…..H^+…..^-O_2CR). Dibbern *et al.*[12] observed no change to the structure of the naturally-occurring polymer upon sonication, indicating that no sonochemically-induced degradation or alternative covalent bond formation was responsible. Although in both publications the chosen sonication time was 3 minutes, the acoustic intensity of the streptavidin system far exceeded that of the poly(glutamic acid) system (150 Wcm^{-2} and 50 Wcm^{-2} respectively[11,12]). The high intensity combined with a prolonged sonication time, with respect to Cavalieri's system[10], may explain the proposed degradation of streptavidin as a mechanism for stabilisation.

The presence of carboxylic acid moieties in poly(methacrylic acid) and their non-covalent interactions could therefore be responsible for the stability of these microspheres in the absence of thiols. Scheme 4.1 shows the potential interactions stabilising PMAA at the oil: water interface, based upon the predictions of Dibbern *et al.*[12]. The pKa of

poly(methacrylic acid) is 5.5[192], therefore at pH 8 a large majority of the acid groups will be deprotonated. As such the main interaction is likely the ion pair hydrogen bond, described by Dibbern as the strongest form of hydrogen bond. This would go some way to explain the stability of the non-crosslinked microspheres.

The average microsphere diameter appears to increase as the percentage of PMAA within the polymer decreases, particularly in the case of the non-functionalised polymers (Figure 4.14). It was therefore initially proposed that the PMAA portions of the chain were solely responsible for the stability of both the functionalised systems, by disulphide crosslinking, and non-functionalised systems, by intermolecular hydrogen bonding.

To further explore the extent of their stability, microspheres of both functionalised and non-functionalised PMAA were monitored over time. Samples of the native microsphere suspension were washed by dialysis and diluted ten-fold in deionised water. The dilute suspensions were then stored at room temperature and imaged at regular intervals. Figure 4.15 depicts the optical micrographs of both $PMAA_{SH(100)}$ and $PMAA_{(100)}$ microspheres with time. Initially, the PMAA and $PMAA_{SH}$-shelled microspheres appeared to possess a very similar morphology to one another with a comparable yield. Over time, however, a distinct loss of yield of non-crosslinked microspheres can be observed, namely between 1 to 2 months at room temperature. This is corroborated by the data collected in Figure 4.17, whereby the average microsphere size and yield are monitored as a function of time. To obtain this data, samples were prepared in triplicate, from which three regions of the slide containing each sample were imaged. The micrographs were then analysed by ImageJ processing software to yield the average values.

Functionalised $PMAA_{SH}$ microspheres exhibited no change in their average diameter with time and only a gradual loss in yield of less than 30 % in two months, compared with 77 % for non-functionalised PMAA-shelled microspheres. It must be noted that this measured loss with respect to time is of washed and diluted microspheres. Unwashed suspensions of tetradecane-filled microspheres with a crosslinked polymeric shell, synthesised during the course of this project, have exhibited stability at room temperature for four years, losing less than 20 % of their yield based on microscopic analysis (Figure 4.16). It is highly unlikely, however, that a microsphere suspension would be stored for administration without extensive washing and purification, therefore monitoring the stability of a washed sample was deemed to provide a more valuable insight into their lifetimes.

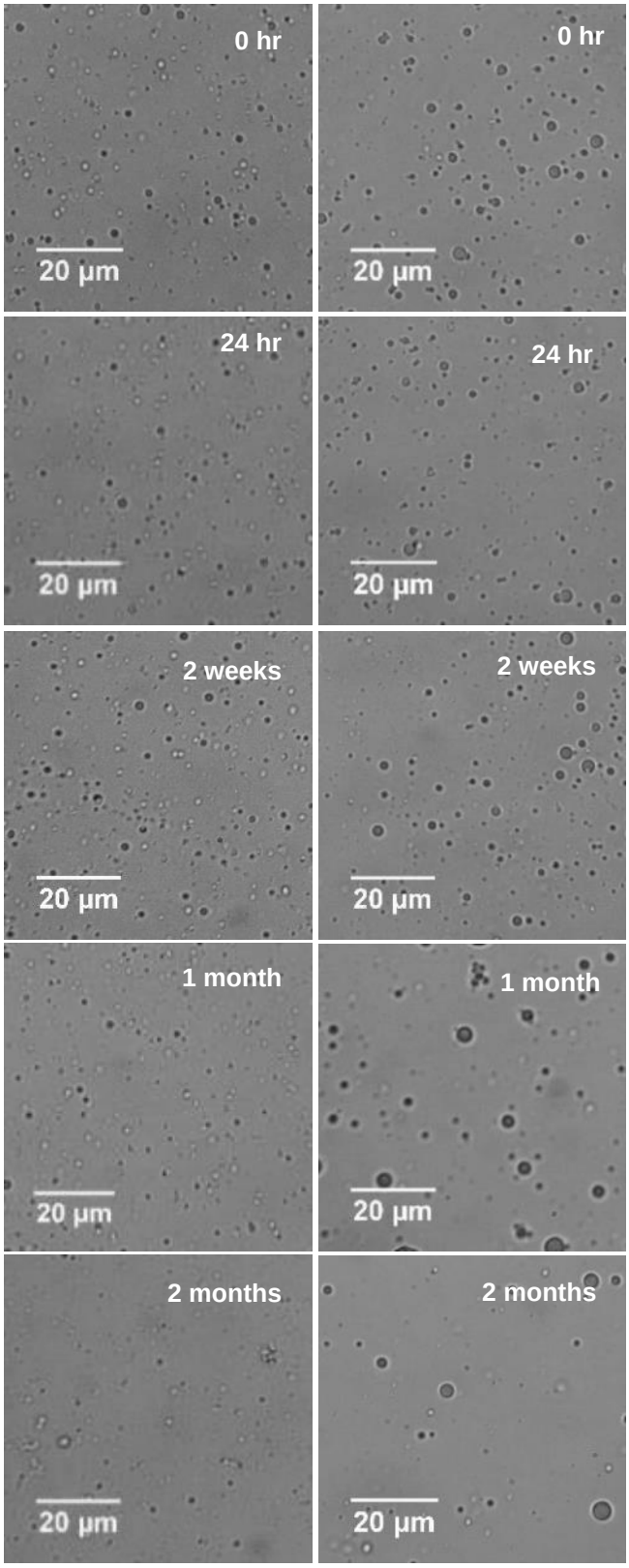

Figure 4.15 - The change in morphology and yield of a dilute solution of $PMAA_{SH(100)}$ (left) and $PMAA_{(100)}$ (right) tetradecane-filled microspheres (100 Wcm^{-2} for 60s).

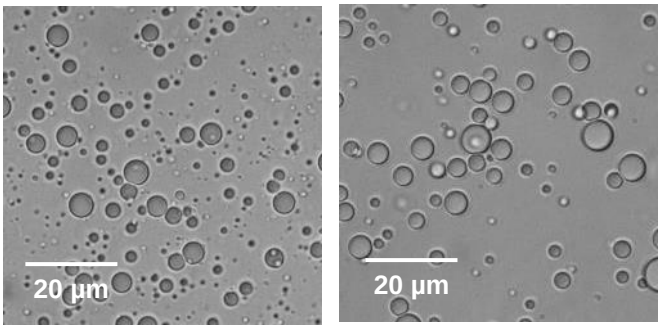

Figure 4.16 – Tetradecane-filled $PMAA_{SH(100)}$-$PNIPAA_{M(100)}$ microspheres after 24 hours, and after 4 years at room temperature (unwashed and undiluted), sonicated at 100 Wcm^{-2} for 60s.

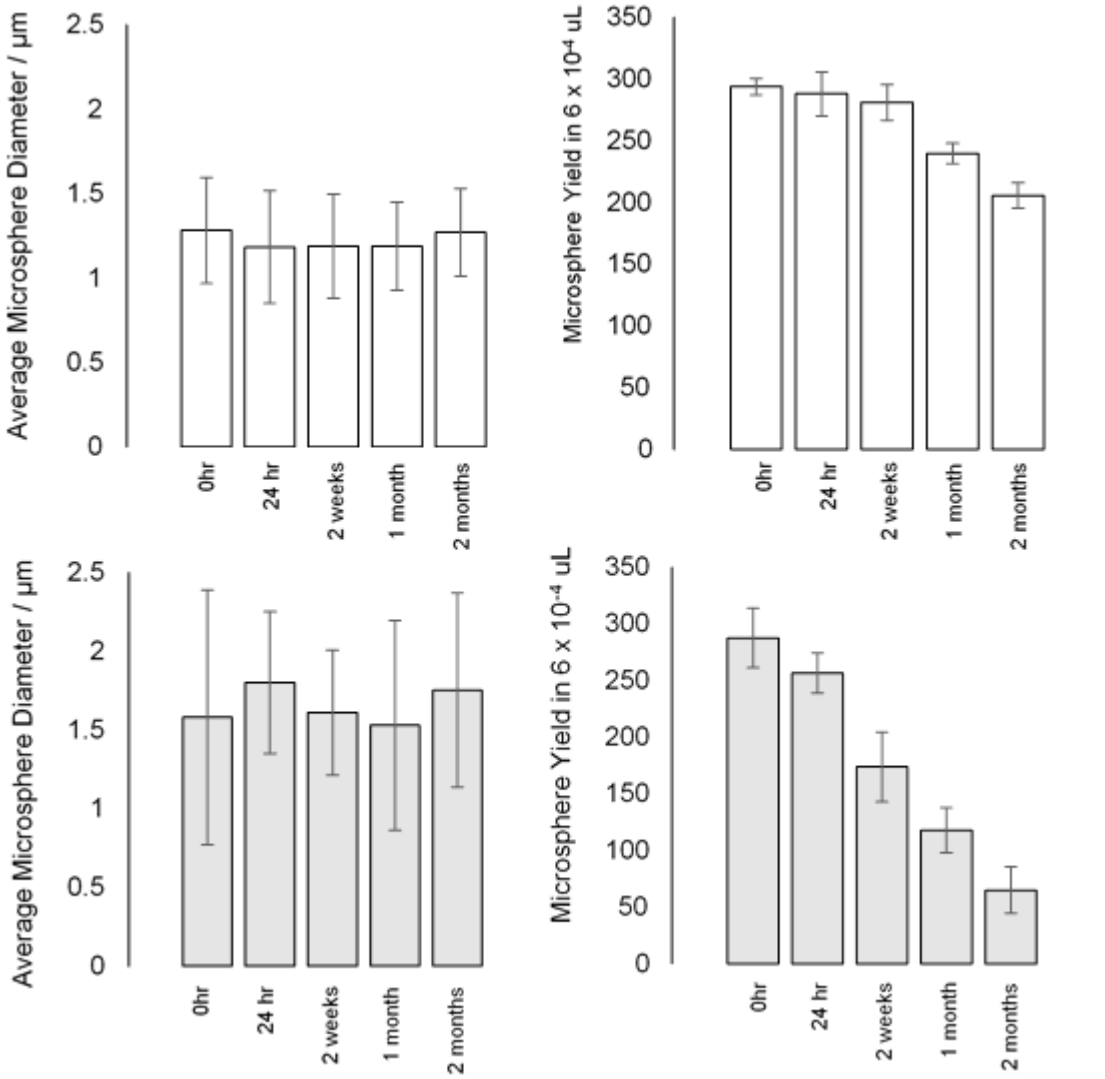

Figure 4.17 – The average microsphere diameter and microsphere yield of $PMAA_{SH(100)}$ microspheres (top row) and $PMAA_{(100)}$ microspheres (bottom row) with time. Samples imaged and analysed in triplicate. Error bars indicate the minimum and maximum average microsphere diameter. Yield calculated as the number of microspheres within region of sample image analysed as a percentage of the sample volume trapped under the cover slip on the microscope slide.

Table 4.3 – The microsphere size and yield of tetradecane-filled $PMAA_{SH}$ and PMAA microspheres after sonication at 100 Wcm^{-2} for 60 s, washing and dilution, and after two months stored at room temperature.

Shell Material	Microsphere Size 0 hr / μm	Yield 0 hr / per 6 x 10^{-4} uL	Microsphere Size 2 months / μm	Yield 2 months / average % loss
$PMAA_{SH(25)}$	1.30 ± 0.45	360 ± 30	1.48 ± 0.22	33
$PMAA_{SH(50)}$	1.29 ± 0.13	320 ± 60	1.33 ± 0.18	21
$PMAA_{SH(75)}$	1.22 ± 0.47	340 ± 60	1.39 ± 0.29	32
$PMAA_{SH(100)}$	1.27 ± 0.32	290 ± 10	1.26 ± 0.27	29
$PMAA_{(25)}$	1.63 ± 0.84	290 ± 60	1.86 ± 0.99	80
$PMAA_{(50)}$	1.72 ± 0.86	330 ± 40	1.79 ± 0.73	71
$PMAA_{(75)}$	1.69 ± 0.49	260 ± 40	1.64 ± 0.65	66
$PMAA_{(100)}$	1.50 ± 0.75	280 ± 30	1.52 ± 0.49	77

Table 4.3 compares the size and stability of all synthesised $PMAA_{SH}$ and PMAA microspheres after sonication and after storage for two months at room temperature. Although the PMAA microspheres possess a larger average diameter and wider size distribution than $PMAA_{SH}$ microspheres, neither analogues exhibit a major shift in diameter or size distribution with time, indicative of loss of yield by coalescence or Ostwald ripening as a result of shell degradation and potential porosity. This is a particularly insightful observation for the non-functionalised PMAA microspheres, as it not only confirms the presence of a polymer layer at the oil:aq interface, but also indicates that the intermolecular interactions are sufficient to stabilise the dispersion with respect to phase separation for a period comparable to that of some conventional surfactants[203]. It was therefore important to determine whether any additional interactions were stabilising the system beyond non-covalent interactions.

The proposed mechanism for microsphere loss of both analogues is believed to be a result of simple degradation. The reductive degradation of protein microspheres and microbubbles *in vitro* has previously been described[7,9], and an acidic environment below pH 5 leads to protonation of PMAA (pKa 5.5)[192] and subsequent precipitation of the polymer (Section 3.7). At pH 7 in deionised water, however, these microspheres were not

subjected to reducing agents, proteases or the risk of complexation with certain buffers[204] . In alternative microsphere systems, storage in water has actually shown to improve stability due to the exertion of osmotic pressure upon the microspheres[205]. As such the precise mechanism of degradation is largely unknown, however it is likely a result of the inherent instability of particular microspheres as opposed to an external influence. Further investigation into the behaviour of microsphere systems under a range of conditions may elucidate to the mechanism of degradation.

The same analysis was conducted for microspheres synthesised using the di- and triblock copolymers to determine the size and stability of both the functionalised and non-functionalised analogues with time (Figure 4.18). The functionalised block copolymeric microspheres were larger on average than those of the $PMAA_{SH}$ microspheres, and this was thought to be due to the presence of non-crosslinking $PNIPAA_{M}$ in the shell, and the reduced likelihood of available thiols upon sonochemical formation[10]. An increase in diameter was also observed between non-functionalised PMAA and diblock PMAA-$PNIPAA_{M}$ microspheres, and it was subsequently proposed that for both analogues the microsphere size is dependent upon the percentage of PMAA within the shell, capable of forming intermolecular covalent and non-covalent bonds.

Figure 4.19 quantifies the change in size and yield of $PMAA_{SH(100)}$-$PNIPAA_{M(100)}$ and $PMAA_{(100)}$-$PNIPAA_{M(100)}$ microspheres with time. After two months, approximately 78 % of non-thiol crosslinked microspheres and 34 % of thiol crosslinked microspheres were lost, comparable to those of the $PMAA_{(100)}$ and $PMAA_{SH(100)}$ microspheres. Table 4.4 compares the change in size and yield of all thiolated di-and triblock and non-thiolated di- and triblock microspheres after two months at room temperature. As previously demonstrated, the average microsphere diameter decreases with increasing PMAA percentage within the polymer chains of both the thiolated and non-thiolated microspheres, further indicating that stability at the interface is induced by PMAA or $PMAA_{SH}$. The long-term stability of the microspheres, however, is independent of PMAA percentage and is instead dependent upon the presence of disulphide crosslinking within the microsphere shells. This would suggest that the interactions stabilising the non-thiol functionalised microspheres are less stable that covalent disulphide crosslinks.

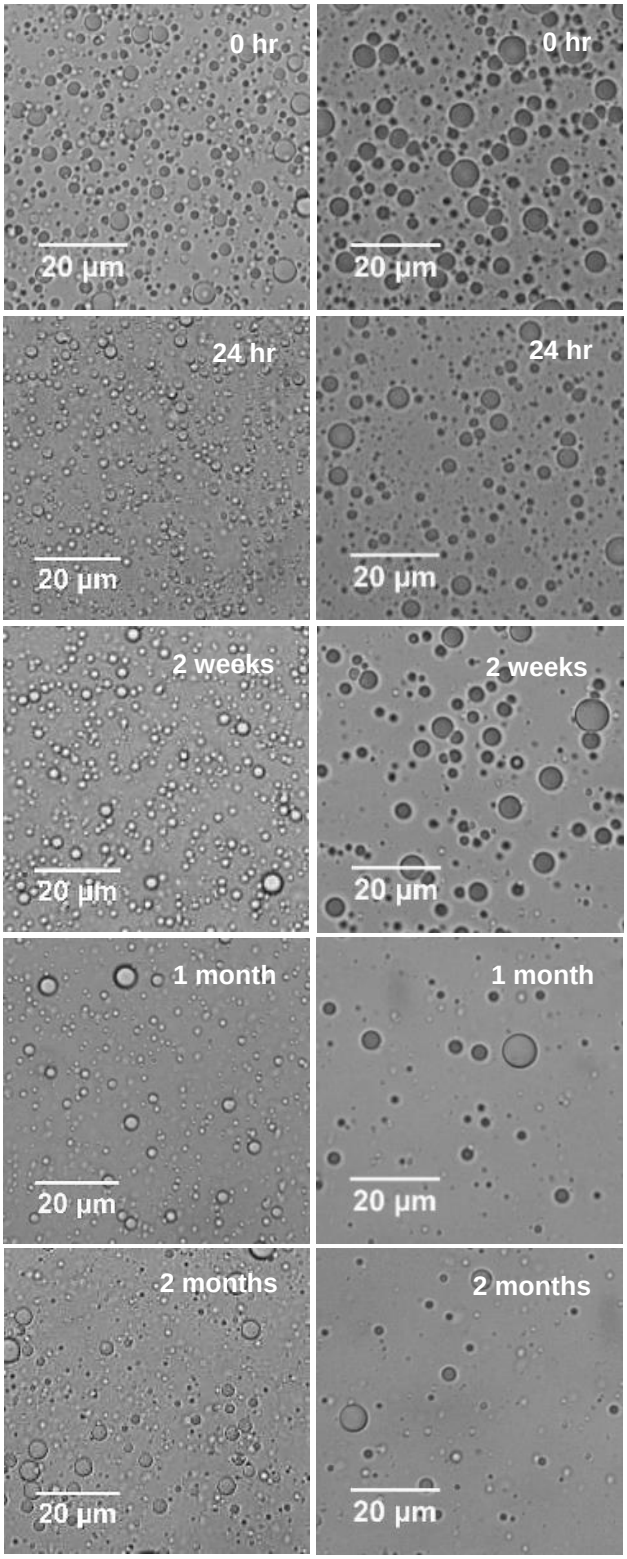

Figure 4.18 - The change in morphology and yield of a dilute solution of diblock $PMAA_{SH(100)}$-$PNIPAA_{M(100)}$ (left) and $PMAA_{(100)}$-$PNIPAA_{M(100)}$ (right) tetradecane-filled microspheres (100 Wcm^{-2} for 60s).

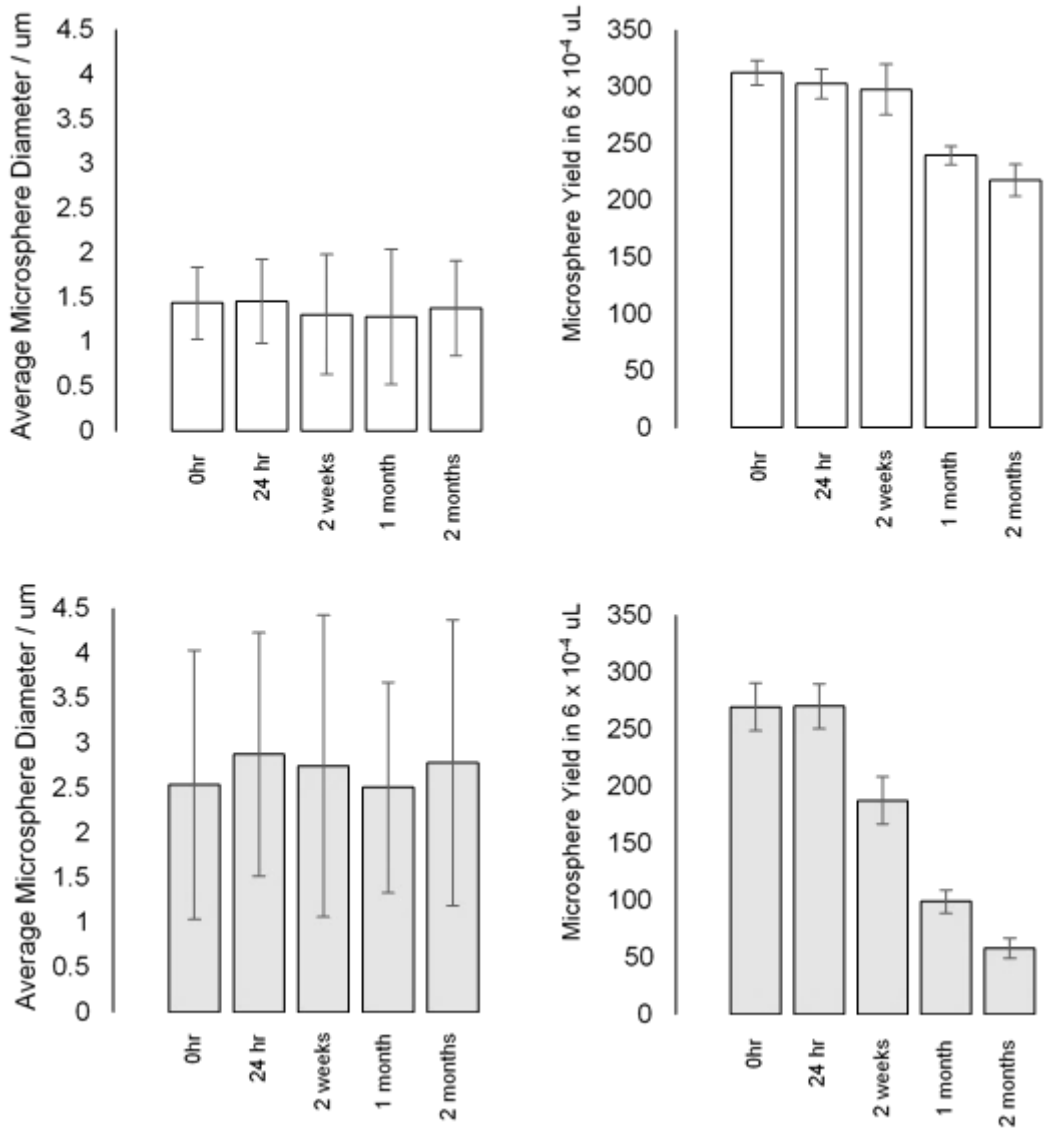

Figure 4.19 - The average microsphere diameter and microsphere yield of $PMAA_{SH(100)}$-$PNIPAA_{M(100)}$ microspheres (top row) and $PMAA_{(100)}$-$PNIPAA_{M(100)}$ microspheres (bottom row) with time. Samples were imaged and analysed in triplicate. Error bars indicate the maximum and minimum average microsphere diameter.

Table 4.4 - The size and yield of tetradecane-filled thiolated and non-thiolated diblock (top) and triblock (bottom) microspheres after sonication at 100 Wcm^{-2} for 60 s, washing and dilution, and after two months at room temperature.

Shell Material	Microsphere Size 0 hr / μm	Yield 0 hr / per 6 x 10^{-4} uL	Microsphere Size 2 months / μm	Yield 2 months / average % loss
$PMAA_{SH(25)}$-$PNIPAA_{M(100)}$	1.68 ± 0.86	340 ± 50	1.76 ± 1.01	41
$PMAA_{SH(50)}$-$PNIPAA_{M(100)}$	1.53 ± 0.31	290 ± 30	1.64 ± 0.95	36
$PMAA_{SH(75)}$-$PNIPAA_{M(100)}$	1.65 ± 0.47	280 ± 30	1.51 ± 0.66	29
$PMAA_{SH(100)}$-$PNIPAA_{M(100)}$	1.49 ± 0.39	320 ± 10	1.45 ± 0.53	34
$PMAA_{(25)}$-$PNIPAA_{M(100)}$	2.67 ± 1.72	290 ± 20	2.49 ± 1.46	73
$PMAA_{(50)}$-$PNIPAA_{M(100)}$	2.63 ± 1.85	290 ± 40	2.66 ± 1.39	81
$PMAA_{(75)}$-$PNIPAA_{M(100)}$	2.51 ± 1.39	330 ± 40	2.41 ± 1.81	90
$PMAA_{(100)}$-$PNIPAA_{M(100)}$	2.48 ± 1.46	260 ± 20	2.69 ± 1.61	78
$PMAA_{SH(25)}$-$PNIPAA_{M(100)}$-$PMAA_{SH(25)}$	1.63 ± 0.38	300 ± 50	1.68 ± 0.54	26
$PMAA_{SH(50)}$-$PNIPAA_{M(100)}$-$PMAA_{SH(25)}$	1.57 ± 0.49	280 ± 30	1.59 ± 0.38	34
$PMAA_{SH(75)}$-$PNIPAA_{M(100)}$ - $PMAA_{SH(50)}$	1.46 ± 0.51	280 ± 30	1.62 ± 0.24	38
$PMAA_{SH(100)}$-$PNIPAA_{M(100)}$-$PMAA_{SH(50)}$	1.31 ± 0.68	320 ± 10	1.39 ± 0.71	21
$PMAA_{(25)}$-$PNIPAA_{M(100)}$-$PMAA_{(25)}$	2.61 ± 1.31	290 ± 60	2.55 ± 1.26	68
$PMAA_{(50)}$-$PNIPAA_{M(100)}$-$PMAA_{(50)}$	2.45 ± 1.08	280 ± 40	2.48 ± 1.61	73
$PMAA_{(75)}$-$PNIPAA_{M(100)}$-$PMAA_{(75)}$	2.20 ± 1.26	260 ± 40	2.32 ± 1.46	66
$PMAA_{(100)}$-$PNIPAA_{M(100)}$ - $PMAA_{(100)}$	1.98 ± 1.17	280 ± 30	2.03 ± 1.26	73

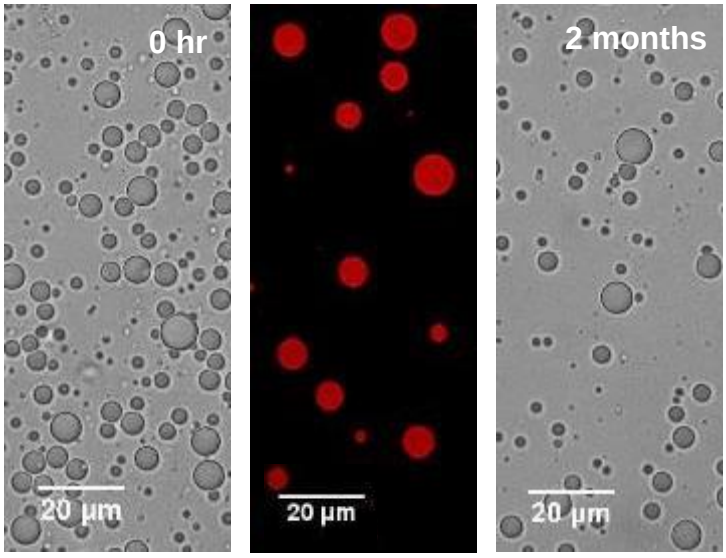

Figure 4.20 – Micrographs of tetradecane-filled PNIPAA$_{M(100)}$ microspheres immediately after sonication (left), LCSM micrograph of Sudan III-saturated tetradecane-filled PNIPAA$_{M(100)}$ microspheres, dialysed and diluted ten-fold (centre), and after 2 months at room temperature (right).

Poly(N-isopropylacrylamide) undergoes hydrogen bonding with water and intermolecular hydrogen bonding between the secondary amine and carbonyl in a similar fashion to PMAA (Scheme 4.1), and should therefore be capable of forming these intermolecular hydrogen bonds across a microsphere shell surface. To confirm whether PNIPAA$_M$ contributes to the intermolecular shell stabilisation of block copolymeric microspheres, tetradecane-filled PNIPAA$_M$ microspheres were prepared.

After rationalising the inter- and intramolecular interactions stabilising non-thiolated PMAA microspheres, and observing microsphere formation from diblock PMAA-PNIPAA$_M$, the formation and stability of tetradecane-filled PNIPAA$_M$ microspheres (Figure 4.20) supports the idea that PNIPAA$_M$ portions of diblock copolymers also contribute to intermolecular stability at the interface. This is achieved either by non-covalent hydrogen bonding or alternative interactions not yet characterised. The average diameter of PNIPAA$_M$ microspheres upon synthesis was found to be 3.09 ± 1.18 µm, larger than that of the homopolymeric and block copolymer microspheres. After two months at room temperature, approximately 72 % of microspheres were lost, comparable with both PMAA and block copolymeric PMAA-PNIPAA$_M$ microspheres.

Microspheres were also successfully generated employing P(MMA-co-NIPAA$_M$) copolymers as the shell material with an average diameter of 3.11 ± 1.13 µm, a comparable morphology to their homopolymeric PNIPAA$_M$ analogues (Figure 4.21 and Table 4.5). Block copolymers of thiolated and non-thiolated PMAA$_{(100)}$-P(MMA-co-NIPAA$_M$) exhibit smaller average diameters and size distributions that were attributed to the presence of the poly(methacrylic acid) both with and without the pendant thiol functionalities (Figure 4.22). This behaviour is analogous to that of the thiolated and non-thiolated PMAA and PNIPAA$_M$ di- and triblock copolymers of increasing PMAA block size, and was once again believed to be a result of the enhanced intermolecular interactions of PMAA at the shell surface relative to PNIPAA$_M$.

Table 4.5 – A comparison of the average diameters of tetradecane-filled microspheres utilising LCST-modified P(MMA-co-NIPAA$_M$) copolymer as a shell material. All sonicated at 100 Wcm^{-2} for 60s.

Shell Material	Microsphere Size / µm (100 Wcm^{-2})
PNIPAA$_{M(100)}$	3.09 ± 1.18
P(MMA-co-NIPAA$_M$)	3.11 ± 1.13
PMAA$_{SH(100)}$-P(MMA-co-NIPAA$_M$)	1.99 ± 0.71
PMAA$_{(100)}$-P(MMA-co-NIPAA$_M$)	2.60 ± 1.18

It was suggested by Suslick et al.[12] that microspheres of non-thiol containing polymers may form a solid aggregate microsphere structure as opposed to core-shell microspheres. Laser scanning confocal microscopy was used as a technique to determine whether this was the case for non-thiol containing microspheres synthesised during the course of this project.

Figure 4.20 and Figure 4.21 reveal the successful formation and encapsulation of tetradecane within PNIPAA$_M$ and P(MMA-co-NIPAA$_M$) polymeric shells. The red fluorescence observed in the LCSM micrographs originates from the lipophilic dye Nile Red saturating the tetradecane encapsulant, as prepared in Experiment 2.2.5, confirming the core-shell structure of the microspheres. The entire core of the microspheres fluoresces, highlighting the discrete distribution of microspheres within the sample. The increased emission observed on the perimeter is likely a result of dye staining the interior of the shell.

Laser scanning confocal microscopy was employed as a technique to observe the thermoresponsiveness of microsphere systems and is discussed in more detail in Chapter 5.

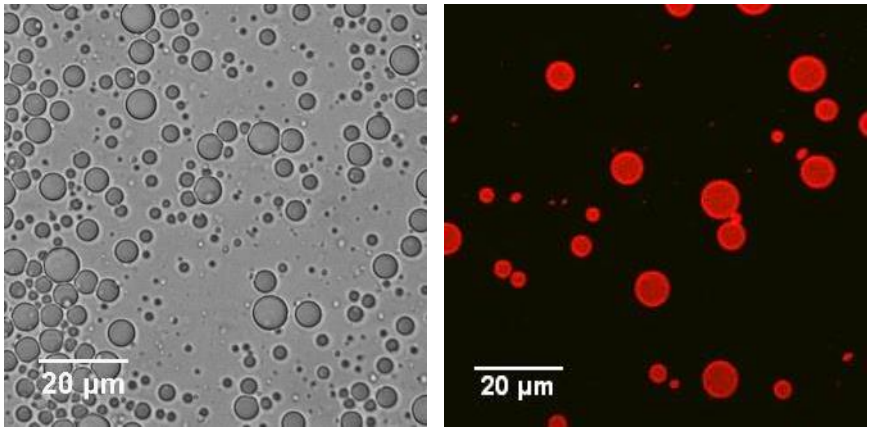

Figure 4.21 – Optical micrograph of tetradecane-filled P(MMA-co-NIPAA$_M$) microspheres (left) and LCSM micrograph of Sudan III-saturated tetradecane-filled P(MMA-co-NIPAA$_M$) microspheres (right). Sonicated at 100 Wcm^{-2} for 60s.

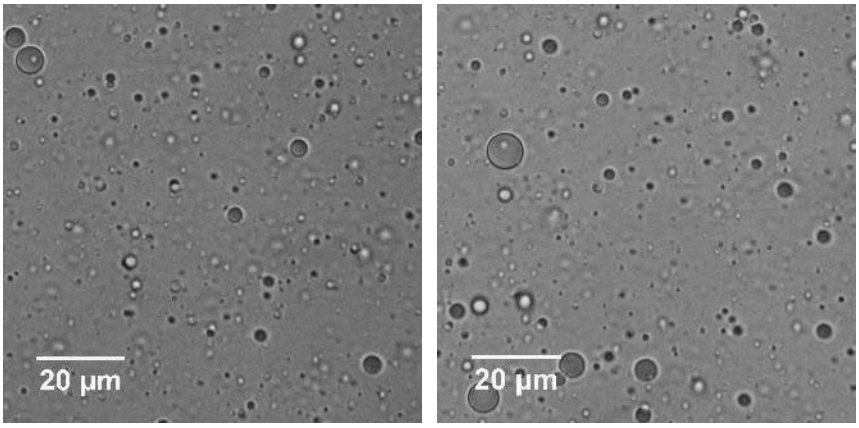

Figure 4.22 – Tetradecane-filled PMAA$_{SH}$-P(MMA-co-NIPAA$_M$) microspheres (left) and PMAA-P(MMA-co-NIPAA$_M$) microspheres (right), sonicated at 100 Wcm^{-2} for 60s.

To determine whether the non-thiolated polymers undergo any alternative sonochemically-induced covalent cross-linking reactions, samples of polymer in buffer were sonicated in conditions similar to those employed during microsphere synthesis, although in the absence of an encapsulant species. The samples were then dried in an oven to yield the sonicated polymer (Experiment 2.2.12).

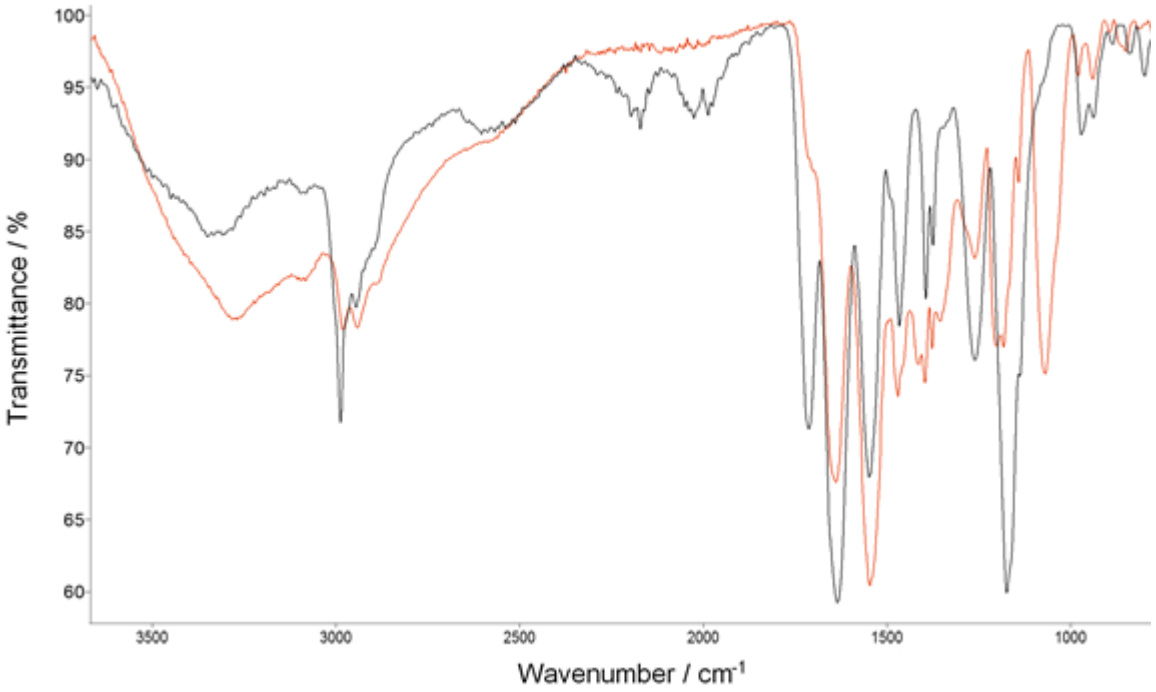

Figure 4.23 – FT-IR spectra of native $PMAA_{(100)}$-$PNIPAA_{M(100)}$ (black) and $PMAA_{(100)}$-$PNIPAA_{M(100)}$ sonicated at 100 Wcm^{-2} for 60 s (red).

Figure 4.23 compares the spectra of unsonicated $PMAA_{(100)}$-$PNIPAA_{M(100)}$ and $PMAA_{(100)}$-$PNIPAA_{M(100)}$ sonicated at 100 Wcm^{-2} for 60 s. The partial loss of the peak at 1750 cm^{-1} corresponding to the carboxylic acid carbonyl peak is indicative of a sonochemically-induced reaction. The twin peak at 1200-1300 cm^{-1} corresponding to the C-O stretch of a carboxylic functionality is also reduced, as with the thiolated polymers (Figure 3.41), and the peak at 1000-1100 cm^{-1} is shown in the literature to be associated with an anhydride functionality[197]. The formation of an acid anhydride may explain the shift in peaks from those of a carboxylic acid to those characteristic of an ester. Yang and Rubner [206,207] observed the thermally-induced formation of acid anhydride bonds between analogous poly(acrylic acid) (PAA) during hydrogen-bonded layer-by-layer ultrathin film formation at 175 ºC over a period of 3 hours, therefore it is entirely possible that this reaction may be facilitated by a sonochemical protocol. According to Yang and Rubner, the anhydride linkages were shown to rehydrolyse immediately upon exposure to water, however alternative reports in the literature[208] indicate that the breakdown of anhydrides in water is a slow reaction, which would correlate with the observed degradation data reported for microspheres in solution relative to their thiol-crosslinked counterparts (Figure 4.17 and

Figure 4.19). The conventional mechanism for the formation of acid anhydride is shown in Figure 4.24.

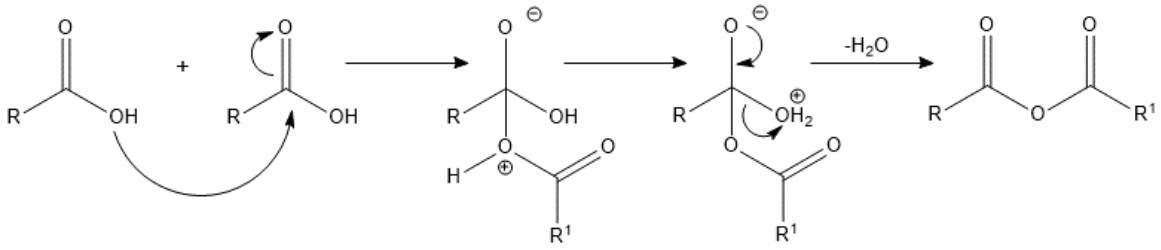

Figure 4.24 - The conventional mechanism for condensation of carboxylic acids to yield acid anhydride.

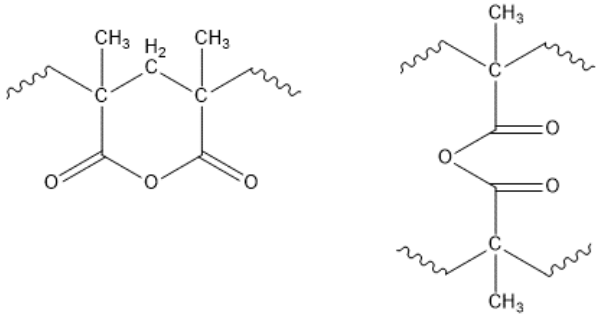

Figure 4.25 – The anhydride structures proposed by Grant and Grassie[208]. Formation between adjacent anhydride groups (left), and non-adjacent inter- and intramolecular anhydride formation (right).

Grant and Grassie[208] proposed two mechanisms upon the thermal decomposition of poly(methacrylic acid) at 200 °C, a minor depolymerisation reaction into MAA monomer, and the main reaction of anhydride formation from the elimination of water, named anhydropoly(methacrylic acid). Although the localised hot spots created during cavitation far exceed the temperatures required for thermal decomposition, it initially seemed unlikely that a sonochemically-induced reaction conducted in water could yield a product analogous to that of a thermal decomposition reaction.

The importance of partial insolubility as a result of amphiphilicity has been reported as essential to the successful formation of thiolated $PMAA_{SH}$ microspheres[10], the disulphide

crosslinks are insoluble in water, thus stabilising the microsphere shells. Hydrolysis of the C-O-C functionalities of anhydrides in water would suggest that no induced amphiphilicity or insolubility would be achieved upon thermal decomposition of hydrophilic PMAA. Grant and Grassie[208] instead reported that the main product of thermal decomposition, anhydropoly(methacrylic acid), was, in fact, insoluble in both water and methanol, suitable solvents for native PMAA. It is therefore possible that a sonochemically-induced mechanism may yield a similar crosslinked polymer, analogous to the product of thermal degradation and capable of forming stable microsphere shells. The question of how this insolubility is achieved may be due both to the rigidity of the anhydride structures generated and the presence of crosslinks.

The two proposed anhydride structures are shown in Figure 4.25. The first is anhydride formation within a single chain, leading to the formation of six-membered glutaric anhydride-type rings, and the second is the inter- and intramolecular "crosslinking" of carboxylic acid moieties to form anhydrides analogous to isobutyric acid. A combination of characterised rigid glutaric anhydride chains with occasional isobutyric crosslinks were reported by Grant and Grissie[208] as the conclusive explanation for the insolubility of anhydropoly(methacrylic acid). It now forms the rationale behind the stability of non-thiolated poly(methacrylic acid) microspheres synthesised during the course of this project.

The potential formation of acid anhydride crosslinks during sonochemical synthesis has not previously been reported. It is a discovery that expands the scope for future sonochemical microsphere syntheses without the need for thiol functionalities, and it demonstrates additional covalent interactions between acids beyond the non-covalent stabilisation mechanisms reported by Dibbern *et al.*[12]. Interestingly, upon analysis of sonicated and native poly(L-glutamic acid) samples to rationalise the formation of microspheres in the absence of disulphide crosslinks, Dibbern reported no modification of the polymer, however characterisation was limited to mass spectrometry[12].

The encapsulation efficiency of the disulphide-crosslinked and the proposed anhydride-crosslinked microspheres has been characterised, alongside various release mechanisms, and is discussed in Chapter 5.

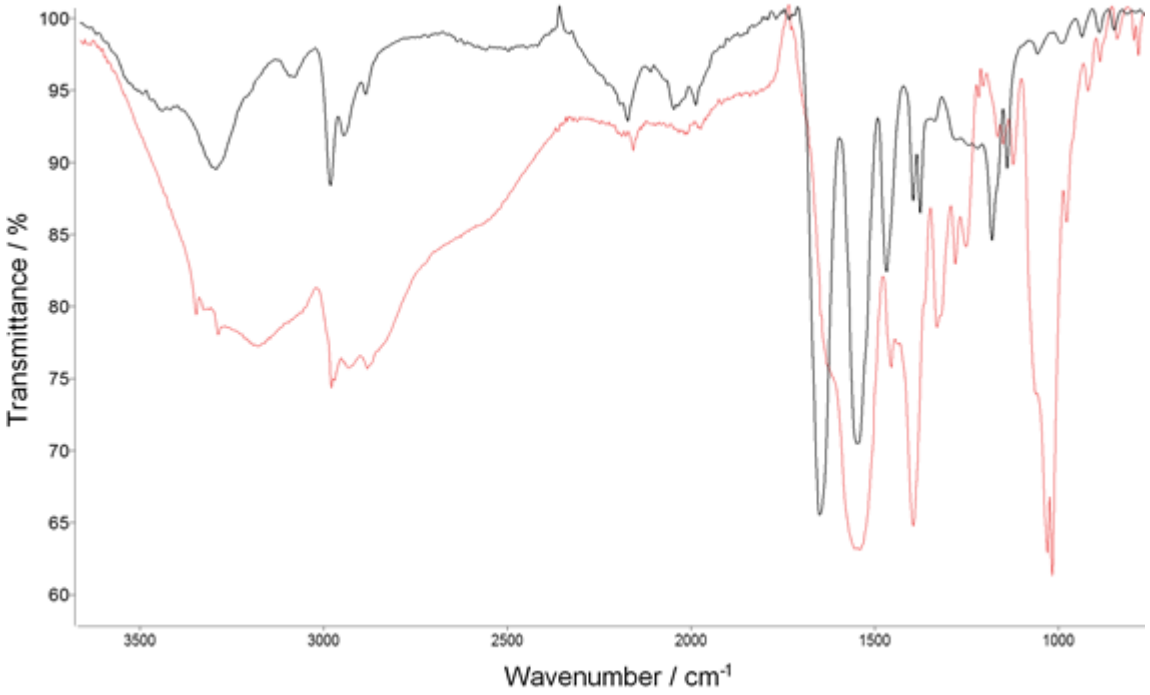

Figure 4.26 - FT-IR spectra of PNIPAA$_{M(100)}$ (black) and PNIPAA$_{M(100)}$ sonicated at 100 Wcm^{-2} for 60s (red).

Figure 4.26 shows the FT-IR spectra of sonicated (red) and unsonicated PNIPAA$_{M(100)}$ (black), revealing some loss of the distinctive double peaks corresponding to the carbonyl stretch of the amide between 1500-1700 cm^{-1}. The peaks at 1400 cm^{-1} are more consistent with the OH bend of a carboxylic acid (Figure 3.40), whilst the strong peak at 1000-1100 cm^{-1} may correspond to an anhydride or alcohol.

Amides are the least reactive of all carboxylic acid derivatives, but may be hydrolysed to their parent carboxylic acid in the presence of an acid or base[209]. There are no previous reports of ultrasound-induced hydrolysis of PNIPAA$_M$, therefore the precise mechanism is not known. However, due to the unusual reaction pathways facilitated by ultrasound and sonochemistry, it is possible that PNIPAA$_M$ undergoes a degree of sonochemically-induced hydrolysis to acrylic acid (AAc) at the surface of the sphere. These AAc moieties would then be capable of undergoing the same proposed covalent and non-covalent interactions as PMAA, thus stabilising the microsphere. Complete hydrolysis would lead to a loss of thermoresponsive character, however a degree of hydrolysis may instead cause an increase in the measured LCST of PNIPAA$_M$ due to the presence of hydrophilic AAc units. The

thermoresponsive release behaviour of $PNIPAA_M$-containing microspheres is described further in Chapter 5.

Whilst the two mechanisms describing sonochemically-induced crosslinking in non-thiolated PMAA and $PNIPAA_M$ microspheres are postulations based upon the FT-IR data and observed microsphere stability, they form the basis for further understanding of the precise interactions stabilising microspheres in the absence of disulphide crosslinks.

4.1.7 The Effect of pH on Microsphere Morphology

When preparing the different microsphere systems during the course of this project, polymers were first solubilised in pH 8 tris acetate buffer to ensure that all acid groups within the PMAA portions of the polymer were fully deprotonated. In the thiolated poly(methacrylic acid) systems, amphiphilicity within the polymer therefore originates solely from the presence of the pendant thiol functionalities. It has previously been reported that, in an acidified environment, $PMAA_{SH}$ microspheres will aggregate due to protonation of the ionised acid groups and subsequent aggregation to exclude water, characterised by the hydrophobic effect.

Since the discovery of potential anhydride crosslinking within the shells of non-thiol functionalised polymers, it was considered pertinent to compare the response of these microspheres to acidification to establish whether non-crosslinked pendant carboxylate functionalities remain in the shell. The homopolymeric PMAA microspheres in particular will likely aggregate at any pH if the shell is entirely comprised of insoluble crosslinked PMAA. The discrete, free-flowing distribution of microspheres observed in previous samples (Figure 4.15) are instead indicative of a percentage of hydrophilic ionised carboxylate functionalities present in the shell, analogous to thiol cross-linked microspheres. It was therefore postulated that, once protonated in acidic environments below the pKa of PMAA (pKa = 5.5), these microspheres would aggregate in the same fashion.

Figure 4.27 and Figure 4.28 compare the response of tetradecane-filled thiolated $PMAA_{SH(100)}$ and non-thiolated $PMAA_{(100)}$ microspheres to changes in solution pH. In both samples the microspheres are discretely distributed in the bulk phase between pH 6 and pH

10, and aggregation of microspheres can be observed at pH 4 below the pKa of PMAA. This would indicate that a number of hydrophilic carboxylate ions are present in the shell, stabilising the microspheres with respect to aggregation.

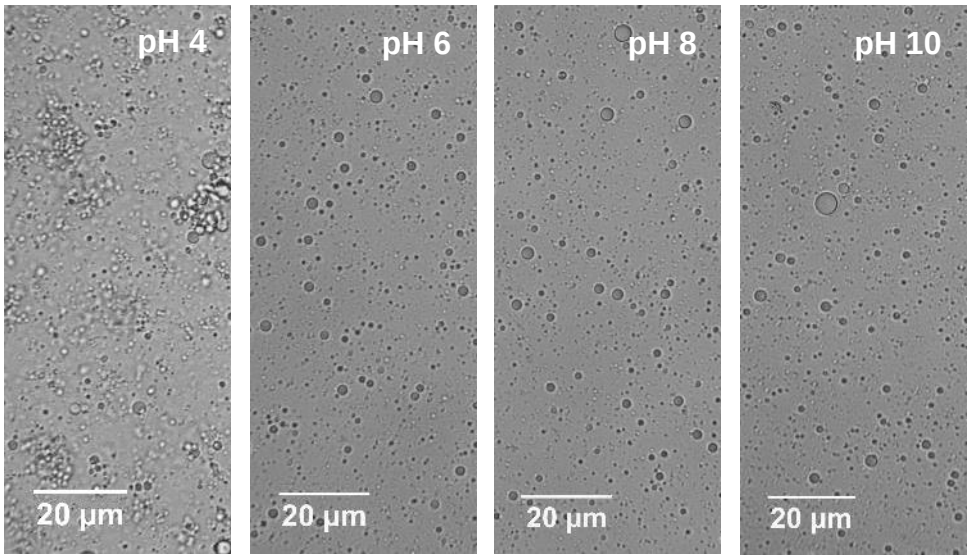

Figure 4.27 – Tetradecane-filled $PMAA_{SH(100)}$ microspheres after 24 hours stored at room temperature in deionised water, and incubation for 2 hours at pH 4, 6, 8 and 10.

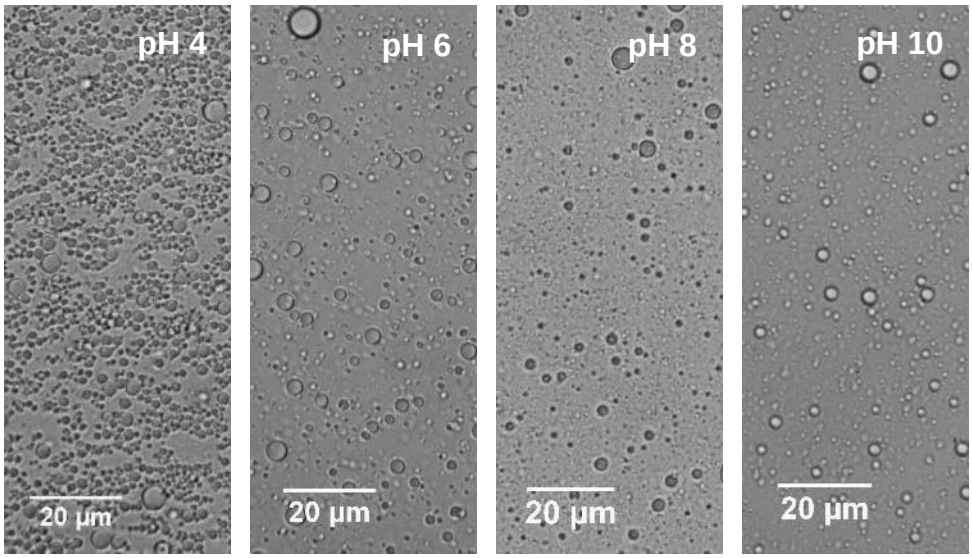

Figure 4.28 - Tetradecane-filled $PMAA_{(100)}$ microspheres after 24 hours stored at room temperature in deionised water, and incubation for 2 hours at pH 4, 6, 8 and 10.

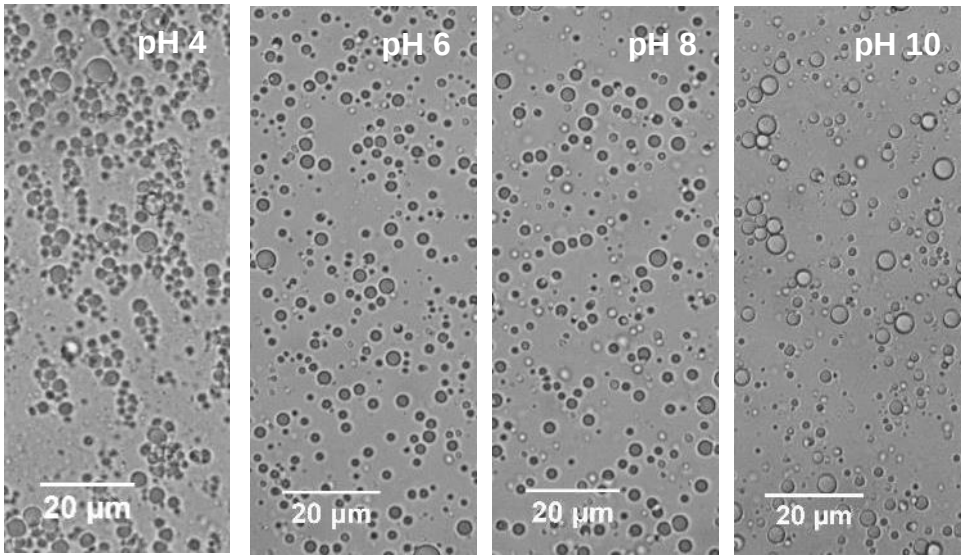

Figure 4.29 – Tetradecane-filled $PMAA_{SH(100)}$-$PNIPAA_{M(100)}$ after 24 hours in deionised water, then incubated at pH 4,6,8 and 10 for 2 hours.

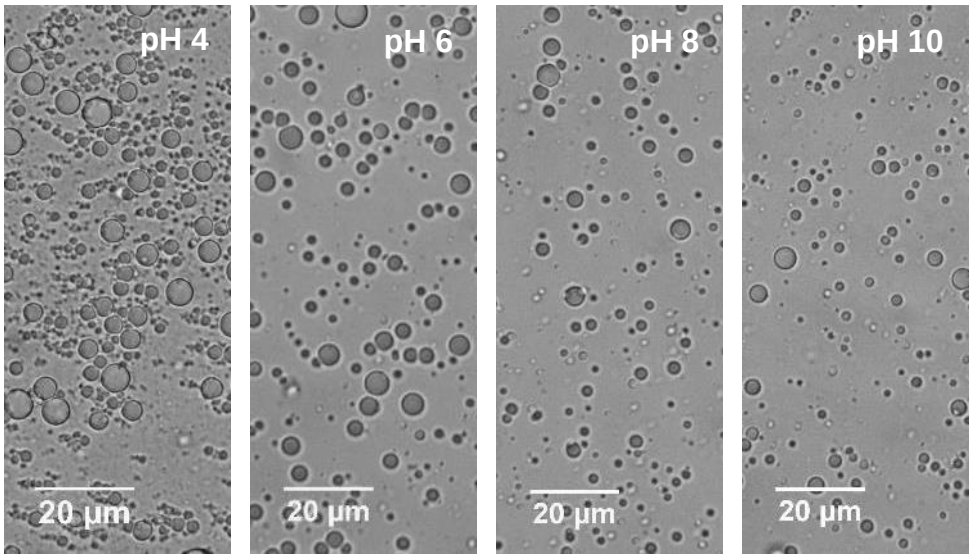

Figure 4.30 – $PMAA_{(100)}$-$PNIPAA_{M(100)}$ after 24 hours in deionised water, then incubated at pH 4,6,8 and 10 for 2 hours.

The behaviour of block copolymers in solutions of increasing pH were then compared, as shown in the images of thiolated and non-thiolated $PMAA_{(100)}$-$PNIPAA_{M(100)}$ (Figure 4.29 and Figure 4.30). $PNIPAA_M$ portions of the microspheres do not induce pH responsiveness, therefore it was interesting to observe aggregation to this degree in the thiol cross-linked and anhydride crosslinked block copolymers, assumed to be originating solely from the

protonated PMAA portions. Alternatively, microspheres generated from polymers in the absence of PMAA blocks, $PNIPAA_M$ and $P(MMA\text{-}co\text{-}NIPAA_M)$, did not undergo as extensive aggregation (Figure 4.31 and Figure 4.32), further supporting the evidence that only ionisable PMAA portions induce aggregation.

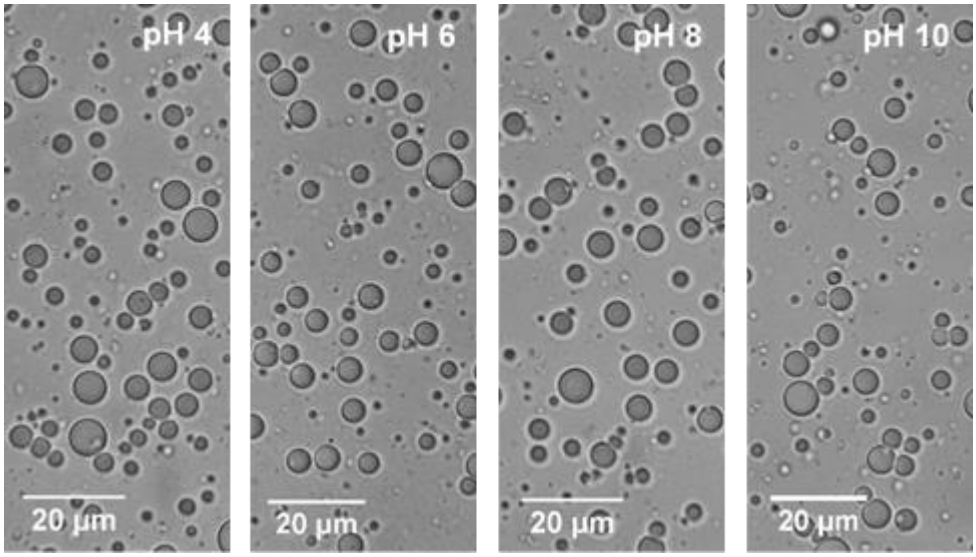

Figure 4.31 - $PNIPAA_{M(100)}$ after 24 hours in deionised water, then incubated at pH 4,6,8 and 10 for 2 hours.

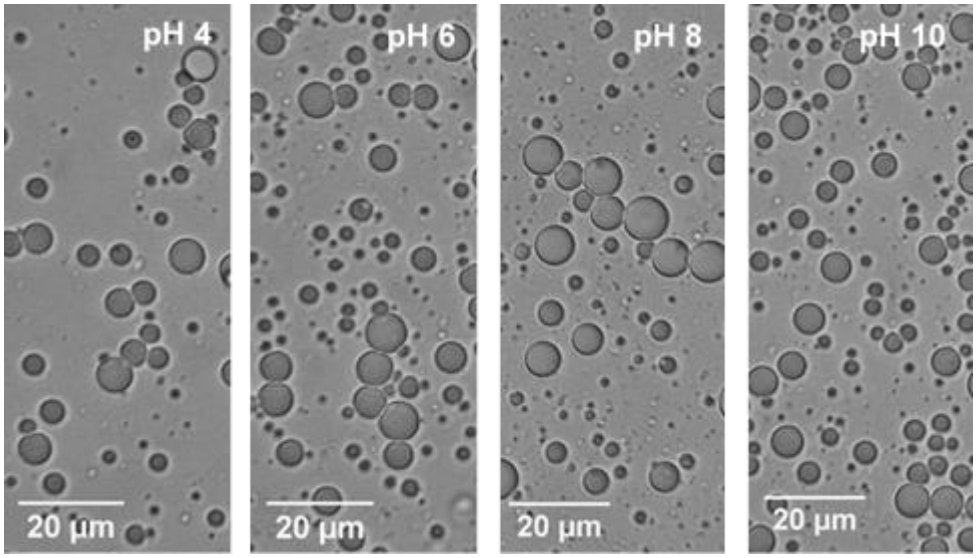

Figure 4.32 – $P(MMA\text{-}co\text{-}NIPAA_{M(100)})$ after 24 hours in deionised water, then incubated at pH 4,6,8 and 10 for 2 hours.

Once the conditions for the sonochemical synthesis had been determined, the next stage was to demonstrate the encapsulation of a range of hydrophobic and hydrophilic species to determine the capability of the novel sonochemically-generated synthetic microspheres as versatile delivery vehicles.

4.2 Encapsulation within Polymeric Microspheres

The encapsulation of hydrophobic species within sonochemically-generated proteinaceous microspheres has been well reported in the literature[2,14,51] and, more recently, the scope of research has extended to encapsulation within synthetic polymeric $PMAA_{SH}$ microspheres[10]. This section reports the encapsulation of hydrophobic and hydrophilic species within thiolated and non-thiolated synthetic polymeric microspheres.

4.2.1 Encapsulation of Hydrophobic Species

In order to characterise the impact of encapsulants on the size of sonochemically-produced $PMAA_{SH}$ and PMAA microspheres and their block copolymers, microspheres were synthesised as per the protocol outlined in Experiment 2.2.5 and 2.2.9.

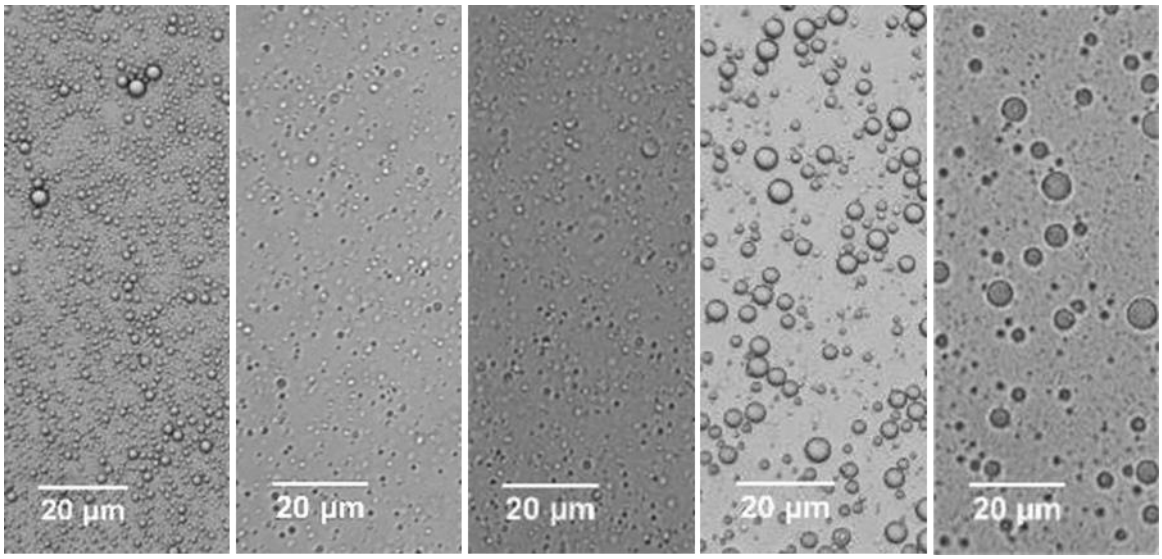

Figure 4.33 – $PMAA_{SH(100)}$ microspheres containing (from left to right): tetradecafluorohexane (TDFH), tetradecane, isopropyl myristate (IPM), soybean oil, and vegetable oil. All sonicated at 100 Wcm^{-2} for 60 s.

Table 4.6 – The viscosities and densities of encapsulant species at room temperature.

Encapsulant	Viscosity at Room Temperature / mPas	Density / gcm^{-3}	Solubility in Water / mgL^{-1}
Tetradecafluorohexane	0.63[210]	1.67[211]	0.38
Tetradecane	2.08[212]	0.76[213]	3.30×10^{-4}
Isopropyl Myristate	6.50[214]	0.85	0.02
Soybean Oil	47.00[215]	0.92	/
Vegetable Oil	40.00-60.00[215]	/	/

Makino *et al.*[60] reported a decrease in the average diameter of BSA microcapsules containing hydrophobic liquids with increasing viscosity. There was no clear mechanism proposed for this observation other than attribution to the clearer interface established between more viscous oils and the aqueous phase. The reported viscosities, densities and solubilities of hydrophobic species encapsulated within microspheres are shown in Table 4.6. Tetradecane, although not the most viscous solvent, exhibits a very low miscibility with water, which justifies the small average diameter and size distribution of tetradecane-filled microspheres (Figure 4.33 and Figure 4.34). Perfluorohexane (TDFH) microspheres, with a comparable average diameter, can be employed as a more biocompatible alternative with no cell activation or observed anti-inflammatory response[216]. Cavalieri *et al.*[10] observed the synthesis of $PMAA_{SH}$ microbubbles alongside perfluorohexane-filled microspheres, and attributed this to the partial evaporation of TDFH into the gas core of temporary microbubbles formed upon air introduction into the system and foaming. The gas phase TDFH is reportedly stabilised by the osmotic pressure placed upon the microbubble, enabling crosslinking of the polymer shell at the bubble interface.

No microbubbles were observed in polymeric TDFH microspheres or any other oil-filled polymeric microsphere systems during the course of this project, and this was believed to be a result of moving the horn tip after initial interfacial disruption to minimise air introduction into the system. Microbubbles can be distinguished from oil-filled microspheres by their "glass bottle bottom" appearance when viewed using an optical microscope, as seen in the micrographs of air-filled lysozyme microbubbles (Figure 4.11), whereby the interior remains out of focus and there is poor definition between the microsphere shell and core. Conversely, oil-filled microspheres display a homogeneous core and a well-defined shell (Figure 4.33).

Isopropyl myristate was employed to measure the release of encapsulated species by partitioning into a layer of IPM deposit. Microspheres were therefore generated to determine whether spheres containing IPM would form during sonochemically-induced release experiments, discussed further in Chapter 1. Although the measured viscosity of IPM is higher than that of tetradecane, IPM exhibits better miscibility in water, which may account for the slight increase in average size relative to tetradecane-filled microspheres. This further contradicts Makino's observations of decreasing microsphere diameter with increasing encapsulant viscosity but supports the theory that decreasing miscibility of the oil phase with water facilitates the formation of smaller microspheres.

Although soybean oil and vegetable oil blends possess far higher viscosities than the synthetic oils, the inherent inhomogeneity and impurities within naturally-occurring oils may contribute to the larger average diameters and size distributions observed (Figure 4.34). Their successful synthesis does, however, demonstrate a means to encapsulate an entirely natural, biocompatible material for a range of applications, particularly nutrient or flavour encapsulation as discussed in Section 1.2.3. All unwashed samples of microspheres exhibited stability of at least one month, with the observed loss in yield for soybean and vegetable oil comparable to those of the synthetic oils.

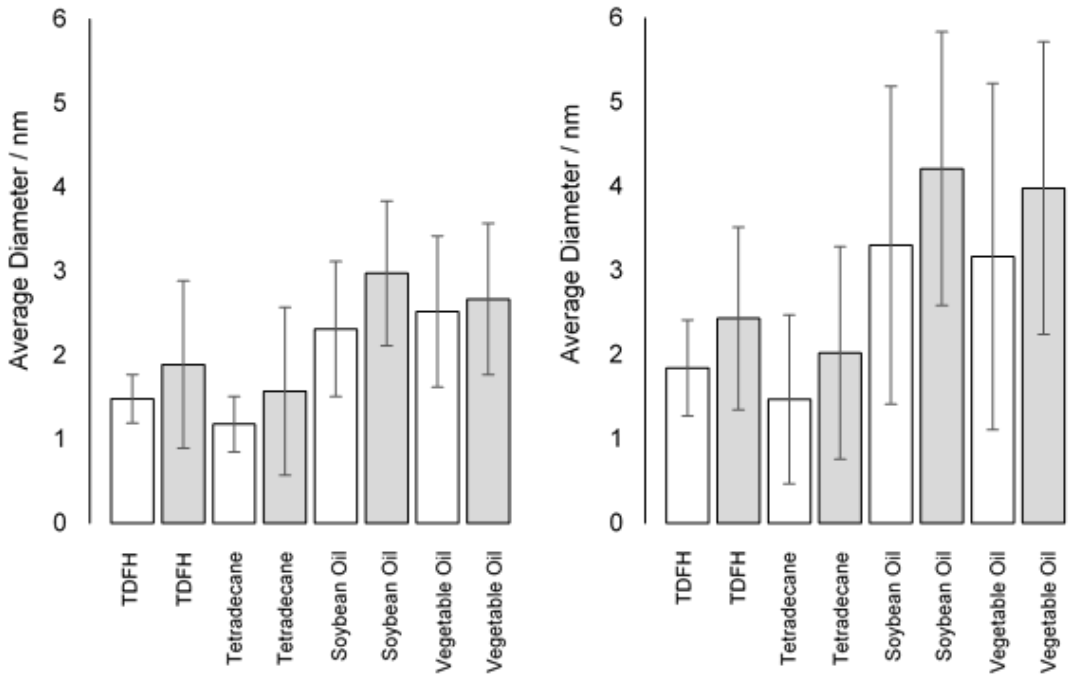

Figure 4.34 – The effect of encapsulant on the average diameter and size distribution of thiolated $PMAA_{SH(100)}$ (white) and non-thiolated $PMAA_{(100)}$ (grey) (left), and thiolated (white) and non-thiolated (grey) $PMAA_{(100)}$-$PNIPAA_{M(100)}$ (right) microspheres, sonicated at 100 Wcm^{-2} for 60 s.

The data in Figure 4.35 and Table 4.7 comparing the effect of encapsulant species on the size and size distribution largely corroborates the data shown in Table 4.3 for tetradecane-filled PMAA and $PMAA_{SH}$ microspheres (also shown in Table 4.7) regarding the effect of polymer chain length on the size and size distribution of the microspheres. The non-thiolated polymers produce larger microspheres with a wider size distribution on average than their thiolated analogues, however the microsphere size is independent of polymer molecular weight.

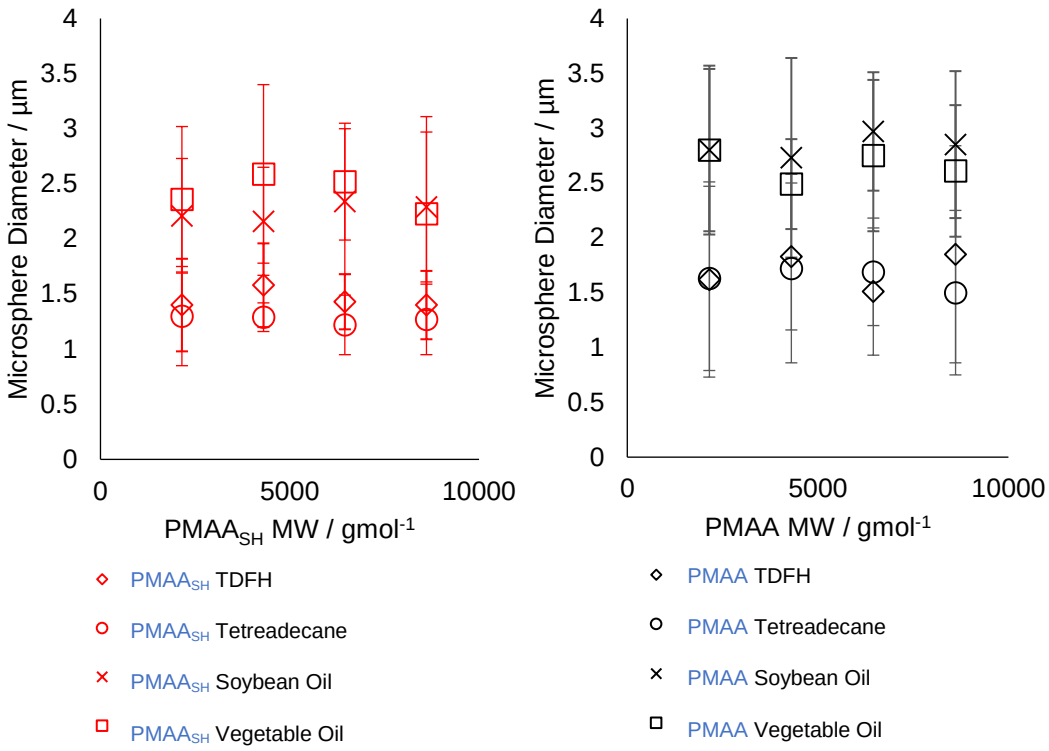

Figure 4.35 – Comparing the effect of PMAA molecular weight on the microsphere diameter of oil-filled homopolymeric-shelled PMAA$_{SH}$ and PMAA microspheres reveals no trend between molecular weight and average microsphere diameter. Samples were imaged and analysed in triplicate. Error bars indicate the maximum and minimum average microsphere diameter.

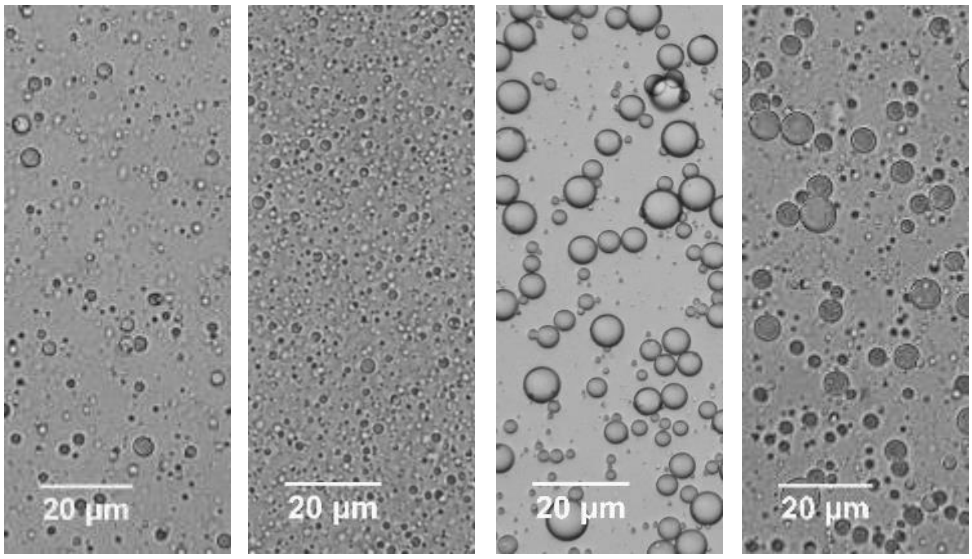

Figure 4.36 - PMAA$_{SH(100)}$-PNIPAA$_{M(100)}$ microspheres containing (from left to right): tetradecafluorohexane (TDFH), tetradecane, soybean oil and vegetable oil. All sonicated at 100 Wcm^{-2} for 60 s.

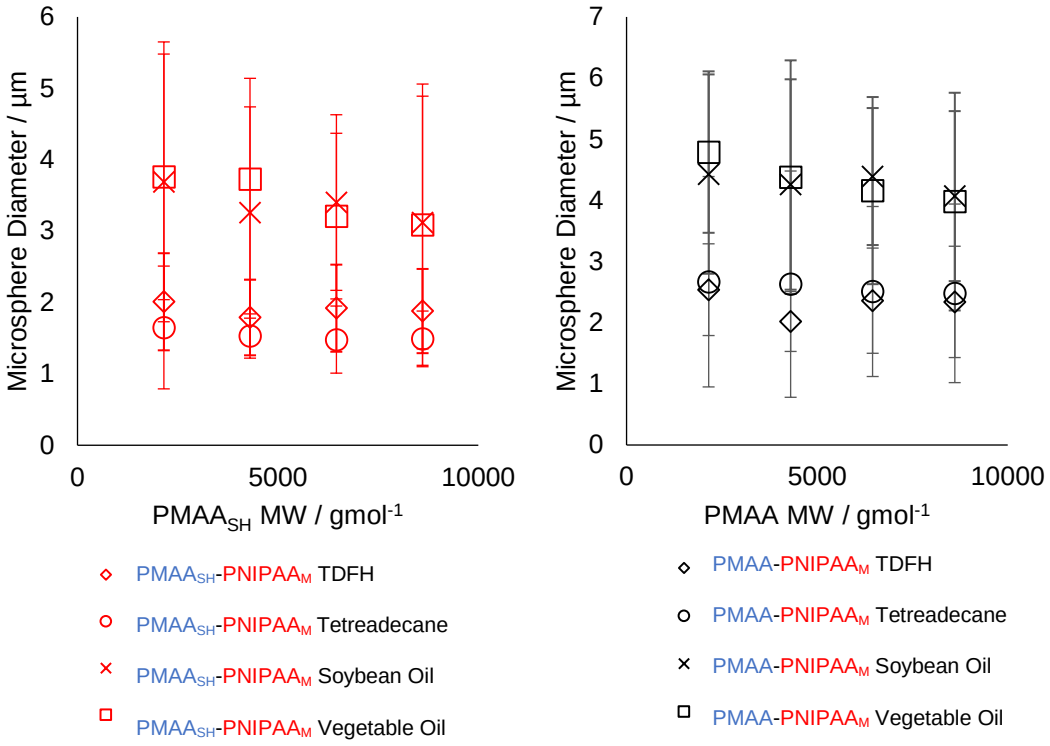

Figure 4.37 - Comparing the effect of PMAA molecular weight on the average microsphere diameter of oil-filled diblock copolymer-shelled microspheres reveals a general decrease in average diameter with increasing PMAA MW and MAA:NIPAA$_M$ ratio in the diblock chains. Samples were imaged and analysed in triplicate. Error bars indicate the maximum and minimum average diameter.

The thiolated and non-thiolated block copolymeric microspheres exhibit size trends comparable to those for the homopolymer microspheres containing different encapsulants, whereby the average microsphere diameter is dependent on the miscibility of the encapsulant species in water, albeit with larger average diameters and broader size distributions (Figure 4.36 and Table 4.7). Once again, the average diameter was largely dependent on the relative percentage of PMAA within the polymer chains, as shown in Figure 4.37, with the microspheres exhibiting a general decrease in average diameter with increasing PMAA block length, and increasing MAA:NIPAA$_M$ repeat unit ratio within the block copolymer.

Table 4.7 – The effect of encapsulant species on the average diameter of synthetic polymeric microspheres, sonicated at 100 Wcm^{-2} for 60s.

Shell Material	TDFH	Tetradecane	Soybean Oil	Vegetable Oil
$PMAA_{SH(25)}$	1.40 ± 0.42	1.30 ± 0.45	2.21 ± 0.52	2.36 ± 0.66
$PMAA_{SH(50)}$	1.58 ± 0.38	1.29 ± 0.13	2.16 ± 0.49	2.59 ± 0.81
$PMAA_{SH(75)}$	1.43 ± 0.25	1.22 ± 0.27	2.34 ± 0.66	2.52 ± 0.53
$PMAA_{SH(100)}$	1.40 ± 0.31	1.27 ± 0.32	2.29 ± 0.68	2.23 ± 0.88
$PMAA_{(25)}$	1.62 ± 0.89	1.63 ± 0.84	2.80 ± 0.77	2.80 ± 0.74
$PMAA_{(50)}$	1.83 ± 0.67	1.72 ± 0.86	2.73 ± 0.91	2.49 ± 0.41
$PMAA_{(75)}$	1.51 ± 0.58	1.69 ± 0.49	2.97 ± 0.54	2.75 ± 0.69
$PMAA_{(100)}$	1.85 ± 0.99	1.50 ± 0.75	2.85 ± 0.67	2.61 ± 0.60
$PMAA_{SH(25)}$-$PNIPAA_{M(100)}$	2.01 ± 0.68	1.65 ± 0.86	3.69 ± 1.96	3.76 ± 1.72
$PMAA_{SH(50)}$-$PNIPAA_{M(100)}$	1.79 ± 0.53	1.53 ± 0.31	3.26 ± 1.48	3.73 ± 1.41
$PMAA_{SH(75)}$-$PNIPAA_{M(100)}$	1.92 ± 0.61	1.48 ± 0.47	3.40 ± 1.23	3.21 ± 1.16
$PMAA_{SH(100)}$-$PNIPAA_{M(100)}$	1.88 ± 0.59	1.49 ± 0.39	3.12 ± 1.77	3.09 ± 1.97
$PMAA_{(25)}$-$PNIPAA_{M(100)}$	2.54 ± 0.75	2.67 ± 1.72	4.43 ± 1.63	4.79 ± 1.32
$PMAA_{(50)}$-$PNIPAA_{M(100)}$	2.02 ± 0.49	2.63 ± 1.85	4.26 ± 1.72	4.38 ± 1.91
$PMAA_{(75)}$-$PNIPAA_{M(100)}$	2.36 ± 0.86	2.51 ± 1.39	4.39 ± 1.12	4.16 ± 1.53
$PMAA_{(100)}$-$PNIPAA_{M(100)}$	2.34 ± 0.91	2.48 ± 1.46	4.07 ± 1.39	3.98 ± 1.78
$PNIPAA_{M}$	3.68 ± 1.92	3.09 ± 1.18	5.17 ± 1.32	4.62 ± 1.29

4.2.2 Encapsulation of Inverse Water-in-Tetradecane Emulsions

To extend the scope of sonochemically-generated microspheres as delivery vehicles for hydrophilic species, mechanisms to facilitate their encapsulation have been investigated. Gedanken has successfully encapsulated the drugs tetracycline[13] and gemcitabine[80] within BSA microspheres by partial solubilisation of the drugs in the oil phase upon sonication,

however a more universal protocol would facilitate the encapsulation of other hydrophilic species and, more importantly, aqueous phases. Skinner *et al.*[7] have since established a mechanism for their encapsulation through the use of inverse water-in-oil (W/O) emulsions.

The synthesis of microspheres by sonication is dependent on simultaneous emulsification and encapsulation to yield the resultant microspheres, essentially a stabilised oil-in-water emulsion. Skinner[7] employed the same sonochemical protocol for the encapsulation of W/O emulsions by deposition of a sonochemically-prepared W/O emulsion onto the protein solution, followed by sonication at the interface to form a stable W/O/W double emulsion.

Emulsions are metastable systems of two dispersed immiscible fluids, stabilised by a surfactant. Oil-in-water (O/W) emulsions are more commonly reported in the literature, but their mechanisms of stabilisation differ from those of inverse W/O emulsions. O/W emulsions are stabilised by both steric and electrostatic repulsions, whereas W/O emulsions are stabilised solely by the steric repulsions of the dispersed water droplets due to the low conductivity of the oil phase[217]. W/O emulsions often possess much lower stability due to the mobility of water droplets and their tendency to coalesce. As such, many W/O emulsions are actually solid or semi-solid and further stabilisation is induced by fat crystallisation[217].

Mechanisms for emulsification include homogenisation, either by simple mixing, the use of a high speed or high pressure homogeniser, or sonochemical mixing. Ultrasonic emulsification consists of two significant steps. The first involves interfacial disruption, leading to the explosive dispersion of the discrete droplets into the continuous phase; whilst the second is cavitation-driven droplet breakdown leading to a very small droplet size, known as a nanoemulsion.

Canselier *et al.*[218] have summarised the contributory variables that determine emulsion morphology. It is common during emulsion formation for the less viscous liquid to form the continuous phase, generating O/W emulsions, however selection of the correct surfactant, a favourable oil:water ratio and use of a high sonochemical intensity will yield the desired W/O emulsion. Sonication time will also impact the droplet size, short irradiation will lead to a course polydisperse emulsion of larger droplets, whilst longer sonication will enable sufficient cavitation-driven droplet breakdown to generate the desired stable nanoemulsion.

Dispersed droplets within emulsions adopt a spherical shape to minimise surface area and surface energy. Although nanoemulsions with low polydispersity and small droplet size are more desirable, the pressure upon the interface of small droplets far greater exceeds that of large droplets, as described by the Laplace pressure (Equation 4.8 and 4.9). The pressure on the concave face of an emulsion droplet (P_{in}) will always exceed the pressure of the convex face (P_{out}). As the radius of curvature (r) increases, the difference between P_{in} and P_{out} will tend to zero. Decreasing the curvature and increasing the surface area (δA) and interfacial tension (γ) leads to an unfavourable increase in the Gibbs free energy (δG).

$$P_{in} = P_{out} + \left(\frac{2\gamma}{r}\right) \tag{4.8}$$

$$\delta G = \gamma(\delta A)_{T,P} \tag{4.9}$$

In order to overcome this and stabilise nanoemulsions, a surfactant is used to lower the interfacial tension and stabilise the dispersed water droplets with respect to Ostwald ripening and coalescence, two mechanisms that seek to reduce the energy of a system by driving the formation of larger dispersion droplets.

The phenomenon of Ostwald ripening is driven by the inherent instability of smaller particles with a larger surface area:volume ratio and greater solubility in the immiscible bulk. Molecules at the interface of a droplet have more energy than those in the bulk of the droplet, and in small droplets the molecules at the interface diffuse into the continuous bulk phase[219]. The diffused aqueous molecules subsequently join larger droplets, leading small droplets to become smaller, and larger droplets to increase in size and stability (Figure 4.38). Skinner[7] observed that a small addition of salt has a stabilising effect on the emulsion by reducing aqueous droplet size. It was proposed that salt increases the stability of the surfactant head group, thus reducing the likelihood of Ostwald ripening or coalescence and phase separation.

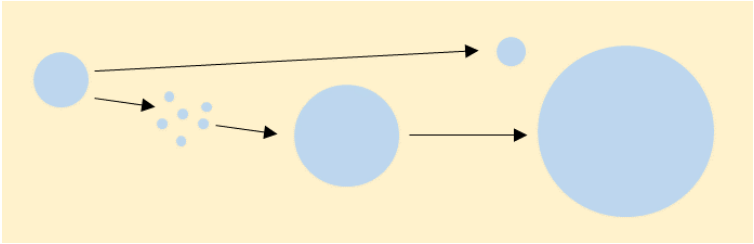

Figure 4.38 – The effect of Ostwald ripening on an aqueous droplet (blue) in an oil phase (yellow).

The challenge when encapsulating hydrophilic species within microspheres is to first stabilise the aqueous dispersion within the continuous oil phase and to ensure that the emulsion remains intact upon secondary sonication to form the microspheres and W/O/W double emulsion.

The hydrophilic-lipophilic balance scale is a ranking of the hydrophilicity of a surfactant. In general, surfactants with a low hydrophilic-lipophilic balance (HLB) will stabilise water-in-oil emulsions. Although they contain both hydrophobic and hydrophilic portions, the surfactant should have more affinity for the continuous phase. Span 80® (Figure 4.39) was chosen as an appropriate non-ionic surfactant based upon the successful formation of W/O emulsions reported by Skinner *et al*.[7] for encapsulation within lysozyme microspheres. It has a low HLB value of 4.3 and high hydrophobic character, and has been reported in the literature as a suitable surfactant for the formation of stable emulsions of water in decane, dodecane and hexane[220]. Capdevila *et al*.[220] attributed the observed stability to the defined interface of more viscous oils and low susceptibility of Ostwald ripening due to the poor solubility of water in the oil phase. It was reported, however, that the oil viscosity had no direct impact on droplet size. Increasing the surfactant:oil ratio, on the other hand, was shown to produce smaller droplets. A higher concentration of Span 80® in the oil phase means more surfactant is readily available to stabilise the interface.

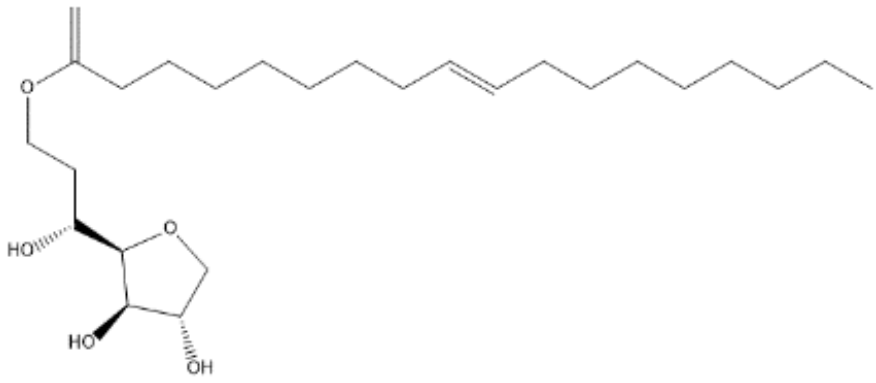

Figure 4.39 – Span 80® non-ionic surfactant.

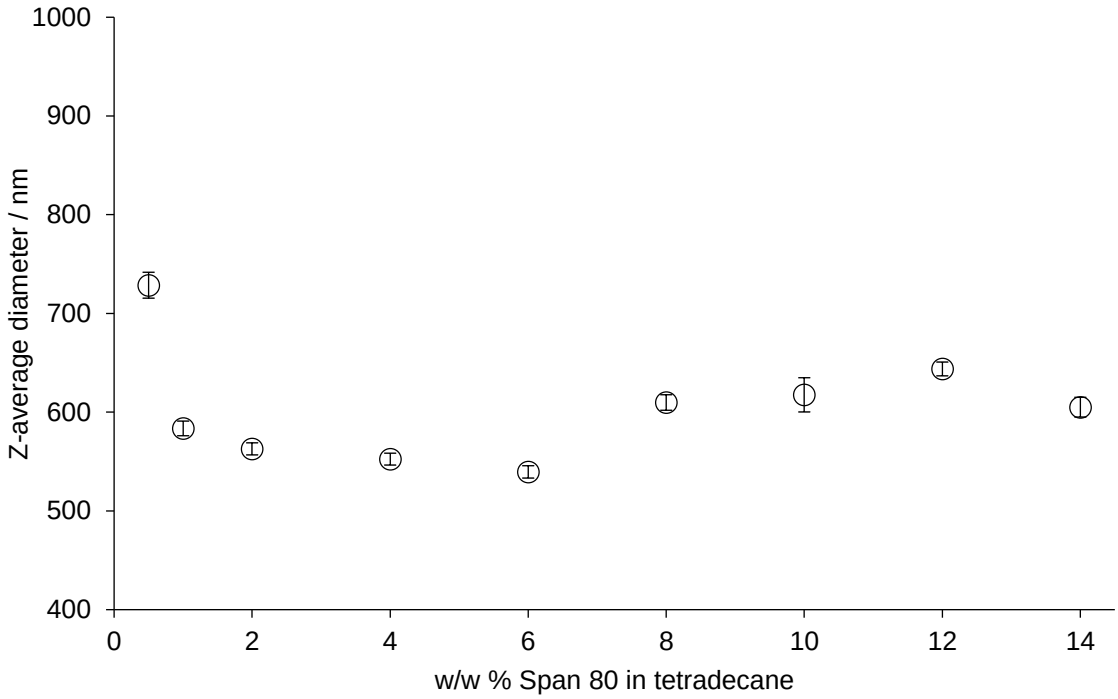

Figure 4.40 - The effect of increasing Span 80® concentration on the Z-average diameter of 3M NaCl aqueous droplets dispersed in tetradecane (40:60), sonicated at 100 Wcm^{-2} for 60s.

Optimisation reactions were conducted in order to determine the conditions required to generate a stable W/O emulsion by sonochemical emulsification. Emulsions were prepared as per the protocol outlined in Experiment 2.2.6 and analysed by dynamic light scattering. Prior to analysis, emulsions were diluted to enable the discrete distribution of dispersed droplets to be analysed. Concentrated samples may be compromised by multiple scattering, whereby light scattered from one particle or droplet is rescattered, resulting in an artificially low measured particle size.

Firstly, the effect of increasing Span 80® concentration on the aqueous droplet size was measured (Figure 4.40). Emulsions of 1M sodium chloride (NaCl) solution in tetradecane were prepared by sonication at 100 Wcm^{-2} for 60 s. Between 0.5 and 6 w/w % Span 80® in tetradecane, the increasing concentration leads to a drop in Z-average diameter of the dispersed droplets. Beyond this, however, the diameter increases again. The mechanism for this increase is not entirely known, but it is likely a result of increased packing of the bulky hydrophilic head group within the aqueous core of the inverse emulsion and the

subsequent compact arrangement and alignment of alkyl tails extending into the oil phase at increased concentrations[221], as depicted in Figure 4.41. As a result, 4 w/w % was chosen as the appropriate Span 80® concentration for future preparations. Although producing emulsions with a comparable droplet diameter, it was shown upon further investigation to determine emulsion stability that the use of 2 w/w % Span 80® surfactant concentration did not produce emulsions with the stability of those containing 4 w/w % Span 80®.

It must be noted that the Z-average diameter represents the hydrodynamic diameter of the dispersed droplets. The hydrodynamic diameter consists of the physical diameter of the dispersed sphere, plus the double layer surrounding the particle, called the Debye length. In a continuous oil phase, the double layer will be larger and more diffuse due to the presence of significantly fewer ions in oil than water[222].

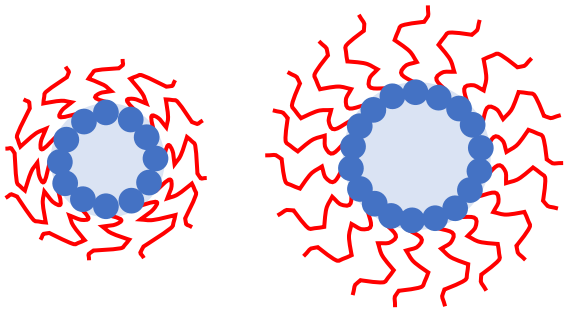

Figure 4.41 – Proposed packing of surfactant at the oil:water interface of dispersed aq droplets in tetradecane at increasing Span 80® concentration.

The next variable to optimise was that of the salt concentration of the dispersed aqueous phase (Figure 4.42). The addition of even a low concentration of salt (0.01 M) greatly reduces the Z-average diameter of the aqueous droplets, yet beyond this the increasing salt concentration does not significantly impact the emulsion morphology. The presence of increasing electrolyte concentration does, however, improve the stability of the emulsions with respect to coalescence and Ostwald ripening[7,223,224]. Koroleva and Yurtov[224] have reported a critical NaCl concentration of 0.012 M in the aqueous phase of aq-in-oil emulsions, stabilised with Span 80®, beyond which dispersed droplets will be stable against Ostwald ripening. Below this concentration, the osmotic pressure exceeds the Laplace pressure and the droplets are susceptible to coarsening.

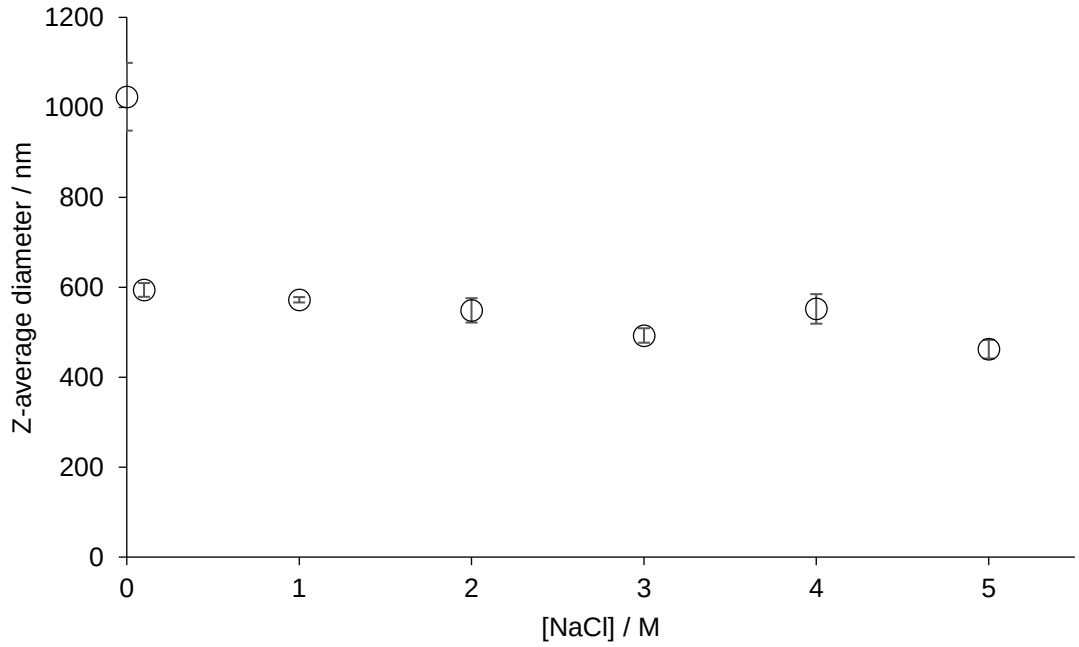

Figure 4.42 – The effect of salt concentration on the average diameter of aqueous droplets dispersed in tetradecane (40:60), stabilised with 4 % Span 80® surfactant, sonicated at 100 Wcm^{-2} for 60 s.

As a final comparison to ensure that the chosen acoustic intensity and sonication time were appropriate, samples of 1M NaCl-in-4 % Span 80®-in-tetradecane (40:60) were sonicated at 100 Wcm^{-2} and 219 Wcm^{-2} for increasing sonication times (Figure 4.43). For both intensities, the Z-average diameter of dispersed aqueous droplets initially decreases with sonication time, in agreement with the observations of Canselier *et al.*[218]. Beyond 3 minutes sonication at 219 Wcm^{-2} and 5 minutes at 100 Wcm^{-2}, the Z-average diameter begins to increase again. Based on the observations of the effects of sonication power on microsphere morphology of tetradecane-filled polymer microspheres (Figure 4.7), the proposed mechanism of air introduction and reduced efficiency due to foaming was therefore believed to be responsible for the increase in Z-average diameter, contradicting the observations of Canselier[201]. Another possible explanation for the observed increase could be a result of droplet coalescence, which would be more prevalent over longer periods of sonication and at higher sonication intensities due to aggressive mixing. However more aggressive mixing of small volumes also leads to air introduction and foaming, thus reducing mixing efficiency. A chosen sonication time and power of 5 minutes at 100 Wcm^{-2} was employed, generating emulsions with droplet diameters approximately 100 nm smaller than those sonicated for 60 s due to increased cavitation-driven droplet breakdown.

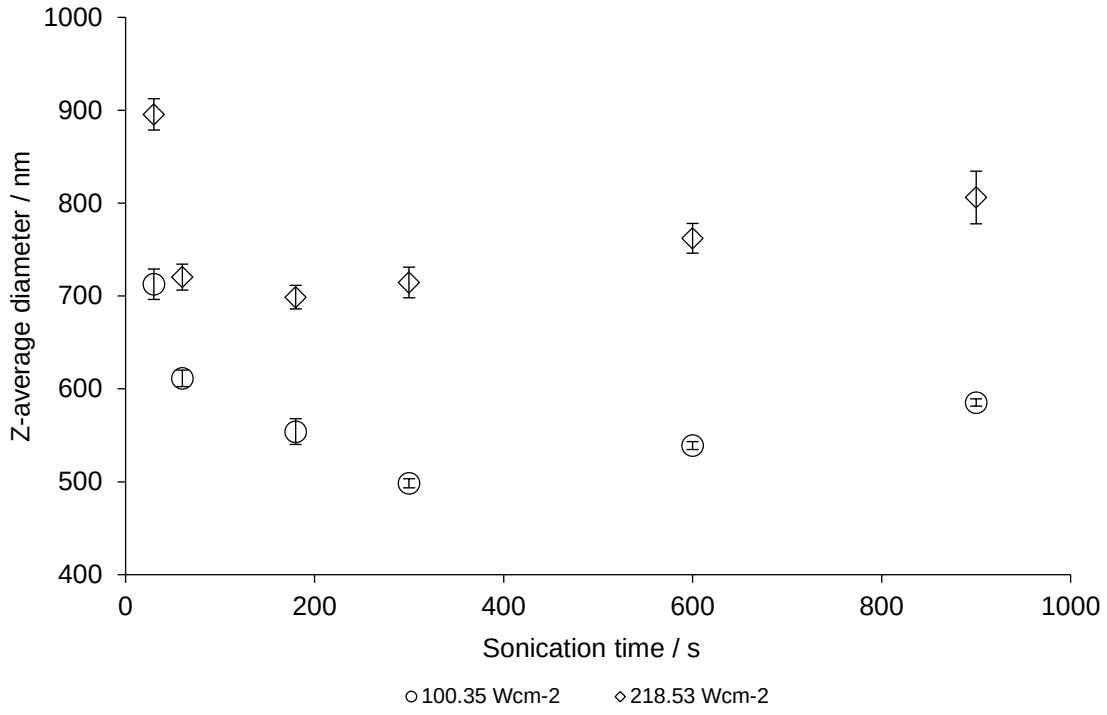

Figure 4.43 – A comparison of the dispersed droplet size of 1M NaCl-in-4 % Span 80®-in-tetradecane emulsions (40:60) sonicated at 100 Wcm^{-2} and 219 Wcm^{-2} for increasing insonation times.

The stability of emulsions synthesised with increasing aq:oil ratios, stored at room temperature, were measured as a function of the partitioned aqueous phase from the emulsified layer after 24 hours. 1 mL samples were prepared of 10-50 % 1 M NaCl-in-tetradecane at increasing Span 80® concentrations and sonicated for 5 minutes at 100 Wcm^{-2}. After 24 hours, the partitioned aqueous phase was extracted from the base of the centrifuge tube using a microsyringe, and the release was reported as a percentage of the entire encapsulated volume (Figure 4.44).

Emulsions prepared containing no Span 80® underwent complete phase separation after 24 hours. Partitioning in fact occurred almost immediately after sonication due Ostwald ripening and coarsening. As the concentration of Span 80® was increased, the emulsions are stabilised with respect to phase separation. Beyond 3 w/w % Span 80®, phase separation for all emulsions, with the exception of 50:50 aq:oil emulsions, was essentially non-existent after 24 hours, and those prepared with 6 % Span 80® retained their stability for up to 1 month.

Samples with higher aq percentages of up to 95 %, stabilised with 17-41 % Span 80®, have been reported in the literature[220]. However, the observed droplet diameters were almost ten times larger than those of the emulsions prepared during the course of this project and also exceeded the diameter of many of the microspheres prepared throughout this project. An aq:oil ratio of 40:60 was therefore considered appropriate to maximise aq loading whilst generating dispersions of a suitable droplet diameter for encapsulation.

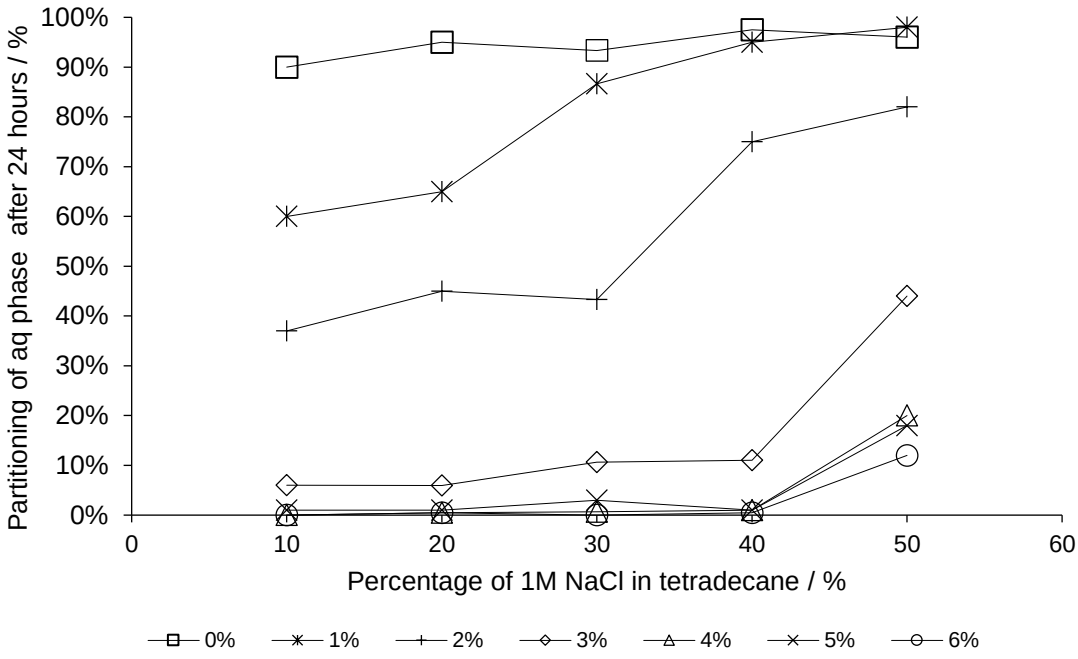

Figure 4.44 – Partitioning of the aqueous phase from 1M NaCl-in-tetradecane emulsions with increasing Span 80® concentrations after 24 hours. Percentage values in legend indicates Span 80 w/w % in tetradecane.

The chosen optimised conditions are in agreement with those reported by Skinner *et al.*[7]. 100 µM of emulsion, consisting of 40:60 1M NaCl-in-4 % Span 80®-in-tetradecane, was deposited onto solutions of polymer in buffer, and samples were sonicated for 60s in order to compare the microsphere morphologies to those containing hydrophobic tetradecane, prepared under the same reaction conditions.

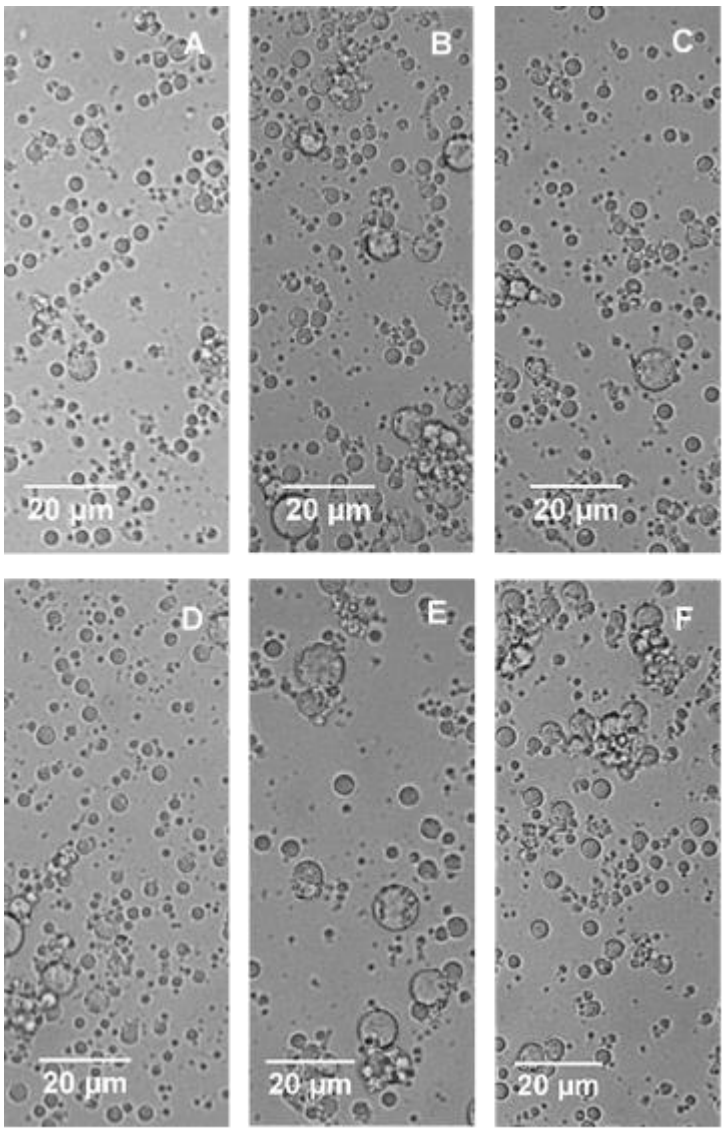

Figure 4.45 – Comparing the size of thiolated $PMAA_{SH(100)}$ and di- and triblock copolymeric $PMAA_{SH(100)}$-shelled microspheres (A-C), containing 1M NaCl-in-4 w/w % Span 80® in tetradecane (40:60), and their non-thiolated analogues (D-F). Sonication at 100 Wcm^{-2} for 60s.

Figure 4.45 compares the size of thiolated and non-thiolated polymer-shelled microspheres containing the optimised W/O emulsion as previously described. The observed trends are comparable to those of oil-filled microspheres (Table 4.8), with thiolated polymers forming smaller microspheres on average than their non-thiolated analogues and average diameter decreasing with increasing PMAA MW in block copolymeric microspheres (Figure 4.46 and Figure 4.47). The spheres were larger on average than oil-filled microspheres prepared under the same conditions, and this was attributed to the less defined interface between the emulsion and the buffer phase due to the miscible aqueous droplets.

Table 4.8 – Comparing the morphologies of thiolated and non-thiolated PMAA based homopolymeric and block copolymer-shelled emulsion filled microspheres. (1M NaCl-in-4 w/w % Span 80®-in-tetradecane (40:60), sonicated at 100 Wcm^{-2} for 60 s).

Shell Material	Microsphere Size / μm
$PMAA_{SH(25)}$	2.49 ± 1.51
$PMAA_{SH(50)}$	2.34 ± 1.19
$PMAA_{SH(75)}$	2.63 ± 1.02
$PMAA_{SH(100)}$	2.46 ± 1.21
$PMAA_{(25)}$	2.81 ± 1.66
$PMAA_{(50)}$	2.61 ± 1.41
$PMAA_{(75)}$	2.96 ± 1.92
$PMAA_{(100)}$	2.70 ± 1.69
$PMAA_{SH(25)}$-$PNIPAA_{M(100)}$	4.07 ± 1.51
$PMAA_{SH(50)}$-$PNIPAA_{M(100)}$	3.82 ± 1.65
$PMAA_{SH(75)}$-$PNIPAA_{M(100)}$	3.68 ± 1.79
$PMAA_{SH(100)}$-$PNIPAA_{M(100)}$	3.75 ± 1.53
$PMAA_{(25)}$-$PNIPAA_{M(100)}$	5.21 ± 2.17
$PMAA_{(50)}$-$PNIPAA_{M(100)}$	4.95 ± 1.93
$PMAA_{(75)}$-$PNIPAA_{M(100)}$	4.28 ± 2.16
$PMAA_{(100)}$-$PNIPAA_{M(100)}$	3.87 ± 2.53
$PMAA_{SH(25)}$-$PNIPAA_{M(100)}$-$PMAA_{SH(25)}$	4.73 ± 1.55
$PMAA_{SH(50)}$-$PNIPAA_{M(100)}$-$PMAA_{SH(50)}$	3.98 ± 1.96
$PMAA_{SH(75)}$-$PNIPAA_{M(100)}$-$PMAA_{SH(75)}$	3.55 ± 1.37
$PMAA_{SH(100)}$-$PNIPAA_{M(100)}$-$PMAA_{SH(100)}$	3.01 ± 1.51
$PMAA_{(25)}$-$PNIPAA_{(100)}$-$PMAA_{(25)}$	4.96 ± 1.84
$PMAA_{(50)}$-$PNIPAA_{(100)}$-$PMAA_{(50)}$	4.62 ± 2.03
$PMAA_{(75)}$-$PNIPAA_{(100)}$-$PMAA_{(75)}$	4.04 ± 1.61
$PMAA_{(100)}$-$PNIPAA_{(100)}$-$PMAA_{(100)}$	3.69 ± 2.04
$PNIPAA_{M}$	5.48 ± 2.91
P(MMA-co-$NIPAA_{M}$)	4.83 ± 2.52
PMAA-(MMA-co-$NIPAA_{M}$)	3.88 ± 2.50
$PMAA_{SH}$-(MMA-co-$NIPAA_{M}$)	3.72 ± 2.47

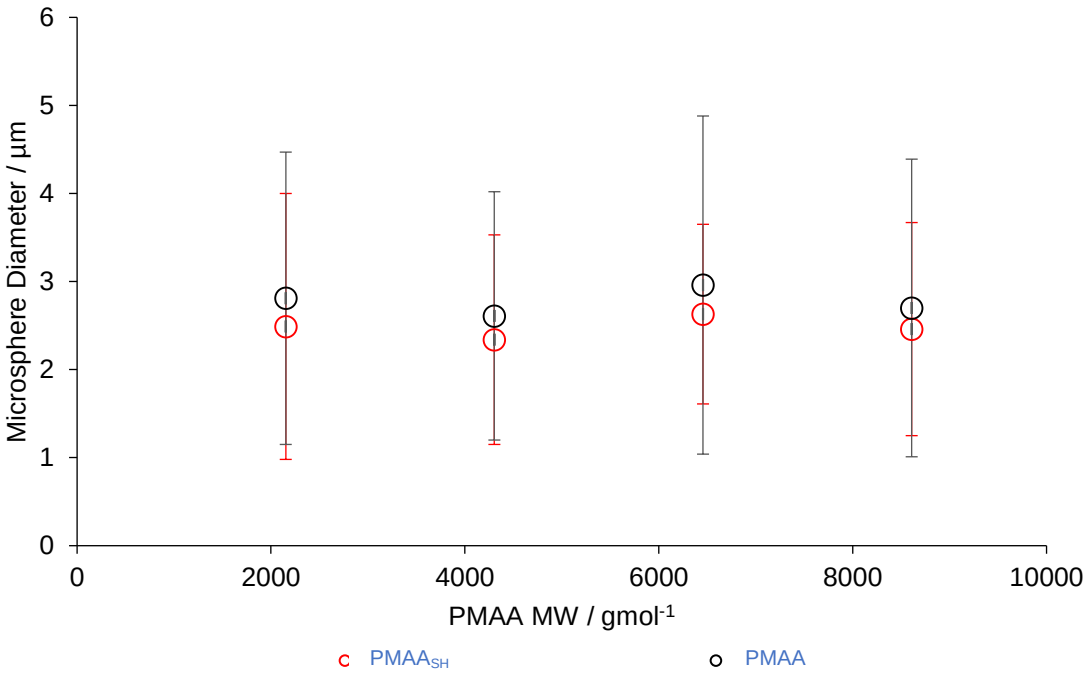

Figure 4.46 – Comparing the average microsphere diameter of homopolymeric $PMAA_{SH}$ and PMAA-shelled microspheres of increasing molecular weight, containing 1M NaCl-in-4 w/w % Span 80®-in-tetradecane (40:60), sonicated at 100 Wcm^{-2} for 60 s. Samples were imaged and analysed in triplicate. Error bars indicate the maximum and minimum average diameter.

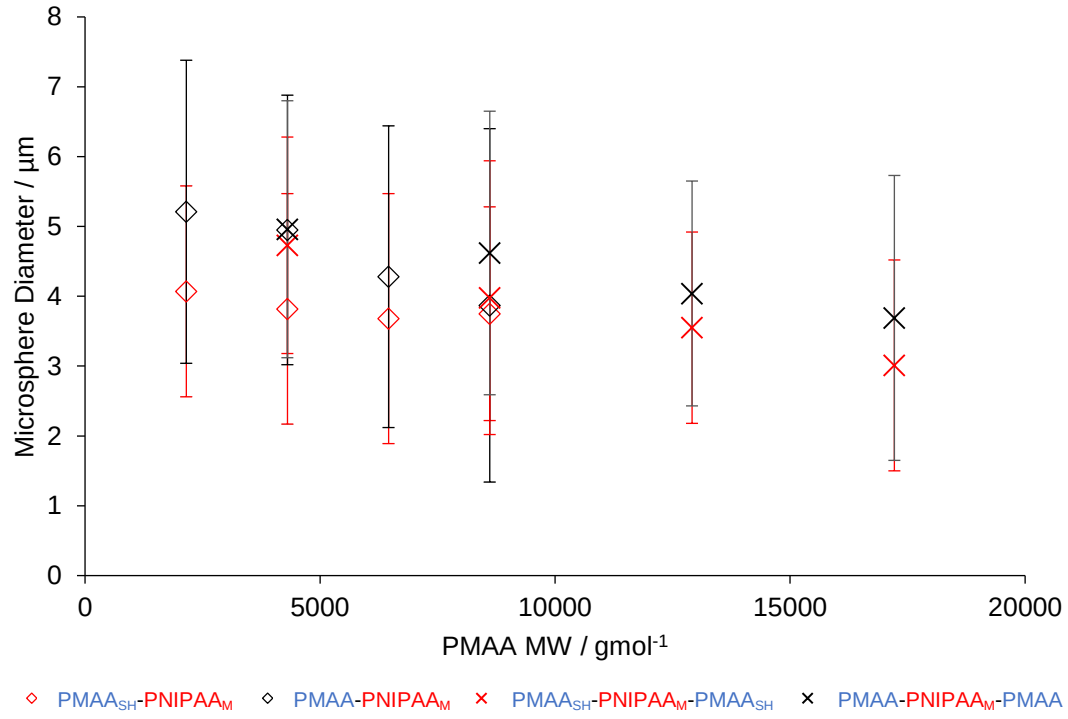

Figure 4.47 - Comparing the average microsphere diameter of thiolated and non-thiolated di-and triblock copolymer-shelled microspheres of increasing PMAA MW, containing 1M NaCl-in-4 w/w % Span 80®-in-tetradecane (40:60), sonicated at 100 Wcm^{-2} for 60 s. Samples were imaged and analysed in triplicate. Error bars indicate the maximum and minimum average diameter.

Inhomogeneities are clearly present within the core of larger microspheres on the micrographs, however due to the limitations of the optical microscopy, these same inhomogeneities characteristic of an emulsion-filled core could not easily be seen in the smaller spheres. To ensure that all microspheres contained a W/O emulsion, and that smaller microspheres were not simply encapsulating a partitioned oil phase, laser scanning confocal microscopy was employed.

Optimised emulsions were prepared as described in Experiment 2.2.6. Prior to sonochemical emulsification, 1M NaCl was saturated with the fluorescent dye 5,6-carboxyfluorescein, an aqueous dye with an excitation and emission wavelength of 492 nm and 517 nm respectively (Figure 4.48). The tetradecane phase was saturated with lipophilic stain Nile Red (ex. 552 nm em. 636 nm) (Figure 4.48).

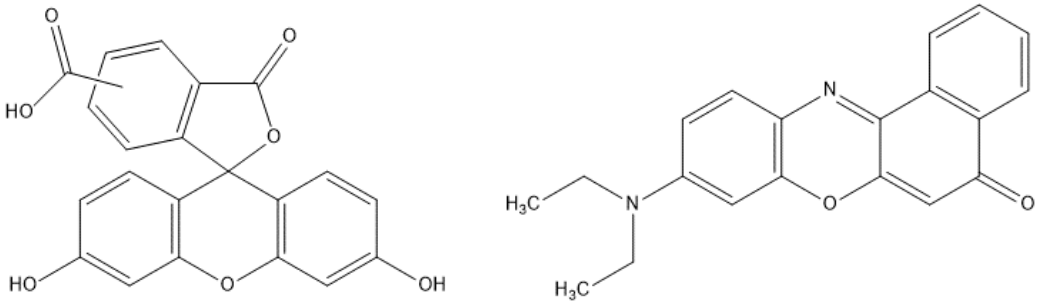

Figure 4.48 - Fluorescent dyes 5,6-carboxyfluorescein (left) and Nile Red (right).

Figure 4.49 reveals the LSCM micrographs of emulsion-filled $PMAA_{SH}$ microspheres, sonicated a 100 Wcm^{-2} for 60 s. The argon laser (488 nm) was used to excited 5,6-carboxyfluorescein (LHS), whilst the HeNe laser (543 nm) excited the Nile Red fluorophore within the continuous oil phase.

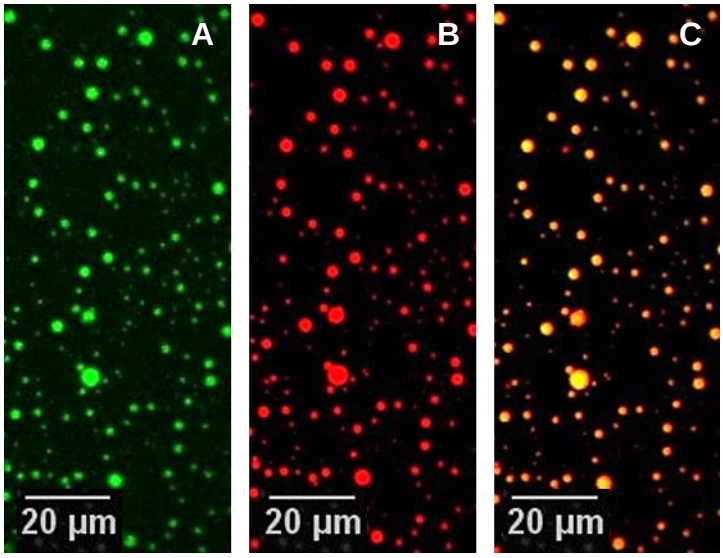

Figure 4.49 – LSCM micrographs of emulsion-filled $PMAA_{SH(100)}$ microspheres containing 5,6-carboxyfluorescein-saturated 1M NaCl-in-4 w/w % Span 80®-in-tetradecane saturated with Nile Red (40:60). A = 5,6-carboxyfluorescein emission in aqueous phase excited by argon laser (488 nm), B = Nile Red emission in oil phase excited by HeNe laser (543 nm), C = Excitation of both fluorophores within emulsion. Sonicated at 100 Wcm^{-2} for 60 s then washed and diluted ten-fold.

It is interesting to note that there is no visible 5,6-carboxyfluorescein staining of the outer surface of the microspheres or in the bulk phase buffer. This was the case for all emulsion-filled microspheres and indicates that minimal emulsion degradation occurred upon the second sonication to form the microspheres (Figure 4.50). Analysis of the confocal micrographs reveal few inhomogeneities or large droplets within the core of the microspheres, suggesting that the emulsion has not coarsened upon secondary sonication and has maintained its morphology as a fine nanoemulsion. This is also true for non-functionalised PMAA emulsion-filled microspheres (Figure 4.50).

The LCSM micrographs reveal that almost all microspheres contain the W/O nanoemulsion for each microsphere system prepared. This is a promising result as it not only confirms the capability of the polymers synthesised to successfully encapsulate both hydrophobic and hydrophilic species, but also supports previous reports in the literature that the conditions used to synthesise the emulsions generate nanoemulsions that retain their morphology upon secondary sonication and encapsulation.

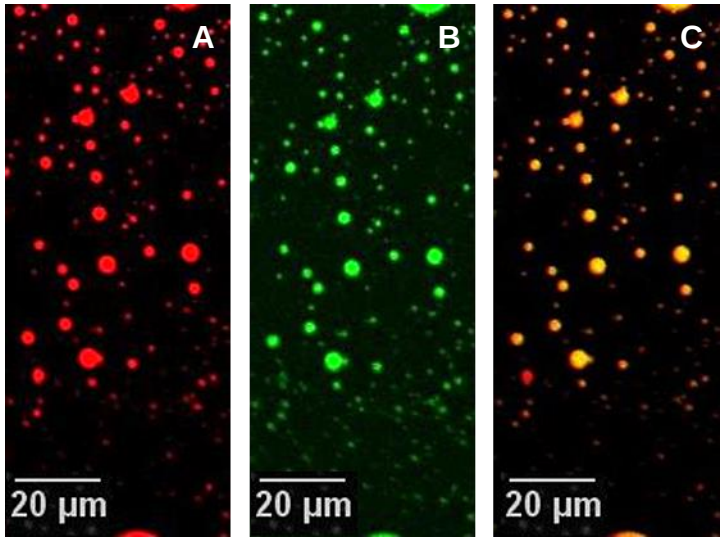

Figure 4.50 - LSCM micrographs of emulsion-filled $PMAA_{(100)}$ microspheres containing 5,6-carboxyfluorescein-saturated 1M NaCl-in-4 w/w % Span 80®-in-tetradecane saturated with Nile Red (40:60). A = Nile Red emission excited by HeNe laser (543 nm), B = 5,6-carboxyfluorescein emission excited by argon laser (488 nm), C = Excitation of both fluorophores within emulsion. Sonicated at 100 Wcm^{-2} for 60 s, then washed and diluted ten-fold.

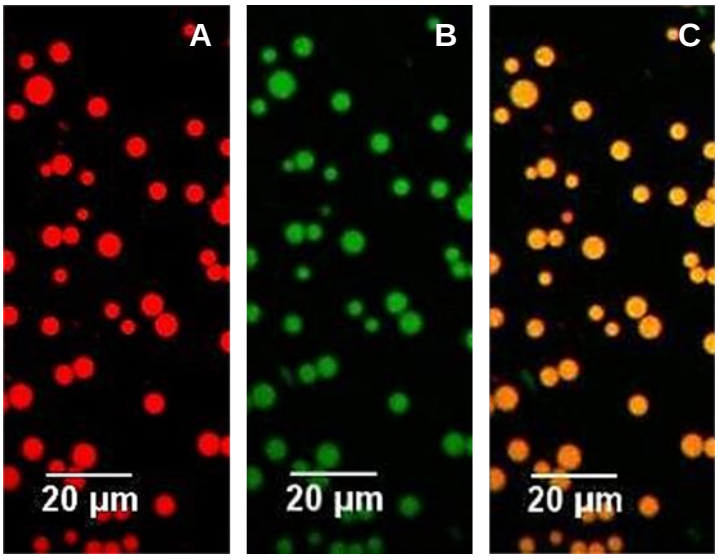

Figure 4.51 - LSCM micrographs of emulsion-filled $PMAA_{SH(100)}$-$PNIPAA_{M(100)}$ microspheres containing 5,6-carboxyfluorescein-saturated 1M NaCl-in-4 w/w % Span 80®-in-tetradecane saturated with Nile Red (40:60). A = Nile Red emission excited by HeNe laser (543 nm), B = 5,6-carboxyfluorescein emission excited by argon laser (488 nm), C = Excitation of both fluorophores within emulsion. Sonicated at 100 Wcm^{-2} for 60 s then washed and diluted ten-fold.

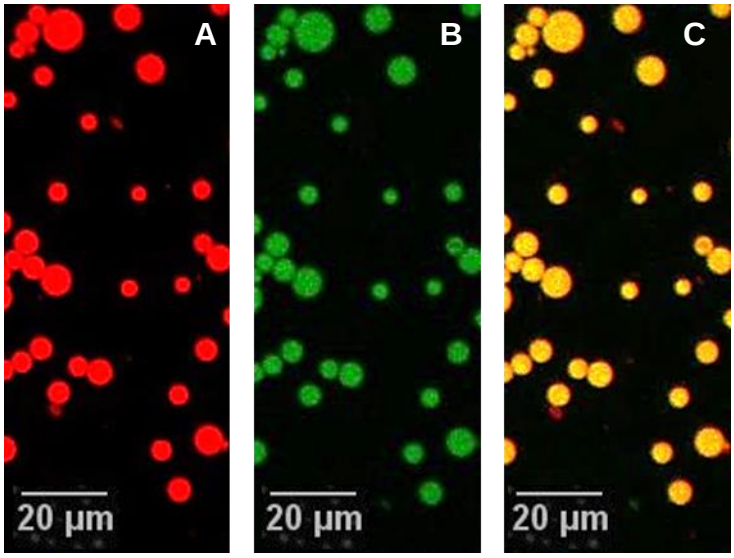

Figure 4.52 - LSCM micrographs of emulsion-filled $PMAA_{(100)}$-$PNIPAA_{M(100)}$ microspheres containing 5,6-carboxyfluorescein-saturated 1M NaCl-in-4 w/w % Span 80®-in-tetradecane saturated with Nile Red (40:60). A = Nile Red emission excited by HeNe laser (543 nm), B = 5,6-carboxyfluorescein emission excited by argon laser (488 nm), C = Excitation of both fluorophores within emulsion. Sonicated at 100 Wcm^{-2} for 60 s then washed and diluted ten-fold.

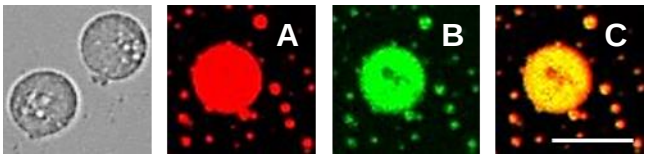

Figure 4.53 – An example of aqueous droplet coalescence within $PNIPAA_{M(100)}$ emulsion-filled microspheres containing 5,6-carboxyfluorescein-saturated 1M NaCl-in-4 w/w % Span 80®-in-tetradecane saturated with Nile Red (40:60). A = Nile Red emission excited by HeNe laser (543 nm), B = 5,6-carboxyfluorescein emission excited by argon laser (488 nm), C = Excitation of both fluorophores within emulsion. Sonicated at 100 Wcm^{-2} for 60 s. The argon laser (B) highlights regions of emulsion partitioning and the overlaid image (C) reveals localised oil regions within the core. Scale bar 5 µm.

The confocal microscope has an optical slice of 1 µm depth, therefore all colocalised regions in the overlaid image with yellow fluorescence correspond to dispersed aqueous droplets of less than 1 µm in diameter, in agreement with the optimisation data. Figure 4.53 demonstrates an example where partitioning of the oil and aqueous phases has occurred

within the microsphere. The distribution of Nile Red fluorescence (red) appears relatively homogeneous, however, the image highlighting the 5,6-carboxyfluorescein fluorophore (green) reveals a dark region within the microsphere that may easily be mistaken for a trapped air bubble. It is only upon analysis of the overlaid image (right), that a partitioned oil region within the microsphere is evident.

The majority of inhomogeneities in emulsion-filled microspheres arose from the presence of trapped air pockets within the microsphere core, particularly in larger microspheres. Sonication of polymer solutions at the air:aq interface determined that air-filled microbubbles could not be synthesised in the same way as lysozyme microbubbles (Figure 4.11), therefore it was interesting to observe the encapsulation of air bubbles within emulsion-filled spheres. The entrapment of air within the emulsion was attributed to the affinity between tetradecane and air. The foaming ability of a particular liquid is inversely proportional to surface tension[225]. Water, for example, with a surface tension of 72.8 mN/m at 20 °C, is unable to form a foam without the use of a surfactant due to its poor affinity for air. Tetradecane, however, has a low surface tension of 26.56 mN/m at 20 °C[226]. Krasowska *et al*.[227] have reported the immersion of air bubbles attached to a hydrophobic surface upon immersion into an aqueous liquid. Teflon surfaces of increasing roughness were immersed in water and the retention of air bubbles on the surface were monitored by high speed imaging. It is therefore entirely possible that during interfacial disruption upon sonication, the affinity of tetradecane for air facilitates the introduction of air into the microspheres, the air pockets are stabilised by the tetradecane and the foam remains trapped.

Figure 4.54 and Figure 4.55 demonstrate the presence air inhomogeneities trapped within emulsion-filled microspheres. As mentioned, air pockets were only present in larger microspheres, it was therefore established that the entrapment of air bubbles was responsible for the observed increased in size. It is important to note that air entrapment did not occur when encapsulating a simple hydrophobic liquid, therefore the presence of surfactant is likely the origin of long-term air bubble stability within the emulsion-filled spheres.

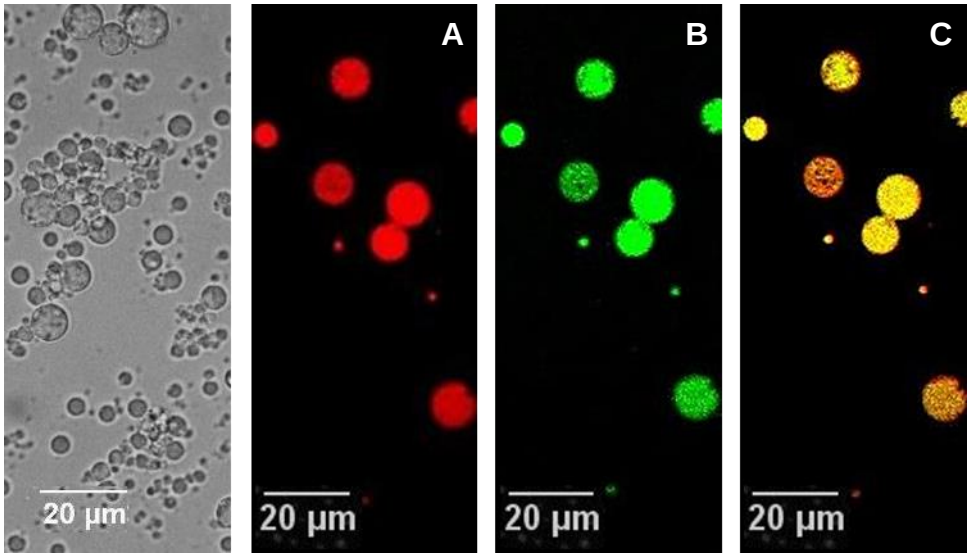

Figure 4.54 – Optical micrograph and LSCM micrographs (washed and diluted ten-fold) of emulsion-filled PNIPAA$_M$ microspheres containing 5,6-carboxyfluorescein-saturated 1M NaCl-in-4 w/w % Span 80®-in-tetradecane saturated with Nile Red (40:60). A = Nile Red emission excited by HeNe laser (543 nm), B = 5,6-carboxyfluorescein emission excited by argon laser (488 nm), C = Excitation of both fluorophores within emulsion. Sonicated at 100 Wcm^{-2} for 60 s.

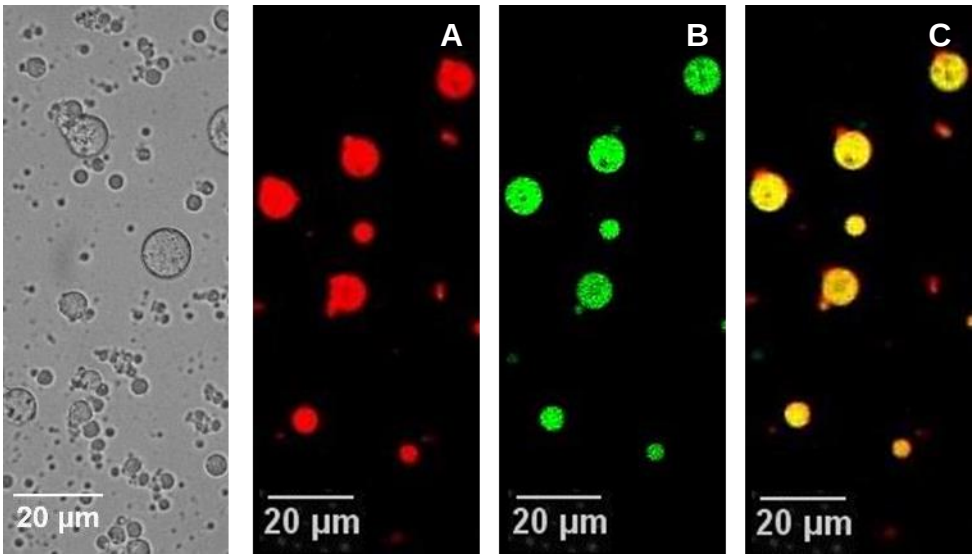

Figure 4.55 - Optical micrograph and LSCM micrographs (washed and diluted ten-fold) of emulsion-filled P(MMA-co-NIPAA$_M$) microspheres containing 5,6-carboxyfluorescein-saturated 1M NaCl-in-4 w/w % Span 80®-in-tetradecane saturated with Nile Red (40:60). A = Nile Red emission excited by HeNe laser (543 nm), B = 5,6-carboxyfluorescein emission excited by argon laser (488 nm), C = Excitation of both fluorophores within emulsion. Sonicated at 100 Wcm^{-2} for 60 s.

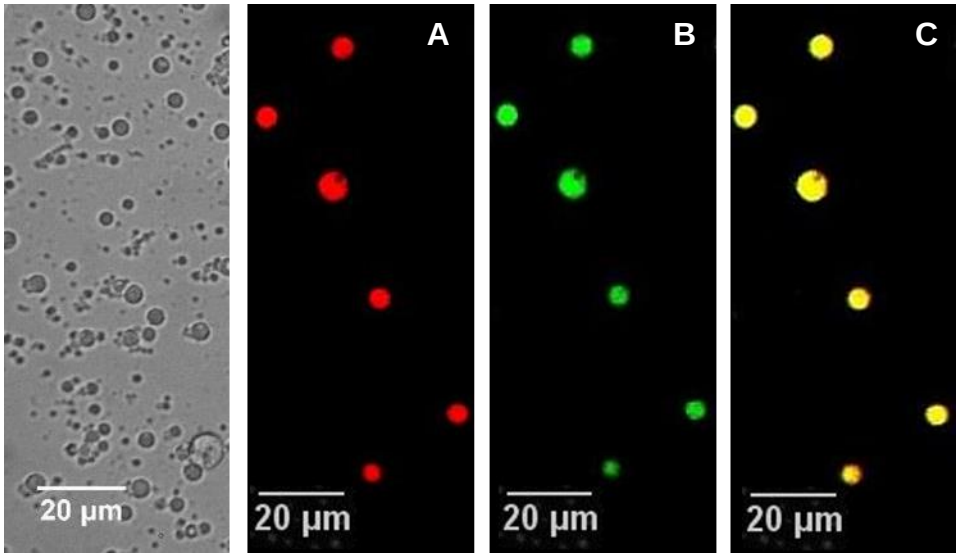

Figure 4.56 - Optical micrograph and LSCM micrographs (washed and diluted ten-fold) of emulsion-filled $PMAA_{SH}$-P(MMA-co-$NIPAA_M$) microspheres containing 5,6-carboxyfluorescein-saturated 1M NaCl-in-4 w/w % Span 80®-in-tetradecane saturated with Nile Red (40:60). A = Nile Red emission excited by HeNe laser (543 nm), B = 5,6-carboxyfluorescein emission excited by argon laser (488 nm), C = Excitation of both fluorophores within emulsion. 100 Wcm^{-2} for 60 s.

4.2.3 Optimisation of Water-in-Natural Oil Emulsions

The optimisation and encapsulation of water-in-tetradecane emulsions provide an excellent model for other emulsified systems in order to encapsulate and deliver hydrophilic species. Naturally-occurring oils are a biocompatible alternative to tetradecane, and the successful encapsulation of a range of synthetic and natural oils within polymeric microspheres, generated during the course of this project, demonstrates the potential for these phases to be encapsulated containing an aqueous dispersion.

Inverse water-in-fluorocarbon emulsions have not been widely reported in the literature[228,229]. The large majority of fluorosurfactants are water-soluble, yielding O/W emulsions. Commercially available non-ionic oil-soluble fluorosurfactants, Zonyl® FSO and Zonyl® FSN (Sigma Aldrich – since discontinued), were employed to model the emulsions generated by Krafft *et al.*[228]. A range of optimisations were conducted, including

varying the aq:oil ratio, the percentage of surfactant and the mechanistic conditions, however, no iterations yielded a stable emulsion.

Attention was instead directed towards the synthesis and optimisation of inverse water-in-natural oil emulsions. Polychniatou *et al.*[230] have compared non-ionic surfactants for the successful formation of water-in-olive oil emulsions containing a maximum loading of 2 v/v% water and a surfactant concentration of between 2-10 w/w %. A decrease in droplet size with increasing emulsifier ratio was observed between 0-8 w/w %, and the inverse emulsions exhibited long term stability. Span 20® (HLB = 8.6) (Figure 4.57) was determined as the most appropriate surfactant to generate water-in-olive oil emulsions.

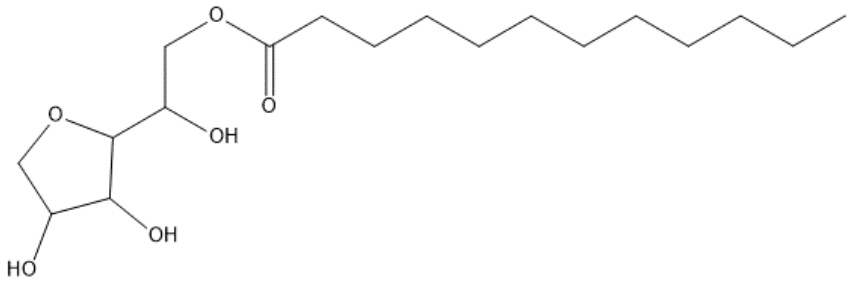

Figure 4.57 – Span 20® non-ionic surfactant.

As an initial investigation, emulsions of an increasing aq:oil ratio from 10-40 v/v% 1M NaCl were prepared at increasing concentration of Span 20®. Beyond 20 v/v%, phase separation was relatively instantaneous for all samples, therefore analysis by dynamic light scattering was not possible. To optimise aq loading whilst achieving stability, 10 v/v% 1M NaCl was chosen (Figure 4.58).

The values are in agreement with light scattering data reported by Polychniatou *et al.*[230], but, interestingly, the dispersion droplets generated were considerably smaller on average than those of 1M NaCl-in-Span 80®-in-tetradecane emulsions. As previously mentioned, Capdevila *et al.*[220] reported no relationship between oil viscosity and droplet size on the formation of inverse W/O emulsions with Span 80®, however naturally-occurring oils such as olive oil are comprised of a range of additional surface active compounds such as phospholipids and fatty acids which may influence the emulsion morphology. Beyond a concentration of 5 w/w % Span 20®, the emulsions were far too viscous.

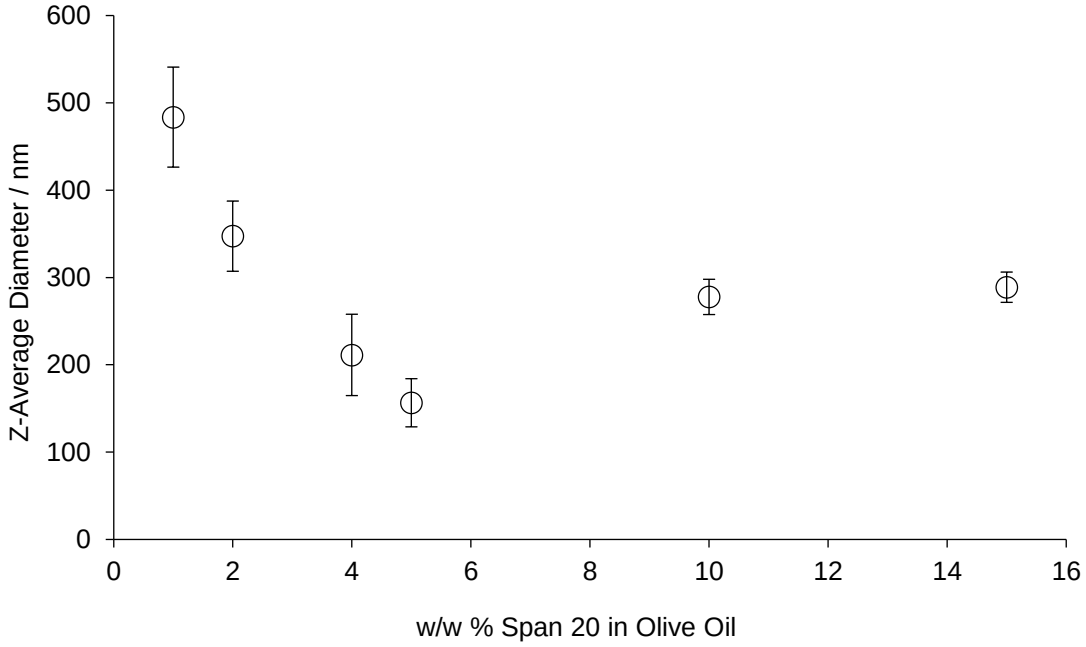

Figure 4.58 – The effect of increasing Span 20® concentration on the Z-average diameter of 1M NaCl-in-Span 20®-in-olive oil emulsions (10:90). Sonicated at 100 Wcm^{-2} for 300 s.

To demonstrate the encapsulation of water-in-olive oil emulsions within polymeric microspheres, $PMAA_{SH(100)}$ and diblock $PMAA_{SH(100)}$-$PNIPAA_{M(100)}$ microspheres were generated containing 5,6-carboxyfluorescein-saturated 1M NaCl-in-5 % Span 20®-in-olive oil emulsions (Figure 4.59). The microspheres are larger than those containing tetradecane-based emulsions, this may be due both to the presence of impurities within naturally-occurring oils, as was the case for natural oil-filled microspheres, and the presence of trapped air bubbles within the microspheres. Regions of dense fluorescence indicate partitioning of the aqueous and oil phases within the microspheres, particularly in image D. This same degree of partitioning throughout the microspheres was not observed in the synthetic oil emulsion-filled microspheres, confirming that the water-in-olive oil emulsions do not possess the same stability upon secondary sonication to form the spheres. The lack of fluorescence in the bulk phase would suggest, however, that this partitioning occurs after encapsulation.

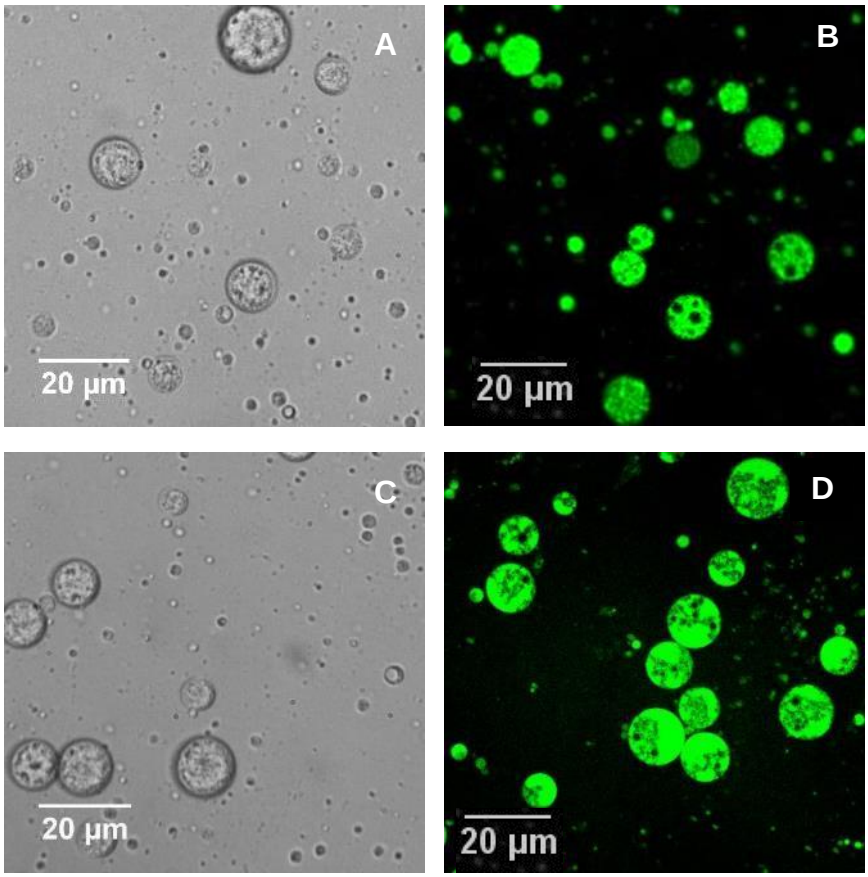

Figure 4.59 - Optical micrographs and LSCM micrographs (washed and diluted ten-fold) of emulsion-filled $PMAA_{SH}$ (A and B) and $PMAA_{SH}$-$PNIPAA_M$ (C and D) microspheres containing 5,6-carboxyfluorescein-saturated 1M NaCl-in-5 w/w % Span 20®-in-olive oil (10:90). Sonicated at 100 Wcm^{-2} for 60 s.

4.3 Chapter Summary

In this chapter, the synthesis of microspheres employing $PMAA_{SH}$-based polymers, characterised in Chapter 3, and the encapsulation of a range of hydrophobic species as well as hydrophilic species in W/O emulsions has been demonstrated. The effect of modifying parameters, including sonication power and time, encapsulant species and shell species, on the size distribution and stability of microspheres has also been analysed. Whilst no trends in size and size distribution could be observed between microsphere samples employing $PMAA_{SH}$ homopolymers of increasing chain length, increasing the ratio of $PNIPAA_M$ to $PMAA_{SH}$ in the block copolymer chains led to an increase in microsphere size and size

distribution. It was therefore initially postulated that sonochemically-induced covalent disulphide crosslinks and intermolecular non-covalent bonding in $PMAA_{SH}$ was solely responsible for the stability of microsphere shells.

The successful synthesis of novel microspheres containing non-thiolated PMAA was also achieved, generating microspheres with comparable morphologies and stability to their thiolated $PMAA_{SH}$-containing analogues. The same observed increases in size and size distribution with decreasing PMAA percentage in block copolymer chains were attributed to the reduced availability of PMAA intermolecular non-covalent bonding sites in the shell. Changes in the infra-red spectra of sonicated PMAA-containing polymers relative to a non-sonicated sample indicated intermolecular bonding beyond the predicted non-covalent hydrogen bonding, and a novel sonochemically-induced anhydride covalent crosslink was proposed as the bonding mechanism.

In addition, microspheres of $PNIPAA_M$ and LCST-modified P(MMA-co-$NIPAA_M$) have been successfully synthesised, disproving the theory that only $PMAA_{SH}$ and PMAA are capable of induced stability in the shell species. Microspheres were also shown to possess long term stability, and whilst non-covalent interactions are proposed as the main mechanism for shell stabilisation, a greater understanding of the interactions stabilising these shells is required.

All polymers synthesised were capable of encapsulating a range of synthetic and naturally-occurring oils, demonstrating their versatility as synthetic shell species. The encapsulation of W/O emulsions was also achieved, and the incorporation of both the hydrophobic and hydrophilic dispersed phase was confirmed by fluorescent labelling and analysis by LSCM.

Following the synthesis and characterisation of the microspheres, successfully employing synthesised polymers incorporating a thermoresponsive component into the shell material, their tolerance to a range of environmental conditions including temperature was analysed, and the results are discussed in Chapter 5.

5 Encapsulation and Release

Having demonstrated that microspheres encapsulating hydrophobic and hydrophilic species could be successfully formed from synthetic polymers in both the presence and absence of thiol functionalities, the next step was to determine their behaviour in response to various disruptive conditions. Of particular interest was the use of elevated temperature to stimulate the thermoresponsive behaviour of $PNIPAA_M$ portions within the microsphere shells.

5.1 Encapsulation Efficiency

In order to compare the encapsulation efficiency of tetradecane-filled thiol crosslinked polymers and those stabilised by the newly proposed sonochemical formation of anhydride crosslinks, samples were prepared as outlined in Experiment 2.2.5. Microspheres encapsulating Sudan III-saturated tetradecane were synthesised by sonication at 100 Wcm^{-2} for 60s. To quantify the amount of tetradecane trapped within the microspheres, 2 mL isopropyl myristate (IPM) was deposited as a layer onto the unwashed, undiluted microsphere dispersion. Any unencapsulated tetradecane partitions into the hydrophobic solvent and the concentration of Sudan III in IPM was then measured by UV absorbance against a control of 100 % unencapsulation to determine the degree of entrapment. The control absorbance of 100 µL Sudan III-soaked tetradecane with pH 8 tris acetate buffer in the absence of solubilised polymer was measured as 8.81×10^{-2} at 480 nm, corresponding to a concentration of 2.97 µM. This is in agreement with the concentration of 100 µL unsonicated Sudan III-saturated tetradecane partitioned into 2 mL IPM, confirming that sonication and emulsification with buffer does not impact the measured absorbance.

Sudan III was chosen as an appropriate dye over Nile Red for the purpose of release measurements by absorbance due to its bright red colour with strong absorbance in the visible spectrum (Figure 5.1). Release of Sudan III-saturated tetradecane into isopropyl myristate upon mechanical or chemical release from lysozyme and $PMAA_{SH}$ microspheres has previously been demonstrated by Skinner[6], therefore the mechanism was applied to measure the encapsulation efficiency and thermoresponsive release of tetradecane from the microspheres synthesised in Chapter 4.

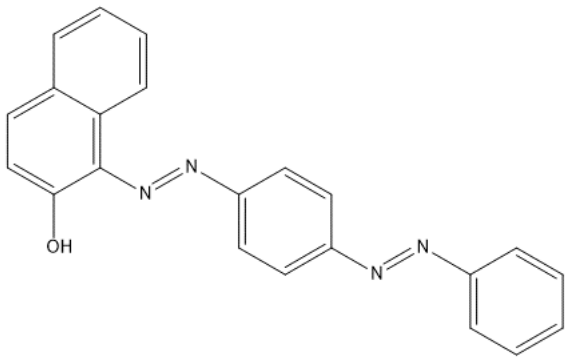

Figure 5.1 – Sudan III lyophilic dye.

Table 5.1 lists the encapsulation efficiencies (EE) of all thiolated and non-thiolated microsphere systems immediately after sonication and after storage at room temperature for 24 hours. The measure of encapsulation efficiency was not conducted to determine loss from microspheres with time, as measured by optical microscopy in Section 4.1.6, but to provide comparison for release experiments conducted to determine the extent of initiated release by various mechanisms as a percentage of the overall measured release.

The encapsulation efficiency for thiolated microsphere samples was very high, with all samples exhibiting more than 95 % EE after 24 hours. No direct correlation could be made between PMAA chain length and encapsulation efficiency in both the homopolymeric and block copolymer microsphere samples, however the encapsulation efficiencies of thiolated microspheres exceeded those of their non-thiolated analogues on average, with less release into IPM observed over 24 hours. This was attributed to the enhanced stabilisation effects of disulphide crosslinking, rapidly stabilising the oil:water interface upon sonication by radically-induced covalent crosslinking.

Microspheres synthesised from polymers lacking PMAA portions still exhibited encapsulation efficiencies of more than 80 %, indicative of alternative interactions stabilising the polymer at the oil:aq interface.

Table 5.1 – Encapsulation efficiency of Sudan III-saturated tetradecane-filled microspheres, sonicated at 100 Wcm^{-2} for 60 s, at 0 hr and after 24 hr. Error not indicated due to single measurements and very small measured loss in encapsulant over 24 hours.

Shell Material	EE 0 hr / %	EE 24 hr / %	Loss in EE / %	Shell Material	EE 0 hr / %	EE 24 hr / %	Loss in EE / %
$PMAA_{SH(25)}$	98.75	96.88	1.86	$PMAA_{(25)}$	98.64	96.89	1.75
$PMAA_{SH(50)}$	99.61	98.93	0.67	$PMAA_{(50)}$	96.08	89.35	6.73
$PMAA_{SH(75)}$	99.42	98.04	1.38	$PMAA_{(75)}$	94.47	91.34	3.13
$PMAA_{SH(100)}$	99.46	99.43	0.03	$PMAA_{(100)}$	97.56	95.70	1.86
$PMAA_{SH(25)}$-$PNIPAA_{M(100)}$	99.01	96.91	2.10	$PMAA_{(25)}$-$PNIPAA_{M(100)}$	96.23	91.41	4.82
$PMAA_{SH(50)}$-$PNIPAA_{M(100)}$	98.92	97.79	1.13	$PMAA_{(50)}$-$PNIPAA_{M(100)}$	97.12	89.55	7.57
$PMAA_{SH(75)}$-$PNIPAA_{M(100)}$	99.06	98.85	0.21	$PMAA_{(75)}$-$PNIPAA_{M(100)}$	98.47	95.65	2.82
$PMAA_{SH(100)}$-$PNIPAA_{M(100)}$	99.41	98.96	0.45	$PMAA_{(100)}$-$PNIPAA_{M(100)}$	94.42	91.86	2.56
$PMAA_{SH(25)}$-$PNIPAA_{M(100)}$-$PMAA_{SH(25)}$	98.88	97.61	1.27	$PMAA_{(25)}$-$PNIPAA_{M(100)}$-$PMAA_{(25)}$	94.22	89.06	5.16
$PMAA_{SH(50)}$-$PNIPAA_{M(100)}$-$PMAA_{SH(50)}$	98.71	98.17	0.54	$PMAA_{(50)}$-$PNIPAA_{M(100)}$-$PMAA_{(50)}$	97.99	93.68	4.31
$PMAA_{SH(75)}$-$PNIPAA_{M(100)}$-$PMAA_{SH(75)}$	98.49	96.25	2.24	$PMAA_{(75)}$-$PNIPAA_{M(100)}$-$PMAA_{(75)}$	98.45	95.24	3.21
$PMAA_{SH(100)}$-$PNIPAA_{M(100)}$-$PMAA_{SH(100)}$	99.62	99.12	0.50	$PMAA_{(100)}$-$PNIPAA_{M(100)}$-$PMAA_{(100)}$	97.72	95.18	2.57
				$PNIPAA_{M}$	94.59	89.36	5.23
				P(MMA-co-$NIPAA_{M}$)	89.68	81.74	7.94
$PMAA_{SH}$-(MMA-co-$NIPAA_{M}$)	98.59	95.69	2.90	PMAA-(MMA-co-$NIPAA_{M}$)	93.29	88.74	4.55

Qualitative analysis of microsphere formation and encapsulation has been determined by optical microscopy, the results of which are detailed in Chapter 3, but it can also be employed alongside LSCM to observe the effects of various release mechanisms on microsphere morphology.

5.2 Non-Specific Release Mechanisms

The use of non-specific release mechanisms, such as mechanical disruption by sonication[10,14] or a reducing agent to break the disulphide linkages of thiol-functionalised microsphere shells[7,8], have been previously described in the literature. Before testing the thermoresponsive behaviour of polymeric microspheres containing $PNIPAA_M$ portions in the shell, it was important to determine whether all microspheres could release their contents in response to mechanical disruptions, a reductive environment, or at extreme pH. Poly(methacrylic acid)-based microspheres have already demonstrated pH responsive aggregation below the pKa of the polymer (pKa = 5.5) (Section 4.1.7), confirming the presence of some remaining exposed carboxylate functionalities on the surface of the spheres. It was therefore interesting to observe whether extreme pH would induce effects beyond aggregation, such as instability and release. Any release after incubation at pH 13 was also measured.

Denaturation of proteins in strong acidic and basic environments by disulphide cleavage and disruption of non-covalent interactions has been previously reported[231,232]. Extremely acidic and strongly alkaline pH environments may therefore induce the same destructive effects in the shells of thiolated and non-thiolated synthetic polymeric microspheres. Figure 5.2 shows the effects of acidification to pH 1 on the behaviour of $PMAA_{SH}$, PMAA and $PNIPAA_M$ microspheres. In images A, C and E, microspheres are distributed throughout the buffer bulk phase after sonication. Upon acidification, extensive aggregation was observed in the samples containing $PMAA_{SH}$ and PMAA shell species, and the microspheres formed a viscous gel-like "plug" on top of the buffer phase (B and D). Figure 5.3 shows an optical micrograph of the aggregated microspheres on acidification. Some microsphere growth was observed, likely as a result of the destructive effects of concentrated acid on the microsphere shell and subsequent coalescence, however, due to the extent of aggregation, microspheres and coalesced droplets appear to remain

immobilised in the gel-like aggregate. As a result, very little release into IPM was observed (Table 5.2), less than 1 % and 9 % for $PMAA_{SH}$ and PMAA respectively in excess of unencapsulated oil released into IPM as a result of inherent encapsulation efficiency after 24 hours (Table 5.1). Similar behaviour was also observed for block copolymeric microspheres, suggesting that the presence of the protonated carboxylic acid functionalities leads to aggregation and exclusion of the acidified aqueous phase, as opposed to release.

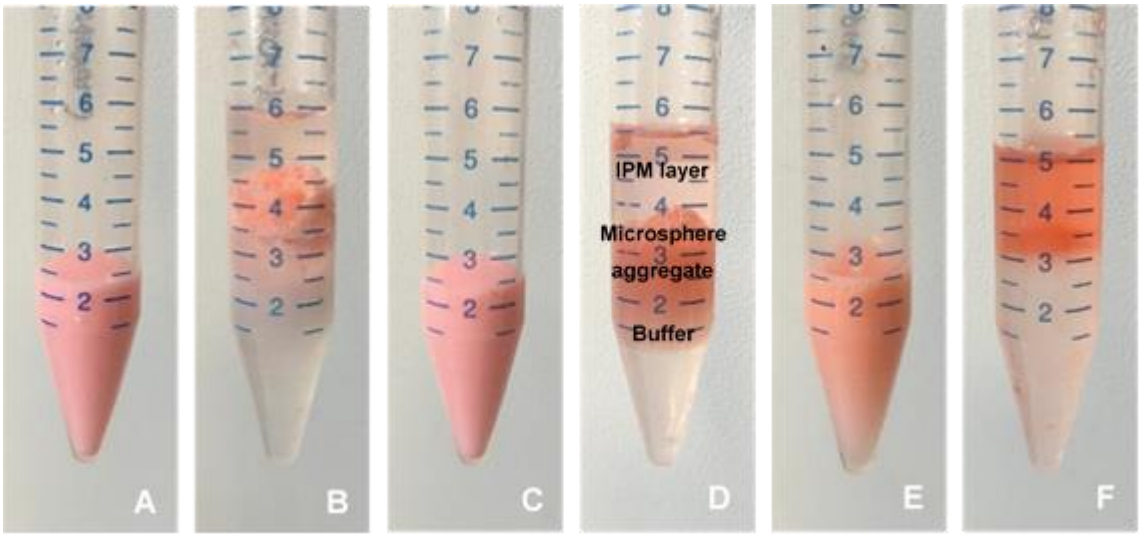

Figure 5.2 – Sudan III-saturated tetradecane-filled $PMAA_{SH(100)}$, $PMAA_{(100)}$ and $PNIPAA_{M(100)}$ microspheres (A, C and E) and $PMAA_{SH(100)}$, $PMAA_{(100)}$ and $PNIPAA_{M(100)}$ microspheres acidified to pH 1 for one hour, then layered with IPM (B, D and F).

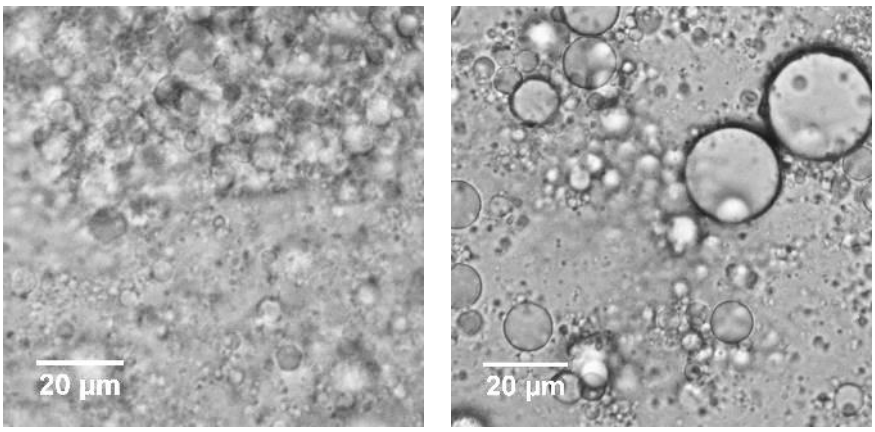

Figure 5.3 – Optical micrographs of $PMAA_{SH(100)}$ microspheres incubated for one hour at pH 1 (left) and pH 13 (right).

Microspheres in the absence of PMAA or $PMAA_{SH}$ exhibited very different behaviour, as shown by $PNIPAA_M$ microspheres in Figure 5.2 E and F. Upon acidification, $PNIPAA_M$ and P(MMA-co-$NIPAA_M$) microspheres underwent almost immediate collapse, releasing approximately 75 % and 85 % of their encapsulant into the IPM phase respectively (Table 5.2). As mentioned in Section 3.7, amides undergo hydrolysis to the parent carboxylic acid in the presence of dilute acids[209]. It is therefore possible that, in acidic environments of high concentration and low pH, this reaction is extensive enough to disrupt the non-covalent interactions stabilising the microspheres, leading to collapse and release.

Incubation with concentrated sodium hydroxide (NaOH) at pH 13 led to some observed release of tetradecane, denoted by the pink hue in the IPM layer after its addition, and aggregation of microspheres into a distinct layer (Figure 5.4 A). This contradicts the behaviour of microspheres in basic environments observed in Section 4.1.7, whereby ionisation of exposed carboxylic acid functionalities beyond the pKa of PMAA (pKa = 5.5) leads to a discrete distribution of microspheres. Upon gentle agitation to facilitate release into IPM, a stable emulsion was formed with the IPM layer, preventing quantification by UV/Vis spectroscopy. The same partial release behaviour into IPM was observed for all samples, suggesting that all polymeric microsphere shells possess less stability at highly alkaline pH. Figure 5.3 shows an optical micrograph of a sample taken from stable emulsion formed with IPM. Microsphere aggregates can be observed in large buffer droplets of millimetres in diameter within IPM in a crude O/W/O emulsion.

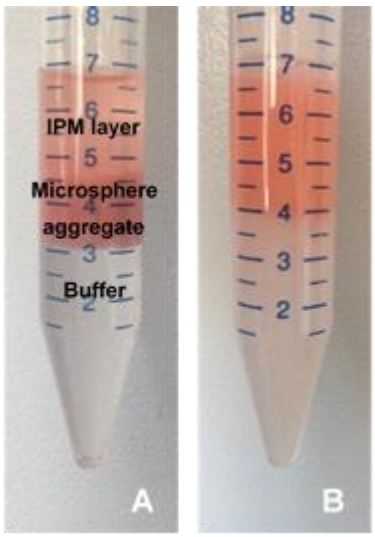

Figure 5.4 - Sudan III-saturated tetradecane-filled $PMAA_{SH}$ microspheres incubated at pH 13 for one hour (A), and after shaking to facilitate partitioning of the oil into the IPM layer (B).

The next disruption mechanism to be investigated was the reductive cleavage of disulphide bonds by DL-dithiothreitol (DTT), which proceeds via sequential disulphide exchange, as shown in Figure 5.5[233]. The reaction works successfully beyond pH 7, due to the required deprotonation of the DTT thiol functionalities (pKa = 9.2). Due to the specificity of the reducing agent for disulphide crosslinks, it was postulated that only polymeric microspheres containing cross-linked disulphide bridges would be affected. Polymers with thiol-functionalities possessed between 6-30 % functionalisation, depending on the percentage of 30 % thiolated PMAA portions within the block copolymers. The reductive effects of an excess of DTT will cleave the disulphide crosslinks and may be sufficient to create voids in the shell from which the encapsulant can escape. Since demonstrating the successful synthesis of microspheres in the absence of thiol functionalities, however, it is possible that the selective cleavage of disulphide crosslinks may be insufficient to disrupt the microsphere structure to the extent that it facilitates release. Additional interactions will exist between the non-functionalised repeat units in addition to disulphide bridges within the shell of thiol-functionalised microspheres, inducing shell stabilisation.

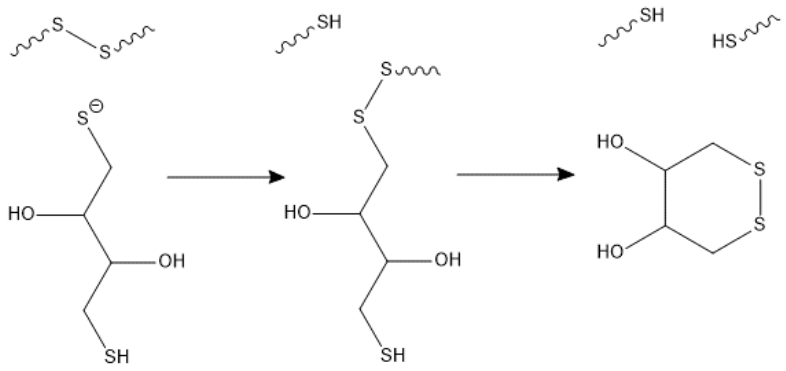

Figure 5.5 – The reduction of disulphide bonds by DL-dithiothreitol.

Figure 5.6 and Figure 5.7 reveal the consequences of incubating tetradecane-filled $PMAA_{SH}$ and PMAA microspheres with 60 mg/mL DTT for 1 hour. Contrary to predictions, both the thiolated and non-thiolated microspheres undergo a degree of reductive degradation, leading to encapsulant release. Reports in the literature regarding the DTT-induced cleavage of lysozyme disulphide links prior to microsphere formation indicate that DTT addition should occur no more than a few minutes prior to sonication to prevent potential further degradation of the protein structure[3,7,14], although the precise mechanism of further

degradation is not specified. It is therefore possible that, akin to the effects of extreme pH on non-covalent interactions within the shell, the reductive environment also facilitates degradation of the microspheres by disruption of the non-covalent interactions. The precise mechanism of this is unknown, but release from both thiol-containing and non-thiol containing microspheres was observed for all microsphere systems.

Whilst it is possible that a degree of reductive degradation in microsphere samples may have occurred over a shorter timescale than the 1 hour incubation period given, agitation of the DTT-treated microsphere suspensions to optimise partitioning of the released phase into the IPM led to temporary contamination of the IPM phase with the microsphere suspension. It was therefore imperative that complete re-equilibration of the two phases had occurred prior to removing an aliquot from the IPM layer for analysis. Although not the most efficient mechanism to facilitate real-time measurements, partitioning of the released encapsulant species into IPM provides a quantitative value for the extent of release from microspheres, initiated by an external mechanism.

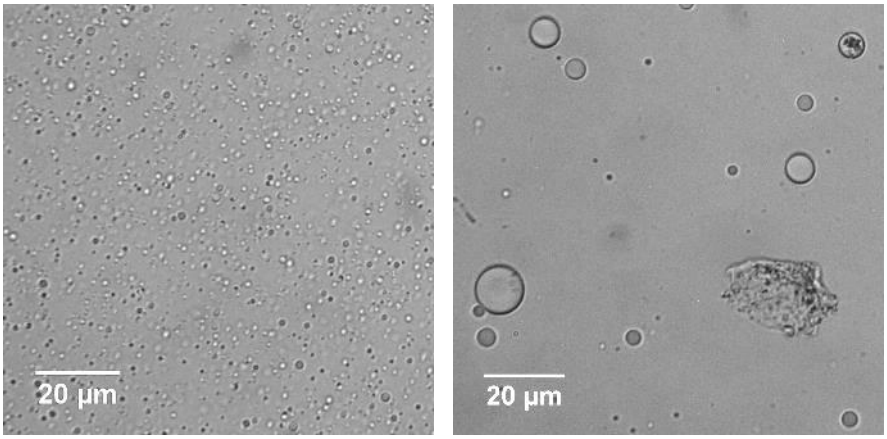

Figure 5.6 – $PMAA_{SH(100)}$ microspheres (sonicated at 100 Wcm^{-2} for 60s) prior to DTT addition (left) and after exposure to 60 mg/mL DTT for 1 hour at room temperature (right).

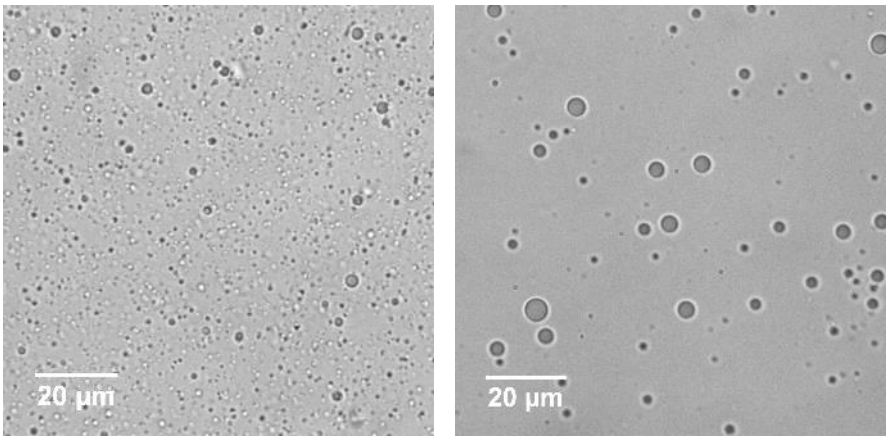

Figure 5.7 – $PMAA_{(100)}$ microspheres (sonicated at 100 Wcm^{-2} for 60s) prior to DTT addition (left) and after exposure to 60 mg/mL DTT for 1 hour at room temperature (right).

The final non-specific release mechanism to be investigated was that of encapsulant species by mechanical disruption. Samples of microspheres were sonicated at 219 Wcm^{-2} for five minutes and left to equilibrate, after which time 2 mL of IPM was charged to the sonicated dispersion and release into IPM was measured by UV/Vis spectroscopy. Over 50 % release was observed for all sonicated samples and, as with the other non-specific release mechanisms, no trends were observed based on molecular weight or degree of thiolation. To ensure that the absorbance measurements were not contaminated by sonicated shell fragments within the IPM layer, two control reactions were performed. The first modelled 100 % release of the labelled tetradecane into IPM without sonication, and the second measured sonication of polymer in buffer in the absence of an encapsulant. The measured contamination in IPM of the second control after equilibration was negligible at less than 1 % of the "100 % release" control.

Table 5.2 - Percentage release of Sudan III-saturated tetradecane-filled microspheres, sonicated at 100 Wcm^{-2} for 60 s, after incubation with 60 mg/mL DTT for 1 hour, incubation at pH 1 for 1 hour, and after sonochemical disruption for 5 min at 219 Wcm^{-2}.

Shell Material	60 mg/mL DTT / %	pH 1 / %	US 219 Wcm^{-2} 5 min / %	Shell Material	60 mg/mL DTT / %	pH 1 / %	US 219 Wcm^{-2} 5 min / %
$PMAA_{SH(25)}$	51 ± 4	2 ± 1	76 ± 6	$PMAA_{(25)}$	69 ± 4	7 ± 4	65 ± 5
$PMAA_{SH(50)}$	64 ± 2	2 ± 2	69 ± 7	$PMAA_{(50)}$	72 ± 3	9 ± 2	51 ± 6
$PMAA_{SH(75)}$	50 ± 3	3 ± 1	70 ± 4	$PMAA_{(75)}$	73 ± 6	6 ± 4	72 ± 4
$PMAA_{SH(100)}$	47 ± 5	2 ± 1	71 ± 6	$PMAA_{(100)}$	70 ± 4	6 ± 3	60 ± 4
$PMAA_{SH(25)}$-$PNIPAA_{M(100)}$	65 ± 6	6 ± 2	71 ± 5	$PMAA_{(25)}$-$PNIPAA_{M(100)}$	41 ± 6	11 ± 4	76 ± 6
$PMAA_{SH(50)}$-$PNIPAA_{M(100)}$	73 ± 5	7 ± 3	88 ± 4	$PMAA_{(50)}$-$PNIPAA_{M(100)}$	72 ± 5	8 ± 6	66 ± 5
$PMAA_{SH(75)}$-$PNIPAA_{M(100)}$	66 ± 6	6 ± 2	65 ± 6	$PMAA_{(75)}$-$PNIPAA_{M(100)}$	57 ± 5	6 ± 5	75 ± 7
$PMAA_{SH(100)}$-$PNIPAA_{M(100)}$	45 ± 6	9 ± 5	72 ± 5	$PMAA_{(100)}$-$PNIPAA_{M(100)}$	83 ± 9	10 ± 3	72 ± 3
$PMAA_{SH(25)}$-$PNIPAA_{M(100)}$-$PMAA_{SH(25)}$	51 ± 5	7 ± 3	55 ± 6	$PMAA_{(25)}$-$PNIPAA_{M(100)}$-$PMAA_{(25)}$	85 ± 4	5 ± 6	68 ± 6
$PMAA_{SH(50)}$-$PNIPAA_{M(100)}$-$PMAA_{SH(50)}$	65 ± 5	7 ± 4	73 ± 8	$PMAA_{(50)}$-$PNIPAA_{M(100)}$-$PMAA_{(50)}$	63 ± 10	10 ± 3	82 ± 6
$PMAA_{SH(75)}$-$PNIPAA_{M(100)}$-$PMAA_{SH(75)}$	45 ± 6	6 ± 3	55 ± 4	$PMAA_{(75)}$-$PNIPAA_{M(100)}$-$PMAA_{(75)}$	57 ± 5	9 ± 5	68 ± 4
$PMAA_{SH(100)}$-$PNIPAA_{M(100)}$-$PMAA_{SH(100)}$	46 ± 5	12 ± 3	62 ± 6	$PMAA_{(100)}$-$PNIPAA_{M(100)}$-$PMAA_{(100)}$	82 ± 6	9 ± 4	74 ± 3
				$PNIPAA_{M}$	94 ± 2	73 ± 4	65 ± 3
				P(MMA-co-$NIPAA_{M}$)	90 ± 3	85 ± 6	75 ± 6
$PMAA_{SH}$-(MMA-co-$NIPAA_{M}$)	51 ± 6	11 ± 5	68 ± 6	PMAA-(MMA-co-$NIPAA_{M}$)	88 ± 5	15 ± 3	71 ± 6

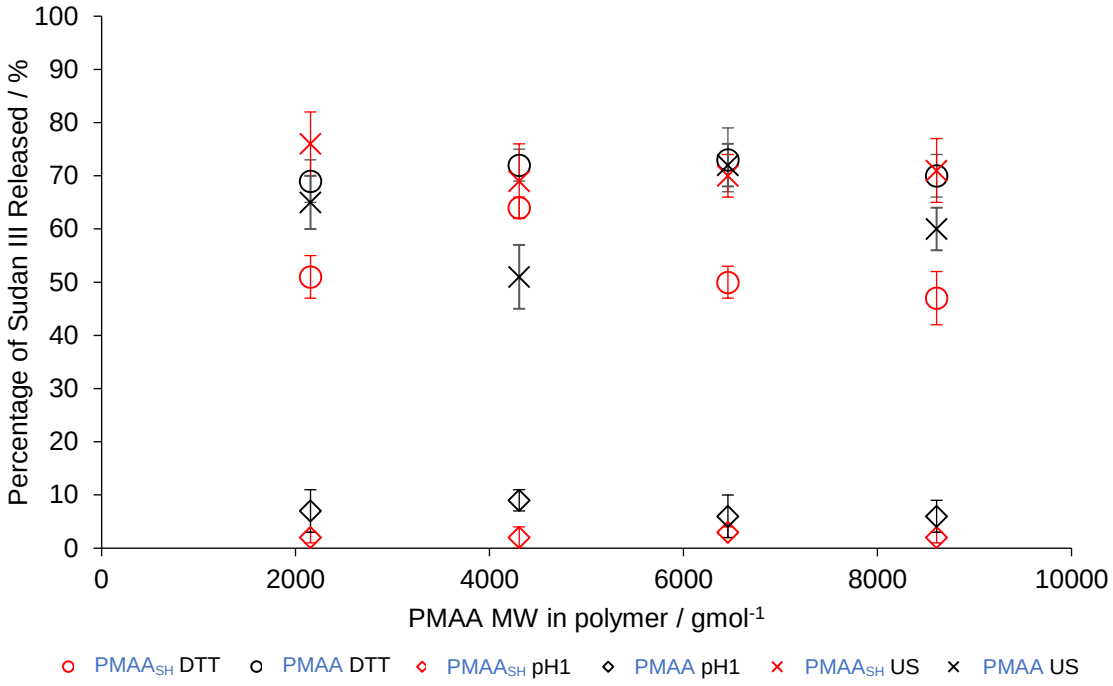

Figure 5.8 – Comparing the extent of release from thiolated and non-thiolated Sudan III-saturated tetradecane-filled PMAA microspheres of increasing PMAA molecular weight by non-specific release mechanisms. Measurements were conducted in triplicate.

Figure 5.8 compares the extent of Sudan III-saturated tetradecane release from thiolated and non-thiolated PMAA-shelled microspheres via the non-specific release mechanisms, tabulated in Table 5.2. As described, no clear trends in release behaviour can be observed in any of the mechanisms as a result of increasing PMAA molecular weight or thiolation.

Although the homopolymeric microspheres exhibited no trends in microsphere size with increasing PMAA molecular weight upon synthesis, the di- and triblock block copolymer-shelled microspheres exhibited an increase in average diameter and size distribution with decreasing PMAA block molecular weight (Table 4.1 and Table 4.4). It was therefore interesting to note that no trends were observed in the release behaviour of these microsphere systems by non-specific release methods, as shown in Table 5.2 and summarised in Figure 5.9 and Figure 5.10. These findings do, however, highlight the non-specific nature of their mechanisms as opposed to thermally-induced release, which is dependent on the stimuli-responsive component within the microsphere shell and therefore more likely to be dependent on shell composition.

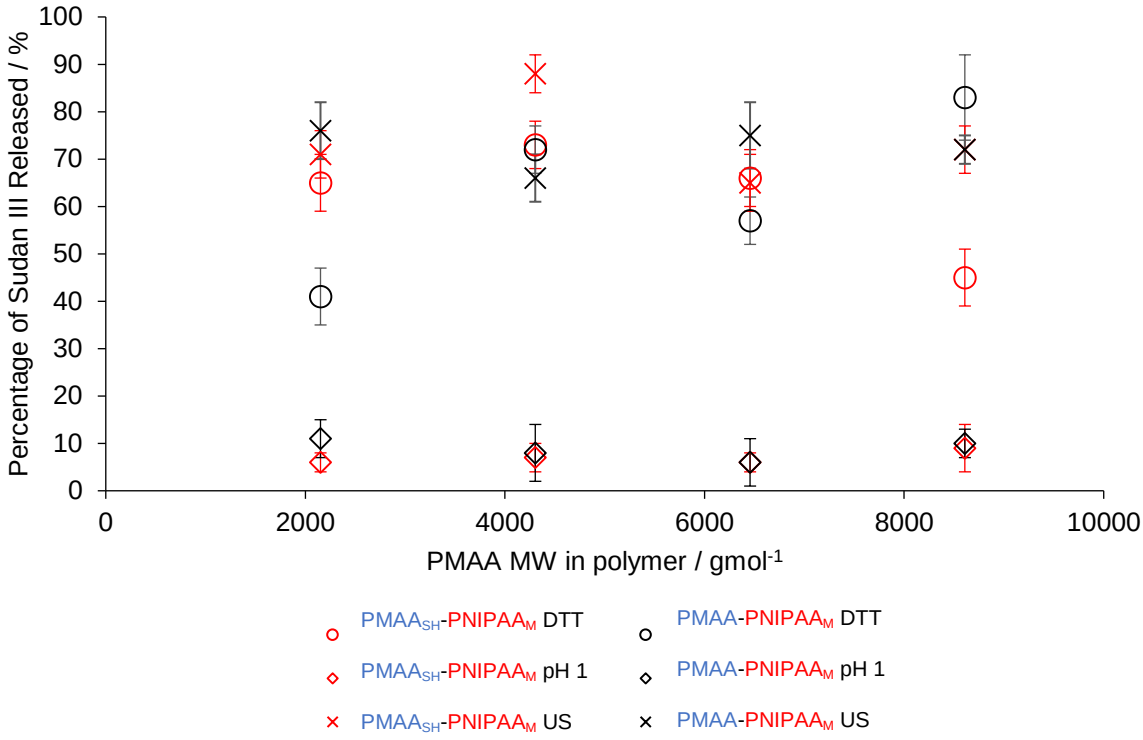

Figure 5.9 - Comparing the extent of release from thiolated and non-thiolated Sudan III-saturated tetradecane-filled diblock PMAA-PNIPAA$_M$ microspheres by non-specific release mechanisms. Measurements were conducted in triplicate.

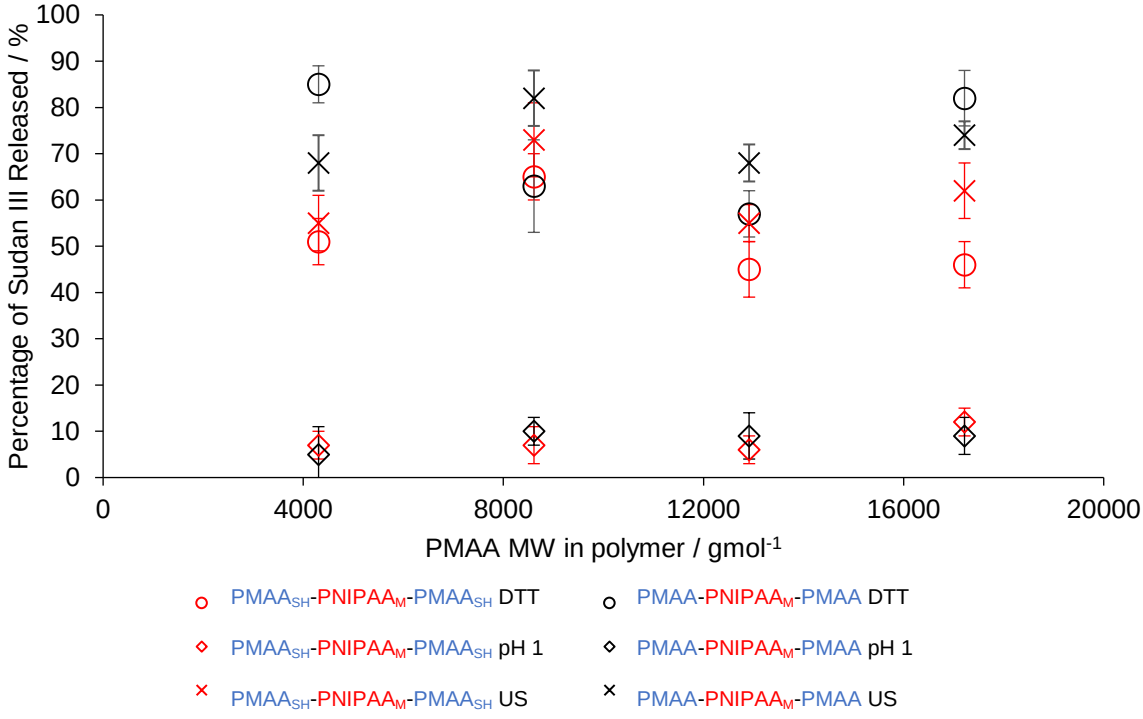

Figure 5.10 - Comparing the extent of release from thiolated and non-thiolated Sudan III-saturated tetradecane-filled triblock PMAA-PNIPAA$_M$-PMAA microspheres by non-specific release mechanisms. Measurements were conducted in triplicate.

Whilst the majority of non-specific release mechanisms investigated facilitated release from all microspheres systems synthesised, the incorporation of thermoresponsive polymers within microsphere shells was performed to facilitate the selective release of encapsulant species in response to an increase in surrounding temperature.

5.3 Thermoresponsive Release of Hydrophobic Species

The main focus of this project was to design of stimuli-responsive microspheres with the ability to release a payload in response to an external environmental stimulus. Release by non-specific mechanisms such as mechanical disruption and extreme pH has been documented, however these mechanisms are generic and facilitate release from all polymeric microsphere systems. It was therefore pertinent to explore the selective thermoresponsive behaviour of polymeric microspheres containing $PNIPAA_M$ portions, which, as an independent polymer and block copolymer, exhibits physiochemical changes beyond the LCST of 31 °C. It was proposed, however, that due to the additional covalent and non-covalent stabilisation of the shell species, the observed LCST for the stimuli-responsive microspheres would exceed that of the free chains.

As predicted, entrapment of stimuli-responsive $PNIPAA_M$ within the microsphere shell led to an increase in the LCST. There are two possible reasons for the observed increase, the first is likely due to the stabilisation effect of additional interactions across the surface of the microsphere on formation, whilst the second may be a result of partial hydrolysis of $PNIPAA_M$ at the shell surface into hydrophilic acrylic acid moieties. These potential hydrolysed repeat units would be present in all $PNIPAA_M$-containing microspheres and would be capable of modifying the LCST in a similar way to copolymerisation with hydrophobic MMA, as previously described.

The LCST was determined by gradual heating of the fluorescent microsphere samples until microsphere deformation and coalescence was observed. Microspheres were analysed in real-time via optical microscopy using the LSCM microscope by heating samples in 1 ºC increments and equilibrating the sample for ten minutes. Microspheres containing $PNIPAA_M$ portions underwent thermoresponsive physiochemical changes at the elevated temperatures of 36-38 °C once incorporated into the microsphere shells, making them an

ideal candidate for *in vivo* applications. It was not possible, however, to image the microspheres during real-time heating, as convection within the sample greatly affected the image quality during laser micrograph acquisition.

Once the sample LCST of stimuli-responsive polymers had been determined by real-time analysis, a sample of tetradecane-filled microspheres was deposited onto a microscope slide and heated to 38 ºC on an IKA® RCT Basic digital heated stirrer plate equipped with a thermometer. Images were taken after 5, 10 and 30 minutes to determine the extent of microsphere collapse.

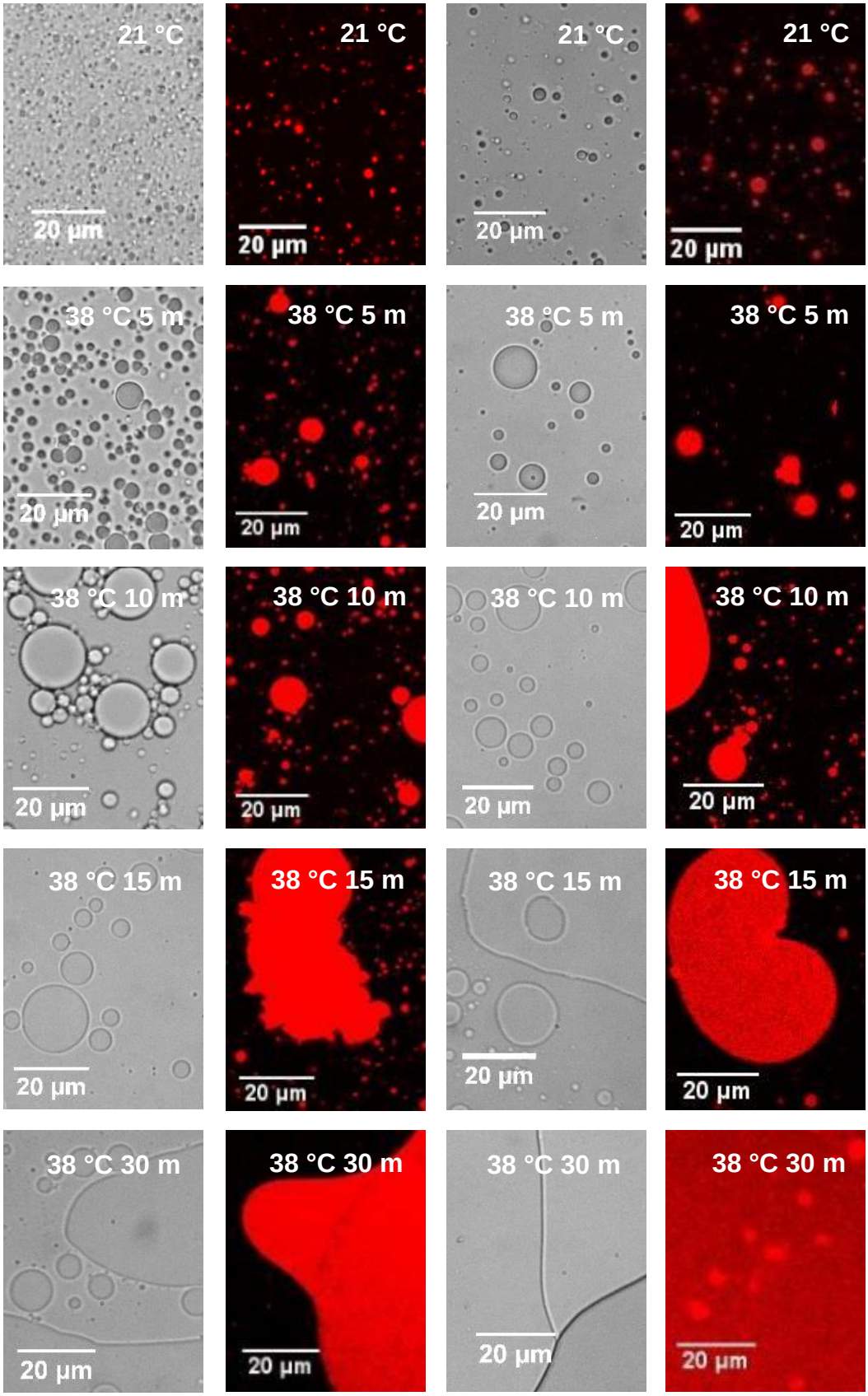

Figure 5.11 - Optical and LSCM micrographs of $PMAA_{SH(100)}$-$PNIPAA_{M(100)}$ (left) and $PMAA_{(100)}$-$PNIPAA_{M(100)}$ (right) at room temperature and after 5, 10, 15 and 30 minutes heated to 38 °C.

Figure 5.11 compares the behaviour of thiolated and non-thiolated PMAA-PNIPAA$_M$ microspheres in response to elevated temperatures. The first change observed in both systems is the apparent growth of larger microspheres, this is unlikely due to diffusion of species into the core as initially the shell appears intact. It may instead be a result of shell degradation and coagulation of nearby oil droplets, as can clearly be observed in the LSCM image of PMAA-PNIPAA$_M$ after 15 minutes at 38 °C. A lack of observed microsphere shell rupture or bursting is also indicative of gradual shell degradation and subsequent release as opposed to simple burst release. This would suggest that the larger droplets are, in fact, free oil puddles that have undergone shell degradation and are therefore able to coalesce. It was not possible to quantitively measure the change in shell thickness by microscopy alone, but a qualitative change in the shell appearance was noted.

After 30 minutes, both systems exhibited extensive coalescence. However, regions of discretely distributed microspheres still remained, suggesting that 30 minutes was insufficient for complete degradation and release. As an alternative method of analysis, samples of Sudan III-saturated tetradecane-filled microspheres were prepared as previously described, 2 mL of IPM was then deposited as a layer on top of the microsphere dispersion and each centrifuge tube was submerged in a water bath set to 38 °C to equilibrate. The dispersion was gently agitated and samples were taken at regular intervals for analysis by UV/Vis.

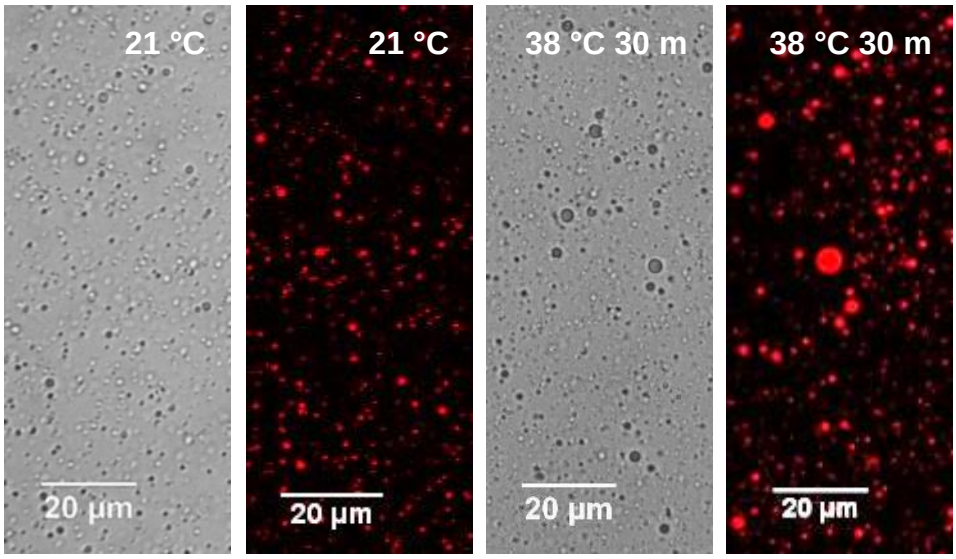

Figure 5.12 – Optical and LSCM micrographs of PMAA$_{SH(100)}$ at room temperature and after 30 minutes heated to 38 °C.

As a control, the behaviour of $PMAA_{SH}$ and PMAA-shelled microspheres, in the absence of thermoresponsive $PNIPAA_{M}$ portions, were analysed on heating. Poly(methacrylic acid) and its thiolated analogue are not thermoresponsive polymers, therefore no major changes in microsphere yield or morphology were expected to be observed upon heating. Figure 5.12 demonstrates the stability of $PMAA_{SH(100)}$ microspheres with respect to heating at 38 °C for 30 minutes. The yield is comparable to those imaged at room temperature, and the microsphere size was largely consistent between samples, with some sporadic growth observed. A small amount of aggregation was evident after 30 minutes, however no regions of microsphere deformation and coalescence as a result of shell rupture were seen upon LSCM imaging. Figure 5.13 shows the behaviour of non-thiolated $PMAA_{(100)}$ microspheres on heating. As with $PMAA_{SH}$, a small amount of microsphere growth and aggregation was observed after 30 minutes, but neither systems exhibit regions of significant growth or rupture and remained a relatively discrete distribution. The $PMAA_{SH}$ and PMAA microspheres therefore served as controls for comparison.

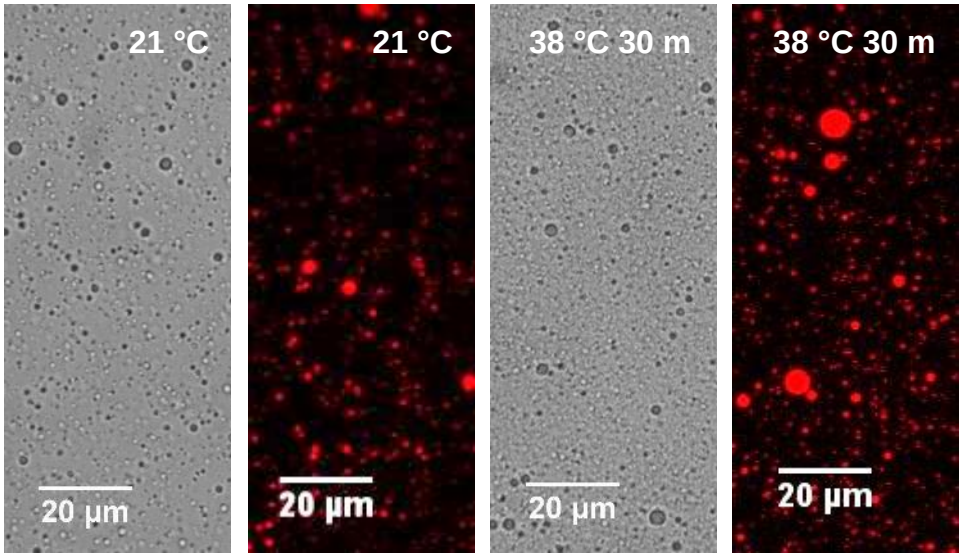

Figure 5.13 - Optical and LSCM micrographs of $PMAA_{(100)}$ at room temperature and after 30 minutes heated to 38 °C.

It was initially assumed that the thermoresponsiveness of $PNIPAA_M$ portions within the microsphere shell and subsequent release would be instantaneous, analogous to the thermoresponsive behaviour of the polymers in Chapter 3. However, the elevated LCST and predicted interactions stabilising the microsphere shell instead indicate that, although the thermoresponsive behaviour of the entrapped polymer may be quick, the effect of $PNIPAA_M$ collapse on release occurs over a longer timescale. The release experiments conducted on the heated stage revealed clear degradation over the course of 30 minutes, however the degree of degradation over a short timescale was attributed in part to the small volume analysed.

Analysis of samples heated within the sample vial were conducted to better simulate the response of an administered sample of the delivery vehicles. Release experiments into IPM were initially performed over a timescale of up to 3 hours, however no release was observed by UV/Vis. In some cases, an inaccurate increase in absorbance was measured due to contamination of the IPM phase upon agitation and insufficient re-equilibration prior to analysis. As such, the experiments were repeated over a longer timescale of 24 and 48 hours to determine whether tetradecane was released into IPM.

Table 5.3 - Percentage release of Sudan III-saturated tetradecane-filled microspheres, sonicated at 100 Wcm^{-2} for 60 s, after incubation at 38 °C for 24 and 48 hours.

Shell Material	24 hr 38 °C / %	48 hr 38 °C / %	Shell Material	24 hr 38 °C / %	48 hr 38 °C / %
$PMAA_{SH(25)}$	1 ± 1	1 ± 1	$PMAA_{(25)}$	6 ± 1	7 ± 1
$PMAA_{SH(50)}$	1 ± 1	1 ± 2	$PMAA_{(500)}$	5 ± 1	7 ± 1
$PMAA_{SH(75)}$	1 ± 1	1 ± 1	$PMAA_{(75)}$	6 ± 1	6 ± 1
$PMAA_{SH(100)}$	1 ± 1	1 ± 1	$PMAA_{(100)}$	8 ± 1	9 ± 1
$PMAA_{SH(25)}$-$PNIPAA_{M(100)}$	30 ± 2	40 ± 1	$PMAA_{(25)}$-$PNIPAA_{M(100)}$	59 ± 1	83 ± 1
$PMAA_{SH(50)}$-$PNIPAA_{M(100)}$	40 ± 2	53 ± 1	$PMAA_{(50)}$-$PNIPAA_{M(100)}$	61 ± 1	75 ± 1
$PMAA_{SH(75)}$-$PNIPAA_{M(100)}$	33 ± 2	50 ± 1	$PMAA_{(75)}$-$PNIPAA_{M(100)}$	56 ± 1	68 ± 1
$PMAA_{SH(100)}$-$PNIPAA_{M(100)}$	33 ± 1	45 ± 2	$PMAA_{(100)}$-$PNIPAA_{M(100)}$	31 ± 2	51 ± 1
$PMAA_{SH(25)}$-$PNIPAA_{M(100)}$-$PMAA_{SH(25)}$	36 ± 2	47 ± 1	$PMAA_{(25)}$-$PNIPAA_{M(100)}$-$PMAA_{(25)}$	38 ± 2	72 ± 1
$PMAA_{SH(50)}$-$PNIPAA_{M(100)}$-$PMAA_{SH(50)}$	40 ± 2	46 ± 1	$PMAA_{(50)}$-$PNIPAA_{M(100)}$-$PMAA_{(50)}$	35 ± 2	63 ± 1
$PMAA_{SH(75)}$-$PNIPAA_{M(100)}$-$PMAA_{SH(75)}$	39 ± 1	51 ± 1	$PMAA_{(75)}$-$PNIPAA_{M(100)}$-$PMAA_{(75)}$	33 ± 2	62 ± 2
$PMAA_{SH(100)}$-$PNIPAA_{M(100)}$-$PMAA_{SH(100)}$	38 ± 3	47 ± 2	$PMAA_{(100)}$-$PNIPAA_{M(100)}$-$PMAA_{(100)}$	34 ± 1	41 ± 3
			$PNIPAA_{M(100)}$	57 ± 2	92 ± 3

Table 5.3 outlines the release profiles of Sudan III-saturated tetradecane-filled microspheres, heated to 38 °C over a timescale of 24 and 48 hours. As expected, microspheres in the absence of thermoresponsive $PNIPAA_M$ exhibit negligible release over 48 hours of less than 10 % for both thiol-functionalised and unfunctionalised PMAA. For the stimuli-responsive block copolymeric microsphere systems, between 30-61 % release was observed after 24 hours and up to 83 % release was measured after 48 hours. Although no dependence on PMAA percentage within the chain was observed for the thiolated block

copolymeric microspheres, a clear inverse relationship between PMAA block length in the copolymer chains and degree of thermoresponsive release can be observed for the non-thiolated microsphere samples. This would suggest that the disulphide crosslinks induce additional stability, capable of inhibiting the degree of thermoresponsive collapse.

The marked difference in measured release with respect to the homopolymer microspheres demonstrates the stimuli-responsive behaviour of the polymeric microspheres and gives some indication as to the release mechanism. A gradual degradation and thinning of the shell on heating was proposed, as $PNIPAA_M$ within each layer of the shell is exposed to the buffer and undergoes a conformational change resulting in weakening and thinning of the shell. It also suggests that $PNIPAA_M$ portions are located across the surface of the shell as opposed to localised, which may have instead resulted in a burst-like release.

Poly(N-isopropylacrylamide) exhibited more extensive release than microspheres containing PMAA portions of over 90 % (Figure 5.14), which would suggest that both thiolated and non-thiolated PMAA confer additional stability upon the microsphere shell. Covalent disulphide crosslinking or the newly proposed formation of anhydride linkages across the surface of the spheres, in addition to non-covalent interactions, appear to immobilise $PNIPAA_M$ to an extent, inhibiting the thermoresponsive behaviour. An additional investigation was conducted to determine the release behaviour of tetradecane into IPM from polymeric microspheres with shell material containing LCST-modified P(MAA-co-$NIPAA_M$) (Table 5.4). Real-time analysis was employed to determine the LCST of the microspheres, and an elevated LCST of 33 ºC was observed. The P(MMA-co-$NIPAA_M$) microspheres exhibited comparable release behaviour to $PNIPAA_M$ microspheres, releasing over 85 % of their encapsulant after 48 hours at 33 ºC.

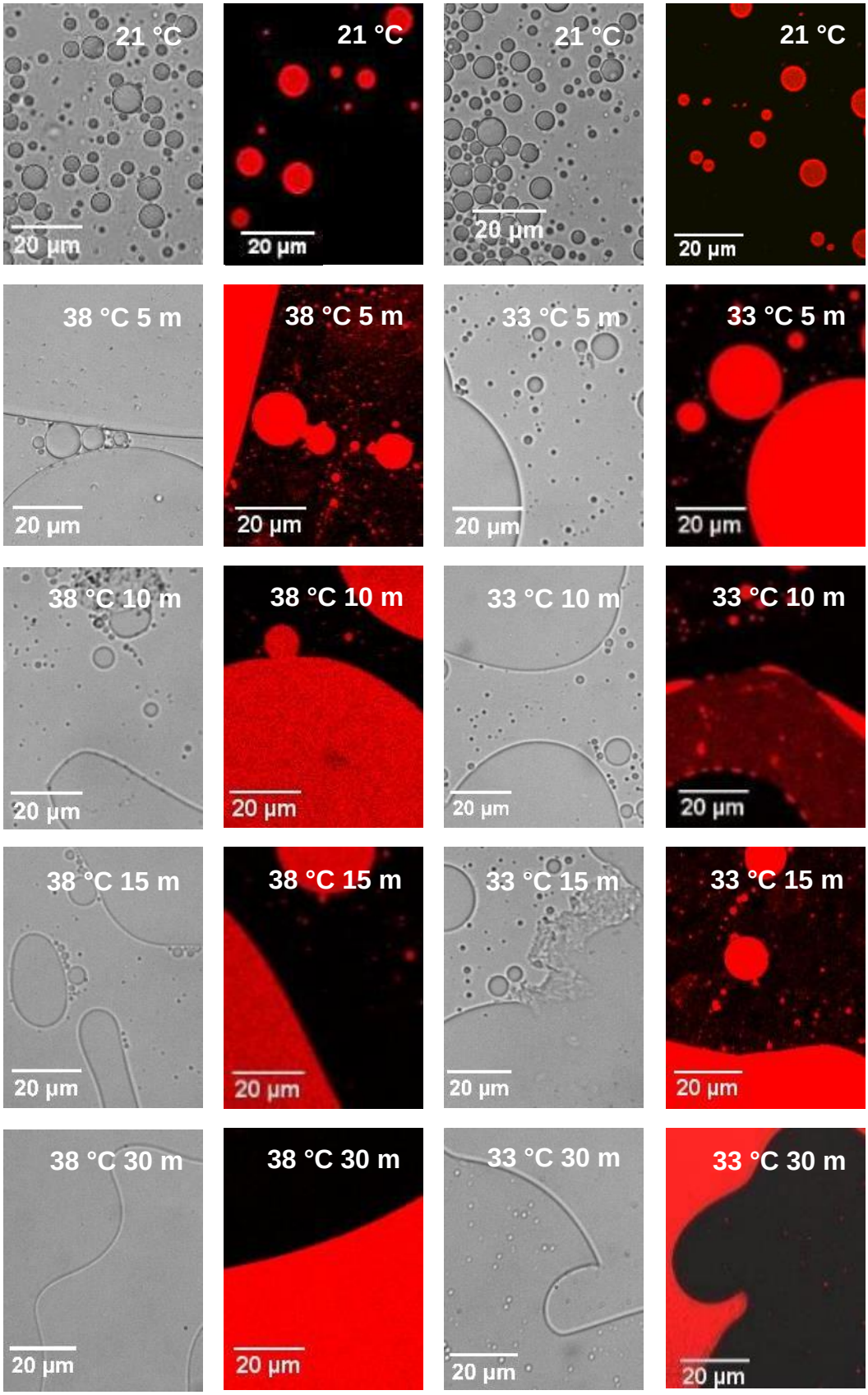

Figure 5.14 - Optical and LSCM micrographs of PNIPAA$_{M(100)}$ (left) (observed LCST 38 ºC) and LCST-modified P(MMA-co-NIPAA$_M$) (right) (observed LCST 33 ºC) at room temperature and after 5, 10, 15 and 30 minutes heated to 38 and 33 °C respectively.

Table 5.4 - Encapsulation efficiency of Sudan III-saturated tetradecane-filled LCST-modified microspheres, sonicated at 100 Wcm^{-2} for 60 s, after incubation at 33 °C for 24 and 48 hours.

Shell Material	24 hr 33 °C / %	48 hr 33 °C / %
P(MMA-co-NIPAA$_M$)	67 ± 1	77 ± 3
PMAA$_{(100)}$-(MMA-co-NIPAA$_M$)	61 ± 1	79 ± 2
PMAA$_{SH(100)}$-(MMA-co-NIPAA$_M$)	55 ± 2	56 ± 2

PNIPAA$_M$ and P(MMA-co-NIPAA$_M$)-shelled microspheres in the absence of PMAA, shown in Figure 5.14, exhibited comparable behaviour on heating. After only five minutes, a distinct loss in the number of discrete microspheres can be observed. After 30 minutes, the majority of microspheres have undergone degradation and very few discrete microspheres remain on the slide. As with the other thermoresponsive microspheres, additional stabilising interactions led to an increase in the observed LCST of MMA-co-NIPAA$_M$-shelled polymeric microspheres, relative to the free polymer.

5.4 Thermoresponsive Release of Hydrophilic Species

The release of hydrophilic species from lysozyme microspheres by mechanical disruption, monitored by a change in conductivity, has been previously reported in the literature[7]. Skinner *et al.*[7] observed an increase in solution conductivity upon the sonochemical disruption of 6.1 M NaCl-in-tetradecane microspheres. The observed increase in conductivity upon disruption was due to the presence of released NaCl into the bulk phase after partitioning from the oil continuous phase, demonstrating a mechanism with which the release of hydrophilic species can be quantified. Upon analysis of the control, whereby a volume of NaCl corresponding to 100 % release was charged to the solution prior to sonochemical disruption of tetradecane-filled microspheres, a decrease in conductivity to was observed. Skinner[7] attributed this to possible adsorption of NaCl to broken charged protein fragments, generated by the sonochemical destruction of the microsphere shells.

In order to determine the release of hydrophilic species from polymeric microspheres, samples of thiolated and non-thiolated homo, di- and triblock copolymers containing 100 MAA repeat units were prepared as per the protocol outlined in Experiment 2.2.9 with 5 M NaCl solution forming the aqueous phase of the emulsion. The undiluted microsphere samples were then transferred into two 1 mL microcuvettes containing a dialysis window in the lid to enable the passage of sodium chloride into 20 mL bulk deionised water within a centrifuge tube, without risk of contamination by shell fragments (Figure 5.15). It was assumed that, due to the gentle release mechanism of thermally-initiated release with respect to sonochemical disruption, the small charged shell fragments, as proposed by Skinner[7], would not be produced. After 48 hours, the centrifuge tubes were agitated by shaking to ensure that any released NaCl would diffuse into the bulk phase. A timescale of 48 hours was chosen due to the observed stability of tetradecane-filled microspheres on heating by extraction into IPM.

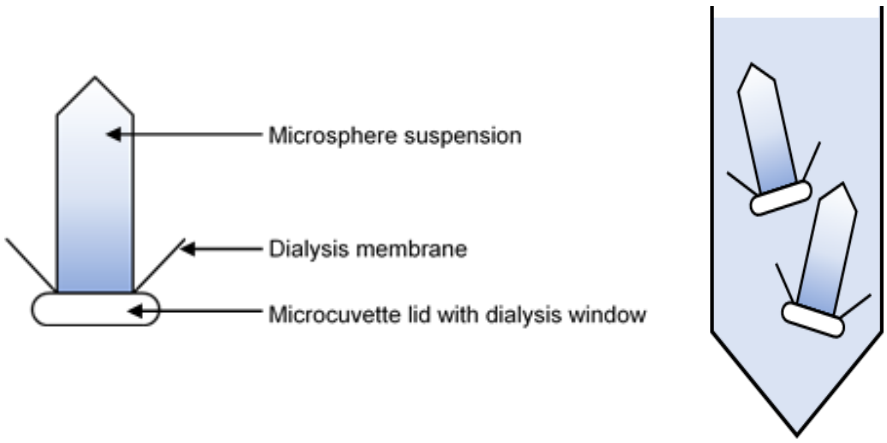

Figure 5.15 – The experimental setup employed to measure the release of hydrophilic species from 5 M NaCl-in-tetradecane-filled polymeric microspheres (within the microcuvettes) via dialysis.

Figure 5.16 shows the difference in measured conductivity between 5 M NaCl-in-tetradecane emulsion-filled microspheres stored at room temperature for 48 hours, and those incubated in a water bath at 40 ºC for the same duration. A sample of 100 µL 40:60 5 M NaCl-in-tetradecane emulsion with 2 mL pH 8 tris acetate buffer in two 1 mL microcuvettes, stored at 40 ºC for 48 hours, was employed as a control to mimic 100 % release. The bulk phase of pH 8 tris acetate buffer also possessed its own conductivity of

237 µScm^{-1}, therefore the difference in conductivity between room temperature samples and heated samples was deemed a more accurate quantification of the release.

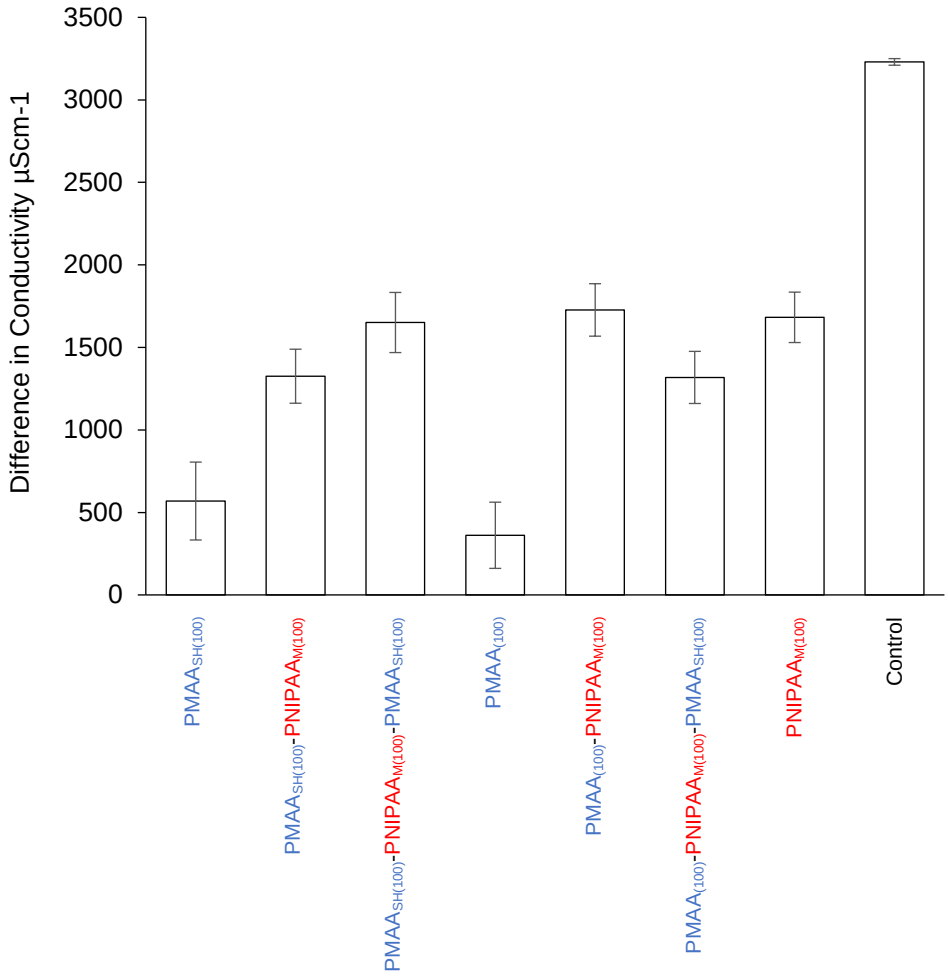

Figure 5.16 – The difference in conductivity between 5M NaCl-in-tetradecane-filled polymeric microspheres, incubated at 40 ºC for 48 hours, and control microsphere dispersions stored at room temperature.

The observed release from the thermoresponsive polymeric microspheres was between 40-55 % relative to the control, whilst for the homopolymeric microspheres no release beyond 15 % was observed. This indicates selective thermoresponsive release of $NaCl_{(aq)}$ from the $PNIPAA_M$-containing microspheres. Although a preliminary investigation, these results demonstrate a mechanism which can be applied to model the release of aqueous hydrophilic drugs from encapsulated water-in-oil emulsions. It would be of interest to determine the

effect of PMAA chain length on aqueous release, to see whether the values corroborate the trends observed during labelled tetradecane release.

It can be concluded from the data presented in this chapter that it is possible to form thermoresponsive microspheres, from the thiol-functionalised and non-thiol-functionalised polymers synthesised in Chapter 3, capable of release their contents in the region of 36-38 ºC. Whilst the LCST of microspheres was shown to be unaffected by the presence of disulphide crosslinks or the PMAA chain length within the polymer shell material, the degree of thermoresponsive release from microspheres in the absence of disulphide crosslinks was shown to be dependent on PMAA block length. The data corroborates the size distribution data for the microspheres, discussed in Chapter 4, whereby microspheres containing disulphide crosslinks within the shell were smaller on average than their non-thiolated analogues, and exhibited greater long-term stability. Thermoresponsive release from LCST-modified polymers at 33 ºC was also successfully demonstrated.

Release of hydrophilic species from thermoresponsive microspheres was achieved after 48 hours at 40 ºC, although it was not possible to observe trends between different polymers due to insufficient material. Further investigation will determine whether the behaviour observed during tetradecane release into IPM will corroborate the release behaviour of hydrophilic species.

6 Conclusions

The main aims of this thesis, outlined in Chapter 1, were to broaden the scope of sonochemically-produced polymeric microspheres as stimuli-responsive delivery vehicles, employing novel thermoresponsive shell species, capable of releasing their payload in response to changes in the surrounding temperature.

In Chapter 3, the synthesis of biocompatible polymers for use as microsphere shell species was addressed. $PMAA_{SH}$ has been reported as a suitable synthetic alternative for the sonochemical synthesis of polymeric microspheres analogous to those with a proteinaceous shell[6,10]. The focus was therefore to build upon these investigations by employing the versatility of RAFT polymerisation as a means to generate polymeric and block copolymeric shell species of PMAA. This was accomplished by incorporating the thermoresponsive polymer poly(N-isopropylacrylamide) (LCST = 31 ºC) to facilitate the synthesis of thermoresponsive delivery vehicles. PMAA and di- and triblock copolymers of PMAA-$PNIPAA_M$ and PMAA-$PNIPAA_M$-PMAA with varying PMAA chain lengths were prepared, and the characteristic LCST of $PNIPAA_M$ was found to remain unchanged upon block copolymerisation. Subsequently, novel PMAA-based diblock copolymers incorporating LCST-modified P(MMA-co-$NIPAA_M$) were synthesised by RAFT polymerisation, with a modified LCST of 28 ºC, as determined by DLS and UV/Vis spectroscopy.

The dependence of successful sonochemical microsphere synthesis upon the presence of thiol functionalities within the PMAA has been previously reported[6,10], Chapter 3 also reports the functionalisation of PMAA blocks within the synthesised block copolymers. Carbodiimide cross-coupling was employed to functionalise the carboxylic acid moieties of the methacrylic acid repeat units and a degree of thiolation of approximately 30 % of PMAA within each polymer was achieved. Functionalisation of PMAA within thermoresponsive and novel LCST-modified thermoresponsive block copolymers was also found to have no impact on the LCST.

Once the polymers and functionalised polymers had been synthesised by RAFT polymerisation and their thermoresponsive behaviour characterised, their use as shell species for the synthesis of novel thermoresponsive polymeric microspheres was investigated, as outlined in Chapter 4.

Chapter 4 first reports the characterisation and optimisation of the ultrasound horn setup and simple one-pot sonochemical protocol, first described by Suslick and coworkers[1,15], for the synthesis of small microspheres (<7 μm) with narrow polydispersities, appropriate for use as intravenous delivery vehicles. Calorimetry was employed to determine the acoustic intensity applied to a system during sonication, and Fricke dosimetry was used to approximate radical production. With regards to microsphere production, variables including the sonication time and applied acoustic intensity were addressed, and evidence of disulphide crosslinking within the microsphere shells, induced by sonochemically-generated superoxide radicals, was determined by the use of a tert-butanol radical trap and sonochemical synthesis in the absence of oxygen. Experiments were compared against a well-characterised lysozyme microsphere system, and it was discovered that, unlike lysozyme, the synthetic polymers generated in Chapter 3 were capable of forming microspheres under nitrogen and in a chemically-purged environment devoid of superoxide radicals. Further characterisation by modifying the degree of thiolation found that the polymers were capable of forming microspheres in the absence of thiol residues altogether. Microspheres have been successfully synthesised in the absence of thiol functionalities[11,12], however this is the first report of the successful sonochemical synthesis of these polymeric and block copolymeric microspheres employing non-thiolated synthetic polymers. The proposed mechanism for stabilisation was a combination of non-covalent interactions and sonochemically-induced anhydride crosslinks.

Microsphere size was found to be largely dependent upon the percentage of poly(methacrylic acid) within the polymer chains. Thiolated PMAA-based microspheres were smaller than their non-thiolated analogues, and this was attributed to the presence of disulphide crosslinks, formed between polymer chains at the interface to stabilise the dispersed oil droplets. It was proposed that PMAA was responsible for stabilising the microspheres, either by disulphide bridges or alternative interactions, however microspheres in the absence of PMAA were also successfully formed. $PNIPAA_M$ and LCST-modified P(MMA-co-$NIPAA_M$) formed tetradecane-filled microspheres exhibiting long-term stability. Their diameter was larger on average that those of PMAA containing alternatives, but their synthesis demonstrates that PMAA is not the only polymer inducing stability in the shell of the block copolymeric microspheres. The proposed mechanism for stabilisation, based on the FT-IR spectra, was partial hydrolysis of $NIPAA_M$ repeat units to the parent acrylic acid, facilitating interactions in the shell analogous to those of PMAA.

Both the thiolated and non-thiolated polymers were capable of encapsulating a range of hydrophobic species and hydrophilic species within preformed W/O emulsions; the method of which was first reported recently by Skinner *et al.*[7]. In addition to tetradecane, biocompatible and natural alternatives of perfluorohexane, soybean oil and vegetable oil were encapsulated, demonstrating the versatility of the synthetic polymers as shell species. Optical and confocal microscopy were used to confirm the encapsulation of tetradecane and water-in-tetradecane emulsions within the polymeric microspheres. Along with water-in-tetradecane emulsions, the previously unreported encapsulation of water-in-olive oil emulsions within $PMAA_{SH}$ and $PMAA_{SH}$-$PNIPAA_{M}$ microspheres was demonstrated, further widening the scope of synthetic polymeric microspheres as biocompatible delivery vehicles.

Finally, the thermoresponsive release from thiolated and non-thiolated $PNIPAA_{M}$ and LCST-modified P(MMA-co-$NIPAA_{M}$)-containing polymeric microspheres was reported in Chapter 5, alongside other non-specific mechanisms for release including sonochemical disruption and a reductive environment.

Microspheres were heated to beyond the LCST, and breakdown was observed by optical microscopy to occur between 37-38 ºC (32-33 ºC for LCST-modified polymers), attributed to the immobilisation of thermoresponsive $PNIPAA_{M}$ within the microsphere shell. Thermoresponsive release was quantified by UV/Vis spectroscopy and was observed visually by the deformation and coalescence of Nile Red-labelled tetradecane phases during LSCM analysis.

In order to quantify the release from W/O emulsion-filled microspheres, an emulsion of 5M NaCl-in-tetradecane was encapsulated, and an increase in conductivity of the bulk phase on heating to 38 ºC was measured. Although reproducibility between samples of $PMAA_{SH(100)}$ and $PMAA_{(100)}$-based polymers and block copolymers was observed, the investigations were considered preliminary due to insufficient yields of polymers with alternative molecular weights. The data does, however, provide a starting point from which further release experiments of hydrophilic materials can be pursued.

To summarise, by combining the synthesis of thermoresponsive polymers with controlled molecular weights by the facile technique of RAFT polymerisation and the simple sonochemical synthesis of microspheres containing both lyophilic and aqueous phases, the

formation of thiolated and novel non-thiolated thermoresponsive microspheres, including those with a modified LCST, has been achieved.

The field of controlled drug delivery has received a lot of focus in recent years, in order to optimise the delivery of potent or volatile drugs to a desired location with a timely release profile. Whilst sonochemically-generated microspheres have demonstrated their potential as viable delivery vehicles both *in vitro* and *in vivo*[9,81,93,100], there are still mechanistic limitations to overcome. The primary obstacle is the restriction of the technique with respect to scale-up for industrial or commercial production. Adaption of the technique into a continuous flow system may go some way to improve production efficiency, however the importance of prolonged exposure to ultrasound for control over microsphere size and polydispersity has been demonstrated in Chapter 3. Zhou *et al*.[61] have recently designed a novel flow-through sonochemical technique for the generation of monodisperse lysozyme microbubbles, yet the method is still limited by its benchtop size and gaseous encapsulant. Whilst the use of sonochemical mechanisms for microsphere synthesis on a commercial or industrial scale may be some way off, its application in "on-demand" microsphere synthesis is currently viable, provided the microsphere morphologies, loading and release profiles are strictly controlled.

The size and polydispersity of sonochemically-generated microspheres currently restricts their use as commercially available drug delivery vehicles. When designing a drug delivery vehicle, their loading must be precisely determined in order to safely administer a known dosage with a predetermined release profile. Combining sonochemical techniques with a mechanism such as microfluidics may facilitate the formation of microspheres with the stability of sonochemically-crosslinked microspheres, and the monodispersity of microspheres generated by microfluidics.

To enable the microspheres generated during this project to be employed as drug delivery vehicles and make a valuable contribution to the field of controlled drug delivery, the following areas and limitations must be addressed:

1. To achieve greater control over the size and polydispersity of sonochemically-generated microspheres, and to fully characterise the covalent and non-covalent interactions within the shell contributing to microsphere stability, particularly those of non-thiol crosslinked polymeric microspheres.

2. To measure the encapsulation efficiency and long-term stability of biocompatible and naturally-occurring oils within the polymeric microspheres as alternatives to tetradecane, and to further characterise the morphology and encapsulation of water-in-natural oil emulsions.
3. Comprehensive release studies of the thermoresponsive release mechanisms of stimuli-responsive microspheres, and determination of the influence of pH on the LCST and release behaviour of the dual-stimuli responsive microspheres.

In order to further the investigations into the use of these stimuli-responsive polymers as shell species for the synthesis of thermoresponsive microspheres, the recommendations for future work are as follows:

1. Surface functionalisation of the microspheres for targeted delivery applications, possibly employing the carbodiimide cross-coupling reaction in order to react with the free carboxylate functionalities on the microsphere shell surface.
2. To demonstrate the encapsulation of a drug, capable of maintaining its biological activity upon thermoresponsive release.
3. Incorporation of an alternative stimuli-responsive component into the shell species, such as photoresponsive pyrenylmethylesters[234] for applications in agrochemicals. Alternatively, the incorporation of bioadhesive components may be explored to improve retention times at target sites[109].
4. To further probe the stabilising interactions within the shell, in order to gain a greater understanding of and optimise the encapsulation and release process, and to demonstrate the reproducibility of LCST-modified release by incorporating alternative copolymers into the shell species with N-isopropylacrylamide.

The work outlined in this thesis provides a novel contribution to the valuable development of sonochemically-generated stimuli-responsive microspheres for use in the field of drug delivery.

7 References

1. Suslick, K. S., Grinstaff, M. W., Kolbeck, K. J. & Wong, M. Characterization of sonochemically prepared proteinaceous microspheres. *Ultrason. Sonochem.* **1,** S65–S68 (1994).

2. Suslick, K. S. & Grinstaff, M. W. Protein microencapsulation of nonaqueous liquids. *J. Am. Chem. Soc.* **112,** 7807–7809 (1990).

3. Cavalieri, F., Ashokkumar, M., Grieser, F. & Caruso, F. Ultrasonic synthesis of stable, functional lysozyme microbubbles. *Langmuir* **24,** 10078–10083 (2008).

4. Shimanovich, U., Eliaz, D., Aizer, A., Vayman, I., Michaeli, S., Shav-Tal, Y. & Gedanken, A. Sonochemical Synthesis of DNA Nanospheres. *ChemBioChem* **12,** 1678–1681 (2011).

5. Skirtenko, N., Tzanov, T., Gedanken, A. & Rahimipour, S. One-step preparation of multifunctional chitosan microspheres by a simple sonochemical method. *Chem. - A Eur. J.* **16,** 562–567 (2010).

6. Skinner, E. Sonochemical Production of Hollow Polymer Microspheres for Responsive Delivery. (2013).

7. Skinner, E. K. & Price, G. J. Encapsulation and release of aqueous components from sonochemically produced protein microspheres. *Chem. Commun.* **48,** 9260 (2012).

8. Li, Z., Zhang, C., Wang, B., Wang, H., Chen, X., Möhwald, H. & Cui, X. Sonochemical fabrication of dual-targeted redox-responsive smart microcarriers. *ACS Appl. Mater. Interfaces* **6,** 22166–22173 (2014).

9. Cui, X., Guan, X., Zhong, S., Chen, J., Zhu, H., Li, Z., Xu, F., Chen, P. & Wang, H. Multi-stimuli responsive smart chitosan-based microcapsules for targeted drug delivery and triggered drug release. *Ultrason. Sonochem.* **38,** 145–153 (2017).

10. Cavalieri, F., Zhou, M., Caruso, F. & Ashokkumar, M. One-pot ultrasonic synthesis of multifunctional microbubbles and microcapsules using synthetic thiolated macromolecules. *Chem. Commun.* **47,** 4096 (2011).

11. Avivi, S. & Gedanken, A. S–S bonds are not required for the sonochemical formation of proteinaceous microspheres: the case of streptavidin. *Biochem. J.* **366,** 705–707 (2002).

12. Dibbern, E. M., Toublan, F. J. J. & Suslick, K. S. Formation and characterization of polyglutamate core-shell microspheres. *J. Am. Chem. Soc.* **128,** 6540–6541 (2006).

13. Avivi, S., Nitzan, Y., Dror, R. & Gedanken, A. An Easy Sonochemical Route for the Encapsulation of Tetracycline in Bovine Serum Albumin Microspheres. *J. Am. Chem. Soc.* **125,** 15712–15713 (2003).

14. Zhou, M., Leong, T. S. H., Melino, S., Cavalieri, F., Kentish, S. & Ashokkumar, M. Sonochemical synthesis of liquid-encapsulated lysozyme microspheres. *Ultrason. Sonochem.* **17,** 333–337 (2010).

15. Wong, M. & Suslick, K. Sonochemically-produced Haemoglobin Microbubbles. *Mat. Res. Soc. Symp. Proc* **372,** 89–94 (1995).

16. Ashokkumar, M., Leong, T. S. H. & Martin, G. Ultrasonic encapsulation – A review. *Ultrason. Sonochem.* **35,** 605–514 (2017).

17. Suslick, K. S. The Chemistry of Ultrasound. *Yearb. Sci. Futur.* 138–155 (1994).

18. Richards, W. T. & Loomis, A. L. The Chemical Effects of High Frequency Sound Waves I. a Preliminary Survey. *J. Am. Chem. Soc.* **49,** 3086–3100 (1927).

19. Mason, T. J. & Peters, D. *Practical Sonochemistry: Power Ultrasound Uses and Applications*. (Woodhead Publishing Limited, 2002).

20. Peters, D. Ultrasound in materials chemistry. *J. Mater. Chem.* **6,** 1605 (1996).

21. Raichel, D. R. & Hansen, U. J. The Science and Applications of Acoustics. *J. Acoust. Soc. Am.* **114,** 21 (2003).

22. Suslick, K. S. & Price, G. J. Applications of Ultrasound to Materials Chemistry. *Annu. Rev. Mater. Sci.* **29,** 295–326 (1999).

23. Suslick, K. & Crum, A. Sonochemistry and Sonoluminescence. *Encycl. Acoust.* 271–281 (1997).

24. Lord Rayleigh. VIII. On the pressure developed in a liquid during the collapse of a spherical cavity. *Philos. Mag. Ser. 6* **34,** 94–98 (1917).

25. Suslick, K., McNamara III, W. B. & Didenko, Y. Hot Spot Conditions during Multi-Bubble Cavitation. *Sonochemistry and Sonoluminescence* 191–204 (1999).

26. Leighton, T. G. *The Acoustic Bubble*. (Academic Press, 1997). doi:10.1121/1.410082

27. Ashokkumar, M. The characterization of acoustic cavitation bubbles – An overview. *Ultrason. Sonochem.* **18,** 864–872 (2011).

28. Riesz, P. & Kondo, T. Free radical formation induced by ultrasound and its biological implications. *Free Radic. Biol. Med.* **13,** 247–270 (1992).

29. Cravotto, G. & Cintas, P. Power ultrasound in organic synthesis: moving cavitational chemistry from academia to innovative and large-scale applications. *Chem. Soc. Rev.* **35,** 180–196 (2006).

30. Suslick, K. S., Hammerton, D. & Cline, R. The Sonochemical Hotspot. *Am. Chem. Soc.* **108,** 5641–5642 (1986).

31. Suslick, K. S., Didenko, Y., Fang, M. ., T, H., Kolbeck, K. ., McNamara, W. ., Mdleleni, M. . & Wong, M. Acoustic cavitation and its chemical consequences. *Philos. Trans. R. Soc.* **357,** 335–353 (1999).

32. Chen, D., Sharma, S. K. & Mudhoo, A. *Handbook on Applications of Ultrasound: Sonochemistry for Sustainability*. (CRC Press, 2011). doi:10.1201/b11012-16

33. Putterman, S. J. Sonoluminescence: Sound into Light. *Sci. Am.* **272,** 46–51 (1995).

34. Matula, T. J., Roy, R. A., Mourad, P. D., McNamara III, W. B. & Suslick, K. S. Comparison of Multibubble and Single-Bubble Sonoluminescence Spectra. *Phys. Rev. Lett.* **75,** 2602–2605 (1995).

35. McMurray, H. N. & Wilson, B. P. Mechanistic and Spatial Study of Ultrasonically Induced Luminol Chemiluminescence. *J. Phys. Chem. A* **103,** 3955–3962 (1999).

36. Wei, Z., Kosterman, J. A., Xiao, R., Pee, G. Y., Cai, M. & Weavers, L. K. Designing and characterizing a multi-stepped ultrasonic horn for enhanced sonochemical

performance. *Ultrason. Sonochem.* **27,** 325–333 (2015).

37. Margulis, M. A. *Sonochemistry and Cavitation*. (Gordon and Breach, 1995).

38. Flannigan, D. J. & Suslick, K. S. Plasma line emission during single-bubble cavitation. *Phys. Rev. Lett.* **95,** (2005).

39. Suslick, K. S. & Flint, E. B. Sonoluminescence from non-aqueous liquids. *Nature* **330,** 553–555 (1987).

40. Suslick, K. The Chemical Effects of Ultrasound. *Sci. Am.* 80–86 (1989).

41. Mason, T. J., Joyce, E., Phull, S. S. & Lorimer, J. P. Potential uses of ultrasound in the biological decontamination of water. in *Ultrason. Sonochem.* **10,** 319–323 (2003).

42. Mason, T. J. The design of ultrasonic reactors for environmental remediation. *Advences in sonochemistry* **6,** 247–268 (2001).

43. Ashokkumar, M. Applications of ultrasound in food and bioprocessing. *Ultrason. Sonochem.* **25,** 17–23 (2015).

44. Mitragotri, S. Healing sound: the use of ultrasound in drug delivery and other therapeutic applications. *Nat. Rev. Drug Discov.* **4,** 255–260 (2005).

45. Miller, D. L., Smith, N. B., Bailey, M. R., Czarnota, G. J., Hynynen, K. & Makin, I. R. S. Overview of Therapeutic Ultrasound Applications and Safety Considerations. *J. Ultrasound Med.* **31,** 623–634 (2012).

46. Jewell, M. L., Solish, N. J. & Desilets, C. S. Noninvasive body sculpting technologies with an emphasis on high-intensity focused ultrasound. *Aesthetic Plast. Surg.* **35,** 901–912 (2011).

47. Harvey, C., Pilcher, J., Eckersley, R., Blomley, M. & Cosgrove, D. Advances in Ultrasound. *Clin. Radiol.* **57,** 157–17 (2002).

48. Ranganayakulu, S. V. Ultrasound applications in Medical Sciences. *IJMTER* **3,** 287–293 (2016).

49. VanWijk, M. J., VanBavel, E., Sturk, A. & Nieuwland, R. Microparticles in

cardiovascular diseases. *Cardiovasc. Res.* **59,** 277–287 (2003).

50. Avivi, S. & Gedanken, A. The preparation of avidin microspheres using the sonochemical method and the interaction of the microspheres with biotin. *Ultrason. Sonochem.* **12,** 405–409 (2005).

51. Gedanken, A. Preparation and properties of proteinaceous microspheres made sonochemically. *Chem. - A Eur. J.* **14,** 3840–3853 (2008).

52. Cui, X., Wang, B., Zhong, S., Li, Z., Han, Y., Wang, H. & Moehwald, H. Preparation of protein microcapsules with narrow size distribution by sonochemical method. *Colloid Polym. Sci.* **291,** 2271–2278 (2013).

53. Grinstaff, M. W. & Suslick, K. S. Air-filled proteinaceous microbubbles: synthesis of an echo-contrast agent. *Proc. Natl. Acad. Sci. U. S. A.* **88,** 7708–7710 (1991).

54. Lysozyme. *Biol. Pages* (2001). at <http://www.biology-pages.info/L/Lysozyme.html>

55. Schutt, E. G., Pelura, T. J. & Hopkins, R. M. Osmotically stabilized microbubble sonographic contrast agents. *Acad. Radiol.* **3 Suppl 2,** S188–S190 (1996).

56. Tan, S., Mettu, S., Biviano, M. D., Zhou, M., Babgi, B., White, J., Dagastine, R. R. & Ashokkumar, M. Ultrasonic synthesis of stable oil filled microcapsules using thiolated chitosan and their characterization by AFM and numerical simulations. *Soft Matter* **12,** 7212–7222 (2016).

57. Shimanovich, U., Volkov, V., Eliaz, D., Aizer, A., Michaeli, S. & Gedanken, A. Stabilizing RNA by the sonochemical formation of RNA nanospheres. *Small* **7,** 1068–1074 (2011).

58. Han, Y., Radziuk, D., Shchukin, D. & Moehwald, H. Stability and size dependence of protein microspheres prepared by ultrasonication. *J. Mater. Chem.* **18,** 5162–5166 (2008).

59. Zhou, M., Cavalieri, F. & Ashokkumar, M. Tailoring the properties of ultrasonically synthesised microbubbles. *Soft Matter* **7,** 623–630 (2011).

60. Makino, K., Mizorogi, T., Ando, S., Tsukamoto, T. & Ohshima, H. Sonochemically

prepared bovine serum albumin microcapsules: Factors affecting the size distribution and the microencapsulation yield. *Colloids Surfaces B Biointerfaces* **22,** 251–255 (2001).

61. Zhou, M., Cavalieri, F., Caruso, F. & Ashokkumar, M. Confinement of acoustic cavitation for the synthesis of protein-shelled nanobubbles for diagnostics and nucleic acid delivery. *ACS Macro Lett.* **1,** 853–856 (2012).

62. Davidov-Pardo, G., Arozarena, I., Navarro, M. & Marin-Arroyo, M. R. *Microencapsulation and Microspheres for Food Applications*. *Microencapsul. Microspheres Food Appl.* (2015). doi:10.1016/B978-0-12-800350-3.00023-6

63. Sun, Q. & Deng, Y. In situ synthesis of temperature-sensitive hollow microspheres via interfacial polymerization. *J. Am. Chem. Soc.* **127,** 8274–8275 (2005).

64. O'Donnell, P. B. & McGinity, J. W. Preparation of microspheres by the solvent evaporation technique. *Adv. Drug Deliv. Rev.* **28,** 25–42 (1997).

65. Sharma, N., Madan, P. & Lin, S. Effect of process and formulation variables on the preparation of parenteral paclitaxel-loaded biodegradable polymeric nanoparticles: A co-surfactant study. *Asian J. Pharm. Sci.* **11,** 404–416 (2016).

66. Sinha, V. R. & Trehan, A. Biodegradable microspheres for protein delivery. *J. Control. Release* **90,** 261–280 (2003).

67. Kozlovskaya, V., Kharlampieva, E., Mansfield, M. L. & Sukhishvili, S. A. Poly(methacrylic acid) hydrogel films and capsules: Response to pH and ionic strength, and encapsulation of macromolecules. *Chem. Mater.* **18,** 328–336 (2006).

68. Chai, F., Sun, L., He, X., Li, J., Liu, Y., Xiong, F., Ge, L., Webster, T. J. & Zheng, C. Doxorubicin-loaded poly (lactic-co-glycolic acid) nanoparticles coated with chitosan/alginate by layer by layer technology for antitumor applications. *Int. J. Nanomedicine* **12,** 1791–1802 (2017).

69. Decher, G. & Hong, J. D. Buildup of ultrathin multiplayer films by a self-assembly process. II. Consecutive absorption of anionie and cationic bipolar amphiphiles and polyeleetrolytes on charged surfaces. *Ber Bunsen-Ges Phys Chem* **95,** 1430–1434 (1991).

70. Zelikin, A. N., Quinn, J. F. & Caruso, F. Disulfide cross-linked polymer capsules: En route to biodeconstructible systems. *Biomacromolecules* **7,** 27–30 (2006).

71. Stride, E. & Edirisinghe, M. Novel microbubble preparation technologies. *Soft Matter* **4,** 2350 (2008).

72. Radulescu, D., Schwade, N., Wawro, D. & USA, M. T. I. Paclitaxel-Loaded Biodegradable Microspheres Manufactured by Ink-Jet Technology. in *11th Int. Symp. Expo. Recent Adv. Drug Deliv. Syst.* 1–5 (2003). doi:10.1007/s13398-014-0173-7.2

73. Farook, U., Stride, E. & Edirisinghe, M. . Preparation of suspensions of phospholipid-coated microbubbles by coaxial electrohydrodynamic atomization. *J. R. Soc. Interface* **6,** 271–277 (2009).

74. Farook, U., Edirisinghe, M. J., Stride, E. & Colombo, P. Novel co-axial electrohydrodynamic in-situ preparation of liquid-filled polymer-shell microspheres for biomedical applications. *J. Microencapsul.* **25,** 241–247 (2008).

75. Pareta, R. & Edirisinghe, M. J. A novel method for the preparation of biodegradable microspheres for protein drug delivery. *J. R. Soc. Interface* **3,** 573–582 (2006).

76. Ahmad, Z., Zhang, H. ., Farook, U., Edirisinghe, M., Stride, E. & Colombo, P. Generation of multilayered structures for biomedical applications using a novel tri-needle coaxial device and electrohydrodynamic flow. *J. R. Soc. Interface* **5,** 1255–1261 (2008).

77. Collins, D. J., Neild, A., DeMello, A., Liu, A.-Q. & Ai, Y. The Poisson distribution and beyond: methods for microfluidic droplet production and single cell encapsulation. *Lab Chip* **15,** 3439–3459 (2015).

78. Talu, E., Hettiarachchi, K., Powell, R. L., Lee, A. P., Dayton, P. A. & Longo, M. L. Maintaining monodispersity in a microbubble population formed by flow-focusing. *Langmuir* **24,** 1745–1749 (2008).

79. Grinberg, O., Shimanovich, U. & Gedanken, A. Encapsulating bioactive materials in sonochemically produced micro- and nano-spheres. *J. Mater. Chem. B* **1,** 595–605 (2013).

80. Grinberg, O., Gedanken, A., Patra, C. R., Patra, S., Mukherjee, P. & Mukhopadhyay, D. Sonochemically prepared BSA microspheres containing Gemcitabine, and their potential application in renal cancer therapeutics. *Acta Biomater.* **5,** 3031–3037 (2009).

81. Gedanken, A., Shimanovich, U., Shav-Tal, Y., Michaeli, S., Eliaz, D., Aizer, A., Cavaco-Paulo, A. M. & Zigdon, S. Proteinaceous microspheres for targeted RNA delivery made by ultrasonic emulsification method. *J. Mater. Chem. B* 82–90 (2013).

82. Agnihotri, N., Mishra, R., Goda, C. & Arora, M. Microencapsulation – A Novel Approach in Drug Delivery : A Review. *J. Pharm. Sci.* **2,** 1–20 (2012).

83. Avivi, S., Felner, I., Novik, I. & Gedanken, A. The preparation of magnetic proteinaceous microspheres using the sonochemical method. *Biochim. Biophys. Acta - Gen. Subj.* **1527,** 123–129 (2001).

84. Krishnamurthy, R., Lumpkin, J. A. & Sridhar, R. Inactivation of lysozyme by sonication under conditions relevant to microencapsulation. *Int. J. Pharm.* **205,** 23–34 (2000).

85. Ward, M. A. & Georgiou, T. K. Thermoresponsive Polymers for Biomedical Applications. *Polymers (Basel).* **3,** 1215–1242 (2011).

86. Kim, K. K. & Pack, D. W. in *BioMEMS Biomed. Nanotechnol.* 19–50 (2006). doi:10.1007/978-0-387-25842-3_2

87. Hernot, S. & Klibanov, A. L. Microbubbles in ultrasound-triggered drug and gene delivery. *Adv. Drug Deliv. Rev.* **60,** 1153–1166 (2008).

88. Fujishige, S., Kubota, K. & Ando, I. Phase transition of aqueous solutions of poly(N-isopropylacrylamide) and poly(N-isopropylmethacrylamide). *J. Phys. Chem.* **93,** 3311–3313 (1989).

89. Cheng, C. J., Chu, L. Y., Ren, P. W., Zhang, J. & Hu, L. Preparation of monodisperse thermo-sensitive poly(N-isopropylacrylamide) hollow microcapsules. *J. Colloid Interface Sci.* **313,** 383–388 (2007).

90. Choi, C.-H., Jung, J.-H., Kim, D.-W., Chung, Y.-M. & Lee, C.-S. Novel one-pot route to monodisperse thermosensitive hollow microcapsules in a microfluidic

system. *Lab Chip* **8,** 1544 (2008).

91. Grinberg, O., Hayun, M., Sredni, B. & Gedanken, A. Characterization and activity of sonochemically-prepared BSA microspheres containing Taxol - An anticancer drug. *Ultrason. Sonochem.* **14,** 661–666 (2007).

92. Grinberg, O. & Gedanken, A. The development and characterization of starch microspheres prepared by a sonochemical method for the potential drug delivery of insulin. *Macromol. Chem. Phys.* **211,** 924–931 (2010).

93. Wu, S., Jiang, W., Zhang, X., Sun, H., Zhang, W., Dai, J., Liu, L., Chen, X. & Li, F. A sonochemical route for the encapsulation of drug in magnetic microspheres. *J. Magn. Magn. Mater.* **324,** 124–127 (2012).

94. Makino, K., Mizorogi, T., Ando, S., Tsukamoto, T. & Ohshima, H. Sustained release of hydrophobic materials from sonochemically prepared bovine serum albumin microcapsules. *Colloids Surfaces B Biointerfaces* **23,** 59–64 (2002).

95. Reytblat, I., Lipovsky, A. & Gedanken, A. DNA Microspheres Coated with Bioavailable Polymer as an Efficient Gene Expression Agent in Yeasts. *J. Nanomater.* **2016,** 1–8 (2016).

96. Shimanovich, U., Tkacz, I. D., Eliaz, D., Cavaco-Paulo, A., Michaeli, S. & Gedanken, A. Encapsulation of RNA molecules in BSA microspheres and internalization into trypanosoma brucei parasites and human U2OS cancer cells. *Adv. Funct. Mater.* **21,** 3659–3666 (2011).

97. Rytblat, I., Wu, N., Xu, H., Gedanken, A. & Lin, X. In vitro studies of polyethyleneimine coated miRNA microspheres as anticancer agents. *Nano Res.* **9,** 1609–1617 (2016).

98. Toublan, F. J. J., Boppart, S. & Suslick, K. S. Tumor targeting by surface-modified protein microspheres. *J. Am. Chem. Soc.* **128,** 3472–3473 (2006).

99. Klibanov, A. L. Targeted delivery of gas-filled microspheres, contrast agents for ultrasound imaging. *Adv. Drug Deliv. Rev.* **37,** 139–157 (1999).

100. Xu, F., Zhao, T., Yang, T., Dong, L., Guan, X. & Cui, X. Fabrication of folic acid functionalized pH-responsive and thermosensitive magnetic chitosan microcapsules

via a simple sonochemical method. *Colloids Surfaces A Physicochem. Eng. Asp.* **490,** 22–29 (2016).

101. Cosgrove, D. Ultrasound contrast agents: An overview. *Eur. J. Radiol.* **60,** 324–330 (2006).

102. Postema, A. W., Frinking, P. J. A., Smeenge, M., De Reijke, T. M., De La Rosette, J. J. M. C. H., Tranquart, F. & Wijkstra, H. Dynamic contrast-enhanced ultrasound parametric imaging for the detection of prostate cancer. *BJU Int.* **117,** 598–603 (2016).

103. Otto, C. M. *The Practice of Clinical Echocardiography*. (Saunders/Elsevier, 2012).

104. Korpanty, G., Grayburn, P. A., Shohet, R. V & Brekken, R. A. Targeting vascular endothelium with avidin microbubbles. *Ultrasound Med. Biol.* **31,** 1279–1283 (2005).

105. Kopczyńska, E. & Makarewicz, R. Endoglin - A marker of vascular endothelial cell proliferation in cancer. *Contemp. Oncol.* **16,** 68–71 (2012).

106. Poehlmann, M., Grishenkov, D., Kothapalli, S. V. V. N., Härmark, J., Hebert, H., Philipp, A., Hoeller, R., Seuss, M., Kuttner, C., Margheritelli, S., Paradossi, G. & Fery, A. On the interplay of shell structure with low- and high-frequency mechanics of multifunctional magnetic microbubbles. *Soft Matter* **10,** 214–26 (2013).

107. Díaz-López, R., Tsapis, N. & Fattal, E. Liquid perfluorocarbons as contrast agents for ultrasonography and 19F-MRI. *Pharm. Res.* **27,** 1–16 (2010).

108. Webb, A. G., Wong, M., Kolbeck, K. J., Magin, R. & Suslick, K. S. Sonochemically produced fluorocarbon microspheres: a new class of magnetic resonance imaging agent. *J. Magn. Reson. Imaging* **6,** 675–683 (1996).

109. Vasir, J. K., Tambwekar, K. & Garg, S. Bioadhesive microspheres as a controlled drug delivery system. *Int. J. Pharm.* **255,** 13–32 (2003).

110. Genta, I., Conti, B., Perugini, P., Pavanetto, F., Spadaro, A. & Puglisi, G. Bioadhesive microspheres for ophthalmic administration of acyclovir. *J. Pharm. Pharmacol.* **49,** 737–742 (1997).

111. Gouveia, I. C. Synthesis and characterization of a microsphere-based coating for textiles with potential as an in situ bioactive delivery system. *Polym. Adv. Technol.* **23,** 350–356 (2012).

112. Angel, U., Silva, C. M., Cavaco-Paulo, A. & Gedanken, A. Attaching different kinds of proteinaceous nanospheres to a variety of fabrics using ultrasound radiation. *Isr. J. Chem.* **50,** 524–529 (2010).

113. Dubey, R., Shami, T. C. & Bhasker Rao, K. U. Microencapsulation technology and applications. *Def. Sci. J.* **59,** 82–95 (2009).

114. Zhou, M., Cavalieri, F. & Ashokkumar, M. in *Handb. Ultrason. Sonochemistry* 1021–1047 (2016). doi:10.1007/978-981-287-278-4_22

115. Tzhayik, O., Cavaco-Paulo, A. & Gedanken, A. Fragrance release profile from sonochemically prepared protein microsphere containers. *Ultrason. Sonochem.* **19,** 858–863 (2012).

116. Nogueira Rodrigues Teixeira, C. S. Microencapsulation of Perfumes For Application in Textile Industry. *Dissertation* (2010).

117. Ciriminna, R. & Pagliaro, M. Sol–gel microencapsulation of odorants and flavors: opening the route to sustainable fragrances and aromas. *Chem. Soc. Rev. Chem. Soc. Rev* **42,** 9243–9250 (2013).

118. Fan, L., Jin, R., Le, X., Zhou, X., Chen, S., Liu, H. & Xiong, Y. Chitosan microspheres for controlled delivery of auxins as agrochemicals. *Microchim. Acta* **176,** 381–387 (2012).

119. Terada, T., Ohtsubo, T., Iwao, Y., Noguchi, S. & Itai, S. Evaluation of the Thermosensitive Release Properties of Microspheres containing an Agrochemical Compound. *Chem. Pharm. Bull* **65,** 49–55 (2017).

120. Young, R. J. & Lovell, P. A. *Introduction to polymers*. (CRC Press, 2011).

121. Dietrich, B. Origins and Devlopment of Initiation of Free Radical Polymerization Processes. *Int. J. Polym. Sci.* **2009,** (2009).

122. Solomon, D. H. Nitroxide-mediated living radical polymerisation - CSIROpedia.

Pers. Commun. (2009). at <https://csiropedia.csiro.au/nitroxide-mediated-living-radical-polymerisation/>

123. Matyjaszewski, K. & Spanswick, J. Controlled/living radical polymerization. *Mater. Today* **8,** 26–33 (2005).

124. Chiefari, J., Chong, Y. K., Ercole, F., Krstina, J., Jeffery, J., T Le, T. P., A Mayadunne, R. T., Meijs, G. F., Moad, C. L., Moad, G., Rizzardo, E. & Thang, S. H. Living Free-Radical Polymerization by Reversible Addition-Fragmentation Chain Transfer: The RAFT Process. *Macromolecules* **31,** 5559–5562 (1998).

125. Lowe, A. B. & McCormick, C. L. Reversible addition-fragmentation chain transfer (RAFT) radical polymerization and the synthesis of water-soluble (co)polymers under homogeneous conditions in organic and aqueous media. *Prog. Polym. Sci.* **32,** 283–351 (2007).

126. Lu, L., Yang, N. & Cai, Y. Well-controlled reversible addition-fragmentation chain transfer radical polymerisation under ultraviolet radiation at ambient temperature. *Chem. Commun.* 5287–5288 (2005).

127. Moad, G., Mayadunne, R. T. A., Rizzardo, E., Skidmore, M. & Thang, S. H. Kinetics and mechanism of RAFT polymerization. *ACS Symp. Ser.* **854,** 520 (2003).

128. Moad, G., Rizzardo, E. & Thang, S. H. Radical addition-fragmentation chemistry in polymer synthesis. *Polymer (Guildf).* **49,** 1079–1131 (2008).

129. Keddie, D. J., Moad, G., Rizzardo, E. & Thang, S. H. RAFT agent design and synthesis. *Macromolecules* **45,** 5321–5342 (2012).

130. Ganachaud, F., Monteiro, M. J., Gilbert, R. G., Dourges, M. A., Thang, S. H. & Rizzardo, E. Molecular weight characterization of poly(N-isopropylacrylamide) prepared by living free-radical polymerization. *Macromolecules* **33,** 6738–6745 (2000).

131. Moad, G. & Solomon, D. H. The Chemistry of Radical Polymerization. 665 (2005). at <http://books.google.com/books?hl=en&lr=&id=Gj1hgUhBWLkC&pgis=1>

132. Moad, G., Chiefari, J., Mayadunne, R. T. A., Moad, C. L., Postma, A., Rizzardo, E. & Thang, S. H. Initiating free radical polymerization. *Macromol. Symp.* **182,** 65–80

(2002).

133. Chong, Y. K. B., Krstina, J., Le, T. P. T., Moad, G., Postma, A., Rizzardo, E. & Thang, S. H. Thiocarbonylthio Compounds [S=C(Ph)S - R] in Free Radical Polymerization with Reversible Addition-Fragmentation Chain Transfer (RAFT Polymerization). Role of the Free-Radical Leaving Group (R). *Macromolecules* **36,** 2256–2272 (2003).

134. Chaduc, I., Lansalot, M., D 'agosto, F. & Charleux, B. RAFT Polymerization of Methacrylic Acid in Water. *Macromolecules* **45,** 1241–1247 (2012).

135. Truong, N. P., Quinn, J. F., Anastasaki, A., Rolland, M., Vu, M. N., Haddleton, D. M., Whittaker, M. R. & Davis, T. P. Surfactant-free RAFT emulsion polymerization using a novel biocompatible thermoresponsive polymer. *Polym. Chem.* **8,** 1353–1363 (2017).

136. Rieger, J., Zhang, W., Stoffelbach, F. & Charleux, B. Surfactant-free RAFT emulsion polymerization using poly(N,N -dimethylacrylamide) trithiocarbonate macromolecular chain transfer agents. *Macromolecules* **43,** 6302–6310 (2010).

137. Huang, W., Gu, W., Yang, H., Xue, X., Jiang, B., Zhang, D., Fang, J., Chen, J., Yang, Y. & Guo, J. Preparation and properties of branched polystyrene through radical suspension polymerization. *Polymers (Basel).* **9,** (2017).

138. Zhang, Z., Zhu, X., Zhu, J., Cheng, Z. & Zhu, S. Thermal-initiated reversible addition-fragmentation chain transfer polymerization of methyl methacrylate in the presence of oxygen. *J. Polym. Sci. Part A Polym. Chem.* **44,** 3343–3354 (2006).

139. Rizzardo, E., Moad, G. & Thang, S. Reversible Addition Fragmentation Chain Transfer (RAFT) Polymerisation. *Mater. Matters* **5,** 2–8 (2010).

140. Patten, T. E. & Matyjaszewski, K. Atom transfer radical polymerization and the synthesis of polymeric materials. *Adv. Mater.* **10,** 901–915 (1999).

141. Matyjaszewski, K. Features of Controlled 'Living' Radical Polymerizations - Matyjaszewski Polymer Group - Carnegie Mellon University. (2001). at <http://www.cmu.edu/maty/crp/features.html#first-order-kinetics>

142. Braunecker, W. A. & Matyjaszewski, K. Controlled/living radical polymerization:

Features, developments, and perspectives. *Prog. Polym. Sci.* **32,** 93–146 (2007).

143. Chong, B. Y. K., Le, T. P. T., Moad, G., Rizzardo, E. & Thang, S. H. A more versatile route to block copolymers and other polymers of complex architecture by living radical polymerization: the RAFT process. *Macromolecules* **32,** 2071–2074 (1999).

144. Nicolaÿ, R., Kwak, Y. & Matyjaszewski, K. Synthesis of poly(vinyl acetate) block copolymers by successive RAFT and ATRP with a bromoxanthate iniferter. *Chem. Commun. (Camb).* **35,** 5336–8 (2008).

145. Keddie, D. J. A guide to the synthesis of block copolymers using reversible-addition fragmentation chain transfer (RAFT) polymerization. *Chem. Soc. Rev.* **43,** 496–505 (2014).

146. Mayadunne, R. T. A., Rizzardo, E., Chiefari, J., Krstina, J., Moad, G., Postma, A. & Thang, S. H. Living polymers by the use of trithiocarbonates as reversible addition-fragmentation chain transfer (RAFT) agents: ABA triblock copolymers by radical polymerization in two steps. *Macromolecules* **33,** 243–245 (2000).

147. Mayadunne, R. T. A., Jeffery, J., Moad, G. & Rizzardo, E. Living free radical polymerization with reversible addition-fragmentation chain transfer (RAFT polymerization): Approaches to star polymers. *Macromolecules* **36,** 1505–1513 (2003).

148. Nasrullah, M. J., Vora, A. & Webster, D. C. Block copolymer synthesis via a combination of ATRP and RAFT using click chemistry. *Macromol. Chem. Phys.* **212,** 539–549 (2011).

149. Anandhakumar, S., Nagaraja, V. & Raichur, A. M. Reversible polyelectrolyte capsules as carriers for protein delivery. *Colloids Surfaces B Biointerfaces* **78,** 266–274 (2010).

150. Bergmann, C. P. & Stumpf, A. in *Dent. Ceram. Microstruct. Prop. Degrad.* 9–13 (2013). doi:10.1007/978-3-642-38224-6_2

151. Yang, C. & Cheng, Y. L. RAFT synthesis of poly(N-isopropylacrylamide) and poly(methacrylic acid) homopolymers and block copolymers: Kinetics and

characterization. *J. Appl. Polym. Sci.* **102,** 1191–1201 (2006).

152. Pelet, J. M. & Putnam, D. High molecular weight poly(methacrylic acid) with narrow polydispersity by RAFT polymerization. *Macromolecules* **42,** 1494–1499 (2009).

153. Nejad, E. H., Castignolles, P., Gilbert, R. G. & Guillaneuf, Y. Synthesis of methacrylate derivatives oligomers by dithiobenzoate-RAFT- mediated polymerization. *J. Polym. Sci. Part A Polym. Chem.* **46,** 2277–2289 (2008).

154. Petko, D. & Shipp, D. Synthesis of Poly (Methacrylic Acid) using RAFT Polymerization. 54–57 (2006). at <www.clarkson.edu/honors/research/summer_papers/Petko-Danielle.doc>

155. Sprong, E., De Wet-Roos, D., Tonge, M. P. & Sanderson, R. D. Characterization and rheological properties of model alkali-soluble rheology modifiers synthesized by reversible addition-fragmentation chain-transfer polymerization. *J. Polym. Sci. Part A Polym. Chem.* **41,** 223–235 (2003).

156. Schmaljohann, D. Thermo- and pH-responsive polymers in drug delivery. *Adv. Drug Deliv. Rev.* **58,** 1655–1670 (2006).

157. Schild, H. G. Poly(N-isopropylacrylamide): experiment, theory and application. *Prog. Polym. Sci.* **17,** 163–249 (1992).

158. American Cyanamid Company, Brochure IC3-1354-500-4/63, N-isopropylacrylamide. (1963).

159. Scarpa, J. S., Letourneau, R. L., Lindeman, L. P., Stone, E. W. & Maki, A. H. The change in the hyperfine coupling constants of the Slow Hydrogen-Deuterium Exchange in a Non-a-helical Polyamide. *J. Chem. Phys* **37,** (1962).

160. Pelton, R. Poly(N-isopropylacrylamide) (PNIPAM) is never hydrophobic. *J. Colloid Interface Sci.* **348,** 673–4 (2010).

161. Fundueanu, G., Constantin, M., Stanciu, C., Theodoridis, G. & Ascenzi, P. PH- and temperature-sensitive polymeric microspheres for drug delivery: The dissolution of copolymers modulates drug release. *J. Mater. Sci. Mater. Med.* **20,** 2465–2475 (2009).

162. Yan, Y., Huang, L., Zhang, Q. & Zhou, H. Concentration effect on aggregation and dissolution behavior of poly(N-isopropylacrylamide) in water. *J. Appl. Polym. Sci.* **132,** 41669 (2015).

163. Ray, B., Okamoto, Y., Kamigaito, M., Sawamoto, M., Seno, K.-I., Kanaoka, S. & Aoshima, S. Effect of Tacticity of Poly(N-isopropylacrylamide) on the Phase Separation Temperature of Its Aqueous Solutions. *Polym. J.* **37,** 234–237 (2005).

164. Yarin, A. & Zhang, Y. Stimuli-responsive copolymers of n-isopropyl acrylamide with enhanced longevity in water for micro- and nanofluidics, drug delivery and non-woven applications. *J. Mater. Chem.* **19,** 4732–4739 (2009).

165. Furyk, S., Zhang, Y., Ortiz-Acosta, D., Cremer, P. S. & Bergbreiter, D. E. Effects of end group polarity and molecular weight on the lower critical solution temperature of poly(N-isopropylacrylamide). *J. Polym. Sci. Part A Polym. Chem.* **44,** 1492–1501 (2006).

166. Schild, H. G. & Tirrell, D. A. Microcalorimetric detection of lower critical solution temperatures in aqueous polymer solutions. *J. Phys. Chem.* **94,** 4352–4356 (1990).

167. Feil, H., Bae, Y. H., Feijen, J. & Kim, S. W. Effect of comonomer hydrophilicity and ionization on the lower critical solution temperature of N-isopropylacrylamide copolymers. *Macromolecules* **26,** 2496–2500 (1993).

168. Jain, K., Vedarajan, R., Watanabe, M., Ishikiriyama, M. & Matsumi, N. Tunable LCST behavior of poly(N-isopropylacrylamide/ionic liquid) copolymers. *Polym. Chem.* **6,** 6819–6825 (2015).

169. Abraham, T. N., Raj, V., Prasad, T., Kumar, P. R. A., Sreenivasan, K. & Kumary, T. V. A novel thermoresponsive graft copolymer containing phosphorylated HEMA for generating detachable cell layers. *J. Appl. Polym. Sci.* **115,** 52–62 (2010).

170. Shieh, Y.-T., Lin, P.-Y., Chen, T. & Kuo, S.-W. Temperature-, pH- and CO2-Sensitive Poly(N-isopropylacryl amide-co-acrylic acid) Copolymers with High Glass Transition Temperatures. *Polymers (Basel).* **8,** 434 (2016).

171. Yoshida, R., Uchida, K., Kaneko, Y., Sakai, K., Kikuchi, A., Sakurai, Y. & Okano, T. Comb-type grafted hydrogels with rapid deswelling response to temperature

changes. *Nature* **374,** 240–242 (1995).

172. Bulmus, V., Stayton, P. & Hoffman, A. Site-Specific Polymer-Streptavidin Bioconjugate for pH-Controlled Binding and Triggered Release of Biotin. *Bioconjugate Chem* **11,** 78−83 (2000).

173. Pollet, B. G. Let's Not Ignore the Ultrasonic Effects on the Preparation of Fuel Cell Materials. *Electrocatalysis* **5,** 330–343 (2014).

174. García, D. M., Escobar, J. L., Bada, N., Casquero, J., Hernáez, E. & Katime, I. Synthesis and characterization of poly(methacrylic acid) hydrogels for metoclopramide delivery. *Eur. Polym. J.* **40,** 1637–1643 (2004).

175. Bassuoni, Y. F., Elzanfaly, E. S., Essam, H. M. & Zaazaa, H. E.-S. Development and validation of stability indicating TLC densitometric and spectrophotometric methods for determination of Clobetasol propionate. *Bull. Fac. Pharmacy, Cairo Univ.* **54,** 165–174 (2016).

176. Lewis, I., Jofre, F., Anderson, M. E. & Markley, J. L. Propionic Acid (C3H6O2). *Biol. Magn. Reson. Data Bank, Univ. Wisconsin Syst.* at <http://bmrb.wisc.edu/metabolomics/mol_summary/show_data.php?molName=propionic_acid&id=bmse000179&whichTab=1>

177. Johnson, C. S. Diffusion Ordered Nuclear Magnetic Resonance Spectroscopy: Principles and Applications. *Prog. NMR Spectrosc.* **34,** 203–256 (1999).

178. Kerssebaum, R. & Salnikov, G. DOSY and Diffusion by NMR - A Tutorial for TopSpin 2.0. 1–32 (2002). at <http://www.nmr.ucdavis.edu/docs/dosy.pdf>

179. Li, Q., Bao, Y., Wang, H., Du, F., Li, Q., Jin, B. & Bai, R. A facile and highly efficient strategy for esterification of poly(meth)acrylic acid with halogenated compounds at room temperature promoted by 1,1,3,3-tetramethylguanidine. *Polym. Chem.* **4,** 2891 (2013).

180. Winnik, F. M. Fluorescence Studies of Aqueous Solutions of Poly (N-isopropylacrylamide) below and above Their LCST. *Macromolecules* **242,** 233–242 (1990).

181. Zhang, Y., Furyk, S., Bergbreiter, D. E. & Cremer, P. S. Specific ion effects on the

water solubility of macromolecules: PNIPAM and the Hofmeister series. *J. Am. Chem. Soc.* **127,** 14505–14510 (2005).

182. Beals, M., Gross, L. & Harrell, S. MAINTAINING CELLULAR CONDITIONS: pH AND BUFFERS. *Univ. Tennessee* (1999). at <http://www.tiem.utk.edu/~gross/bioed/webmodules/phbuffers.html>

183. Malvern Instruments Ltd. Polymer Characterisation Using Light Scattering Techniques and Equipment From Malvern Instruments. (2005). at <http://www.azonano.com/article.aspx?ArticleID=1232>

184. Malvern Instruments Ltd. Zetasizer Nano Series. 1–20 (2017).

185. Instruments, M. Dynamic Light Scattering. *Malvern Guid.* 1–6 (2011).

186. Cruickshank Miller, C. The Stokes Einstein Law for Diffusion in Solution. *Proc. R. Soc. London. Ser. A, Contain. Pap. a Math. Phys. Character* **106,** 724–749 (1924).

187. Chen, A., Wu, D. & Johnson, C. S. Determination of Molecular Weight Distributions of Polymers by Diffusion-Ordered NMR. *J. Am. Chem. Soc.* **117,** 7965–7970 (1995).

188. Boyd, A. How to Prepare Samples for NMR. *Heriot-Watt Univ.* (1999). at <http://nmr.chem.umn.edu/samprep.html>

189. Tang, T., Castelletto, V., Parras, P., Hamley, I. W., King, S. M., Roy, D., Perrier, S., Hoogenboom, R. & Schubert, U. S. Thermo-responsive poly(methyl methacrylate)-block-poly(N- isopropylacrylamide) block copolymers synthesized by RAFT polymerization: Micellization and gelation. *Macromol. Chem. Phys.* **207,** 1718–1726 (2006).

190. Topp, M. D. C., Dijkstra, P. J., Talsma, H. & Feijen, J. Thermosensitive Micelle-Forming Block Copolymers of Poly(ethylene glycol) and Poly(N - isopropylacrylamide). *Macromolecules* **30,** 8518–8520 (1997).

191. Adelsberger, J., Kulkami, A., Jain, A., Wang, W., Bivigou-Koumba, A. M., Busch, P., Pipich, V., Holderer, O., Hellweg, T., Laschewsky, A., Müller-Buschbaum, P. & Papadakis, C. M. Thermoresponsive PS-b-PNIPAM-b-PS Micelles: Aggregation behavior, segmental dynamics, and thermal response. *Macromolecules* **43,** 2490–2501 (2010).

192. Zhang, J. & Peppas, N. A. Molecular interactions in poly(methacrylic acid)/poly(N-isopropyl acrylamide) interpenetrating polymer networks. *J. Appl. Polym. Sci.* **82,** 1077–1082 (2001).

193. Mukherji, D., Wagner, M., Watson, M. D., Winzen, S., de Oliveira, T. E., Marques, C. M. & Kremer, K. Relating side chain organization of PNIPAm with its conformation in aqueous methanol. *Soft Matter* **12,** 7995–8003 (2016).

194. Guerrero-Sanchez, C., O'Brien, L., Brackley, C., Keddie, D. J., Saubern, S. & Chiefari, J. Quasi-block copolymer libraries on demand via sequential RAFT polymerization in an automated parallel synthesizer. *Polym. Chem.* **4,** 1857 (2013).

195. Haven, J. J., Guerrero-Sanchez, C., Keddie, D. J., Moad, G., Thang, S. H. & Schubert, U. S. One pot synthesis of higher order quasi-block copolymer libraries via sequential RAFT polymerization in an automated synthesizer. *Polym. Chem.* **5,** 5236–5246 (2014).

196. ThermoFisher & Scientific. Carbodiimide Crosslinker Chemistry. *Thermo Fish. Sci.* (2016). at <https://www.thermofisher.com/uk/en/home/life-science/protein-biology/protein-biology-learning-center/protein-biology-resource-library/pierce-protein-methods/carbodiimide-crosslinker-chemistry.html>

197. Infrared spectroscopy absorption table. *OChemOnline* 1–7 (2013). at <http://www.ochemonline.com/Infrared_spectroscopy_absorption_table>

198. Silverstein, R. M., Bassler Clayton G. & C., M. T. *Spectrometric identification of organic compounds*. (Wiley and Sons, 1981). doi:10.1016/0022-2860(76)87024-X

199. Iida, Y., Yasui, K., Tuziuti, T. & Sivakumar, M. Sonochemistry and its dosimetry. *Microchem. J.* **80,** 159–164 (2005).

200. Mason, T. J. *Advances in Sonochemistry - Volume 5*. (JAI Press, 1999).

201. Qsonica. Qsonica Sonicators. *QSonica Ultrason. Liq. Process.* (2016). at <http://www.sonicator.com/literature/faq.shtml>

202. Tauber, A., Mark, G., Schuchmann, H.-P. & von Sonntag, C. Sonolysis of tert-butyl alcohol in aqueous solution. *J. Chem. Soc. Perkin Trans. 2* **2,** 1129–1136 (1999).

203. Cho, Y. H., Kim, S., Bae, E. K., Mok, C. K. & Park, J. Formulation of cosurfactant free o/w microemulsion using nonionic surfactant mixtures. *J. Food Sci.* **73,** 115–121 (2008).

204. Stoll, V. S. & Blanchard, J. S. in *Guid. to Protein Purif.* **Volume 182,** 24–38 (Academic Press, 1990).

205. Bittner, B., Witt, C., Mäder, K. & Kissel, T. Degradation and protein release properties of microspheres prepared from biodegradable poly(lactide-co-glycolide) and ABA triblock copolymers: influence of buffer media on polymer erosion and bovine serum albumin release. *J. Control. Release* **60,** 297–309 (1999).

206. Quinn, J. F., Johnston, A. P. R., Such, G. K., Zelikin, A. N. & Caruso, F. Next generation, sequentially assembled ultrathin films: beyond electrostatics. *Chem. Soc. Rev.* **36,** 707 (2007).

207. Sung, Y. Y. & Rubner, M. F. Micropatterning of polymer thin films with pH-sensitive and cross-linkable hydrogen-bonded polyelectrolyte multilayers. *J. Am. Chem. Soc.* **124,** 2100–2101 (2002).

208. Grant, D. . & Grassie, N. The Thermal Decomposition of Poly(methacrylic Acid). *Polymer (Guildf).* **1,** 125–134 (1959).

209. O'Connor, C. Acidic and basic amide hydrolysis. *Q. Rev. Chem. Soc.* **24,** 553 (1970).

210. Morgado, P., Black, J., Lewis, J. Ben, Iacovella, C. R., McCabe, C., Martins, L. F. G. & Filipe, E. J. M. Viscosity of liquid systems involving hydrogenated and fluorinated substances: Liquid mixtures of (hexane+perfluorohexane). *Fluid Phase Equilib.* **358,** 161–165 (2013).

211. Tetradecafluorohexane 99%. *Sigma Aldrich* (2017). at <http://www.sigmaaldrich.com/catalog/product/aldrich/281042?lang=en&region=GB>

212. Dymond, J. H. & O/ye, H. A. Viscosity of Selected Liquid n-Alkanes. *J. Phys. Chem. Ref. Data* **23,** 41–53 (1994).

213. Tetradecane ≥99%. *Sigma Aldrich* (2017). at <http://www.sigmaaldrich.com/catalog/product/aldrich/172456?lang=en&region=

GB>

214. Committee to Evaluate Drugs. Isopropyl Myristate. *Sigma Aldrich* 5–7 (2010). at <http://www.sigmaaldrich.com/catalog/product/aldrich/172472?lang=en&region=GB>

215. Diamante, L. M. & Lan, T. Absolute Viscosities of Vegetable Oils at Different Temperatures and Shear Rate Range of 64 . 5 to 4835 s − 1. *J. Food Process.* 1–6 (2014). doi:10.1155/2014/234583

216. Haufe, D., Dahmen, K. G., Tiebel, O., Hubler, M. & Koch, T. Effect of perfluorohexane on the expression of cellular adhesion molecules and surfactant protein A in human mesothelial cells in vitro. *Artif Cells Blood Substit Immob. Biotechnol* **39,** 239–246 (2011).

217. Ushikubo, F. Y. & Cunha, R. L. Stability mechanisms of liquid water-in-oil emulsions. *Food Hydrocoll.* **34,** 145–153 (2014).

218. Canselier, J. P., Delmas, H., Wilhelm, A. M., Abismaïl, B., Delmas, H., Wilhelm, A. M. & Ultrasound, B. A. Ultrasound Emulsification — An Overview. *J. Dispers. Sci. Technol.* **23,** 333–349 (2002).

219. Jiao, J. & Burgess, D. J. Ostwald ripening of water-in-hydrocarbon emulsions. *J. Colloid Interface Sci.* **264,** 509–516 (2003).

220. Capdevila, M., Maestro, A., Porras, M. & Gutiérrez, J. M. Preparation of Span 80/oil/water highly concentrated emulsions: Influence of composition and formation variables and scale-up. *J. Colloid Interface Sci.* **345,** 27–33 (2010).

221. Wijaya, E. C., Separovic, F., Drummond, C. J. & Greaves, T. L. Micelle formation of a non-ionic surfactant in non-aqueous molecular solvents and protic ionic liquids (PILs). *Phys. Chem. Chem. Phys. Phys. Chem. Chem. Phys* **18,** 24377–24386 (2016).

222. Sjöblom, J. Emulsions and Emulsion Stability. *Emuls. Emuls. Stab.* 185–223 (2006). doi:10.1016/0300-9572(85)90015-2

223. Márquez, A. L., Medrano, A., Panizzolo, L. A. & Wagner, J. R. Effect of calcium salts and surfactant concentration on the stability of water-in-oil (w/o) emulsions prepared with polyglycerol polyricinoleate. *J. Colloid Interface Sci.* **341,** 101–108

(2010).

224. Koroleva, M. Y. & Yurtov, E. V. Effect of ionic strength of dispersed phase on Ostwald ripening in water-in-oil emulsions. *Colloid J. Russ. Acad. Sci. Kolloidn. Zhurnal* **65,** 40–43 (2003).

225. Abbott, S. *Surfactant Science, Principles and Practice*. (Creative Commons BY-ND, 2015). at <https://www.stevenabbott.co.uk/practical-surfactants/the-book.php>

226. Surface tension values of some common test liquids for surface energy analysis. *DataPhysics Instruments GmbH* **49,** 0–4 (2017).

227. Krasowska, M., Zawala, J. & Malysa, K. Air at hydrophobic surfaces and kinetics of three phase contact formation. *Adv. Colloid Interface Sci.* **147–148,** 155–169 (2009).

228. Krafft, M. P. & Riess, J. G. Reverse water-in-fluorocarbon emulsions as a drug delivery system: an in vitro study. *Colloids Surfaces A Physicochem. Eng. Asp.* **147,** 309–315 (1999).

229. Sadtler, V. M., Krafft, M. P. & Riess, J. G. Achieving stable, reverse water-in-fluorocarbon emulsions. *Angew. Chemie* **35,** 1976–1978 (1996).

230. Polychniatou, V. & Tzia, C. Study of Formulation and Stability of Co-surfactant Free Water-in-Olive Oil Nano- and Submicron Emulsions with Food Grade Non-ionic Surfactants. *J Am Oil Chem Soc* **91,** 79–88 (2014).

231. Bull, H. B. & Neurath, H. The denaturation and hydration of proteins: II. Surface denaturation of egg albumin. *J. Biol. Chem.* **118,** 163–175 (1937).

232. Workentin, M. S. Functional Condensation Polymers. *Synthesis (Stuttg).* 2794–2794 (2002). doi:10.1055/s-2002-35996

233. Cleland, W. W. Dithiothreitol, a New Protective Reagent for SH Groups. *Biochemistry* **3,** 480–482 (1964).

234. Bertrand, O. & Gohy, J.-F. Photo-responsive polymers: synthesis and applications. *Polym. Chem.* **44,** 5539–5553 (2016).